中国高等科学技术中心

CCAST—WL WORKSHOP SERIES: VOLUME 25

QUARK EFFECTS AND COLLECTIVE MODES INSIDE NUCLEI

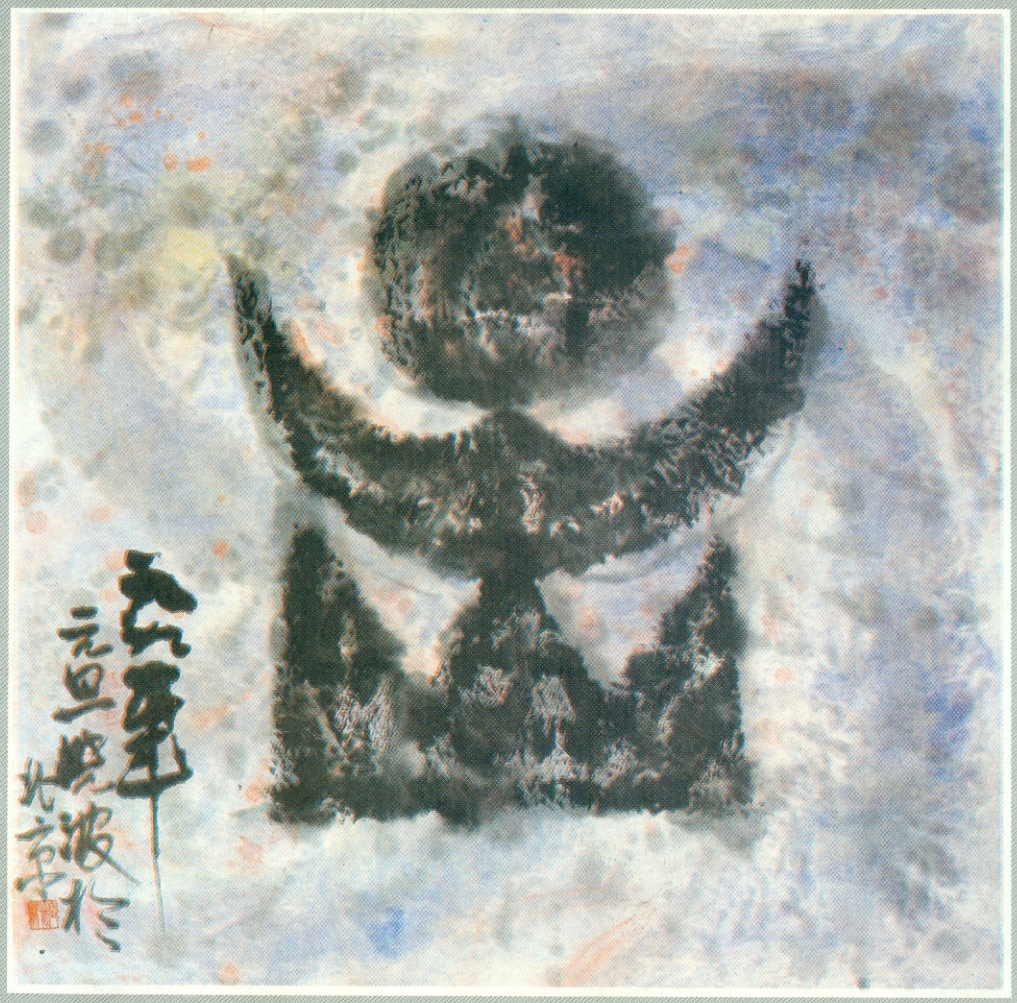

edited by

Zhaoming Qiu, Hongzhou Sun and Enguang Zhao

Beijing **January**, 1993

Preface to the CCAST-World Laboratory Series

The China Center of Advanced Science and Technology (CCAST) was established in Beijing on October 17, 1986 to introduce important frontier areas of science to China, to foster their growth by providing a suitable environment, and to promote free exchange of scientific information between China and other nations.

An important component of CCAST's activities is the organization of domestic and international* symposium/workshops. Each academic year we hold about 15 domestic symposium/workshops which last an average of one month each. The subjects are carefully chosen to cover advanced areas that are of particular interest to Chinese scientists. About 20-60 participants, from senior scientists to graduate students, are selected on a nationwide basis for each program, During each workshop, these scientists hold daily seminars and work closely with each other.

Since 1990, CCAST has also sponsored a vigorous program for young Chinese scientists who have already made world-class contributions and are currently doing research abroad. They return to China to lecture at CCAST and to collaborate with their colleagues at home. In this way, they can bring to China their own expertise, and when they go back to their institutions abroad they will be able to circulate in turn the knowledge they have acquired in China.

China is at a pivotal point in her scientific development. She is gradually emerging as an important and dynamic force in shaping the advanced science and technology of the future. This series is part of this remarkable evolution. It records the effort, dedication, and sharing of knowledge by the Chinese scientists, at home and abroad.

T. D. Lee

*The CCAST international symposium/workshop series is published separately by Gordon and Breach Scientific Publishers

Contents

Quark Degrees of Freedom in Nuclear Physics*

Wei-hsing Ma[a], En-guang Zhao[b], Han-xin He[c] and Peng-nian Shen[a]
Center of Theoretical Physics, CCAST(World Laboratory)
P.O.Box 8730 Beijing 100080, China

Abstract

The roles of quark degrees of freedom in nuclear physics are studied in this paper. Our particular interests focus primarily on nuclear force, electromagnetic properties of nucleon in quark model, multiquark clusters in nuclei, and six quark mechanism of pion-nucleus double charge exchange. The present study shows that although there is no unique, explicit experimental evidence so far to prove the presence of quark degrees of freedom in nuclei, it seems to be clear that the quark degrees of freedom may be responsible for theoretically resolving many long-standing puzzle problems in nuclear physics, such as the similarity of experimental charge form factors of ^3H and ^3He, the observed central "hole" of ^3He charge density, and the first minimum location of the experimental angular distribution of 164 MeV double charge exchange reaction $^{18}O(\pi^+,\pi^-)^{18}Ne_{g.s.}$, which are all in strong conflict with conventional hadronic theory with meson currents.

*This work was partly Supported by National Natural Science Foundation of China.

1 Introduction

The traditional picture of the nucleus in low energy nuclear physics is that of an interacting many-body system of structureless, pointlike protons and neutrons. By low energy nuclear physics we understand the region of excitation energies δE smaller than the Fermi energy ($\epsilon_F \approx 30 - 40 MeV$) and momentum transfer $\delta q \leq 1/R$, where R is the nuclear radius.

The situation changes as δE and/or δq is increased by several hundreds of MeV up to a few GeV, the domain of intermediate energies physics. At this point, explicit mesonic degrees of freedom become directly visible. The Pion, in particular, is of fundamental importance. With its small mass of m_π=140 MeV, it is by far the lightest of all mesons. As mesons become important, nucleons begin to reveal their intrinsic structure. Inseparably connected with pionic degrees of freedom is the role of the $\Delta(1232)$, the spin 3/2–isospin 3/2 isobar reached from the nucleon by a strong spin-isospin transition at an excitation energy $\delta E = M_\Delta - M_N =$ 300 MeV, the Δ-nucleon mass difference.

At the same time as these developments proceeded, high energy physics provided strong evidence for the quark structure of hadrons[1]. In particular, since the discover of the J/Ψ particle we have become thoroughly convinced of the quark structure of hadron. As a consequence, there is an obvious necessity to investigate the phenomenology of nuclear constituents and forces from a more fundamental point of view. The relevant issues are masses, size and other static properties of baryons and mesons; meson-baryon coupling constants which related to the description of the long- and intermediate distance properties of the nucleon-nucleon interaction; a description of nucleon-nucleon and nucleon-antinucleon interactions at short distance, where the quark cores of the nucleons overlap, directly in terms of interacting quarks and gluons; and an investigation, both theoretically and experimentally, of possible explicit quark degrees of freedom in nuclei.

Altogether, this is a challenging program, and there is little doubt that activities in this direction will represent a substantial branch of intermediate energy nuclear physics research in coming years.

In this paper, we study quark degrees of freedom in nuclear phenomena. We suggest a hybrid quark hadron model to describe NN interaction in section 2. In section 3, we firstly derive quark- quark interaction from the idea of nontopological soliton theory, and then we calculate static properties of proton and spectroscopy of baryon by use of the quark-quark interaction. In section 4, we present some strong signals for the existence of multiquark clusters in nuclei. As a particularly evident example, we discuss the observed central " hole "

of ^3He charge density in this section in a hybrid quark hadron model. We point out in section 5 that the quark degrees of freedom are responsible for the minimum location of experimental angular distribution of 164 MeV double charge exchange (DCX) reaction. We claim that the 164 MeV DCX reaction may be a good stage for dibaryon, a six-quark cluster, to manifest itself. Finally, we reserve our concluding remarks stemed from the present study for section 6.

2 NN interaction in hybrid quark hadron model

Because of its importance to nuclear physics, the NN interaction gives rise to a large amount of models. Some of them are purely phenomenological, designed to fit the rich body of existing experimental data. As is known, some understandings of the NN interaction have been gained during the last ten years and, in opinion of many, including us, consideration of purely phenomenological potentials without inclusion of well-established theoretical elements is no longer justified. On the other hand, there is now a consensus that a reasonable theoretical approach to the problem of nuclear force can be based on the breaking of the interaction into two parts:

(i) The long range and medium range part where hadronic (mesons and isobars) degrees of freedom provide a very good approximation. In this part, consideration of quark degrees of freedom is uneconomical and unnecessary.

(ii) The short range part where subhadronic (quarks, gluons) degrees of freedom are expected to play a significant role. The problem, however, is to find reliable methods to handle those degrees of freedom.

In fact, at present, the potential models that are the most frequently used in the literatures are the Bonn[2], Paris[3], Super-soft core[4], Reid-soft core[5], Argonne V_{14}[6] and new Bonn potential[7]. They are all derived from hadronic degrees of freedom. For expamle, in the Paris potential the long- and medium-range parts ($r > 0.8$fm) are given by the $(\pi + 2\pi + \omega)$ meson exchange while the short - range part ($r \leq 0.8$fm) is described simply by a phenomenological soft core constrained by experimental data. Therefore, we do need to understand this short-range part of NN interaction theoretically. On the other hand, although these potential models have passed many serious experimental tests with success there exist many difficulties in understanding of data, such as the triton binding energy.

Given the two - body forces, the triton binding energy can be calculated exactly. The

results obtained with different potentials are shown in table 1.

Table 1: The triton binding energy predicted by different two-body interactions.

Potential	Paris[3]	SSC[4]	RSC[5]	$V_{14}^{6)}$	$TRS^{8)}$	New Bonn[7]	Exp.
$E(^3H)$ (Mev)	7.64	7.53	7.35	7.67	7.56	6.70	8.48

Obviously, all these two-body potentials underbind the triton by about 1 MeV. This is a big discrepancy between theory and data, and has to be resolved.

The interaction between quarks is governed by QCD which has two basic properties: asymptotic freedom and confinement. This means that at short distance, the quark-gluon coupling constant becomes so small that the perturbative QCD is applicable. However, at long distance the quarks and gluons interact so strongly that the perturbative calculations are no longer valid. As a result, we propose a hybrid interaction model of quark and hadron to describe NN force. In the model, the quark and gluon exchange interaction is assumed to be dominant only in the region where the two nucleonic clusters overlap, while the hadronic degrees of freedom are effective at the intermediate - and long - ranges. This model has the good feature that it does not need any ambiguous coupling of quarks to mesons. Thus, the equivalent local potential will be cut off sharply at a distance R_c and replaced, outside R_c, by the $(\pi + 2\pi + \omega)$ exchange potential. The two - pion exchange potential can be calculated via dispersion relations in the same way as that in the Paris potential model. The proposed model could be materialized by the following potential

$$V(r) = V_{quark}(r)f(r) + V_{meson}(r)[1 - f(r)] \tag{1}$$

where V_{quark} is given by QCD theory, and $V_{meson} \equiv (\pi + 2\pi + \omega)$ exchange potential. The cut off function is chosen of the form

$$f(r) = \frac{1}{1 + (r/R_c)^\alpha}. \tag{2}$$

The sharpness of $f(r)$ is realized by choosing $\alpha = 10$, R_c is adjusted to fit the deuteron binding energy which yields R_c=0.626 fm. The calculations of different phase shifts and other physical quantities in the hybrid model are in progress.

3 Static properties and spectroscopy of baryon in quark model

Understanding the structure of the nucleon is one of the key issues in both particle and nuclear physics. For example, one needs the proton's charge form factor (and even that of the neutron) to accurately calculate nuclear charge form factors. At the same time the inclusion of nucleon structure in theoretical calculations alters some traditional concepts in nuclear physics. For instance, in mean - field approximation the nuclear saturation is a direct effect of the nucleon motion becoming relativistic[9]. But, if considering quark structure of nucleon the whole saturation mechanism is altered[10]. It is a consequence of the relativistic motion of the quarks, not the nucleons !

The baryons consist of quarks and gluons. The interaction between quarks has been successfully described by a non- Abelian gauge theory called Quantum Chromodynamics (QCD). At present considerable efforts are made to solve the QCD equations on large computers, using Monte Carlo techniques. There is, however, still only limited direct impact of such calculations on the problem of low energy hadron dynamics and nuclear forces. It will be necessary to rely on phenomenological models which incorporate basic properties expected from QCD.

The best known of these models is the MIT bag model[11]. However, the original MIT bag model is not easily compatible with basic nuclear facts. If the bag radius R is adjusted to obtain reasonable baryon masses, one finds $R \geq 1.0fm$! A bag of this size would be difficult to commodate with the observation of well isolated nucleon quasiparticles in nuclei. Also, the mass of the pion as a pair of confined quark and antiquark comes out much too large in the standard bag model. This is a serious point for nuclear physics since the pion compton wavelength $\lambda_\pi = \frac{\hbar}{m_\pi c} = 1.4fm$ defines the natural length scale for nuclei. It is amusing to imagine, for example, how the deuteron would look like if the pion mass were not 140 MeV, but a multiple of 140 MeV. On the other hand, due to the sharp boundary the axial current in MIT bag model is not conserved. This also is a serious point for its application in nuclear physics.

Another commonly used model is harmonic oscillation quark bag model[12]. The boundary of this model is so ambiguous that it is usually named a soft wall potential model in contrast with the hard wall potential of MIT bag model. The radius of nucleon predicted by this model turns out to be also inadequately large.

In fact, in spite of their successes, the static bag models cannot be expected to yield an adequate description of hadronic collisions, $N\bar{N}$ annihilation and many other dynamical phenomena since their noncovariant, non-Hamiltonian formulation. A description of hadron-hadron interactions requires more than bag statics. As a particular example, consider the N-N interaction. The static energy of six-quark bag has been calculated as a function of a shape, or N-N separation, and parameters. Qualitative understanding of the N-N potential was obtained. However, in order to calculate scattering or bound- state quantities, it is usually necessary to insert the " potential" into a Schrodinger, Dirac, or Lippmann-Schwinger equation. This requires a knowledge of the mass parameter which enters in the kinetic-energy term. Static bag models cannot yield the kinetic mass parameter because they are not associated with a complete Hamiltonian. There exist an expression for the energy, a differential equation, and a boundary condition, but no Hamiltonian. Thus, these difficulties spur us to quest for alternative bag formulations which can be described by a complete Hamiltonian and are manifestly covariant.

Friedberg and Lee have proposed a model[13] based on a complete Lagrangian or Hamiltonian formulation of the problem, and which therefore admits dynamical solutions of structure and scattering problems. The model contains only a few adjustable parameters, but is extremely rich in the variety of problems it can address.

We follow closely the idea of Friedberg and Lee[13] who have demonstrated that it is possible to obtain confining quark states from soliton solution of an effective Lagrangian which contains quarks and a scalar σ field. In the Friedberg-Lee's non - topological soliton model[13], the QCD theory is approximated by an effective Lagrangian density

$$\mathcal{L}_{eff} = \bar{\psi}(r)[i\gamma_\mu\partial^\mu - g\sigma(r)]\psi(r) + \frac{1}{2}(\partial_\mu\sigma(r))^2 - U(\sigma) \qquad (3)$$

where $i\bar{\psi}\gamma_\mu\partial^\mu\psi$ describes the quarks as Dirac particles. The last two terms in Eq.(3) describe the scalar soliton field $\sigma(r)$, which represents the complex structure of the vacuum, arising from virtual gluons and quark-pairs interacting among themselves. The non-linearity of the soliton field enters through the self-interaction $U(\sigma)$ of the σ field

$$U(\sigma) = B + a_2\sigma^2(r) + a_3\sigma^3(r) + a_4\sigma^4(r) \qquad (4)$$

where the polynomial terminates in fourth order to ensure renormalizability, even though we are dealing with an effective Lagrangian. $U(\sigma = 0) = B$ is to be identified with the "bag constant" or volume energy density of a cavity. With a suitable adjustment of the constants, the function has two minima, one at $\sigma = 0$, and another, lower minimum, at $\sigma = \sigma_0$. The

physical vacuum corresponds to the second minimum, and the constant B is chosen so that $U(\sigma_0) = 0$. The non-linear features of $U(\sigma)$ permits soliton-like solutions for appropriate choices of parameters. These solutions have the property that quark density $\bar{\psi}\psi$ goes to zero rapidly beyond some radius R which determines the hadron size.

The term $-g\bar{\psi}\sigma(r)\psi$ in Eq.(3) describes interaction of quarks with the soliton field where g is coupling constant between quark and soliton field. In the presence of valence quarks, the $U(\sigma) + g\bar{\psi}\sigma(r)\psi$ may have a minimum near $\sigma(r) = 0$ (the perturbative vacuum). This leads to a cavity in the σ field, which is called the " bag ". The quark dig a hole in the vacuum. This is the origin of confinement in the model. In the model all observed hadrons appear as solitons in the scalar σ field with quarks trapped inside them.

Although there is no direct relation to QCD in Eq.(3), one might think of the σ field as describing the long-range, non- perturbative QCD effects. In fact, by starting from QCD in a finite volume and then taking the infinite-volume limit, Friedberg and Lee found that there is a " phase-transition" phenomenon, which implies the existence of a long-range order in the vacuum for an infinite volume. This long-range order is represented by Lorentz scalars, because of relativistic invariance, such Lorentz scalars can in turn be identified with the phenomenological scalar field used in a soliton bag model of hadrons.

The Hamiltonian density, $\mathcal{H}$, obtained from Eq.(3) can be written

$$\mathcal{H} = \frac{1}{2}\dot{\sigma}^2 + \frac{1}{2}(\vec{\nabla}\sigma(r))^2 + U(\sigma) + \psi^+(-i\vec{\alpha}\vec{\nabla} + \beta g\sigma)\psi \tag{5}$$

with $\vec{\alpha}$ and β being the usual Dirac matrixes. Consider now a classical σ field , for which the conjugate field $\dot{\sigma}$ commutes with σ itself. This means that the state of lowest energy has $\dot{\sigma} = 0$, hence σ is time - independent. The total Hamiltonian is then given by $H = \int d^3r\mathcal{H}$ which can be decomposed into a sum of two terms: a quasiclassical part and a quantum correction, $H = H_{qcl} + H_{cor}$.

Although a complete Lagrangian should also contain the vector, Higgs field and counterterms which are for renormalization purposes, at present stage of our research we shall not consider this complicated case. We also restrict our subsequent discusion to the sector of H_{qcl}. We shall treat H_{cor} as a correction in our coming paper.

The lowest eigenvalue E of the quark-σ field system described by H_{qcl} can be derived by distributing quarks to the same spinor state, but with different colors. Consequently, E is the minimum of $E(\sigma)$ where

$$E(\sigma) = NE_\alpha + \int d^3r\ [\frac{1}{2}(\vec{\nabla}\sigma)^2 + U(\sigma)]. \tag{6}$$

where $\sigma(r)$ is a c-number function of r and the E_α is defined to be the lowest positive eigenvalue of the Dirac equation

$$(-i\vec{\alpha}\cdot\vec{\nabla}+\beta g\sigma)\psi = E_\alpha\psi. \tag{7}$$

From Eqs.(6-7), one sees that the minimum of $E(\sigma)$ occurs when the $\sigma(r)$ field approximately satisfies

$$\frac{d^2\sigma(r)}{d^2r} - \frac{d\,U(\sigma)}{d\sigma} = 0. \tag{8}$$

Eq.(8) provides a good approach to the subject in a sense that the quark density $\bar{\psi}\psi$ goes to zero rapidly beyond some radius R which determines the hadron size and the coupling constant g is negligibly small inside the hadron due to requirement of asymptotic freedom[13].

Substituting Eq.(4) into Eq.(8) and then solving the resulting equation lead to a Woods-Saxon-like expression of the $\sigma(r)$ field,

$$\sigma(r) = \frac{\sigma_0}{1+exp[-m_\sigma(r-R)]} \tag{9}$$

with m_σ^{-1} being the diffusive thickness of the boundary and R stands for the radius of the bag. Eq.(7) shows that the confining potential for quarks is now given by

$$V(r) \equiv g\sigma(r) = \frac{g\sigma_0}{1+exp[-m_\sigma(r-R)]} \tag{10}$$

Consequently, the local quark mass $V(r) = g\sigma(r)$ is small inside the hadron. At the surface of hadron the σ field changes very rapidly towards its vacuum value σ_0. The effective quark mass outside the hadron is given by a value $g\sigma_0$ which can be chosen very large by adjustment of the coupling constant g of quark and σ field.

The model describes a situation where quarks are essentially free inside, with a relatively sharp transition region from inside to outside the hadron.

It should be emphased that in contrast with the work of R. Goldflam and L. Wilets[13] who numerically resolved the coupled differential equation satisfied by ψ and σ in lowest order in σ and obtained their numerical solution of σ, we obtain the analysis expression of σ. Needless to say, this is very easy to use in many cases.

We expand ψ in Eq.(7) in terms of a complete set of orthonormal c-number time-independent spinor functions $u_\alpha(\vec{r})$ and $v_\alpha(\vec{r})$

$$\psi(\vec{r},t) = \sum_\alpha \{u_\alpha(\vec{r})e^{-iE_\alpha t}\ b_\alpha + v_\alpha(\vec{r})e^{iE_\alpha t}\ d_\alpha^+\}, \tag{11}$$

where α denotes the set of quantum numbers necessary to specify the quark states, including flavor. The color degrees of freedom is also assumed to be implicit in the α. Here b_α annihilates a quark and $d^\dagger_\alpha$ creates an antiquark in the orbit α. The $u_\alpha(\vec{r})$ and $v_\alpha(\vec{r})$ are determined by

$$[-i\vec{\alpha}\cdot\vec{\nabla}+\beta V(r)]\begin{Bmatrix}u_\alpha(\vec{r})\\ v_\alpha(\vec{r})\end{Bmatrix}= E_\alpha\begin{Bmatrix}+u_\alpha(\vec{r})\\ -v_\alpha(\vec{r})\end{Bmatrix} \tag{12}$$

with $V(r)=g\sigma(r)$ for massless quarks. The normalization of the Dirac spinors is

$$\int d^3\vec{r}\,u^+_\alpha(\vec{r})u_\alpha(\vec{r}) = \int d^3\vec{r}\,v^+_\alpha(\vec{r})v_\alpha(\vec{r}) = 1. \tag{13}$$

The quark wave function can be written in the form

$$u_{nljm}(\vec{r}) = \begin{pmatrix} ig_{nlj}(r)/r \\ \vec{\sigma}\cdot\hat{r}\,f_{nlj}(r)/r \end{pmatrix}\phi_{ljm}(\hat{r}) \tag{14}$$

with $\phi_{ljm}(\hat{r})$ being the spinor harmonics

$$\phi_{njm}(\hat{r}) = \sum_{m_l,m_s} C^{jm}_{lm_l\frac{1}{2}m_s}\,Y_{lm_l}(\hat{r})\,\chi_{\frac{1}{2}m_s} \tag{15}$$

and the normalization is $\int_0^\infty dr\,[g^2_{nlj}(r)+f^2_{nlj}(r)] = 1$. The antiquark wave functions are obtained by charge conjugation

$$v_{nljm}(\vec{r}) = \eta_c\cdot(-1)^{j-m+l}\begin{pmatrix}\vec{\sigma}\cdot\hat{r}\cdot f_{nlj}(r)/r \\ -i\,g_{nlj}(r)/r\end{pmatrix}\phi_{lj-m}(\hat{r}) \tag{16}$$

where η_c is an arbitrary phase with $|\eta_c|^2=1$.

The upper and lower components of Dirac wave functions $g_\alpha(r)$ and $f_\alpha(r)$ satisfy

$$\begin{aligned}\frac{d\,f_\alpha(r)}{dr} &+ [-m-V(r)+E_\alpha]g_\alpha(r)-\frac{k}{r}f_\alpha(r)=0\\ -\frac{d\,g_\alpha(r)}{dr} &+ [m+V(r)+E_\alpha]f_\alpha(r)-\frac{k}{r}g_\alpha(r)=0\end{aligned} \tag{17}$$

where $\kappa = \mp(j+1/2)$ for $j = l\pm 1/2$. Solving Eq.(17) numerically, we can obtain quark eigenfunctions and eigenvalues in our Woods-Saxon-like confining potential model of quarks.

A calculation for massless non-strange quarks is performed in this work. The theoretical results and comparing to other model predictions are shown in Fig.1-3. The eigenvalues are given in Fig.1, where the energies for $1s_{1/2}$ state in three different bag models have been adjusted to be the same. Our calculation indicates that the confinement of quarks in this model is strongly dependent on the strength of the confining potential, $V_0 = g\sigma_0$. This means that quarks are partially confined in the bag region for finite V_0. This feature of the soliton

model is not particularly troublesome. Furthermore, the limit of large V_0 can be carried out after the completion of the calculations, thus ensuring that no spurious results occur due to discontinuities of the bag surface as is the case in the MIT model.

The behaviors of the upper and lower components of quark wave function are shown in Fig.2 in a comparisive way. Obviously, the two model predictions are quite similar. The maximum of our eigenfunction could be moved towards Regensburg position by changing the radius of our confining bag. This consistency can be thought of as being an evidence that our Woods-Saxon-like confining potential model of quarks has its great validity.

In Fig.3, we show the upper and lower components $u(r) = g(r)/r$ and $v(r) = f(r)/r$ of quark eigenfunctions, respectively, for three different models. As is seen from the figure, at short distance (r $\leq$ 0.8fm) there is no difference between MIT bag model and ours, while at large distance (r $>$ 0.8fm) our model behaves like Regensburg harmonic bag model.

The calculated static properties of nucleon in our Woods-Saxon- like confining potetial bag model are presented in the following:

(1). Charge radii: the charge density is derived from the time- like component of the quark current $Q\bar{\psi}\gamma_\mu\psi$

$$\rho_{ch}(\vec{r}) = \sum_\alpha Q_\alpha u^+_\alpha(\vec{r})u_\alpha(\vec{r})b^+_\alpha b_\alpha \tag{18}$$

where the Q is quark charge and α denotes the occupied quark orbits (including flavor). For three valence quarks forming nucleonic core, the root-mean-square charge radius is then defined by

$$< r^2 > = \int r^2 d^3\vec{r} < N|\rho_{ch}(\vec{r})|N > . \tag{19}$$

For a proton in the state of α

$$< r^2 >_\alpha = 4\pi \int_0^\infty r^2 dr\ [g^2_\alpha(r) + f^2_\alpha(r)]. \tag{20}$$

So, using the $1s_{\frac{1}{2}}$ state wave functions $g_{1s_{\frac{1}{2}}}(r)$ and $f_{1s_{\frac{1}{2}}}(r)$ in Eq.(17), we get the charge radius of proton in $1s_{\frac{1}{2}}$ state, $r_p = 0.87fm$.

(2). Axial charge g_A: Consider now the quark axial current

$$A^i_\mu(\vec{r}) = \bar{\psi}(\vec{r})\gamma_\mu\gamma_5\frac{\tau^i}{2}\psi(\vec{r}). \tag{21}$$

We are interested in the matrix elements of Eq.(21) taken between nucleon quark core states $|N>$, in particular those with i=3 and the space part of A_μ. The axial charge g_A of quark

core can be defined by

$$g_A \cdot < \vec{\sigma}_N \cdot \vec{\tau}_N^3 >= \int d^3\vec{r} < N|\vec{A}^3(\vec{r}, t=0)|N > \tag{22}$$

where $< \vec{\sigma}_N \cdot \vec{\tau}_N >$ refers to the matrix element taken with nucleon (rather than quark) spin and isospin operators. In the absence of center -of- mass correction, with three quarks in $1s_{\frac{1}{2}}$ orbits , one obtains

$$g_A = \frac{5}{3} \cdot 4\pi \int_0^\infty dr\ [g^2_{1s_{\frac{1}{2}}}(r) - \frac{1}{3} f^2_{1s_{\frac{1}{2}}}(r)] = \frac{5}{3}\ [1 - \frac{4}{3} \cdot 4\pi \int_0^\infty f^2_{1s_{1/2}}(r) dr] \tag{23}$$

Therefore, in the non-relativistic quark model with $f(r) = 0$, one obtains the result predicted by the standard SU(4) model: $g_A = \frac{5}{3}$. This should be compared to the empirical value of $g_A = 1.255 \pm 0.006$. Our model gives $g_A = 1.18$ which is better than the MIT model prediction of $g_A = 1.09$.

(3). Magnetic moments: the magnetic moment of nucleon is defined by

$$\mu_N = < N, \frac{1}{2}\frac{1}{2}| \int d^3r [\vec{r} \times \vec{j}]_z |N, \frac{1}{2}\frac{1}{2} >, \tag{24}$$

where the spin s (1/2) and its z-projection $s_z(1/2)$ have been made explicit. $\vec{j}$ is the 3-vector part of electromagnetic current

$$\vec{j} = \sum_\alpha Q_\alpha \bar{u}_\alpha(\vec{r}) \vec{\gamma} u_\alpha(\vec{r}) b^\dagger_\alpha b_\alpha. \tag{25}$$

Then, μ_p can be rewritten as

$$\mu_p = -\frac{2}{3} \cdot 4\pi \mu_N \cdot 2M_N \int_0^\infty r dr\ g_{1s_{\frac{1}{2}}}(r)\ f_{1s_{\frac{1}{2}}}(r) \tag{26}$$

with $\mu_N = \frac{e}{2M_N}$ being nucleon magneton. The corresponding neutron magnetic moment is

$$\mu_n = -\frac{2}{3}\mu_p. \tag{27}$$

Our model prediction for μ_p is 2.27 in the unit of nucleon magneton. We tabulate our calculated results of the r_p, g_A and μ_p in table 2 for comparison with data[15].

Table 2. Static properties of proton from quark core contribution for $V_0 = 4.5 fm^{-1}$, $m_\sigma^{-1} = 0.06 fm$.

	$r_p(fm)$	g_A	μ_p
Exp.	0.87	1.255	2.79
Theor.	0.87	1.128	2.27

The parameters in the present calculations are determined by mass difference of nucleon and isobar, $M_\Delta - M_N$, and stability condition of nucleon, $\frac{dM_N}{db}_{b=0.6} = 0$ where b is the size of bare quark core.

(4). Form factors: In the following, we study the nucleon elastic form factors. Given the electromagnetic current $J_\mu(x)$, the relevant form factors are defined by

$$< N(p',s') \ |J_\mu(0)| \ N(p,s) > = \bar{u}_{s'}(p')\{eF_1(q^2)\gamma_\mu + \frac{e}{2M_N}F_2(q^2)i\sigma_{\mu\nu}q^\nu\}u_s(p) \tag{28}$$

where $u_s(p)$ are the nucleon spinors ($\bar{u}u = 1$), p and p' are incoming and outgoing nucleon four momenta, with $p'^2(p^2) = M_N^2$, the square of the nucleon mass. The q_μ is the four momentum transfers, $q_\mu = (p' - p)_\mu$, and

$$q^2 = q_0^2 - \vec{q}^2 \tag{29}$$

In the Breit-frame, $\vec{p'} = -\vec{p} = \vec{q}/2$ and $q_0 = 0$, we have

$$< N(\frac{\vec{q}}{2},s') \mid J_0(0) \mid N(-\frac{\vec{q}}{2},s) >= \frac{\delta_{s's}}{\sqrt{1+\eta}}G_E(q^2), \tag{30}$$

and

$$< N(\frac{\vec{q}}{2},s') \mid \vec{J}(0) \mid N(-\frac{\vec{q}}{2},s) >= \frac{i < s' \mid \vec{\sigma} \times \vec{q} \mid s >}{2M_N\sqrt{1+\eta}}G_M(q^2) \tag{31}$$

where $\eta = -\frac{q^2}{4M_N^2}$. The charge and magnetic form factors are related to the Dirac and Pauli form factors $F_1(q^2)$ and $F_2(q^2)$ by

$$G_E(q^2) = F_1(q^2) - \eta F_2(q^2), \tag{32}$$

and

$$G_M(q^2) = F_1(q^2) + F_2(q^2). \tag{33}$$

The charge form factors of proton and neutron at the value of $q^2 = 0$ are required to be

$$G_E^p(q^2 = 0) = 1 \ , \qquad G_E^n(q^2 = 0) = 0, \tag{34}$$

while $G_M(q^2 = 0.)$ is related to the magnetic moment of proton or neutron by

$$\mu_{p,n} = \frac{e}{2M_N} G_M^{p,n}(q^2 = 0). \tag{35}$$

The experimental values of $G_M(q^2 = 0)$ for proton and neutron respectively are

$$G_M^p(q^2 = 0) = 2.79\,, \qquad G_M^n(q^2 = 0) = -1.91 \tag{36}$$

The measured form factor follows very closely a dipole form[15]

$$G_D(q^2) = [1 - q^2/0.71]^{-2} \tag{37}$$

with q being in the unit of Gev/c. This is the most salient feature of all the form factors.

There are several models used to fit or predict the nucleon elastic form factors. The traditional vector dominance models (VDM)[16] describe the virtual photon in terms of its hadronic components. The interaction is described by the coupling of a photon to various vector mesons (dominated by ρ at low q^2), which are then absorbed by the nucleon as described by a meson- nucleon form factor. The main problem with VDM model is that they have many free parameters and do not explicitly take into account the quark structure of the nucleon.

Another approach[17] that does explicitly use the valence quark components is the application of perturbative QCD and concepts from dimensional scaling. In this case the interaction is described by the point - like coupling of a virtual photon to a single quark, combined with several hard gluon exchanges between the quarks to keep them flying apart. In practice, the strength of the strong coupling constant $\alpha_s \simeq 0.3$ at experimentally accessible q^2 values makes the perturbative assumption questionable, and so far only the leading order diagram has been calculated.

Of course, some progresses are also being made in predicting the nucleon form factors by evaluating the QCD Lagrangian in Lattice gauge theory and QCD sum Rules[18]. Although quantitative predictions are not possible at present, advances in computer power and calculational techniques make these approaches very promising for the future.

We try to fit the form factors by use of our quark confining model. Considering three quark in proton are in $1s_{\frac{1}{2}}$ orbit, then the electromagnetic form factors of proton are given by

$$G_E^p(q^2) = 4\pi \int_0^\infty dr j_0(qr)[g^2_{1s_{\frac{1}{2}}}(r) + f^2_{1s_{\frac{1}{2}}}(r)], \tag{38}$$

and

$$G_M^p(q^2) = -\frac{4M_N}{q} 4\pi \int_0^\infty dr\, j_1(qr) f_{1,\frac{1}{2}}(r) g_{1,\frac{1}{2}}(r) \tag{39}$$

in leading order in $\eta = -\frac{q^2}{4M_N^2}$. Therefore, given $g_\alpha(r)$ and $f_\alpha(r)$, we can easily obtain the electromagnetic form factors $G_E^p(q^2)$ and $G_M^p(q^2)$. Our theoretical results are shown in Fig.4. As is seen from the comparisons with other phenomenological models, our model seems to be more realistic.

It should be noted that we only calculate the contributions from quark core of nucleon to r_p, g_A, μ_p, $G_E^p(q^2)$ and $G_M^p(q^2)$ in this paper. An actual comparison with the experimental data must require to deal with the contributions from pion cloud surrounding the quark core since a nucleon consists of a quark core and a pion cloud surrounding the core in chiral quark bag model. The charged pions contribute to the total current, and therefore play an important role in determining electromagnetic properties of nucleon. We are going to estimate these contributions.

4 Multiquark clusters in nuclei

Many experimental observables are in strong conflict with the expectation given by traditional nuclear theories involving meson exchange currents, and support the theoretical idea of the formation of multiquark clusters in nuclei[20]. For example, it has been known for over decade that the ^3He charge form factor cannot be understood in terms of the impulse approximation - scattering from nucleons whose charge and current distributions are given by the ^3He wave function. With improved knowledge of the N-N potential and the ability to accurately solve the three - body nuclear problem over the past decade, one must conclude that traditional nuclear physics is not adequate, and non-nucleonic aspects of nuclei must be considered. A number of theorists have attempted to fit the experimental data by introducing meson currents[21], and experiments have also proven the presence of meson currents in nuclei[22]. However, most hadronic theories with meson currents, including Delta contributions[23], fail to fit the ^3He data. This is a serious test of meson exchange currents.

One of the most striking results of traditional hadronic models with meson currents is the prediction that the meson current contributions for ^3He are much smaller than for ^3H. The reason is quite simple. Due to the γ_5 coupling, the largest meson current contributing to three-body charge form factor is the pion pair current depicted in Fig.5, where the photon

is coupling to a $N\bar{N}$ pair.

The operator for the charge part (the fourth component) of the two-body pion pair current is

$$J_0^{\pi NN} = f \frac{F_{\pi NN}(Q^2)\cdot F_{\gamma NN}(K^2)}{\vec{Q}^2+m_\pi^2}(\vec{\sigma}_1\cdot\vec{K})(\vec{\sigma}_2\cdot\vec{Q}) \times[G^{(s)}(K^2)\vec{\tau}_1\cdot\vec{\tau}_2+G^{(v)}(K^2)\tau_{2z}]+(1\rightleftharpoons 2) \quad (40)$$

where $(\vec{K},\vec{Q})$ are the (photon, pion) momenta, f is a constant, the F are the vertex functions contained $N\bar{N}$ pair, and the $\vec{\tau}$ (isospin) and $\vec{\sigma}$ (spin) operators act in nucleonic space 1 and 2. It is clear from Eq.(40) that for values of K^2 such that the isoscalar and isovector nucleonic form factors (G^s, G^v) do not change sign, the isoscalar and isovector terms will contribute constructively for ^3He since the $T_z(^3He)=+\frac{1}{2}$ and destructively for ^3H since the $T_z(^3H)=-\frac{1}{2}$. Thus, we expect that the ^3He and ^3H charge form factors given by traditional hadronic models with meson current should be quite different. Contrary to our expectation, the observables of ^3He and ^3H charge form factors are quite similar to each other. So, this unexpected discrepancy provides a crucial test of the use of meson current in explaining the experimental data.

It is now believed that the conflict between traditional theory and data is a clear signal of explicit quark effects, and a good example for quark nuclear physics. Since the discovery of the J/ψ particle we have become thoroughly convinced that hadron is composed of quarks and gluons. A nucleus can be thought of as being a system of quark clusters. However, since the average distance between the centers of two nucleons in nuclear matter is about the diameter of a nucleon, a sizable fraction of nuclear matter consists of overlapping nucleons. In quark model, this leads to a large probability for a nucleon to be part of a six- or nine-quark cluster. Furthermore, the density of ^3He and ^3H are sufficiently close to the density of nuclear matter to provide important information at internucleon separation of less than 1 fm where quark degrees of freedom might be expected to be important. We claim that a modern concept of the ^3He and ^3H structure should be hybrid: both nucleonic and quark degrees of freedom must be included with care not double count.

Kisslinger and Ma proposed a Hybrid Quark Hadron (HQH) model to describe nuclear structure[24]. In this model, the configuration space is divided into two distinct regions: an interior quark region and an exterior hadronic region. In the interior quark region, nucleon bags overlap and six- and /or nine - quark clusters are formed. One no longer has nucleons. In the exterior hadronic region, quarks are confined within hadrons, and we treat a tradi-

tional nuclear system. The boundary separating these two distinct regions is described by a phenomenological parameter, r_0, in terms of which projection operators can be defined. For bound state, the probability for a nucleon to be part of six-quark cluster is determined by nuclear wave function in the exterior hadronic region[24].

The wave function in the HQH model is defined by projections onto the outer and the inner region. For instance, for two baryon bound system in a channel α, the wave function is given by

$$\psi^{\alpha}_{B_1,B_2} = \begin{cases} \psi_{B_1}(3q)\psi_{B_2}(3q)\Phi^{\alpha}_{B_1,B_2}(r) & r > r_0 \\ \psi^{\alpha}_{6q} = N \sum_i C^{\alpha}_i \psi^i_{\alpha}(6q) & r \leq r_0 \end{cases} \tag{41}$$

Where C^{α}_i are the amplitude of the six-quark configurations $\psi^i_{\alpha}(6q)$ and satisfy $\sum_i \mid C^{\alpha}_i \mid^2 = 1$. N is the normalization constant determined from the probability conservation law, i.e. ,

$$N^2 \equiv P_{6q} = 1 - \int \mid \Phi^{\alpha}_{B_1,B_2}(r) \mid^2 \theta(r - r_0) dr \tag{42}$$

Which $\Phi^{\alpha}_{B_1,B_2}(r)$ being the relative wave functions of the two nucleon system, which is the best known part in the traditional nuclear theory.

The external wave functions for ^3He and ^3H used in our calculations are five channel Faddeev solutions[24] obtained with several two- body potentials, such as Reid soft core, Super soft core and Argonne V_{14}. Corresponding six- and nine - quark cluster probabilities in the ^3He are listed below in %, with $r_0 = 1.0 fm$.

Table 3. Probabilities for six - and nine-quark clusters in ^3He with $r_0 = 1. fm$ for different two-body interaction

interaction	P_{6q}	P_{9q}
Reid soft core	13.396	0.427
super soft core	14.129	0.500
Argonne V_{14}	14.230	0.498

Note that the multiquark cluster probabilities are not very sensitive to the choice of two-body nuclear interaction.

The charge form factors for ^3He and ^3H in the HQH model are given[24] by

$$F_{ch}(q^2) = F^{I.A.}_{ch}(q^2) + F^{M}_{ch}(q^2) + F^{6q}_{ch}(q^2) + F^{9q}_{ch}(q^2) \tag{43}$$

with $F^{I.A.}_{ch}(q^2)$, $F^{M}_{ch}(q^2)$, $F^{6q}_{ch}(q^2)$ and $F^{9q}_{ch}(q^2)$ being contributions from impulse approximation, meson exchange current in the exterior hadronic region, six- , and nine -quark clusters in the

interior quark region, respectively. The detailed description of $F^{I}_{ch}(q^2)$ are given in Ref.(24). As is seen from Ref.(24), the electromagnetic form factors of ^3He and ^3H have been simultaneously reproduced by the HQH model without any adjustment of parameters (i.e., $r_0 = 1$ fm for both ^3He and ^3H). The model works successfully, and is attractive in resolving the long-standing puzzles of the observed similarity of charge form factors for this two three - body systems.

The long-standing puzzle problem for ^3He charge density is the observed central "hole" as shown in Fig.7 by crosses. According to our best knowledge, the observable has not been reproduced by any traditional three - body wave function. We believe this is also suggestive of our hybrid quark hadron model. The reason is quite simple. The density of ^3He can be written as

$$\rho_{r_0}(\vec{r}) = < \psi(^3He) \mid \sum_i e_i \delta^3(\vec{r} - \vec{r}_i) \mid \psi(^3He) > \tag{44}$$

which now depends on r_0. $\psi(^3He)$ in Eq.(44) stands for nuclear wave function of the ^3He. When one calculates the ratio of central density $\rho_{r_0 \neq 0}(r = 0)$ in the HQH model and $\rho_{r_0=0}(r = 0)$ in traditional hadronic model, one may obtain

$$\rho_{r_0 \neq 0}(r = 0) = [1 - P_{6q} - P_{9q}]\rho_{r_0=0}(r = 0) \tag{45}$$

with P_{6q} and P_{9q} being probabilities of six- and nine - quark clusters, respectively. Using the probabilities given in the table 3 , we see that due to the formation of multiquark clusters in ^3He, its charge density at center is greatly reduced. Therefore, the observed central " hole " seems to be naturally understood.

In fact, we have numerically carried out in this paper the Fourier transformation of Eq.(43) and obtained the charge density of the ^3He theoretically. The results are shown in Fig.6 by the solid curve. Indeed, the HQH model gives a perfect fit to the existing data. Comparison with the prediction of traditional nuclear theory with meson current in Ref.(25) shows that the experimental data strongly support our HQH model. Therefore, we may claim that the observed central "hole" of ^3He charge density might be an evident signal for possible existence of multiquark clusters in nuclei.

5 Quark degrees of freedom in DCX reaction

The main interest in pion - nucleus double charge exchange (DCX) reaction stems from the fact that any leading process of DCX must involve two different nucleons, a feature that

is not present in most other nuclear phenomena where two nucleon process appear only as high- order corrections. Thus, pion DCX reactions are ideal for the study of NN correlation at short range. In recent years, a large amount of good quality data from LAMPF, SIN, and TRIUMF has become available. These data have played a decisive role in improving our understanding of the DCX dynamics and in proving, in turn, the existence of six - quark cluster in nuclei.

Comparing the new data to various theoretical calculations done in past decade clearly indicates:

(1). the calculated excitation functions have a wrong energy dependence. The inclusion of medium renormalization effects and meson exchange current help but do not entirely remedy.

(2). the calculated position of the first minimum in the angular distribution at 164 MeV for transition to the analogue state in light nuclei is around 30^0 whereas experimentally it is near 20^0.

(3). an intriguing observation is the existence of large non- analog cross sections for (π^+, π^-) reaction on T=0 nuclei. As can be seen in the oxygen isotopes, at 164 MeV the cross section for $^{16}O(T=0)$ is nearly as large as that for $^{18}O(T=1)$. That is, $R = \frac{\sigma(^{18}O,T=1)}{\sigma(^{16}O,T=0)} = 3:1$ at 164 MeV, but R = 20 : 1 at 292 MeV. The ratios are strongly energy dependent and consequently rule out simple explanations based on conventional nuclear structure.

Keeping these difficulties in ones mind, one may say that we are, indeed, at a gate way to understanding of DCX reaction. In fact, we have carried out a laborious calculation of meson exchange currents in Ref.(27). Our principal finding is that although the meson exchange current theory provides some understanding of the reaction, the three long-standing puzzle problems mentioned here still exist. We have to search for other sources to resolve these difficulties.

We study contributions from six-quark mechanism to cross section of DCX reaction at the Δ (1232) resonance region. We propose a Hybrid Quark Hadron Model for describing DCX reaction to take place. In the model, DCX reaction proceeds in two distinct ways :

(a). At internucleon separation of less than a phenomenological length, r_0, the two nucleons form a six - quark cluster. Thus, DCX proceeds via six - quark cluster mechanism as shown graphically in the Fig.7 where, taking the direct term as an example, a π^+ is absorbed by a down (d) quark which is then turned into an up (u) quark after the absorption, and finally, a π^- is emitted from another d quark which becomes an u quark after the emission.

(b). At internucleon separation of larger than r_0, the two nucleons is in a traditional nuclear system. Thus, DCX proceeds via the conventional mechanism as depicted in Fig.8 where, taking Fig.8 (a) as an example, a π^+ scatters with a neutron to give rise to a $\pi^0 p$ through Δ^+ excitation and the produced π^0 then interacts with the second neutron to give rise to a $\pi^- p$ through Δ^0 excitation. This two - step mechanism is the standard approach used in all literatures.

In the HQH model, the relevant T- matrix of DCX reaction $A(\pi^+,\pi^-)B$ can be written as

$$T(q) = P_{6q} < \psi_{6q} \mid \hat{T}_{6q} \mid \psi_{6q} > +(1 - P_{6q}) < \psi_{pp} \mid \hat{T}_{conv.} \mid \psi_{nn} > \tag{46}$$

Where P_{6q} is given by Eq.(42). The first term in Eq.(46) is the contribution from six- quark cluster mechanism in the interior quark region. The second term represents the hadronic contribution from conventional mechanisms in the exterior hadronic region. We define the scattering amplitude, $F(q)$, in such a way that

$$\frac{d\sigma}{d\Omega} = \mid F(q) \mid^2 \tag{47}$$

with

$$F(q) = -\frac{1}{4\pi} T(q) \tag{48}$$

where the T- matrix elements are given by Eq.(46).

The pion - quark interaction is given by the axial vector interaction: The pion - nucleon interaction is calculated from cloudy bag model[28], i.e.

$$V^{\beta\alpha}_{\vec{K},i} = \frac{1}{2f_\pi} \frac{1}{(2\omega)^{\frac{1}{2}}} \int d^3\vec{x}\ e^{i\vec{K}\vec{x}} \delta(x - R_6) < \beta \mid \bar{q}(\vec{x})\tau_i\gamma_5 q(\vec{x}) \mid \alpha > \tag{49}$$

where α, β are quark wave functions of the system under consideration. $q(x)$ is the quark field and f_π the pion decay constant. Then, the formulae of the T- matrix for quark sector in the HQH model can be written

$$\begin{aligned} T_{6q}(\vec{k},\vec{k}') \;=\; & -(\frac{3}{5})^2(\frac{f_{\pi NN}}{m_\pi})^2 \frac{1}{2\omega_{\vec{k}}} u(kR_6)u(k'R_6) \\ & \int e^{i(\vec{k}-\vec{k}')\cdot\vec{R}}\ P_{6q}(\vec{R})\ d^3\vec{R} \cdot \sum_m < f \mid \sum_{a=1}^{6} \vec{\sigma}_a \cdot \vec{k}'\tau_+(a) \mid m > \\ & \frac{2E_m}{\omega_k^2 - E_m^2} < m \mid \sum_{b=1}^{6} \vec{\sigma}_b \cdot \vec{k}\ \tau_+(b) \mid i > \end{aligned} \tag{50}$$

$u(kR) = \frac{3j_1(kR)}{kR}$ is form factor. R_6 the radius of six - quark bag. $\vec{k}$ and $\vec{k}'$ are the initial and final pion momentum. $\mid i >$, $\mid m >$ and $\mid f >$ are respectively the initial, intermediate and

final states of six - quark clusters. All states are formed by placing six quarks in the lowest energy single quark orbits (n=1, k= - 1). For a bag composed of two neutrons, the initial state is

$$| i > = | 6q\ ,\quad S = 0\ ,\quad T = 1\ ,\quad T_z = -1 >, \tag{51}$$

and for a bag made up of two protons, the final state is

$$| f > = | 6q\ ,\quad S = 0\ ,\quad T = 1\ ,\quad T_z = +1 > . \tag{52}$$

The intermediate states $| m >$ are those connected to $| i >$ and $| f >$ by axial vector pion-quark interaction. These states have S=1, T=0 and S=1, T=2 with eigenvalues of (290+i140) MeV and (500 + i280) MeV[29], respectively.

The matrix elements of the axial vector coupling operator are determined by employing tabulated coefficients of fractional parentage. The essential reduced matrix elements are

$$< S = 1,\ T = 2,\ \| \sum_{a=1}^{6} \sigma_a \cdot \tau_a \| S = 0,\ T = 1 >= 8\sqrt{2}, \tag{53}$$

and

$$< S = 1,\ T = 0,\ \| \sum_{a=1}^{6} \sigma_a \cdot \tau_a \| S = 0,\ T = 1 >= -10. \tag{54}$$

Using the above discussion the T-matrix elements in Eq.(50) can be easily calculated.

The T-matrix elements for the conventional mechanism depicted in Fig.8 have been thoroughly studied in Ref.(30). In order to avoid making the paper of too length we do not give the detailed calculations here. The wave function for two relavent nucleons in ^{18}O is given[31] by

$$\psi_{NN} = 0.948 \mid (1d_{\frac{5}{2}})^2,\ J = 0 > +0.318 \mid (1s_{\frac{1}{2}})^2,\ J = 0 > \tag{55}$$

from which we can easily obtain the probability of six- quark cluster. The calculated probabilities are tabulated in table 4.

Table 4. Dependence of the probability of six- quark cluster on r_0, with nuclear wave function given by Eq.(55).

$r_0(fm)$	0.8	0.9	1.0	1.1	1.2	1.3	1.4
$P_{6q}(\%)$	2.34	3.22	4.25	5.42	6.71	8.10	9.58

The coupling constants used in our present calculations of the conventional mechanisms shown in Fig.8 are

$$\frac{f^2}{4\pi} = 0.081, \qquad \frac{f^{*2}}{4\pi} = 0.36, \qquad f_\Delta = \frac{4}{5} f. \tag{56}$$

for πNN, $\pi N\Delta$ and $\pi\Delta\Delta$ coupling vertices, respectively.

So far, we have only considered the calculations of DCX amplitude from a pair of nucleons. This is the minimum step necessary for the reaction to take place. Of course, in real nuclei nothing prevents the pion from colliding any number of times with other nucleons in the target nucleus. Indeed, such additional collisions give rise to a strong distortion of the pion wave. We follow for this purpose the distortion technique based on the Glauber approximation[31]. In the Glauber multiple scattering theory the amplitude of DCX reaction with the distortion effect included can be written

$$F(q) = \frac{iK}{2\pi} \int d^2\vec{b}\ \ e^{i\vec{q}\vec{b}}\ \ \Gamma_{DCX}(\vec{b})\ \ \Gamma_{DIS}(\vec{b}) \tag{57}$$

with

$$\begin{aligned} \Gamma_{DCX}(\vec{b}) &= \frac{1}{2\pi iK} \int d^2\vec{q} e^{-i\vec{q}\vec{b}} F_{DCX}^{undis}(\vec{q}) \\ &= \frac{1}{2\pi iK} \int d^2\vec{q}\ e^{-i\vec{q}\vec{b}} (-\frac{1}{4\pi} T(\vec{q})) \end{aligned} \tag{58}$$

where $T(\vec{q})$ is given by Eq.(46) ($F_{DCX}^{undis}(\vec{q}) = -\frac{1}{4\pi}T(\vec{q})$), and

$$\Gamma_{DIS}(\vec{b}) = < \psi_i \mid \prod_{l \neq i,j} [1 - \Gamma_l^{(s)}(\vec{b} - \vec{s}_l)] \mid \psi_i > . \tag{59}$$

$\Gamma_l^{(s)}(\vec{b} - \vec{s}_l)$ is isoscalar part of profile function, $\Gamma_l(\vec{b}) = \Gamma_l^{(s)}(\vec{b}) + \Gamma_l^{(v)}(\vec{b})\vec{T}_\pi \cdot \vec{\tau}_l$, and ψ_i are the nuclear wave functions of nuclear core (^{16}O). If we take a spin-isospin average parameterized pion-nucleon elementary amplitude

$$f_{\pi N} = \frac{ik\sigma}{4\pi}(1 - i\rho)e^{-\beta^2 q^2/2} \tag{60}$$

as input in Eq.(59). Then, the $\Gamma_{DIS}(b)$ can be explicitly written as

$$\begin{aligned} \Gamma_{DIS}(b) &= [1 - \frac{\sigma(1-i\rho)}{4\pi} \frac{2\alpha^2}{1+2\alpha^2\beta^2} e^{-\alpha^2 b^2/(1+2\alpha^2\beta^2}]^4 \\ & [1 - \frac{\sigma(1-i\rho)}{2\pi}(\frac{\alpha^2}{1+2\alpha^2\beta^2} - \frac{2\alpha^2}{3(1+2\alpha^2\beta^2)^2} + \frac{2\alpha^2 b^2}{3(1+2\alpha^2\beta^2)^3}) \\ & exp(\frac{-\alpha^2 b^2}{(1+2\alpha^2\beta^2)})]^{12} \end{aligned} \tag{61}$$

for s, p shell nuclei. The parameters σ, ρ, β are energy dependence, and given by experiments. This procedure has long been recognized as a good approximation[32].

A calculation in this HQH model is performed for $^{18}O(\pi^+,\pi^-)^{18}Ne_{g.s.}$ at the energy of 164 MeV. The results are shown in Figs.(9-10).

As is seen from the Fig.9, the conventional mechanism in the exterior hadronic region as shown diagrammatically in Fig.8 does not produce an agreement in both magnitude and the minimum location of the experimental angular distribution. But, the six quark cluster mechanism in the interior quark region as shown graphically in Fig.7 produces a quite good improvement over the conventional calculations. In particular, the minimum location, and shape of the experimental differential cross section seem to be reproduced successfully by the six quark cluster contributions . This result clearly indicates that quark degrees of freedom play an essential role in this peculiar case of DCX reaction.

Fig.10 evidently shows that unlike the amplitude given by the conventional mechanisms which changes its phase at 30^0, the six quark cluster amplitude changes its phase at 21^0. This is a very important feature of our HQH model and leads to a quite good theoretical description of data.

However, the magnitude of the cross section predicted by our HQH model is much larger than data in forward angles. Some further improvements are really needed. We speculate this discrepancy may attribute to contributions from other six-quark cluster mechanisms and from absorption of pions in nucleus, which are not considered in our present calculations.

It is also worthwhile to mention that M. Johnson and his collaborators[33] used ρ meson exchange for short range part of the main diagrams as shown in Fig.8. They found a bad phase compared with experiment. However, without ρ meson, the magnitude of their amplitude was wrong. Thus, Their finding may also be thought of as being a support to our conclusion here that the six-quark cluster contribution is responsible for 164 MeV DCX reaction to take place.

6 Concluding remarks

Based on the point of view of quark structure of hadron we study quark degrees of freedom in NN interaction, spectroscopy of baryon and its static electromagnetic properties, multiquark cluster effect in nuclei and six-quark mechanism of DCX reaction at Δ resonance

region. Our principal findings are as follows:

(1). It has been known from extentive study that quark model gives a natural description of NN interaction at short range. In particular, we see that the one- gluon exchange, which is an essential feature of the quark cluster model, represents an important part of the interaction. For example, the one-gluon exchange together with the quark structure of the baryons yields the short range repulsion both in the NN and YN interaction. However, the quark model description fails to reproduce the intermediate range attraction indispensable for the binding of nucleons in nuclei. The QCD is not applicable at long range where quraks and gluons interact strongly. The perpurbative calculations, i.e., the expansion of physical quantities in terms of a power series in running coupling constant α_s, are no longer valid and NN interaction is quantitatively, successfully described in terms of hadronic degrees of freedom. Thus, we suggest a hybrid model to describe NN interaction. In the hybrid model, quark exchange is assumed to be responsible for short range part and meson exchange for long -and medium - range part of the interaction. The calculations of different phase shifts and other physical quantities in the hybrid model are under way. However, our preliminary results show that the model seems promising.

(2). Under the approximation of Eq.(8), Friedberg and T. D. Lee's non-topological soliton bag model leads naturally to our Woods- Saxon-like confining potential model of quarks. Our model produces a reasonable description of static properties, and electromagnetic form factors of proton. It also agrees with theoretical prejudices based on MIT model. Based on the present form of our model, an attractive quark confining potential model would be developed in terms of inclusion of pion cloud surrounding bare quark core as well recoil correction and mass- of-center motion in defining the wave function. We believe that the soliton bag model can be regarded as satisfactory approximation schemes " bridging" conventional hadron physics and non-perturbative QCD.

(3). Our HQH model gives a good, natural explanation of the observed central "hole" of ^3He charge density. This may be thought of as being an evident signal for a possible existence of multiquark clusters in nuclei since, according to our best knowledge, no other theories could solve this long - standing puzzle problem so far.

(4). Quark degrees of freedom in DCX reaction at 164 MeV are likely responsible for the first minimum location of experimental angular distribution. Our six - quark cluster mechanism produces a favorable agreement with the data. Unlike the amplitude given by conventional mechanism which changes its phase, at least, at 30^0, the amplitude of the quark

part in our HQH model changes its phase at 21^0. This is a very important point of our HQH model and leads to a quite good theoretical description of data.

In summary, the present study shows that the quark degrees of freedom may be so important in modern nuclear physics that it must be considered in any assessment of short range nuclear phenomenon. Along this line, a great deal of work is in abundant demand.

However, it should be noted that there are still some problems with our models presented in this paper. For example, the HQH model is in its infancy. There are many places which should be improved in our present HQH calculations. Therefore, it is difficult to say that our principal finding in this paper is a great evidence for the presence of quark degrees of freedom in nuclei. For this purpose more efforts should be donated.

a) Institute of High Energy Physics, Academia Sinica. P. O. Box 918(4) Beijing 100039, China
b) Institute of Theoretical Physics, Academia Sinica. P. O. Box 8730 Beijing 100080, China
c) China Institute of Atomic Energy. P. O. Box 275(18) Beijing 102413, China

References

[1] F. E. Close, An introduction to quarks and partons, Academic press (New York, 1979)

[2] See e.g. K. Holinde, Phys. Rep. 68 No.3 (1981)

[3] M. Lacombe et al., Phys. Rev. D12,1495(1975); C21,861 (1980);C23,2405 (1981)

[4] R. B. Wiringa, R. A. Smith and T. A. Ainsworth, Phys. Rev. C29, 1207 (1984)

[5] R. V. Reid, Ann. Phys. (N. Y.), 50, 411 (1969)

[6] R. de Tourreil, B. Rouben and D. W. L. Sprung, Nucl. Phys. A242,445 (1975)

[7] R. Machleidt, K. Holinde, and Ch. Elster, Phys. Rep. 149,1 (1987)

[8] R. A. Bradenburg et al., Phys. Rev. C37, 1245 (1988)

[9] D. Serot and J. D. Walecka, Adv. Nucl. Phys. 16, 1 (1986)

[10] P. A. M. Guichon, Phys. Lett. B200, 235 (1988)

[11] A. Chodos, R. L. Jaffe, C. B. Thorn and V. Weisskopf, Phys. Rev. D9, 3471 (1974); A. Chodos, R. L. Jaffe, K. Johnson and C. B. Thorn, Phys. Rev. D10, 2599 (1974)

[12] N. Isgur and G. Karl, Phys. Rev. D19, 2653 (1979); V. Berrad, R. Brockman, M. Schaden, W. Weise and E. Warner, Nucl. Phys. A421, 349 (1984)

[13] R. Friedberg and T. D. Lee, Phys. Rev. D15, 1694 (1977); D14, 1096 (1977); D18,2623 (1978); R. Goldflam and L. Wilets, Phys. Rev. D25(1982)1951

[14] R. Tegen, R. Brockman and W. Weise, Z. Phys. - Atomic and Nuclei, 307, 339 (1982)

[15] G. Hohler et al., Nucl. Phys. B114, 505 (1976);G. G. Simon et al., Z. Naturforsch 35a (1980)1

[16] G. Iachelo, A. Jackson, A. Lande, Phys. Lett. B43, 191 (1973)

[17] S. Brodsky and G. Lepage, Phys. rev. D22, 2157 (1980)

[18] L. S. Kisslinger and Pauchy Hwang et al., Private communication, 1992

[19] G. Hohler et al., Nucl. Phys. B114, 505 (1975)

[20] Wei-hsing Ma and L. S. Kisslinger, Nucl. Phys. A531, 493 (1991)

[21] M. T. Hoftel and W. M. Kloot, Phys. Rev. C15, 404 (1977); W. M. Kloot and J. A. Tjon, Phys. Lett. B61, 356 (1976); C. Hajduk et al., Nucl. Phys. A352, 413 (1981); E. Hadjimichoel et al., Phys. Rev. Lett. 48. 583 (1982)

[22] B. Frois, elecron scattering and few - nucleon systems. Prog. in particle and nuclear physics. Vol.24 , P-1, Edited by A. Faessler, 1990.

[23] H. Hajduk, P. U. Sauer and W. Strueve, Nucl. Phys. A405, 581 (1983)

[24] L. S. Kisslinger, Wei-hsing Ma and P. Hoodbhoy, Nucl. Phys. A459, 645 (1986); Wei-hsing Ma and L. S. Kisslinger, Nucl. Phys. A531. 493 (1991)

[25] J. L. Friar et al., Phys. Rev. C24, 665 (1981)

[26] M. Beyer et al., Phys. Lett. B122, 1 (1983)

[27] Wei- hsing Ma, Meson Exchange Current Mechanism of DCX reaction, Nucl. Phys. A to be published

[28] A. W. Thomas, Preprint Ref.TH. 3368-CERN TRI-pp-82- 29, 1982; A. Miller, Interactional Review of nucl. Phys.. Vol. 1, 1984, Quarks and Nuclei, Edited by W. Weise, p-189

[29] P. W. Mulders and A. W. Thomas, J. Phys. G, Nucl. Phys. 9, 1159 (1983)

[30] Yu Zi-qian, Cai Chong-hai, Ma Wei-hsing, Phys. Rev. C38, 272 (1988); Wei-hsing Ma et al., Nucl. Phys. A481, 793 (1988); E. Oset, D. Strottman et al., Preprint LA-UR-85-175, 1985, Los Alamos. USA

[31] R. J. Glauber, In Boulder Lectures in theoretical Physics, L. G. Dunham and W. E. Brittin, eds. (interscience, New York), pp. 315 (1959)

[32] E. Oset, D. D. Strottman, M. J. Vicente-Vacas and Wei-hsing Ma, Nucl. Phys. A408, 461 (1983); Wei-hsing Ma et al., Nucl. Phys. A481, 793 (1988)

[33] M. B. Johnson et al., Phys. Rev. Lett. 52, 593(1984)

Figure Captions

Fig.1. Scheme of energy levels for a simple quark confinement in three different potentials. I: the scalar vector harmonic potential[14], $U(r) = c(1. + \gamma_0)r^2$; II: infinite square potential[15], and III: our Woods-Saxon-like confining potential model with $V_0 = 7.425fm^{-1}$, $m_\sigma^{-1} = 0.075$ fm and R = 1.1 fm.

Fig.2. Numerical results of Dirac wave functions of the $1s_{\frac{1}{2}}$ state given by two different confining potentials. $g(r)$ and $f(r)$ are the upper and lower components of quark eigenfunctions, respectively. The $g_1(r)$ and $f_1(r)$ (the solid curves) are produced by our confining potential, Eq.(10). The $g_2(r)$ and $f_2(r)$ (the dashed curves) stand for the predictions of Regensburg potential[14], $U(r) = cr^2$.

Fig.3. The upper and lower components of $1s_{\frac{1}{2}}$ state wave functions. The solid lines denote the results of our Woods-Saxon-like potential model, the dotted lines represent the results of infinite square potential (MIT bag model), and the dashed curves are the results of the scalar vector harmonic model[14].

Fig.4. Electromagnmetic form factors of proton in our Woods-Saxon-like confining potential model. a) charge form factor of proton $G_E^p(q^2)$; b) magnetic form factor of proton $G_M^p(q^2)$. The experimental data is taken from Ref.(19).

Fig.5. Two- body meson exchange current: the pion pair current.

Fig.6. ^3He charge density. the dashed curve stands for theoretical prediction by traditional nuclear theory[25]. The solid curve is the prediction of our HQH model. The data comes from Ref.(26).

Fig.7. Six-quark mechanisms of DCX reaction. a) direct term; b) cross term.

Fig.8. Conventional mechanisms of DCX reaction at the Δ resonance region. a) the sequential mechanism; b) the successive mechanism.

Fig.9. Angular distribution of 164 MeV DCX reaction in our HQH model. The curves 1, 2 and 3 denote respectively the contributions from quark part, conventional part in the HQH model and the full HQH model prediction.

Fig.10. Amplitude of 164 MeV DCX reaction in the HQH model versus scattering angles, with $r_0 = 1.0fm$ and without inclusion of width of six quark states.

K^+ NUCLEON TWO-BODY POTENTIAL AND K^+-NUCLEUS OPTICAL POTENTIAL[1]

P.Ning[1,2,3], , E.Zhao[1,3] and P.Li[2]

1.CCAST(World Laboratory) P.O.Box 8730, Beijing 100080
2.Department of Physics, Nankai University, Tianjin 300071, China
3.Institute of theoretical Physics, Academia Sinica, Beijing 100080

PACS. 25·80 -Meson-and hyperon-induced reactions and scattering.

Abstract

The K^+-Nucleon two-body potential is derived in the framework of the constituent quark model and it may provide reasonable explanation for the large K^+-nucleon scattering phase shift of P-wave $I = 0, J = \frac{1}{2}$ channel. On the bases of the derived K^+ -nucleon interaction, the real part of the K^+ -nucleus optical potential is constructed. Reasonable good agreement between theoretical cross section and experimental data may be reached by requiring a weak imgaginary part of the optical potential, as expected for the K^+ -nucleus scattering.

[1]Work supported by National Natural Science Foundation of China and State Education Committee of China

It is well known that the K^+ -nucleus(K^+A) interaction is rather weak on the hadronic scale, corresponding to a mean free path in nuclear matter of roughly 6fm, a typical nuclear size. Interest in K^+A scattering arises from a desire to learn more about nuclear interior structure, more about the K^+ -nucleon (K^+N) and K^+A interaction [1-5]. A Widely accepted approach of constructing the K^+A Optical potential is the "$t\rho$" approximation with nuclear density ρ fixed from electron scatering and the K^+N two-body t-matrix provided by the measured K^+N phase shifts. Although the agreement of the theoretical results with experimental data is fairly reasonable, there are non-negligible differences between the calculated values of cross sections prediced by using different input K^+N phase shifts, resulting in uncertainties in the theory. Furthermore, the K^+N physics is not fundamental.

A more fundamental way to obtain the K^+N two-body potential, by analogy with the nucleon-nucleon case, is to use the so-called constituent quark model (CQM) based on the quark-(anti) quark interaction. A pioneering study of the K^+N interaction at the quark level has been performed by Bender et al.[6,7],but it contains only central part of the K^+N potential and is not able to reproduce the measured K^+N P-awve phase shifts. It was found[6] that spin-orbit (SO) coupling in QCD residual interaction can not be neglected, whereas the especially large scale for the $I = 0, J = \frac{1}{2}$ channel was not reproduced by the K^+N SO potential derived from ref.[8].

The purpose of the present work is twofold: (1) We try to derive a practically useful K^+N two-body potential from quark-(anti) quark interaction based on the existing works. We improve the model of ref.[7] by adding the SO part of one-gluon exchange (OGE) to the effective hamiltonian in CQM for K^+N system and using a new form of the SO part of quark-quark interaction[9]. We give only a brief describtion of the above K^+N interaction model in this letter, complete calculations can be found in later publication[10]. (2) We try to construct the real part of the K^+A optical potential from the derived K^+N two-body potential and make a crude estimate by comparing with experimental cross sections to find the required imaginary part of the K^+A optical potential.

The effective Hamiltonian for the K^+N system is

$$\mathcal{H} = \sum_{i=1}^{4} \frac{\vec{P_i}^2}{2m_q} + \frac{\vec{P_s}^2}{2m_s} + \sum_{i<j}(V_{ij}^{OGE} + V_{ij}^{Conf}) \tag{1}$$

where P_i is the momentum of the ith light quark (numbered from 1 to 4), P_s is the momentum of the strange antiquark (with the number 5). m_q the masses of the light quarks and m_s the strange-quark mass. The potential acting between quarks consists of the one-gluon exchange potential V_{ij}^{OGE} and the confinement potential V_{ij}^{Conf}:

$$V_{ij}^{OGE} = \frac{1}{4}\alpha_s \vec{\lambda_i}\cdot\vec{\lambda_j}\{[\frac{1}{r_{ij}} - \frac{2\pi}{3}\frac{1}{r_{ij}} - \frac{2\pi}{3}\frac{1}{m_i m_j}\vec{\sigma_i}\cdot\vec{\sigma_j}\delta(\vec{r_{ij}}) - \frac{\pi}{2}(\frac{1}{m_i^2} + \frac{1}{m_j^2})\delta(\vec{r_{ij}})]$$
$$-\frac{1}{4}f(r_{ij})[(\vec{r_{ij}}\times\vec{P_{ij}})\cdot(\vec{\sigma_i}+\vec{\sigma_j}) - \frac{1}{3}\vec{r_{ij}}\times(\vec{P_i}+\vec{P_j}) + (\vec{\sigma_i}-\vec{\sigma_j})]\} \tag{2}$$

$$V_{ij}^{Conf} = \begin{cases} -\frac{1}{2}D\vec{\lambda_i}\cdot\vec{\lambda_j}r_{ij}^2 & (for\ a\ pair\ of\ quarks) \\ -\frac{1}{2}D'(-\vec{\lambda_i}\cdot(\vec{\lambda_j})^T)r_{ij}^2 & (for\ a\ quark\ -antiquark\ pair) \end{cases} \tag{3}$$

with

$$\vec{r_{ij}} = \vec{r_i} - \vec{r_j} \tag{4}$$

$$\vec{P_{ij}} = \frac{m_j\vec{P_i} - m_i\vec{P_j}}{m_i + m_j} \tag{5}$$

$$f(r_{ij}) = A_{ij}e^{-\mu_{ij}r_{ij}^2}, \tag{6}$$

α_s is the QCD fine structure constant. λ_i is the set of Gell-Mann matrices acting on quark i. The form of $f(r_{ij})$ is from ref.[9]. The gaussian form is not only easier to use, but it also simulates to some extent the effect of gluon confinement in the nucleon. The strength parameter A_{ij} is defined as

$$A_{ij} = \frac{3}{16}(1+\mu_{ij/2b})^{5/2}\Delta M. \tag{7}$$

For the interaction between light quarks the range parameter $\mu_{ij} = 0.726fm^{-2}, b = 0.36fm^{-2}, \Delta M = 92MeV$. For the interaction between light quark and strange antiquark, according to ref.[10], a factor m_q/m_s should be added in eq.(7). The other parameters are

$$m_q = 0.25GeV \quad m_s = 0.45GeV$$
$$\alpha_s = 0.6 \qquad D \approx D' = 0.33GeV\cdot fm^{-2}$$

The nucleon and kaon are two color-singlet quark clusters. The total wave function depends on the five quark coordinates $x_1, \cdots\cdots, x_s$ and x_s denotes the coordinate of the strange antiquark. In the generator coordinate method (GCM) the trial wave function for the K^+N system has the form

$$\psi = \mathcal{A} \int c(\vec{R}) \psi_{\vec{R}} d^3\vec{R} \tag{8}$$

$$\psi_{\vec{R}} = \phi_{\vec{R}}(\vec{x_1}, \vec{x_2}, \vec{x_3}, \vec{x_4}, \vec{x_5}) x^{SIC} \tag{9}$$

Here χ^{SIC} is the combined spin-isospin-color wave function. The orbital wave function is assumed to be

$$\begin{aligned}\phi_{\vec{R}} = & \left\{ \Pi_{i=1}^{3} (\frac{2\Omega}{\pi})^{3/4} exp[-\Omega(\vec{x_1} + \frac{1+k}{4+k}\vec{R})^2] \right\} (\frac{2\Omega}{\pi})^{3/4} exp[-\Omega(\vec{x_4} - \frac{3}{4+k}\vec{R})^2] \\ & \cdot (\frac{2\Omega K}{\pi})^{3/4} exp[-\Omega k(\vec{x_5} - \frac{3}{4+k}\vec{R})^2]\end{aligned} \tag{10}$$

with $K = m_q/m_s$ and $\Omega = 1.94 fm^{-2}$. By use of the standart moment-expansion technique within the GCM framework we can evaluate the interaction kernel together with the norm kernel of the non-local Hill-Wheeler equation. From these kernels we obtain the central and SO part of the K^+N two-body potential for each isospin channel:

$$V_c^{I=0}(r) = 0.0406 exp(-4.437r^2) + 0.1001 exp(-2.426r^2) - 0.0500 exp(-1.941r^2) \tag{11}$$

$$V_c^{I=1}(r)$$

$$= \frac{0.1839 exp(-4.437r^2) + 0.2001 exp(-2.565r^2) - 0.2002 exp(-2.426r^2) + 0.4508 exp(-1.}{3 - exp(-1.941r^2)} \tag{12}$$

$$V_{SO}^{I=0}(r) = 0.2810 exp(-2.469r^2) + 0.4320 exp(-1.941r^2) \tag{13}$$

$$V_{SO}^{I=1}(r) = \frac{-0.0936 exp(-2.469r^2) - 0.2882 exp(-1.941r^2)}{1 - (0.1310 + 0.6440r^2) exp(-1.941r^2)} \tag{14}$$

The potentia's obtained above are plotted in Fig.1. In order to compare the derived potentials with the experimental data, we calculate the K^+N scattering phase shifts for S-and P-wave. The results show that the potentials may provide reasonable explanation for the K^+N data, particularly for the large phase shift of P-wave $I = 0, J = \frac{1}{2}$ channel[10]. Thus the derived K^+N two-body potential seems to be receivable. The results differ from ref. [8] mainly due to the new form of the SO part of quark-quark interaction.

In order to exam suitability of the resulting K^+N two-body potential, the K^+A optical potential which describes the elastic scattering of K^+ from nuclei is constructed by folding nuclear density ρ with this K^+N interaction. The folding potential has the form

$$V_{opt}(r) = \frac{1}{(2\pi)^3}\int \rho(\vec{q}) t_{ACM}(\vec{q}) exp(-i\vec{q}\cdot\vec{r}) d\vec{q} \tag{15}$$

where t_{ACM} is the K^+N interaction in the K^+-nucleus center of mass system and

$$t_{ACM} = [\frac{E_k(k_c)E_k(k'_c)E_N(k_c)E_N(k'_c)}{E_k(k_A)E_k(k'_A)E_N(k_A)E_N(k'_A)}]^{1/2} t_{2CM} \tag{16}$$

is the transformation from the K^+N center of mass system to that of the K^+ -nucleus. The real parts of the K^+N two-body t-matrix are taken to be the above derived K^+N interaction [see Eq.(11)-(14)], so the real parts of the K^+A optical potential, or equivalently, the imaginary parts of the K^+A optical potenital can be determined more precisely. Following the standard procedure of the folding model, the imaginary parts of the K^+A optical potential, or equivalently, the imaginary parts of the K^+N two-body t-matrix are built in a phenomenological way. Since the real parts appear as a combination of gaussians, the imaginary parts in each isospin channel I are parametrized in the gaussians form:

$$Imt^I_c(q) = \alpha^I_c exp(-\beta_c q^2) \tag{17a}$$

$$Imt^I_{SO}(q) = \alpha^I_{SO} exp(-\beta_{SO} q^2). \tag{17b}$$

The weights α'_c, α'_{so} and the ranges β_c,β_{so} are adjusted such taht the differential cross-section for $K^+ - {}^{12}C$ elastic scattering is fitted at $P_k = 800MeV/c$. We obtained

$$\alpha^{I=0}_c = -0.10GeV$$

$$\alpha^{I=1}_c = -0.05GeV$$

$$\alpha^I_{SO} = 0$$

$$\beta_c = \beta_{SO} = 4.0fm^2$$

The nuclear density $\rho(r)$ for ${}^{12}C$ is given by usual Woods-Saxon form with exactly the same parameters as in our previous papers[1,5].

In view of the importance of nucleon swelling in nucleus[11], we have accounted for this nuclear medium effect by multiplying the K^+N two-body interaction by the density dependent factor $\eta(\rho)$ of ref.[11]:

$$\eta(\rho) = [1 - \frac{\lambda\rho(r)}{2\rho_0}]^{-2} \tag{18}$$

with $\lambda = 0.2$ and $\rho_0 = \frac{1}{6} fm^{-3}$.

The $K^+ - {}^{12}C$ optical potential obtained from the above calculations is displayed on Fig.2. We can see a repulsive real part with the central value of 28.5MeV and a quite shallow imaginary part with the central value of -4.0MeV. After corrections of the relativistic kinematics, the $V_{opt}(r)$ is inserted into the ususl Klein-Gordon equation which is solved to obtain K^+ scattering wave functions and differential cross section at 800MeV/c. The results are shown in Fig.3 and 4. Fig.3 illustrates the variations caused by different values of the range parameter β_c of $\mathrm{Im}t_c^1(q)$ [see eq.(17)] and Fig.4 illustrates the variations caused by the weight parameter α_c. As can be seen, the agreement with the experimental data is quite reasonable and the differential cross section is not very sensitive to the parameters β_c and α_c^I.

From our results of the calculations for the K^+N two-body potential and K^+A optical potential, we have reason to believe that: 1) A practically useful K^+N two-body potential may be obtained from the constituent quark model and it may provide reasonable explanation for the large K^+N scattering phase shift of P-wave $I = 0, J = \frac{1}{2}$ channel. 2) The real part of the K^+A optical potential can be constructed from the derived K^+N two-body potential and reasonable good agreement between theoretical cross section and experimental data may be reached by requiring a weak imaginary part of the optical potential, as expected for the K^+A scattering processes. Indeed, the main features of the obtained K^+A optical potential coincide with the fact that K^+ meson is a weakly absorbed hadronic probe of nuclei,however, do not coinside with a recently published result[13], in which the K^+A optical potential has a quite shallow real part and a strong imaginary part, even both the real and imaginary parts are absorptive in the entire interaction range.

In this work we have concentrated on the $K^+ - {}^{12}C$ scattering. Since the existing data also include scattering from ${}^{40}Ca$, we have performed similar calculations for $K^+ - {}^{40}Ca$ scattering, and we draw again the same conclusion.

1 Halderson D., Ning P. and Philpott R.J., Nucl. Phys. A, 458(1986)605

2 Halderson D., Mo Y. and Ning P., Phys. Rev. Lett., 57(1986)1117.

3 Ning P., High Ener. Phys. Nucl. Phys. (China), 11(1987)708

4 Ning P. and Men D., Chin. J. Nucl. Phys., 11(1989)65.

5 Jiang S., Hu Z., Wu X. and Ning P., Europhys. Lett., 14(1991)217

6 Bender I. and Dosch H.G., Z. Phys. C, 13(1982)69.

7 Bender I., Dosch H.G., Pirner H.J. and Kruse H.G., Nucl. Phys. A,414(1984)359.

8 Mukhopadhyay D. and Pirner H.J., Nucl. Phys. A, 442(1985)605

9 Wang F. and Wong C. W., Nucl. Phys. A, 438(1985)620

10 Ning P., Zhao E. and Li P., in preparing.

11 Brown G. E., Dover C.D., Siegel P.B. and Weise W., Phys. Rev. Lett., 60(1988)2723.

12 Marlow D., Phys. Rev. C, 25(1982)2619.

13 Labarsouque J., Nucl. Phys. A, 506(1990)539

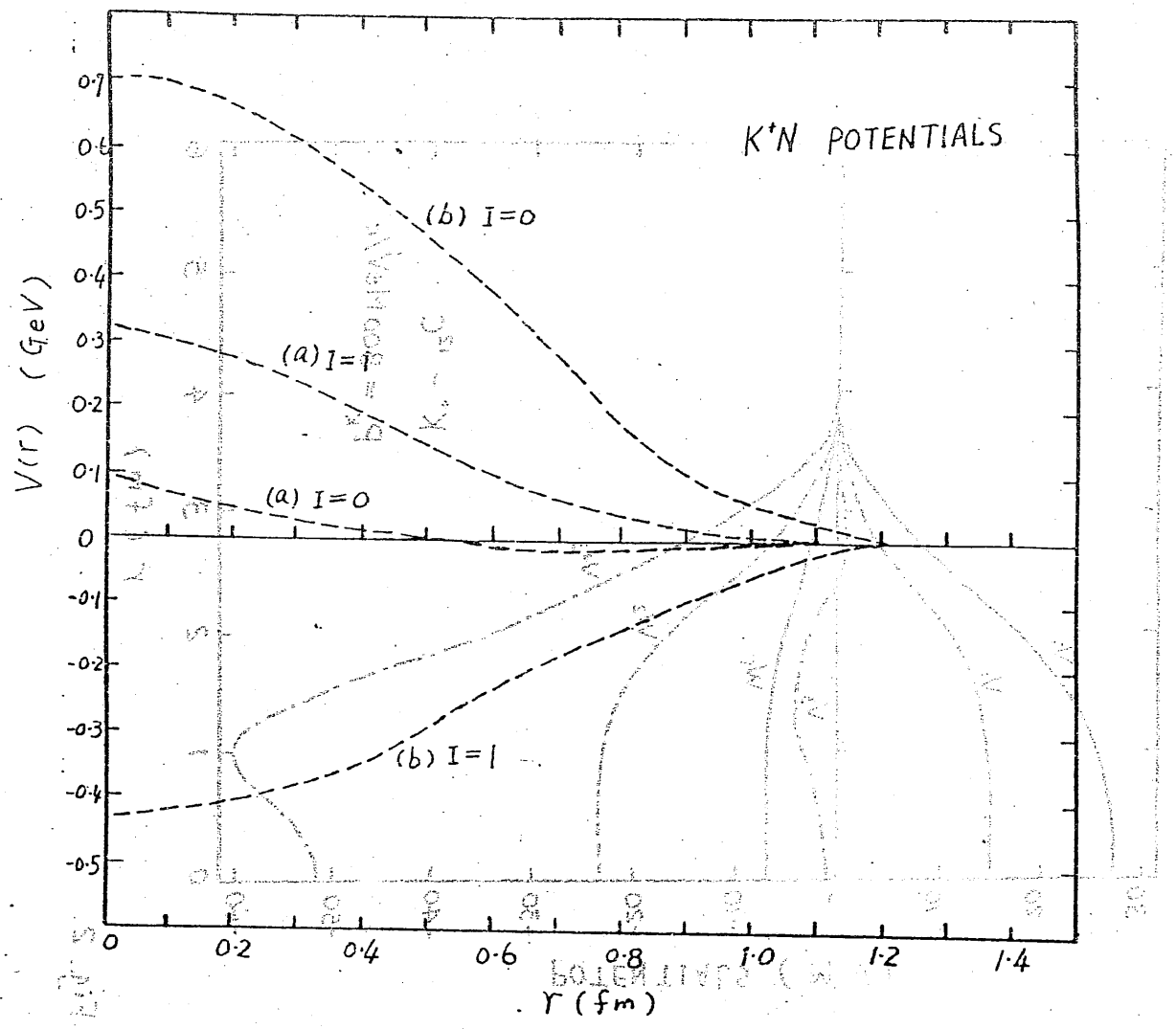
K⁺N POTENTIALS
(b) I=0
(a) I=1
(a) I=0
(b) I=1
V(r) (GeV)
r (fm)
0.7
0.6
0.5
0.4
0.3
0.2
0.1
0
-0.1
-0.2
-0.3
-0.4
-0.5
0
0.2
0.4
0.6
0.8
1.0
1.2
1.4

Fig. 1

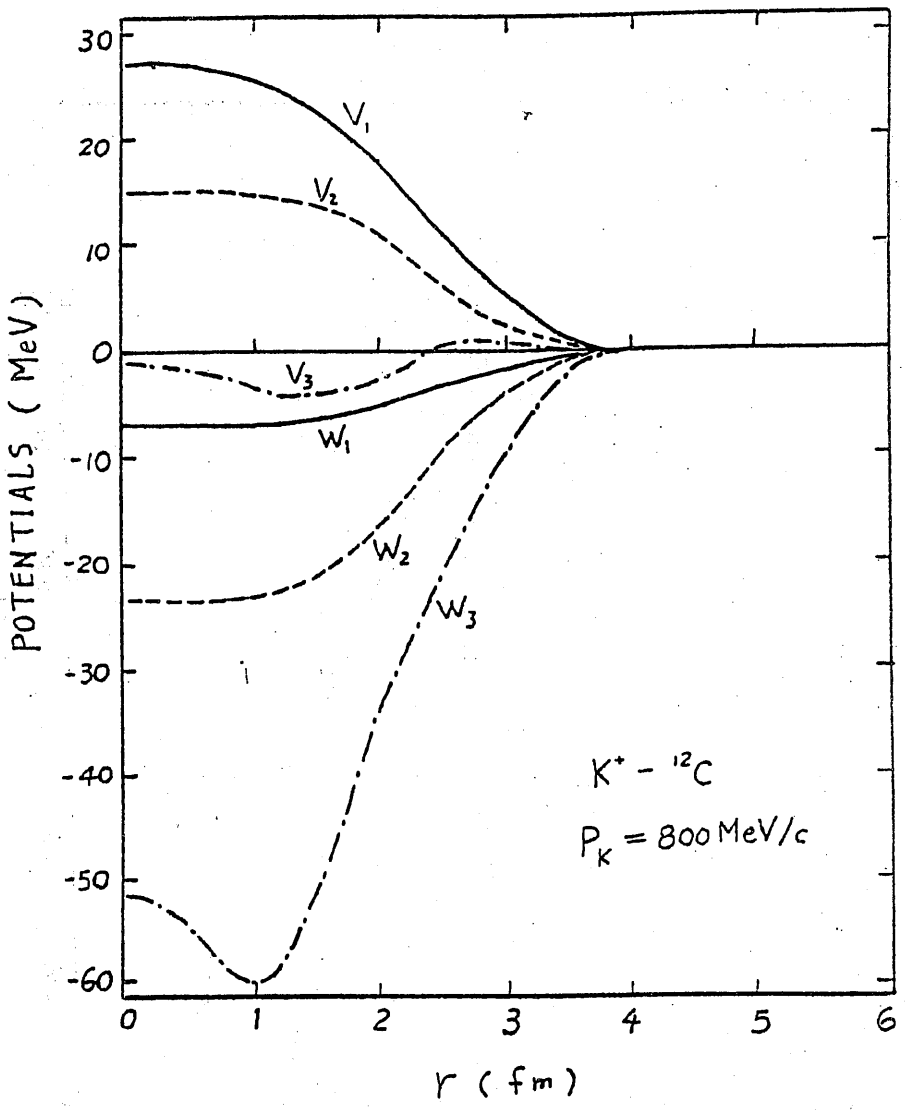
30
20
10
0
-10
-20
-30
-40
-50
-60
0
1
2
3
4
5
6
POTENTIALS (MeV)
r (fm)
V1
V2
V3
W1
W2
W3
K+ - 12C
PK = 800 MeV/c

Fig. 2.

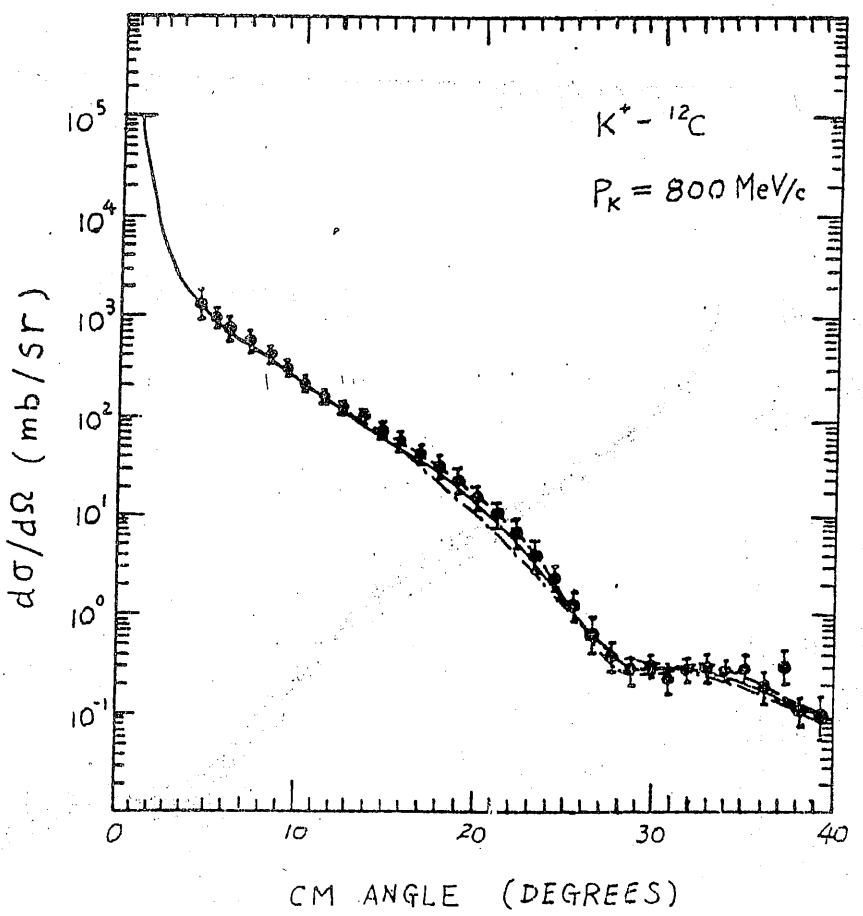
$K^+ - {}^{12}C$
$P_K = 800$ MeV/c
$d\sigma/d\Omega$ (mb/sr)
10^5
10^4
10^3
10^2
10^1
10^0
10^{-1}
0
10
20
30
40
CM ANGLE (DEGREES)

Fig. 3

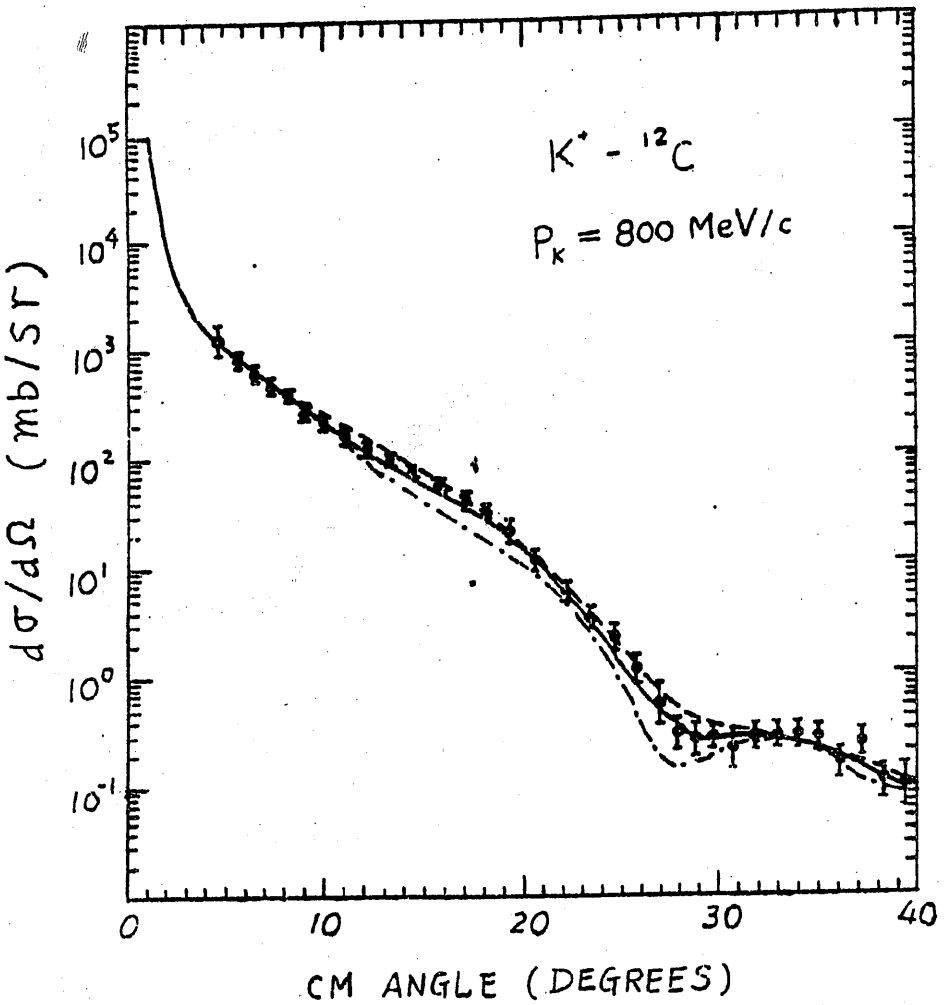
$K^+ - {}^{12}C$
$P_K = 800$ MeV/c
$d\sigma/d\Omega$ (mb/SR)
10^5
10^4
10^3
10^2
10^1
10^0
10^{-1}
0
10
20
30
40
CM ANGLE (DEGREES)

Fig. 4

Quark effect in nucleon-nucleon interaction

Shen Peng-nian and Dong Yubing
CCAST(World Laboratory) P. O. Box 8730, Beijing 100080, P. R. China
Institute of High Energy Physics, Academia Sinica, P. O. Box 918, Beijing 100039, P. R. China

As a basic quantity in nuclear physics, the nucleon-nucleon interaction is well established on the hadron- meson level. This potential is in general described by the meson exchange plus the phenomenological replusive core. It is natural to ask where is the origin of the repulsive core. Is it possible to explain the N-N interaction in the subnucleon degrees of freedom? Since the QCD theory was introduced, developing a quantitative understanding of the N-N interaction in an underlying QCD description has been put into the nuclear physics research program.

It is well known that there are two basic assumptions in the QCD theory, namely, the asymptotic free in the small distance (or large momentum transfer) and the phenomenological confinement in the large separation (or small momentum transfer).

Interaction between quarks is believed to be governed by the QCD theory. At very short distance, the perturbative QCD is applicable. As a result, quarks are considered as some simple particles which interact with each other at least via one-gluon exchange. In terms of this idea, Rujular, Georgi, and Glashow[1] proposed one-gluon exchange potential. Later, by employing that potential, Oka et al.[2] and Faessler[3] et al. calculated the N-N scattering and showed that the short-range repulsion between two nucleons can be obtained via the quark exchange together with the color magnetic interaction. This is a big step toward the understanding of the N-N interaction in the quark-gluon degrees of freedom.

Although the short-range N-N interaction is successfully explained in the subnucleonic degrees of freedom, the phenomenological σ-meson exchange and long-range π-meson exchange must be additionally employed to fit emperical N-N phase shifts. Moreover, in the quark-quark interaction, the phenomenological confinement term should be remained no matter what kind of type it is. Can these phenomenological interactions which have large effects in the medium and long distance be understood in the quark degrees of freedom?

We know that if the distance between quarks is not so short, the perturbative QCD may not be valid again. There should exist the nonperturbative effect of QCD. In 1979,

Shifman, Vainstein, and Zakharov[4] pointed out that when distance between quarks r_{q-q} becomes larger, $q-\bar{q}$ and gg can condensate into the vacuum. They introduced the nonzero $<0|m_q q\bar{q}|0>$ and $<0|\frac{\alpha_s}{\pi}GG|0>$ because of the complicated structure of the nonlinear QCD vacuum. It is obvious that these condensates can contribute to the medium-and long-range q-q interactions. Shen, Li and Guo [5] studied the non- perturbative effect of QCD on the gluon propagator, derived the full gluon-propagator by considering one $q\bar{q}$ or gg condensate and consequentely derived the modified q-q interaction which partially includes the nonperturbative effect of QCD. They also pointed out that the condensation mechanism can automatically give the confinement term r and deconfinement term $-r^3$. Bian and Huang[6] considered more condensates in the ladder approximation in the gluon propagator and obtained $(-1)^k r^{2k+1}$ terms. Referring the confinement potential in the form of (1-exp(-μr)), which obtained from the lattice gauge calculation, we believe that the confinement should behave like linear potential at the short distance and becomes weaker at the longer distance. This is so called the color screening effect. In order to study this effect, Yang, Deng, and Zhang[7] proposed a confinement potential with the shape of the error function.

In order to exam the nonperturbative effect of QCD, we study the hadronic spectrum and N-N interaction by using various types of confinement potentials. In table I, we tabulate the N and Δ spectra, and experimental data. From these results, we see that, although all confinement potential used have the color screening effects (or include the nonperturbative effects) in different ways, the obtained spectra can well fit the experimental data, and the $ar-br^3$ type and error function type potentials look better. This showes that the condensation mechanism may be a better way to take into account the nonperturbative effect of QCD, which can contribute to the medium-range interaction.

However, there is a defect in the $ar-br^3$ type confinement. If we use this type of confinement potential to calculate the N-N scattering, we will find the long-tailed color Van de Waals force. Of course, it is not a physical result, because we ignored the modification factor caused by the non-validity of the formulation in the small q region[5] and higher order condensations. To solve this problem, one of the easiest ways is adopting the error function type confinement potential. By using this potential, we calculate the phase shifts of the N-N interaction.

In this calculation, the trial wave function of the N-N system is taken as

$$\Psi = \Phi^{NN} + \Phi^{c'c',L=0} + \Phi^{c'c',L=2}, \tag{1}$$

where Φ^{NN} is the trial wave function of the N-N channel, which has the form of

$$\Phi^{NN} = A[\psi_A^N \psi_B^N \chi^{NN} Z], \tag{2}$$

$\Phi^{c'c',L=0}$ and $\Phi^{c'c',L=2}$ are distortion function in the compound region for L=0 and L=2, respectively, which take the form of

$$\Phi^{c'c',L=x} = \psi_A^{c'} \psi_B^{c'} \chi^{c'c',L=x} Z, (x = 0 or 2), \tag{3}$$

here $\chi^{c'c',L=x}$ is the resonance type function

$$\chi^{c'c',L=0} = \sum_i a_i^{L=0}\sqrt{4\pi}(\frac{2\lambda_i}{\pi})^{4/3}exp(-\lambda_i R^2), \tag{4}$$

and

$$\chi^{c'c',L=2} = \sum_i b_i^{L=2}\frac{4}{\sqrt{15}}(2\eta_i)^{2/3}(\frac{2\eta_i}{\pi})^{1/4}R^2exp(-\eta_i R^2)Y_{2n}(\hat{R}). \tag{5}$$

The hamiltonian is taken as that in Ref[8]. By using Kamimura variational method, the phase shifts can be obtained. They are plotted in Fig.1. From this figure, it is seen that:

(1) Due to the consideration of the nonperturbative effect of QCD, one can obtain a better agreement between the theoretical result and experimental data.

(2) The strength of the phenomenological σ-meson exchange potential is reduced about 10%. This means that by considering the nonperturbative effect of QCD, one can obtain a reasonable confinement, consequentily, a physical color Van de Waals force. This color Van de Waals force provides part of the medium-range attraction of the nuclear force.

Furthermore, we should point out that by using the $q-\bar{q}$ pair creation model, Yu, Zhang, and Shen obtained a effective one-meson exchange potential and a effective two-meson exchange potential between two nuclears[9]. The result showed that in the q-g level, the obtained one-meson exchange potential is very similar to the conventional one-meson exchange potential at the large distance, and the obtained two-meson exchange potential is somewhat weaker than the σ-meson potential.

Although we can successfully understand the short-range nuclear force and partially explain the medium- and longe-range N-N interactions in the q-g level, we should emphasize that:

(1) There exists the quark effect in the nuclear force.

(2) There should be other nonperturbative QCD effect such as the sea quark effect in the medium-range. In fact, Yu, Zhang, and Shen have shown[10] that the sea quark effect can provide a color independent term in the q-q interaction. As a result, this term would offer a medium-range attraction between two-nucleons. We should put more effects on the investigation of the medium- range nuclear force.

References

1. A. De. Rujula, H. Georgi, and Glashow, Phys. Rev. D12 (1975), 147.
2. M. Oka and K. Yazaki, Prog. Theor. Phys. 66 (1981), 556; 572.
3. A. Faessler, F. Ferhandes, G. Lübeck, and K. Shimizu, Nucl. Phys. A402 (1983), 555
4. M. Shifman, A. Vainstein, and V. Zakharov, Nucl. Phys. B147 (1979), 385.
5. P. N. Shen, X. Q. Li, and X. H. Guo, Commun. Theor. Phys. 16 (1991), 443; Phys. Rev. C45 (1992) 1894.
6. Private communication
7. Yang Hua, Deng Wei-zhen, and Zhang Zong-ye, High energy Phys. and Nucl. Phys. 16 (1992), 241.
8. Zhang zong-ye, Yu You-wen, Shen Peng-nian, Shen Xiao-yan, and Dong Yu-Bing, BIHEP-TH-92-28.
9. Yu You-wen, Zhang Zong-ye, and Shen Peng-nian, Nucl. Phys. A528 (1991), 513.
10. Yu You-wen, Zhange Zong-ye, and Shen Peng-nian, and Shen Xiao- yan, to be published on High Energy Phys. and Nucl. Phys. (1992).
11. Particle Data Group: Phys. Lett. B204 (1988), 1.

Figure Captions

Fig. 1 N-N s-wave phase shift.

Table I. The comparison of the theoretical spectra and experimental data[11] for baryons N and Δ in Gev.

J^p	Error function Conf.	Exp.
$N_{1+/2}$	0.936	0.938
	1.496	1.400÷1.480
	1.736	1.680÷1.740
	1.958	-----
	2.017	-----
	•	
$N_{3+/2}$	1.777	1.690÷1.800
	1.893	----
	1.947	----
	1.974	----
	2.026	----
$N_{5+/2}$	1.724	1.670÷1.690
	1.943	1.880÷2.175
	1.986	N(2.000)
$N_{7+/2}$	1.951	1.950÷2.050
$N_{1-/2}$	1.572	1.520÷1.560
	1.608	1.620÷1.680
	2.089	N(2.090)
$N_{3-/2}$	1.520	1.510÷1.530
	1.672	1.670÷1.730
	2.037	N(2.080)
$N_{5-/2}$	1.630	1.660÷1.690
	2.178	1.900÷2.230
$N_{7-/2}$	2.193	2.120÷2.230
$N_{9-/2}$	2.233	2.100÷2.270

Table I. Continued.

J^P	Error function Conf.	Exp.
$\Delta_{1+/2}$	1.907	1.850÷1.950
	1.923	—
$\Delta_{3+/2}$	1.206	1.230÷1.240
	1.774	1.500÷1.900
	1.856	1.860÷2.160
	1.978	—
$\Delta_{5+/2}$	1.933	1.890÷1.920
	1.975	$\Delta(2.000)$
$\Delta_{7+/2}$	1.924	1.910÷1.960
	2.387	$\Delta(2.390)$
$\Delta_{9+/2}$	2.341	$\Delta(2.300)$
$\Delta_{1-/2}$	1.652	1.600÷1.650
	1.989	1.850÷2.010
$\Delta_{3-/2}$	1.653	1.630÷1.740
	1.988	$\Delta(1.940)$
$\Delta_{5-/2}$	1.925	1.890÷1.960
	2.341	$\Delta(2.350)$
$\Delta_{7-/2}$	2.341	$\Delta(2.200)$
$\Delta_{9-/2}$	2.386	$\Delta(2.400)$

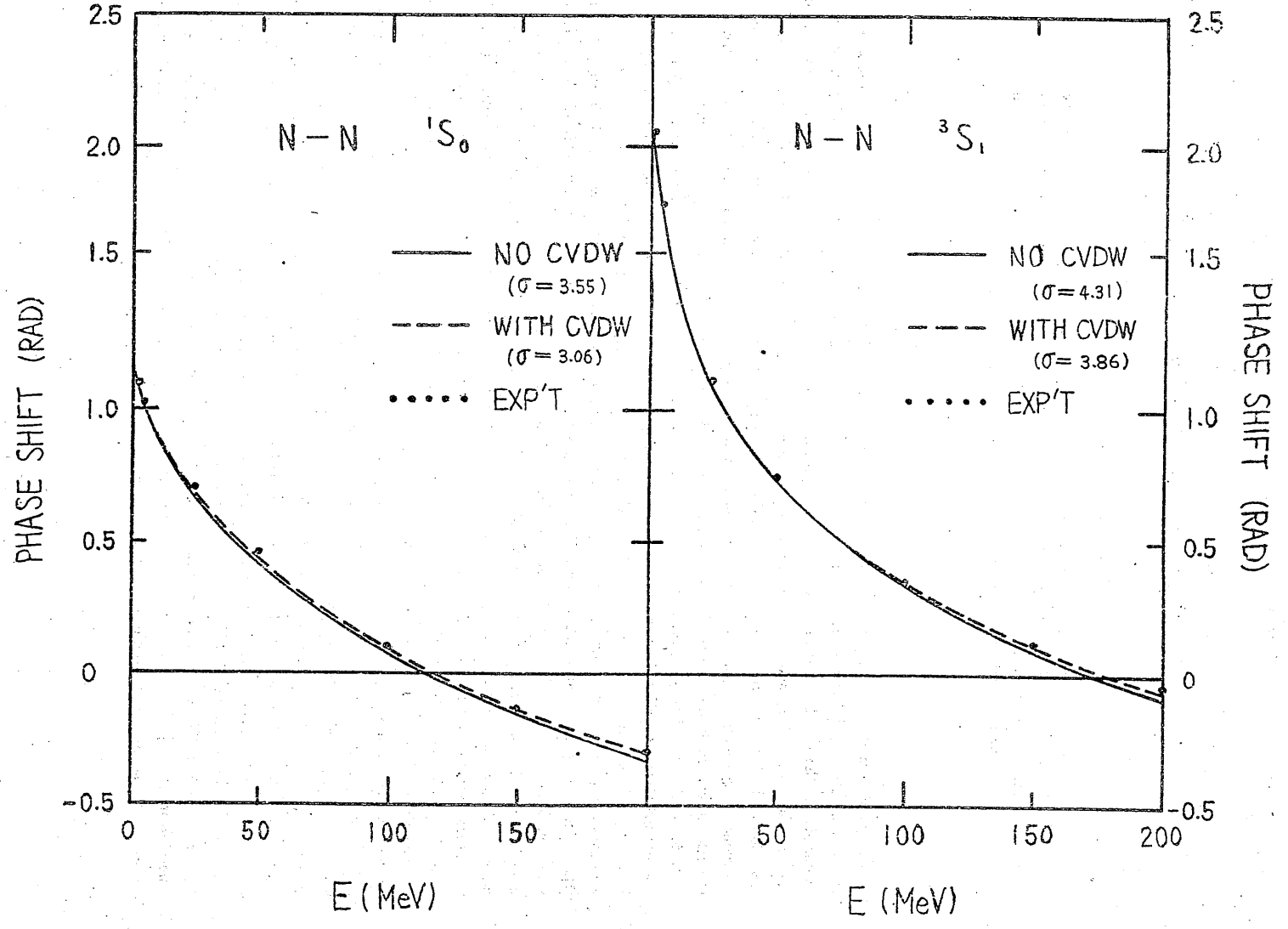
N – N $^1S_0$
N – N $^3S_1$
NO CVDW
(σ = 3.55)
WITH CVDW
(σ = 3.06)
EXP'T
NO CVDW
(σ = 4.31)
WITH CVDW
(σ = 3.86)
EXP'T
PHASE SHIFT (RAD)
PHASE SHIFT (RAD)
E (MeV)
E (MeV)
2.5
2.0
1.5
1.0
0.5
0
-0.5
0
50
100
150
200

Nucleon form factors in a self-induced potential

J.-W. ZHANG[a,b], W. Z. DENG[b], and L. M. YANG[a,b]

[a] *(CCAST (World Laboratory), P. O. Box 1024, Beijing 100080, China*

and

[b]* *Institute of Theoretical Physics and Department of physics, Peking University, Beijing 100871, China*

A generalised Nambu-Jona-Lasinio model is proposed and solved in relativistic Hartree approximation. An effective confining potential for individual quarks is obtained in a self-consistent way through an ansatz on the form of the interaction kernel. Various nucleon form factors and static properties are evaluated comparably with the empirical measurement.

I. INTRODUCTION

Both particle and nuclear physics research has now been probed deeply into the stratification to study the structure of nucleons. To the particle physics point of view, nucleons comprises three quarks interacting through gluon fields in conformity to the possible fundamental theory of quantum chromodynamics (QCD). In the empirical measurement, e.g., for the study of the short range correlation of nucleons, it should be defined exactly for the short range contribution and repulsive core of nucleons, and also for the deep inelastic lepton scattering from nucleons and nuclei collisions in high energy physics. Understanding modern nuclear physics craves for elaborating the internal structure of nucleons, especially the change of such internal structure for nucleons embedded in nuclear medium.

As for nucleons in low lying states it is too involved to be able to make the direct application of QCD for the non-perturbative properties of gluon fields. Theorists have been working for the phenomenology for more than twenty years. Apart from Monte Calo simulations, modeling QCD is now still the only game of the town. There has seen a remarkable proliferation of nucleon models, catologuing from constituent quarks bound in a confining potential [1] to non-topological chiral quark-meson solitons [2]. More recently the Nambu–Jona-Lasinio (NJL) model [3] in basic quark degrees of freedom suitably generalized which links in some ways between the more phenomenological models and QCD becomes increasingly popular [4]. This is because this model, deals explicitly only with the effective interaction between quarks, is a schematic one which consolidates all of the relevant (global) symmetries and main properties as many as possible, and especially visualizes the chiral symmetry breaking pattern [5] of the low energy regime of QCD, but is still sufficiently simple to permit actual calculations. Multi-gluon machanism is frozen and absorbed in an effective interaction between quarks.

The interaction kernel $g_i(x_1, x_2, x_3, x_4)$ of the generalised NJL-type (GNJL) model represents local interaction called as piont contact interaction. One might include six- or more- point fermion terms in principle except for the lowest four-fermion ones, the later is asked to satify Fierz rearrangement invariance, even though it is still quite involved for a pratical calculation. The GNJL lagrangian or the action may be finally fixed exactly by fitting the experimental data. It is expected to accurately describing the properties and predicting some new physics. The color confinement is believed to be stemmed from multi-gluon mechanism, however, it is generally considered that the confinement mechanism of QCD is able to be sustained effectively no matter that GNJL deminishes the glounic degrees of freedom. The relevant confinement sector is hidden in the effective quark-quark interaction kernels in the general formalism [6]. The ambitious aim is to make it clear that how large in amplitude of such gluonic degrees of freedom and their properties would be reattrieved in a generalised formalism. Still now, however, there is no way to

deduce it from the first principles. As a first step we would like to consider valence quarks qqq, sea quark pairs $q\bar{q}$ and diquarks qq and all the other possible kinds of degrees of freedom, and test the effective quark-quark interaction kernels in the composite structure of hadrons by expreiments, then we should improve various concrete forms to give the information and to deminish the uncertainty.

The general form of a GNJL action has been investigated by a number of authors in the past [4,6]. In the present work we take the following one:

$$S = S_0 + S_I \ , \tag{1.1}$$

where

$$S_0 = \int d^4x\, \bar{\psi}(x)\left(i\gamma_\mu \partial^\mu - m_q\right)\psi(x) \ ,$$

$$S_I = \int d^4x\, d^4y \left[\left(\bar{\psi}(x)\Gamma_i\psi(x)\right) g_i(x-y) \left(\bar{\psi}(y)\Gamma_i\psi(y)\right)\right] \ ,$$

with

$$\Gamma_i = \{1, i\gamma_5, \gamma_\mu, \gamma_\mu\gamma_5\} \otimes \{\text{flavor and color}\},$$

only the two-flavor sector is considered here. The interaction kernel g_i's are taken to depend on the difference $(x-y)$ to insure translational invariance. The action preserves the relevent symmetries of QCD, namely (global) color symmetry $SU_c(3)$, chiral symmetry $SU_L(2) \otimes SU_R(2)$, baryon number symmetry and the discrete symmetries $P.C.T.$. Further S_I is chosen to be Fierz invariant, namely,

$$\begin{aligned} S_I = \int d^4x\, d^4y \Big\{ & g_1(x-y)\left((S_{00}^{(x)}S_{00}^{(y)} + P_{00}^{(x)}P_{00}^{(y)}) + (S_{30}^{(x)}S_{30}^{(y)} + P_{30}^{(x)}P_{30}^{(y)})\right) \\ & + g_2(x-y)\left(V_{00}^{(x)}V_{00}^{(y)} + A_{00}^{(x)}A_{00}^{(y)}\right) + g_3(x-y)\left(V_{30}^{(x)}V_{30}^{(y)} - A_{30}^{(x)}A_{30}^{(y)}\right) \\ & + g_4(x-y)\left(V_{00}^{(x)}V_{00}^{(y)} - A_{00}^{(x)}A_{00}^{(y)}\right) + \text{color octet terms}\Big\} \ , \end{aligned} \tag{1.2}$$

where, e.g.,

$$S_{30} = \bar{\psi}(x)\tau\cdot\delta^c\psi(x) \ ,$$

$$P_{08}^c = \bar{\psi}(x)\mathbb{1}\cdot\lambda^c i\gamma_5\psi(x) \ .$$

Here τ is the isospin operator and δ^c, λ^c the $SU_c(3)$ generators. The interaction kernals g_i's are nonlocal and still quite arbitrary apart from their covariance property, but we intend to incorporate in them the general features of QCD, namely, asympototic freedom and confinement.

Since there are so many unknown elements in our model that has to be searched and tested by confronting the deduction with experimental data, we prefer to make simple assumptions. At first we would like to make a drastic approximation on g_i's: All the forms are in the same shape but with different strength. And instantoneous approximation in which the retardation of the quark interation is negnected reduces further the formalism into three space dimensions. Namely we take the following form:

$$g_i(x-x') = c_i\,\delta(t-t')\,g(|\mathbf{x}-\mathbf{x}'|) = c_i\,\delta(t-t')\,g(r) \ , \tag{1.3}$$

where c_i's are constants and $g(r)$ is chosen by the general properties of low energy QCD and from hadron phenomenological. This is the so called static approximation. Nevertheless we should finally reserve the rotational and translational invariance to g_i's.

In Sec. II we will discuss the further simplifying steps, including relativistic mean field (MF) approximation. Nucleon form factors are given in relativistic Hartree approximation (RHA) quark states in one of the simplest forms of the effective quark-quark interaction kernels. In Sec. III, numerical results of various form factors and the corresponding static properties of the nucleon, and a brief discussion will be given.

II. FORMALISM

A. The self-consistent relativistic Hartree approximation

The next major simplifying step is the use of the relativistic MF approximation. As the scalar MF the lowest order self-energy $\Sigma(r)$ is evaluated from the effective interactions $g_1(r)$ which includes confinement and a set of simple particle wave functions is defined.

In nuclear physics MF approach is more familiar to the natural studies. An MF gets out the main contributions of quark interaction as much as possible, and minimizes the residual interactionns. This is from often used bound state method of the resently developed theory dealing with relativistic nuclear many-body problems [7]. The mean field in configuration space breaks the translational invariance of both hadronic states and the physical vacuum. In principle it may be restored by the relativistic momentum projection and boost method to obtain physical hadron states with well-defined momentum.

The MF can also contain confinement to make quarks bound where is single (anti) quark in the vacuum (ground state). Brockmann, Weise and Werner [8] proposed that effective quark-quark contact interaction with position dependent coupling strength postulated to be determined by the multi-gluon sector is impossible to be calculated from first principles, although it is widely believed to be small at origin (hadron center) and increases rapidly towards the hadron surface, even if it has come to scene the assumed color screening effect. Therefore one needs to introduce an effective kernel for induvidual quarks in a phenomenological manner to seek *a posteriori* justification in finding its confomity with the supposed qualitative behavior of the position-dependent coupling strength in the contact interaction.

On the other hand, the quark-quark interaction kernels reduced from the instantoneously approximative Bethe-Salpeter equation verify that one can also obtain a scalar Hartree mean field in the first order, which represents an one-point contribution to the self-energy of quarks. In this work we consider only the Hartree term contribution of the self-energy. The Fork term, which is a two-point one and is of order $O(1/N_c)$, is negnected. This is the same approximation scheme used in the original NJL model. The explicit evaluation of the Fock term is possible by following the method of Ref. [9], but we will not purse this further here. The self-energy of individual quarks in the Hartree vacuum is

$$\Sigma(\mathbf{r}) = \int d\mathbf{r}' g(\mathbf{r},\mathbf{r}') G^{(0)}(\mathbf{r}',\mathbf{r}') = \Sigma(r) \,, \tag{2.1}$$

provided that the two-body-kernel of quarks $g(\mathbf{r},\mathbf{r}')$ is parameterized with qualitative properties of the effective interaction quoted above, in Eq. (2.1) $G^{(0)}(\mathbf{r}',\mathbf{r}')$ is the Green function in the lowest level,

$$G^{(0)}(\mathbf{r}',\mathbf{r}') = \langle 0 | T\left(\psi(\mathbf{r}')\bar{\psi}(\mathbf{r}')\right) | 0 \rangle \,.$$

For the sake of simplicity, in this work we make the following ansatz:

$$g(\mathbf{r},\mathbf{r}') = g(|\mathbf{r}-\mathbf{r}'|) \,,$$

as an instanton-reduced interaction as mentioned in Sec. I (see Eq. (1.3)). This procedure is manifest to keep Lorentz invariance in three-dimensinal space, i.e., the kernel $g(|\mathbf{r}-\mathbf{r}'|)$ is translational and rotational invariant. There are some clues from the results of the lattice gauge simulations of QCD that the confine kernel is approximate linear increase within the intermediate separation between quarks. In practical calculation the effective interaction kernel $g(r)$ is simply taken to be a linear confining form:

$$g(r) = Cr, \quad (C > 0) \,. \tag{2.2}$$

This means that at a short separated distance quarks only weakly interact, while at large distance there is a linear increased confine interaction.

In a trancated quark configuration space of a hadron state, however, the scalar self-energy available above not only breaks chiral symmetry spontaneously, but also provides a confinement part of interaction in Hartree MF level. The interaction which is determined by Dirac equation of independent quarks or anti-quarks in Hartree vacuum,

$$(i\gamma\cdot\nabla - m_q - \Sigma(r))\psi(r) = E_q\psi(r)\ , \tag{2.3}$$

where $\psi(r)$ is the single quark wave function in the sphere self-induced potential $V(r) = m_q + \Sigma(r)$, E_q is the single quark eigenenergy. A solution to the time reverse invariant independent-quark wave function is conventionally obtained in two-component spatial form as:

$$\psi_{njlmt}(r) = \begin{pmatrix} G_{njl}(r)/r \\ i\sigma\cdot\hat{\mathbf{r}}\, F_{njl}(r)/r \end{pmatrix} \left(Y_l(\hat{\mathbf{r}})\chi^s_{1/2}\right)_{jm} \chi^t_{1/2}\ . \tag{2.4}$$

In this work we assume as in soliton models that the three quarks of the baryons are in their ground state with $J^P = \frac{1}{2}^+$ ($\kappa = \frac{1}{2}$) and $J_z = J_3 = \frac{1}{2}$. Solutions of Eq. (2.3) and Eq. (2.1) would be obtained by a standard self-consistent iterative method with the interaction kernel under the assumption of Eq. (2.2).

B. Nucleon form factor definitions

Assuming the quarks to be point-like particles, the nucleon vector current is taken as the sum of the quark currents $\bar{\psi}_q(\mathbf{r})\gamma_\mu\psi_q(\mathbf{r})$, the nucleon axial-vector current as the sum of the quark contributions $\bar{\psi}_q(\mathbf{r})\gamma_\mu\gamma_5\frac{\tau}{2}\psi_q(\mathbf{r})$. The Dirac and Pauli form factors F_1 and F_2 are measured by elastic scattering of electrons on nucleons. The general form of matrix elements of the electromagnetic current $J_\mu(x)$ from Lorentz invariance under reflections and charge conservation between nucleon states is as follows:

$$\langle N(p')|J_\mu(0)|N(p)\rangle = \bar{u}(p',S')[\gamma_\mu F_1(q^2) + \frac{i\sigma_{\mu\nu}q_\nu}{2M_p}F_2(q^2)]u(p,S)\ , \tag{2.5}$$

where $q = p' - p$ is the four-momentum transfer, S the spin. They are related to the Sachs form factors by

$$\begin{aligned} G_E(q^2) &= F_1(q^2) - \eta F_2(q^2)\ , \\ G_M(q^2) &= F_1(q^2) + F_2(q^2)\ , \end{aligned} \tag{2.6}$$

here $\eta = -\frac{q^2}{4M_p^2}$, with normalizations $G_E^p(0) = 1$, $G_M^p(0) \equiv \mu_p = 2.793$ for the proton and $G_M^n(0) \equiv \mu_n = -1.913$ for the neutron. Isoscalar and isovector combinations are

$$\begin{aligned} G^S_{E,M}(q^2) &= \tfrac{1}{2}[G^p_{E,M}(q^2) + G^n_{E,M}(q^2)]\ , \\ G^S_{E,M}(q^2) &= \tfrac{1}{2}[G^p_{E,M}(q^2) - G^n_{E,M}(q^2)]\ , \end{aligned} \tag{2.7}$$

with $G^S_E(0) = G^V_E(0) = \frac{1}{2}$, $G^S_M(0) \equiv \mu_S = 0.440$ and $G^V_M(0) \equiv \mu_V = 2.353$.

The current matrix elements take a simple form in the Breit-Fermi frame (the electron-nucleon certer-of-mass frame) between nucleon states

$$\begin{aligned} \langle N_{S'}(\tfrac{1}{2}\mathbf{q})|J_0(0)|N_S(-\tfrac{1}{2}\mathbf{q})\rangle &= (1+\eta)^{-1/2}G_E(q^2)\delta_{S'S}\ , \\ \langle N_{S'}(\tfrac{1}{2}\mathbf{q})|\mathbb{J}(0)|N_S(-\tfrac{1}{2}\mathbf{q})\rangle &= (1+\eta)^{-1/2}G_M(q^2)\chi^\dagger_{S'}\frac{i\sigma\times\mathbf{q}}{2M_p}\chi_S\ , \end{aligned} \tag{2.8}$$

with $q_\mu = (0,\mathbf{q})$, $p^2 = p'^2 = M_p^2$, $\mathbf{p} = -\mathbf{p}' = -\frac{1}{2}\mathbf{q}$, and $p_0 = E = (4M_p - \mathbf{q}^2)^{1/2}$.

The axial-vector current $\mathbf{A}_\mu$ has isovector property as the Pauli matrix τ. The corresponding matrix elements of this current between nucleon states involve the axial-vector form factor $G_A(q^2)$ and the induced pseudoscalar form factors $G_P(q^2)$ as follows:

$$\langle N(p')|\mathbf{A}_\mu(0)|N(p)\rangle = \bar{u}(p')\left[\gamma_\mu G_A(q^2) + \frac{i\sigma_{\mu\nu}q_\nu}{2M_p}G_P(q^2)\right]\gamma_5\frac{\tau}{2}u(p)\ . \tag{2.9}$$

The axial-vector form factor has the normalization of $G_A(0) \equiv g_A = 1.255 \pm 0.006$. The induced pseudoscalar-vector form factor is connected with the pion-nucleon strong interaction form factor $g_{\pi NN}(q^2)$ as,

$$G_P(q^2) \approx \frac{m_\pi^2}{m_\pi^2 - q^2} \frac{g_{\pi NN}(q^2)}{g_{\pi NN}} G_P(0) ,$$

where the (charge) pion mass $m_\pi = 139.6$ MeV, on pion mass-shell $g^2_{\pi NN}(q^2 = m_\pi^2)/4\pi \approx 14.3$. Also in Breit-Fermi frame one finds for the components of $A^i_\mu = (A^i_0 , \mathbf{A}^i)$:

$$\langle N_{S'T'}(\tfrac{1}{2}\mathbf{q})|A^i(0)|N_{ST}(-\tfrac{1}{2}\mathbf{q})\rangle = \chi^\dagger_{S'}\chi^\dagger_{T'} \left[\frac{E}{M_p} G_A(q^2)\sigma_T + \left(G_A(q^2) + \eta G_P(q^2)\right)\sigma_L\right] \frac{\tau^i}{2}\chi^\dagger_S\chi^\dagger_T , \tag{2.10}$$

while the time component $\langle N_{S'T'}(\frac{1}{2}\mathbf{q})|A^i(0)|N_{ST}(-\frac{1}{2}\mathbf{q})\rangle = 0$ in this frame. Here the transverse and longitudinal spins are $\sigma_T = \sigma - \hat{\mathbf{q}}(\sigma \cdot \hat{\mathbf{q}})$ and $\sigma_T = \hat{\mathbf{q}}(\sigma \cdot \hat{\mathbf{q}})$.

The slope of the form factors at $q^2 = 0$ determines various radii by

$$\langle r^2 \rangle = \frac{6}{G(0)} \left.\frac{dG(q^2)}{dq^2}\right|_{q^2=0} . \tag{2.11}$$

The empirical nucleon charge, magnetic and axial radii are [10]:

$$\begin{aligned}
\langle r_E^2\rangle^{1/2}_{\text{proton}} &= (0.86 \pm 0.01) \text{ fm} , \\
\langle r_E^2\rangle^{1/2}_{\text{neutron}} &= (-0.12 \pm 0.01) \text{ fm} , \\
\langle r_M^2\rangle^{1/2}_{\text{proton}} &= (0.86 \pm 0.06) \text{ fm} , \\
\langle r_M^2\rangle^{1/2}_{\text{neutron}} &= (0.88 \pm 0.07) \text{ fm} , \\
\langle r_A^2\rangle^{1/2}_{\text{nucleon}} &= (0.63 \pm 0.06) \text{ fm} .
\end{aligned}$$

So there are different kinds of radii of the nucleon, its size depends on the probe.

III. NUMERICAL RESULTS AND DISCUSIONS

Within the present framework some static properties of nucleons are investigated. These include magnetic moment μ_N, mean-squied radius $\langle r^2\rangle_N$, and axial-vector couplant ratio (g_A/g_V) for β decay of nucleons, ect.

There would be an appreciable contribution to the energy E_q due to the motion of the center of mass (CM) of the three-quarks system. The expressions for the static quantities need to be modified taking into account CM motion. Then accordingly the corrected expressions for them can be written as

$$\mu_N^{\text{corr}} = \frac{1}{1 + \delta_N + \delta_N^2}\left[3\mu_N + \frac{M_p}{M_N} Q_N(1 - \delta_N)\right] , \tag{3.1}$$

$$\langle r_C^2\rangle^{\text{corr}} = \frac{3}{2 + \delta_N^2} \sum_q \left[\left(1 - \frac{2E_q}{E_N}\right) Q_q + \left(\frac{E_q}{E_N}\right)^2\right] \langle r_C^2\rangle , \tag{3.2}$$

and

$$(g_A/g_V)^{\text{corr}} = \frac{3}{1 + 2\delta_N}(g_A/g_V) , \tag{3.3}$$

where

$$\delta_N^2 = \langle M_N^2/E_N^2\rangle = 1 - \langle \mathbf{P}_N^2\rangle/E_N^2 , \qquad \delta_N = \langle M_N/E_N\rangle \approx \tfrac{1}{2}(1 + \delta_N^2) .$$

Here $\mathbf{P}_N$ is the center-of-mass momentum, and Q_N is the charge of the nucleon. The relativistic energy of the quark core of the nucleon is

$$E_N = \sum_q E_q - E_{\rm int} \,, \tag{3.4}$$

where $E_{\rm int}$ is the energy from the residual scalar and pseudoscalar interaction of Eq. (1.2). To be consistent with the Hartree approximation, the exchange term is also not included in it. The physical mass of the bare nucleon core is

$$M_N = (E_N - \langle \mathbb{P}_N^2 \rangle)^{1/2} \,, \tag{3.5}$$

and $\langle \mathbf{P}_N^2 \rangle$ is evaluated with the usual approximation $\langle \mathbf{P}_N^2 \rangle = \sum_q \langle \mathbf{P}^2 \rangle_q$. Evaluation of the mean-squired average of the independent quark momenta $\langle P_N^2 \rangle_q$ would lead approximately to the correct estimation of the static properties of the nucleon.

TABLE I. List of values in MeV of the parameter C in the kernel Eq. (2.2) fit to a nucleon mass M_N and the correspondingly calculated 'constituent' quark mass at hadron center $M(0)$ and at the quark core radius $M(r_c)$, scalar (E_S) and pseudoscalar (E_P) interaction energies, total energy E_N and the CM momentum $\langle P_N^2 \rangle^{1/2}$.

C	$M(0)$	$M(r_c)$	E_q	E_S	E_P	$\langle P_N^2 \rangle^{1/2}$	E_N	M_N
114	307	375	542	362	172	555	1093	941

TABLE II. Static properties of the nucleon calculated from the relevant form factors and the corresponding CM corrected values. The radii are in fm, magnetic moments in unit of the Bohr magnetons.

$\langle r_E^2 \rangle^{1/2}$	$\langle r_M^2 \rangle^{1/2}$	$\langle r_A^2 \rangle^{1/2}$	μ_p	μ_n	g_A
no CM corrected values					
0.94	0.90	0.95	1.62	-1.08	1.48
with CM corrected values					
0.85	0.81	0.86	1.91	-1.24	1.62

Now we present the calculated nucleon properties with quarks interacting by the linear confining kernel Eq. (2.2). As the only parameter of this schematic model, C in Eq. (2.2) is fixed through fitting the recoiled correction mass of the nucleon M_N to the empirical value. The single quark energy E_q, the residual interaction energy between quarks

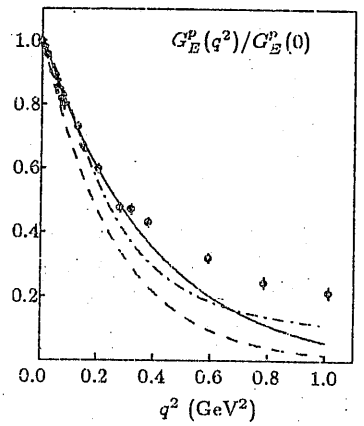

FIG. 1. Proton charge form factor $G_E^p(q^2)/G_E^p(0)$ calculated in the present model (The solid line corresponds to the recoil corrected form factor, the dashed line the bare one.) in comparison with the relativistic confining potential model [11] (dashed-dotted line), as well as with the experimental data.

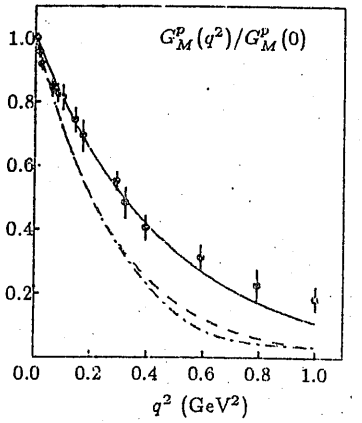

FIG. 2. The same as Fig. 1 for the proton magnetic form factor $G_M^p(q^2)/G_M^p(0)$.

E_{int} and the total CM momentum of the nucleon $\langle P_N^2\rangle^{1/2}$ are listed in Tab. I. Of the interaction energy part, here both scalar and pseudoscalar components, E_S and E_P, respectively, contribute at the Hartree level. The unrecoiled energy E_N in Eq. (3.4) then reduces $\sim \frac{1}{3}$, so the spurious CM energy of the nucleon is approximate equal to the single particle eigen energy of the quarks. It is worth noting that the value of the scalar confining potential $M(r)$ in the center of the nucleon is happened to be about one third of the recoiled mass M_N in Eq. (3.5). This number is the so called "constituent mass" of quarks. Two values of this mass are presented for comparison, one is at the center and another is at the empirical quark core radius $r_c \sim 0.6$ fm.

We show in Figs. 1 and 2 the results obtained for proton electromagnetic form factors $G_E^p(q^2)$ and $G_M^p(q^2)$, respectively, in comparison with the relativistic confining potential model results [11] as well as with the experimental data [12].

The recoil corrections of the quark core are made in similar to Ref. [11]. The details will be given in a subsequent paper where the meson states are also well-treated. The corresponding recoil corrected form factors are shown for comparison. They are generally harder than the static ones.

We observe an fair overall qualitative agreement with the experiment data, with discrepencies quite prominent in the higher $|\mathbf{q}|^2$ region. It is argued that these deviations are caused by the absence of the derect pion meson cloudy

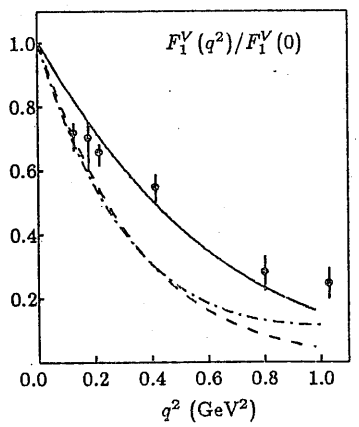

FIG. 3. The same as Fig. 1 for the isovector form factor $F_1^V(q^2)/F_1^V(0)$.

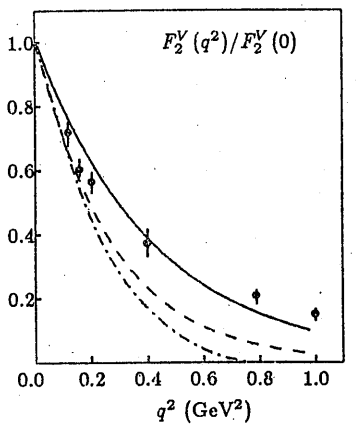

FIG. 4. The same as Fig. 1 for the isovector form factor $F_2^V(q^2)/F_2^V(0)$.

contributions. This model failed to give nuetron charge form factor $G_E^n(q^2)$, while experimentally $G_E^n(q^2)$ is much less than $G_E^p(q^2)$ in the low $|\mathbf{q}^2|$ region, so that $G_E^p(q^2) = G_E^V(q^2)$ according to Eq. (2.7). In order to isolate meson cloudy effects, it always be useful to discuss the isovector parts of the form factors $F_1^V(q^2)$ and $F_2^V(q^2)$ [11,13],

$$F_1^V(q^2) = \frac{1}{1-\eta}\left[G_E^p(q^2) - \tfrac{5}{3}\eta G_M^p(q^2)\right] ,$$
$$F_2^V(q^2) = \frac{1}{1-\eta}\left[\tfrac{5}{3}G_M^p(q^2) - G_E^p(q^2)\right] . \qquad (3.6)$$

Results for Eq. (3.6) are shown in Figs. 3 and 4. Characteristically these again fit the empirical data [14] fairly well. The results for the axial form factor $G_A(q^2)$ in the normalised ratio $G_A(q^2)/G_A(0)$ has been plotted in Fig. 5 in comparison with the experical data [13,14]. The fit is better than that in Ref. [11].

The results of the static properties of the nucleon calculated from the form factors and the corresponding CM recoiled corrected values are listed in Tab. II. The charge radius of the nucleon computed from Eq. (3.2) is $\langle r_E^2\rangle^{1/2} = 0.78$ fm. This value is less that in Ref. [11]. The magnetic radius is 0.83 fm. It is almost the same as the charge radius. They both fit the experimental data well. The axial radius calculated here is not so large as 0.97fm in Ref. [11].

The results of the static properties of the nucleon calculated from the form factors and the corresponding CM recoil correction values are listed in Tab. II. We see the recoil correction gives less radii. This is nothing but through hardening the relevant form factors. The charge radius of the nucleon computed from Eq. (3.2) is $\langle r_E^2\rangle^{1/2} = 0.85$ fm. This value is less than that in Ref. [11]. The magnetic radius is 0.81 fm. It is approximate the same as the charge radius. They both fit the experimental data well. The axial radius calculated here is 0.86 fm. In Ref. [11] it is as large as 0.97fm. The calculated magnetic moments of the nucleon are 30% less in amplitude than the empirical data. The axial-vector couplant, in the other way, is 30% larger. It indicates that corrections from meson cloudy and color gluonic exchange may be significant. It will be our interest of further works.

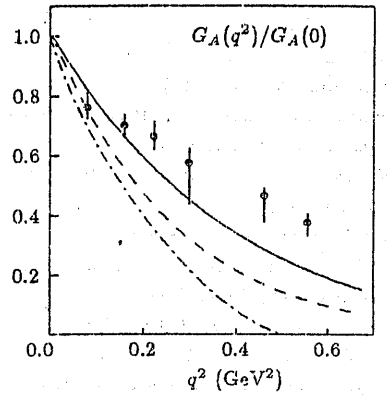

FIG. 5. The same as Fig. 1 for the Axial form factor $G_A(q^2)/G_A(0)$.

Now we would like to make some concluding remarks and discussions of this work. The main ideal of the present approach is to obtain a self-consistent confining potential from the effective quark-quark interaction kernel. The simplest way to realize it is to work in the relativistic Hartree MF. Scalar interaction with the sea quarks in the lowest order gives rise to a self-energy which serves as a scalar potential, or an MF to the lowest energy single particle states. There are other ways of dealing with the MF and the vacuum. For example, quark pair condensation [15] in the quark vacuum by means of the Bogoliubov transformation is formulated, though working with quarks in the MF is essentially working with dressed quarks. Residual interactions will help to restore symmetry violated by the MF approximation [16]. By means of RPA equation it is possible to get the quark structure of hadrons, including the $q\bar{q}$ cloud surrounding the baryons [17]. We expect to reproducing much more better there the properties of nucleons and there radial excited states, including the charge form factors of the nuetron and the Roper resonance.

The single quark wave functions solved by the Dirac Eq. (2.3) is not the eigenstates of the momentum. There are a significant amount of contribution to the total energy of the nucleon by the CM motion. So using the translationally invariant nucleon wave function obtains a significant improve to the static form factors. This correction will be done in a subsequent work by the TDA and RPA approaches in a larger configuration space.

Finally we would like to point out that although we take $g(r)$ to be a linear form in r. it doesn't mean that we should rely on this concrete form of $g(r)$ to get confinement. Actually the similar results will come out irrespectively for the $g(r)$ in different ways. Confinement in this scheme is realized essentially as long as the interaction strength between quarks is large enough so that quark pair condensate prevails in the physical vaccum.

ACKNOWLEDGMENTS

One of the authors (J.-W. Z.) would like to express his thanks to Professor Z.-M. Qiu of CCAST (World Laboratory) and Professor E.-G. Zhao of ITP (Academia Sinica) for their hospitality. His part of this work has been done partly during the CCAST Summer Workshop on Collective Motions and Quark Degrees of Freedom in Nuclei. We preciate various fruitful discussions with Professor X.-J. Qiu, Professor H.-X. He and Professor T.-S. Cheng.

REFERENCES

* Correspondence address.

[1] C. Carl and I. Isgir, Phys. Rev. D **19**, 435 (1979); R. Rith and K. Buck, *ibid.* **42**, 1164 (1991).

[2] See, for example, M. C. Birse, Prog. Part. Nucl. Phys. **20**, 1, (1991) and references therein.

[3] Y. Nambu and G. Jona-Lasinio, Phys. Rev. **122**, 345 (1961); **124**, 246 (1961).

[4] V. Bernard, R. Brockmann, M. Schaden, W. Weise, and E. Wener, Nucl. Phys. A **412**, 349 (1984); T. Hatsuda and T. Kunihino, Prog. Theor. Phys. **74**, 765 (1985); V. Bernard, Phys. Rev. D **34**, 1601 (1986); V. Bernard, U.-G. Meissner, and I. Zahed, *ibid*, **36**, 819 (1987).

[5] J. Cornell, Phys. Rev. D **00**, 1452 (1980); A. Casher, Phys. Lett. **83B**, 395 (1979); J. R. Finger and J. E. Mandula, Nucl. Phys. B **199**, 168 (1982).

[6] W. Z. Deng, J.-W. Zhang, and L. M. Yang, Preprint (1992).

[7] J. D. Welacka and B. D. Serot, Adv. Nucl. Phys. **16**, 1 (1986).

[8] R. Brockmann W. Weise, and E. Werner, Phys. Lett. 122 B (1983) 201.

[9] R. Haag and Th. A. J. Maris, Phys. Rev. **132**, 2325 (1963).

[10] W. Weise, Regensburg Univ., TPR-91-7, (1991)

[11] N. Barik, S. N. Jena, and D. P. Rath, Phys. Rev. D **41**, 1568 (1990).

[12] G. Hohler *et al.*, Nucl. Phys. B **114**, 505 (1976).

[13] R. Tegen, R. Brockmann, and W. Weise, Z. Phys. A **307**, 339 (1982).

[14] E. Amaldi, S. Fubini, and G. Furlan, in *Electroproduction at Low Energy and Hadron Form Factors*, ed., G. Hohler, (springer Tracts in Modern Physics, Vol. 83) (Springer, Berlin, 1979).

[15] P. Biondo and J. Ribeiro, Phys. Rev. D **42**, 1661 (1990).

[16] M. Bando, K. Fujii, Y. Abe, T. Okazaki, and S. Kurada, Phys. Rev. D **33**, 548 (1986).

[17] L. M. Yang, W. Z. Deng, and J.-W. Zhang, in preparation.

QCD and The Pion- Nuclear DCX Reaction

Xiaofu LU[a,b,c], Enguang ZHAO[a,c], Yuxin LIU[a,c] and Jie MENG[a,c]

[a]CCAST(World Laboratory), P. O. Box 8730, Beijing 100080, China

[b]Department of Physics, Sichuan University, Chengdu 610064, China

[c]Institute of Theoretical Physics, Academia Sinica,
P. O. Box 2735, Beijing 100080, China*

December 22, 1992

Abstract

The two nucleon DCX transition matrix element is under consideration in the framework of QCD. The interactions in the DCX process including the perturbative and non-perturbative effects are discussed. The interaction operators are given.

It came as a big surprise, When 1984 the first Pion-nucleus double charge exchange reaction (DCX) measurement below the Δ - resonance had been conducted. Navon et al[1] and later Leith et al[2] measured the DIAS transition on ^{14}C at an incident pion eneryg of $T_\pi = 50MeV$ and found that there the forward angle cross section is as large as at $T_\pi = 300MeV$ and even is close to the forward angle cross section for SCX on ^{14}C at $T_\pi = 50MeV$. This observation was in clear contradiction to expectations. Since the destructive interference of s- and p- waves in the πN- system causes the SCX cross section to undergo a deep minimum near $T_\pi = 50MeV$, one could speculated that also something similar would happen for the DCX process. In order to account for this unexpectedly large DIAS cross section on ^{14}C at $T_\pi = 50MeV$, at first non-nucleonic processes were proposed, such as the double charge exchange on six quark clusters[3]. However, conventional explainations[4] have also been found soon, based on a careful treatment of nucleon-nucleon correlations. Nevertheless, a commou feature of both exotic and conventional explainations is that both these treatments stress the relevance of short distances ($\leq 1fm$) between the nucleons participating in the DCX process[5]. This is a region in which nucleons overlap so that the conventional multiple scattering treatment may be an oversimplification. A more correct consideration of the process occuring at such short distance from quark degrees of freedom is still needed.

*Mailing address

The main purpose of this article is to develop a more sophisticated QCD treatment for the two nucleon DCX transition matrix element, especially to take into accaunt some non-perturbative effects.

The S-metrix of DCX reaction in the Heisenberg Representation can be expressed as

$$\langle pp\,\pi^-|S|nn\,\pi^+\rangle = \frac{1}{(2\pi)^3 2\sqrt{\omega_{\mathbf{k}}\omega_{\mathbf{k}'}}}\int d^4x\int d^4x' e^{i(\mathbf{k}'\cdot\mathbf{x}'-\mathbf{k}\cdot\mathbf{x})} \\ (\Box_x + m_\pi^2)(\Box_{x'}+m_\pi^2)\langle pp|T(\phi_{\pi^-}(x')\phi_{\pi^-}(x))|nn\rangle \tag{1}$$

where the matrix elements can be expressed in figure 1, in which the dashed external lines represent the Green function for the $\phi_{\pi^-}(x)$ field. Considering the Goldstone effect, we have

$$\partial_\mu A^\mu_{u\,d} = i2m_q\overline{u}(x)\gamma_5 d(x)$$
$$\partial_\mu A^\mu_{u\,d} = \sqrt{2}f_\pi m_\pi^2\phi_{\pi^-}(x)$$

where $A^\mu_{u\,d} = \overline{u}\gamma^\mu\gamma_5 d$, From the dynamical spontaneous breacking of chiral symmetry we have the effective lagrangian term[6]

$$-i\frac{\sqrt{2}m_q}{f_\pi}\overline{u}\gamma_5 d\phi_{\pi^+}(x) \tag{2}$$

Using the equation

$$(\Box_x + m_\pi^2)\Delta_F = -i\delta(x-y) \tag{3}$$

where Δ_F is the Feynman propagator for pions, we can get

$$\langle pp\,\pi^-|S|nn\,\pi^+\rangle = \frac{-2}{f_\pi^2}\frac{1}{2(2\pi)^3\sqrt{\omega_{\mathbf{k}}\omega_{\mathbf{k}'}}}\int d^4x\int d^4x' e^{i(\mathbf{k}'\cdot\mathbf{x}'-\mathbf{k}\cdot\mathbf{x})} \\ \langle p\,p|T(m_q\overline{u}\gamma_5 d(x')m_q\overline{u}\gamma_5 d(x))|n\,n\rangle. \tag{4}$$

Making a translation transformation we have

$$\langle pp\,\pi^-|S|nn\,\pi^+\rangle = \frac{-2}{f_\pi^2}\frac{2\pi}{2\sqrt{\omega_{\mathbf{k}}\omega_{\mathbf{k}'}}}\delta(k'+p'-k-p)\int d^4x e^{i(\mathbf{k}'\cdot\mathbf{x})} \\ \langle p\,p|T(m_q\overline{u}\gamma_5 d(x), m_q\overline{u}\gamma_5 d(0))|n\,n\rangle. \tag{5}$$

where $\mathbf{k}'$ is the outgoing momentum of π^-, $\mathbf{k}$ is the incident momentum, $\mathbf{p}'$ is the momentum of $(p\,p)$, $\mathbf{p}$ is the momentum of $(n\,n)$.

We emphasize that the above discussion is based on the nonperturbative effects. In order to carry out the calculation we shall use the QCD sum rule. According to the operator product expansion, we have

$$\begin{aligned} &T(\overline{u}(x)\gamma_5 d(x)\,\overline{u}(0)\gamma_5 d(0)) \\ =&:\overline{u}(x)\gamma_5 d(x)\,\overline{u}(0)\gamma_5 d(0): \\ &+:\overline{u}(0)\gamma_5 d(0)\,\overline{u}(0)\gamma_5 d(0): C_G(x): G^a_{\mu\nu}G^a_{\mu\nu}: \\ &+:\overline{u}(0)\gamma_5 d(0)\,\overline{u}(0)\gamma_5 d(0): C_Q(x)m_q:\overline{q}(0)q(x): \end{aligned} \tag{6}$$

The first term in the right hand side is the perturbative effect, which has the contribution

$$m^2 \int d^4x e^{i(\mathbf{k'}\cdot\mathbf{x})} \langle p\, p| : \overline{u}\gamma_5 d(x), m_q \overline{u}\gamma_5 d(0) : |n\, n\rangle. \tag{7}$$

Because of the energy momentum conservation the lowest order contribution of eq.(8) can be represented by figure 2.

For Fig.2.(1), the contribution is

$$\begin{aligned} &\overline{u}(p_1')g\frac{\lambda^a}{2}\gamma_\mu \frac{1}{(p_1-k'-p_1')^2}\frac{i}{(\not{p}_1-\not{k}'-m)}\gamma_5 d(p_1) \\ &\qquad \overline{u}(p_2')\frac{i\,\lambda^a}{2}\gamma^\mu \frac{i}{(\not{p}_2'+\not{p}_1'-\not{p}_1+\not{k}-m)}\gamma_5 d(p_2) \end{aligned} \tag{8}$$

For Fig.2.(2), the contribution is

$$\begin{aligned} &\overline{u}(p_1')\gamma_5 \frac{i}{(\not{p}_1'+\not{k}'-m)}g\frac{\lambda^a}{2}\gamma_\mu \frac{1}{(p_1-k'-p_1')^2} d(p_1) \\ &\qquad \overline{u}(p_2')\frac{i\,\lambda^a}{2}\gamma^\mu \frac{i}{(\not{p}_2'+\not{p}_1'-\not{p}_1+\not{k}-m)}\gamma_5 d(p_2) \end{aligned} \tag{9}$$

For Fig.2.(3), the contribution is

$$\begin{aligned} &\overline{u}(p_1')g\frac{\lambda^a}{2}\gamma_\mu \frac{1}{(p_1-k'-p_1')^2}\frac{i}{(\not{p}_1-\not{k}'-m)}\gamma_5 d(p_1) \\ &\qquad \overline{u}(p_2')\gamma_5 \frac{i}{(\not{p}_2'+\not{p}_1-\not{p}_1'-\not{k}-m)}g\frac{i\,\lambda^a}{2}\gamma^\mu d(p_2) \end{aligned} \tag{10}$$

For Fig.2.(4), the contribution is

$$\begin{aligned} &\overline{u}(p_1')\gamma_5 \frac{i}{(\not{p}_1+\not{k}'-m)}g\frac{\lambda^a}{2}\gamma_\mu \frac{1}{(p_1-k'-p_1')^2} d(p_1) \\ &\qquad \overline{u}(p_2')\gamma_5 \frac{i}{(\not{p}_2'+\not{p}_1'-\not{p}_1-\not{k}'-m)}g\frac{i\,\lambda^a}{2}\gamma^\mu d(p_2) \end{aligned} \tag{11}$$

For the calculation of the second term of the time-ordered product expansion, namely the contribution of gluon condensation, we adopt the fixed-point gauge technique[7]. In this method we introduce an external gauge field $A_\mu^a(x)$ with the gauge condition $x^\mu A_\mu^a(x) = 0$. The external gauge field $A_\mu^a(x)$ can then be expressed directly in terms of gauge convariant quantities

$$A_\mu(x) = \frac{1}{2}x^\nu G_{\nu\,\mu}(0) + \frac{1}{3}x^\alpha x^\nu D_\alpha G_{\nu\mu}(0) + \cdots. \tag{12}$$

To calculate the contribution of gluon condensation we shall employ the diagram shown as Fig.2'. This contribution can be expressed as

$$-\frac{i}{4}g\frac{\lambda^a}{2}G_{\kappa\lambda}^a(0)\frac{1}{(p^2-m^2)^2}\{\sigma_{\kappa\lambda}(\not{p}+m)+(\not{p}+m)\sigma_{\kappa\lambda}\}, \tag{13}$$

where

$$\sigma_{\kappa\lambda} = \frac{i}{2}(\gamma_\kappa\gamma_\lambda - \gamma_\lambda\gamma_\kappa).$$

After some derivation, we can get all of the contributions from these diagram. For Fig.4.(1), the result is

$$\begin{aligned}\overline{u}(p_1-k'-q)g\frac{\lambda^a}{2}\gamma_\mu\left[f_1(q^2)g^{\mu\nu}+f_2(q^2)\frac{q^\mu q^\nu}{q^2}\right]\frac{k'}{(p_1-k')^2-m^2}\gamma_5 d(p_1)\\ \frac{1}{q^2}\overline{u}(p_2+k+q)g\frac{\lambda^a}{2}\gamma_\nu\frac{\not{k}}{(p_2+k)^2-m^2}\gamma_5 d(p_2)\langle G^a_{\mu\nu}G_{\mu\nu}a\rangle,\end{aligned} \tag{14}$$

where

$$\begin{aligned}f_1(q^2) &= \frac{im^2g^4}{1152\pi^2}\int_0^1(1-x)^3\frac{x(1-x)q^2+3m^2}{(m^2-x(1-x)q^2)^3}dx\\ f_2(q^2) &= \frac{im^2g^4}{1152\pi^2}\int_0^1(1-x)^3\frac{-2x(1-x)}{(m^2-x(1-x)q^2)^3}dx\end{aligned} \tag{15}$$

The result of Fig.4.(2) is the same as that of Fig.4.(1).
For Fig.4.(3), we have

$$\begin{aligned}\overline{u}(p_1-k'-q)g\frac{\lambda^a}{2}\gamma_\mu\frac{1}{q^2}\left[H_1(q^2)g^{\mu\nu}+H_2(q^2)\frac{q^\mu q^\nu}{q^2}\right]\frac{k'}{(p_1-k')^2-m^2}\gamma_5 d(p_1)\\ \frac{1}{q^2}\overline{u}(p_2+k+q)g\frac{\lambda^a}{2}\gamma_\nu\frac{\not{k}}{(p_2+k)^2-m^2}\gamma_5 d(p_2)\langle G^a_{\mu\nu}G_{\mu\nu}a\rangle,\end{aligned} \tag{16}$$

where

$$\begin{aligned}H_1(q^2) &= \frac{ig^4}{2304\pi^2}\int_0^1 x(1-x)\frac{3m^2-2x(1-x)q^2}{(m^2-x(1-x)q^2)^2}dx\\ H_2(q^2) &= \frac{im^2g^4}{2306\pi^2}\int_0^1\frac{-x^2(1-x)^2}{(m^2-x(1-x)q^2)^2}dx\end{aligned} \tag{17}$$

For Fig.4.(4), the corresponding one is

$$\begin{aligned}\overline{u}(p_1-k'-q)\gamma_5\frac{k'}{(p_1-q)^2-m^2}\frac{\lambda^a}{2}\gamma_\mu\frac{1}{q^2}d(p_1)\left[f_1(q^2)g^{\mu\nu}+f_2(q^2)\frac{q^\mu q^\nu}{q^2}\right]\\ \overline{u}(p_2+k+q)g\frac{\lambda^a}{2}\gamma_\nu\frac{\not{k}}{(p_2+k)^2-m^2}\gamma_5 d(p_2)\langle G^a_{\mu\nu}G_{\mu\nu}a\rangle,\end{aligned} \tag{18}$$

For Fig.4.(5), it takes the following form

$$\begin{aligned}\overline{u}(p_1-k'-q)\gamma_5\frac{k'}{(p_1-q)^2-m^2}\frac{\lambda^a}{2}\gamma_\mu\frac{1}{q^2}d(p_1)\left[H_1(q^2)g^{\mu\nu}+H_2(q^2)\frac{q^\mu q^\nu}{q^2}\right]\\ \frac{1}{q^2}\overline{u}(p_2+k+q)g\frac{\lambda^a}{2}\gamma_\nu\frac{\not{k}}{(p_2+k)^2-m^2}\gamma_5 d(p_2)\langle G^a_{\mu\nu}G_{\mu\nu}a\rangle,\end{aligned} \tag{19}$$

The contribution of Fig.4.(6) is the same as that of Fig.4.(4).

The Fig.4.(4), (5) have their exchange terms. They can be given as the followings respectively.

$$\overline{u}(p_1-k'-q)g\frac{\lambda^a}{2}\gamma_\mu\frac{1}{q^2}\left[f_1(q^2)g^{\mu\nu}+f_2(q^2)\frac{q^\mu q^\nu}{q^2}\right]\frac{k'}{(p_1-k')^2-m^2}\gamma_5 d(p_1)$$
$$\frac{1}{q^2}\overline{u}(p_2+k+q)\gamma_5\frac{\not{k}}{(p_2+q)^2-m^2}g\frac{\lambda^a}{2}\gamma_\nu d(p_2)\langle G^a_{\mu\nu}G_{\mu\nu}a\rangle, \tag{20}$$

$$\overline{u}(p_1-k'-q)g\frac{\lambda^a}{2}\gamma_\mu\frac{1}{q^2}\left[H_1(q^2)g^{\mu\nu}+H_2(q^2)\frac{q^\mu q^\nu}{q^2}\right]\frac{k'}{(p_1-k')^2-m^2}\gamma_5 d(p_1)$$
$$\frac{1}{q^2}\overline{u}(p_2+k+q)\gamma_5\frac{\not{k}}{(p_2+k)^2-m^2}g\frac{\lambda^a}{2}\gamma_\nu d(p_2)\langle G^a_{\mu\nu}G_{\mu\nu}a\rangle, \tag{21}$$

The exchange term of Fig.4.(6) takes the same form as Fig.4.(4).

Similarily, we can write down the contributions of Fig.4.(7), (8) as the followings respectively, and Fig.4.(9) has the same result as that of Fig.4.(7).

$$\overline{u}(p_1-k'-q)\gamma_5\frac{k'}{(p_1-q)^2-m^2}\frac{\lambda^a}{2}\gamma_\mu\frac{1}{q^2}d(p_1)\left[f_1(q^2)g^{\mu\nu}+f_2(q^2)\frac{q^\mu q^\nu}{q^2}\right]$$
$$\frac{1}{q^2}\overline{u}(p_2+k+q)\gamma_5\frac{\not{k}}{(p_2+q)^2-m^2}g\frac{\lambda^a}{2}\gamma_\nu d(p_2)\langle G^a_{\mu\nu}G_{\mu\nu}a\rangle, \tag{22}$$

$$\overline{u}(p_1-k'-q)\gamma_5\frac{k'}{(p_1-q')^2-m^2}\frac{\lambda^a}{2}\gamma_\mu\frac{1}{q^2}d(p_1)\left[H_1(q^2)g^{\mu\nu}+H_2(q^2)\frac{q^\mu q^\nu}{q^2}\right]$$
$$\frac{1}{q^2}\overline{u}(p_2+k+q)\gamma_5\frac{\not{k}}{(p_2+k)^2-m^2}\frac{\lambda^a}{2}\gamma_\nu d(p_2)\langle G^a_{\mu\nu}G_{\mu\nu}a\rangle, \tag{23}$$

The third term of eq.(6) is the contribution of quark condensation. In order to determine this contribution it is necessary to consider the following diagrams in Fig.5..

The contribution from Fig.5(1) can be written in the following formula,

$$\overline{u}(p_1-k'-q)g\frac{\lambda^a}{2}\gamma_\mu\frac{1}{q^2}K(q^2)\left(\frac{q^\mu q^\nu}{q^2}-g^{\mu\nu}\right)\frac{i}{\not{p}_1-\not{k}'-m}\gamma_5 d(p_1)$$
$$\frac{1}{q^2}\overline{u}(p_2+k+q)g\frac{\lambda^a}{2}\gamma_\nu\frac{i}{\not{p}_2+\not{k}-m}\gamma_5 d(p_2)\frac{1}{6}\langle\psi\psi\rangle, \tag{24}$$

where

$$K(q^2)=i\frac{m}{q^2} \tag{25}$$

For Fig.5.(2) and (3), we have

$$\overline{u}(p_1-k'-q)\gamma_5\frac{\not{k}'}{(p_1-q)^2-m^2}\frac{\lambda^a}{2}\gamma_\mu\frac{1}{q^2}K(q^2)\left(\frac{q^\mu q^\nu}{q^2}-g^{\mu\nu}\right)d(p_1)$$
$$\overline{u}(p_2+k+q)g\frac{\lambda^a}{2}\gamma_\nu\frac{\not{k}}{(p_2+k)^2-m^2}\gamma_5 d(p_2)\frac{1}{6}\langle\psi\psi\rangle, \tag{26}$$

$$\bar{u}(p_1-k'-q)\gamma_5\frac{\not{k}'}{(p_1-q)^2-m^2}\frac{\lambda^a}{2}\gamma_\mu\frac{1}{q^2}d(p_1)K(q^2)\left(\frac{q^\mu q^\nu}{q^2}-g^{\mu\nu}\right)$$
$$\frac{1}{q^2}\bar{u}(p_2+k+q)\gamma_5\frac{\not{k}}{(p_2+q)^2-m^2}g\frac{\lambda^a}{2}\gamma_\nu d(p_2)\frac{1}{6}\langle\psi\psi\rangle. \tag{27}$$

The next step is to write down the six quark wave function of $(n\,n)$ and $(p\,p)$ in the nucleus and calculate the matrix element. The result will be given in the future.

The authors are grateful for the hospitality of CCAST and this work is also partly supported by the National Natural Science Foundation of China.

REFERENCES

[1] I. M. Navon, et. al., Phys. Rev. Lett. **52** (1984) 105.
[2] M. J. Leitch, et. al., Phys. Rev. Lett. **54** (1985) 1482.
[3] G. A. Miller, Phys. Rev. Lett. **53** (1984) 2008; ibid, Phys. Rev. **C35** (1987) 377.
[4] N. Auerbach, et. al., Phys. Rev. **C38** (1988) 1277.
[5] H. Clement, Prog. Part. Nucl. Phys. bf 29 (1992) 175.
[6] R. T. Cahill and C. D. Roberts, Phys. Rev. **D32** (1985) 2419.
[7] L. J. Reinders, et. al., **127** (1985) 27.

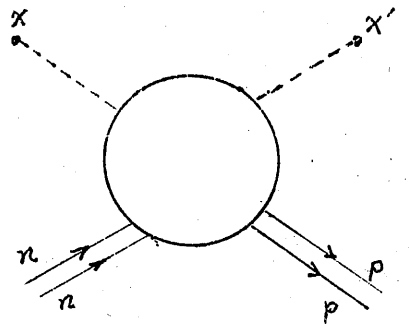

Fig. 1

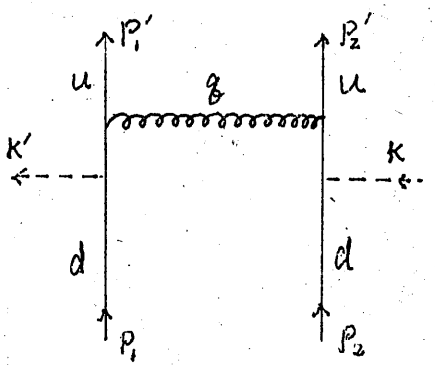

(1)

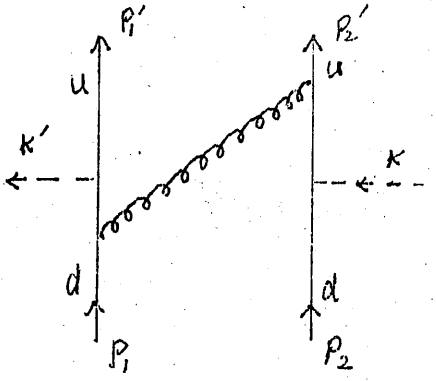

(2)

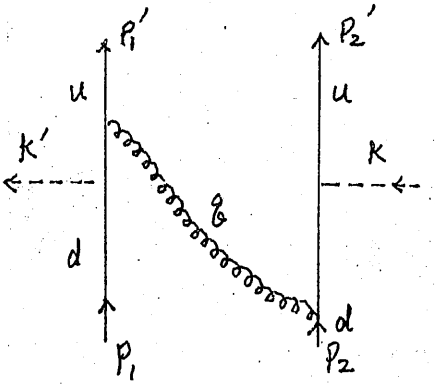

(3)

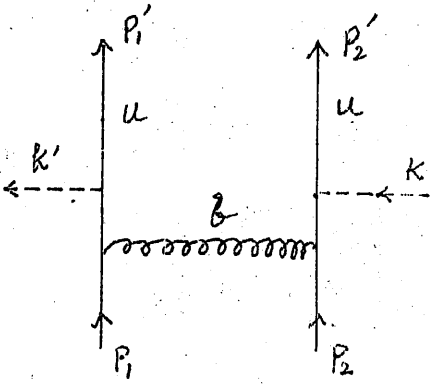

(4)

Fig. 2.

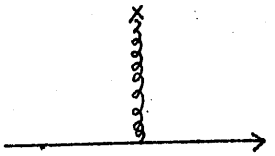

Fig. 3

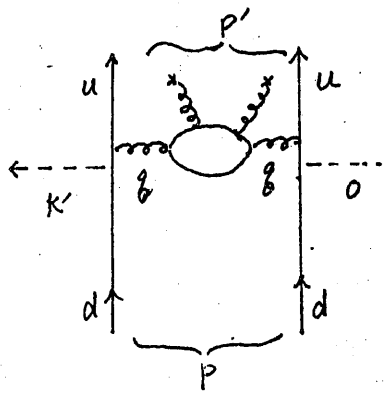

(1)

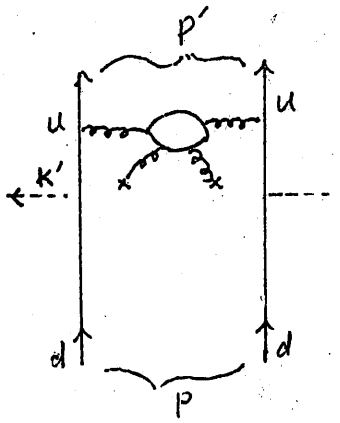

(2)

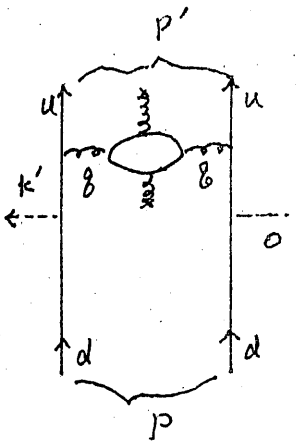

(3)

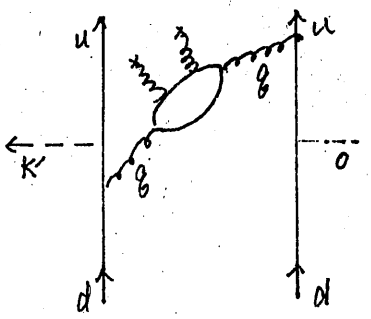

(4)

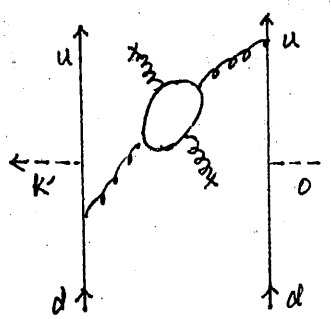

(5)

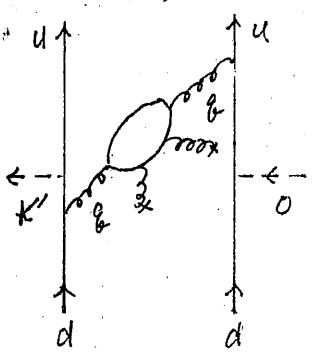

(6)

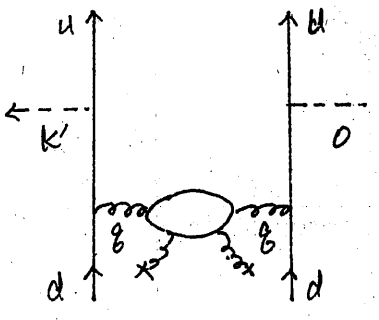

(7)

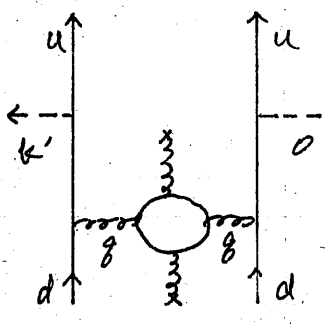

(8)

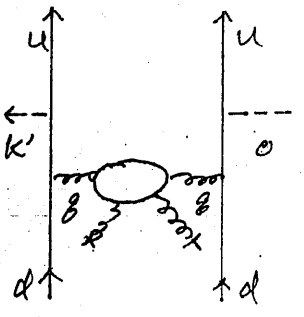

(9)

Fig. 4

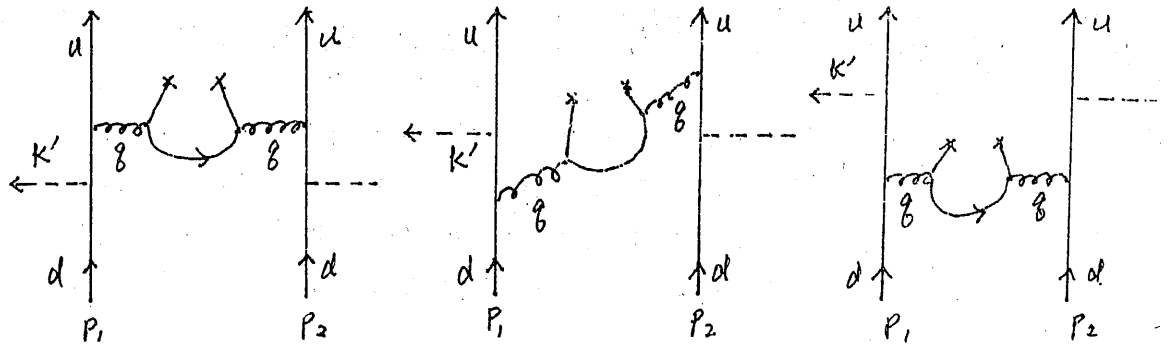

Fig. 5

Relativistic Effective Interaction *

Ma Zhongyu[(1),(2),(3)] and Chen Baoqiu[(2)]
[1)]CCAST, P.O.Box 8730, Beijing 100080, P.R.China
[2)]China Institute of Atomic Energy, Beijing 102413, P.R.China
[3)]Institute of Theoretical Physics, Beijing 100080, P.R.China

October 28, 1992

Abstract

In analogy to the idea of the effective interaction commonly used in the non-relativistic approach, the relativistic effective interactions are adopted to incorporate the relativistic Brueckner-Hartree-Fock (RBHF) results in the relativistic mean field approach (RMF) or relativistic Hartree-Fock approach (RHF). It is desired to remedy the deficiencies of RMF and RHF without losing the features of the relativistic G matrix and at same time retain the simplicity. The relativistic effective interactions are used to describe the ground state properties of nuclei and medium-energy nucleon-nucleus scattering in this paper.

1 Introduction

During past ten years people have devoted considerable efforts on the relativistic approach in nuclear physics[1-3]. One may ask why we need a relativistic approach in nuclear physics. In the non-relativistic approach the nucleus is considered as a collection of non-relativistic nucleons. It is a non-relativistic many-body system. To deal with the non-relativistic many-body problems one starts from a static nucleon-nucleon (NN) interaction, such as

*This work was supported by the National Natural Science Foundation of China

paris, Bonn potentials etc., which fits the low energy NN scattering data, phase shifts and deuteron properties. With the many-body technique one solves the Schrodinger equation. The non-relativistic approach is quite successful in explaining low energy nuclear physics and has provided important insights into nuclear physics. Despite of the success, there are still some longstanding problems, which have to be solved. It is well known that the calculated nuclear matter saturation points can not meet the empirical value. The saturation points calculated with different two-body NN interactions are located in a narrow band, which is called Coester band[4]. Taking account of three and four hole line contribution the results still can't hit the empirical value. Similarly, for three body system with modern NN potentials, the ^3He system is underbound by 0.8 MeV[5] and the calculated rms charge radius is about 9% too large. For finite nuclei, it is necessary to add a phenomenological density dependent term[6]. To show the shell structure the spin-orbit interaction has to be put in by hand. These might suggest that there need some additional mechanisms to let nuclear matter saturate at the right position.

It is known that NN scattering amplitude has large scalar and vector components. The nuclear bulk properties could be mainly described in terms of the scalar and vector components. The Lorentz structure of the interaction provides an additional saturation mechanism, that is not present in the non-relativistic approach. As the nuclear density increases the attractive scalar potential saturates. The vector potential dominates at high density and produces the minimum in the binding curve. The nuclear matter saturation point is reproduced nearly quantitatively in RBHF approach[7]. The relativistic impulse approximation (RIA) is very successful in explaining the scattering of medium-energy proton from nuclei[8]. RIA calculations agree remarkably well with the data, particularly for the spin observables. The Dirac phenomenological optical potential (DPOP) predicted the spin observables much better than the non-relativistic optical potentials[9]. The calculations of the RMF for finite nuclei clearly reveal a shell structure[2]. It is due to the fact that the spin-orbit interaction is obtained naturally in the relativistic approach. These may indicate that the relativistic many-body approach is a useful tool in studying the nuclear structure and nuclear reaction.

In addition, in the future experiments nuclear systems will be examined under extreme conditions of density and temperature. A new generation of accelerators, e.g., RHIC may produce nuclear density of 6 times equilibriun density,

the temperature of nuclear system may reach 100 to 200 MeV. CEBAF will provide continuum electron beam of 4 GeV with high resolutions. The experiments will carry out with high momentum and high energy transfers. The high energy baryon accelerator will provide a complete information of the polarization of the proton-nucleus scattering. These future experiments will clearly involve physics beyond the Schrodinger equation. Therefore, it is necessary to develop a reliable and relativistic theory.

It is commonly accepted that the quantum chromodynamics (QCD) is a fundamental theory of the strong interaction. It has already drawn a lot of interests and has made a significant progress. However, it is still far from complete to use QCD directly to describe many-nucleon systems now. Therefore, to explain the future experiments it is attractive to develop a reliable and practicable model based on the hadronic degrees of freedom. The relativistic many-body approach and the quantum hadrodynamics (QHD)[1-3] is a satisfied candidate. It has been intensively investigated in the past ten years. The simplest model is RMF, which starts from an effective Lagrangian. In this model the meson fields are treated as classical fields. It is considered to be an efficient model to study the nuclear structure and nuclear reaction. However, the effective interactions of a nucleon in the nuclear medium are treated in a rather crude way in this simple model. A more sophisticated and fundamental way to deal with the many-body problem is to start from a static NN force. Taking account of nuclear short range correlations, the relativistic G matrix is evaluated by solving RBHF equation[1,7]. The relativistic G matrix is of density and momentum dependence. Obviously, it is rather complicated. In analogy to the idea of the effective interaction, which we often used in the non-relativistic approach, the relativistic effective interactions are adopted to incorporate the RBHF results in the RMF. The relativistic effective interactions are required to contain as much information of G matrix as possible. They have first to be examined in study of the nuclear structure and nuclear reaction at the normal condition of density and temperature. Then they are ready to be extended to the nuclear system away from the normal condition.

In Sec.2 we briefly present RMF and RBHF and their success and defects in explaining the nuclear structure and nuclear reactions. The relativistic effective interactions, which incorporate the RBHF results, are described in Sec.3. Finally, Sec.4 contains a summary.

2 RMF and RBHF

The RMF approach is to start from an effective Lagrangian,

$$\pounds = \pounds_o + \pounds_I,$$

$$\pounds_o = \overline{\psi}(i\gamma_\mu\partial^\mu - M)\psi + \frac{1}{2}(\partial_\mu\sigma\partial^\mu\sigma - m_\sigma^2\sigma^2) - \frac{1}{4}F_{\mu\nu}F^{\mu\nu} + \frac{1}{2}m_\omega^2\omega_\mu\omega^\mu, \quad (1)$$

$$\pounds_I = g_\sigma\overline{\psi}\sigma\psi - g_\omega\overline{\psi}\gamma_\mu\omega^\mu\psi,$$

$$F_{\mu\nu} = \partial_\mu\omega_\nu - \partial_\nu\omega_\mu,$$

where ψ is the baryon field, σ and ω are the neutral scalar and vector fields, respectively. The effective coupling constants g_σ and g_ω are to be adjusted. The field equations, i.e. the Euler Lagrange equations can be obtained from the effective Lagrangian,

$$(\partial_\mu\partial^\mu + m_\sigma^2)\sigma = g_\sigma\overline{\psi}\psi,$$

$$(\partial_\mu F^{\mu\nu} + m_\omega^2)\omega^\nu = g_\omega\overline{\psi}\gamma^\nu\psi, \quad (2)$$

$$[\gamma^\mu(i\partial_\mu - g_\omega\omega_\mu) - (M - g_\sigma\sigma)]\psi = 0.$$

When the sources are large, the meson field operators can be replaced by their expectation values. The meson fields are treated as classical fields. In the uniform infinite nuclear matter the meson fields are constants. The effective coupling constants are adjusted by fitting the nuclear matter saturation conditions. In this simple approach the nucleon self-energy Σ_s and Σ_o, are constant in the momentum,

$$\Sigma_s = -\frac{g_\sigma^2}{m_\sigma^2}\rho_s, \quad (3)$$

$$\Sigma_o = \frac{g_\omega^2}{m_\omega^2}\rho_B,$$

where ρ_s and ρ_B are the scalar and vector densities, respectively,

$$\rho_s = <\overline{\psi}\psi> = \frac{4}{(2\pi)^3}\int_0^{k_F} d^3k\frac{M^*}{E^*(k)},$$

$$\rho_B = <\overline{\psi}\gamma^\circ\psi> = \frac{2}{3\pi^2}k_F^3, \quad (4)$$

$$M^* = M + \Sigma_s, \qquad E^* = \sqrt{k^2 + M^{*2}}.$$

The incompressibility of nuclear matter K calculated in RMF is about 590 MeV, which is overlarge compared with the experimental value 210±30 MeV. It indicates that the effective interaction calculated in RMF do not have a correct behavior of the density dependence. To solve nuclear structure problems, we deal with a finite system. Therefore, the meson fields are of spatial dependence. For spherical nuclei, the meson fields as well as the scalar and vector potentials depend only on the radius. To solve the Dirac equation the negative energy states are neglected. The positive energy spinors can be written as

$$\psi_\alpha(\mathbf{r}, \sigma, \xi) = \frac{1}{r} \begin{pmatrix} iG_a(r) \\ F_a(r)\sigma \cdot \hat{r} \end{pmatrix} Y_{\kappa m}(\hat{\mathrm{r}}, \sigma)\chi_\tau(\xi), \tag{5}$$

where r, σ, ξ are the space, spin and isospin variables, respectively. The quantum number α refers to (n, κ, m, τ) and a to (n, κ), where n is the principal quantum number, κ=$\pm(j + 1/2)$ for $l = j \pm 1/2$ and τ=1 for proton and -1 for neutron. In order to make a quantitative comparison with actual nuclei some additional dynamics have to be introduced, e.g. γ to account for the Coulomb interaction, ρ meson for the nuclear symmetry energy. Therefore, the upper and lower radial components satisfy the equation,

$$\frac{d}{dr} \begin{pmatrix} G_a(r) \\ F_a(r) \end{pmatrix} = \begin{pmatrix} -\frac{\kappa_a}{r} & M + E_a + \Sigma_s(r) - \Sigma_o(r) \\ M - E_a + \Sigma_s(r) + \Sigma_o(r) & \frac{\kappa_a}{r} \end{pmatrix} \begin{pmatrix} G_a(r) \\ F_a(r) \end{pmatrix}, \tag{6}$$

where

$$\Sigma_s(r) = V_\sigma(r),$$

$$\Sigma_o(r) = V_\omega(r) + V_\rho(r)\tau + \frac{1}{2}(1 + \tau)V_c(r).$$

The scalar and vector potentials are the expectation values of meson fields in the ground states. They depend on the wave function of the ground state and the baryon density. Therefore, the eq.(6) has to be solved self-consistently. In this approach, there are only four adjustable parameters, the coupling constantsg_σ,g_ω, g_ρ and the scalar meson mass m_σ. The other quantities, such as masses of nucleon,ω and ρ meson and the strength of electromagnetic interaction α are taken their physical values. Actually, the g_σ, g_ω and g_ρ are adjusted by the nuclear matter saturation properties. This method

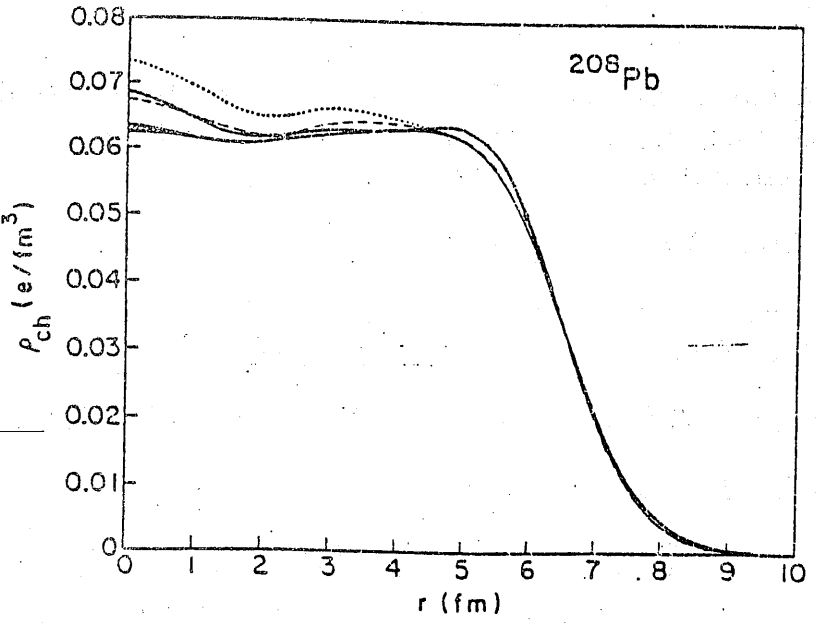

Figure 1: Charge density distribution for ^{208}Pb [10]. The shaded region represents the experimental data. The solid curve is calculated in RMF. The dotted and dashed curves are the results of DDHF and DDHF+RPA, respectively.

has turned out to be a very successful tool for the description of nuclear structure. First, the shell structures appear automatically due to the spin-orbit interaction, which is obtained naturally in the relativistic approach. The ground state properties of all closed-shell nuclei, such as charge density distribution, binding energy per nucleon, rms charge radius, right ordering of single particle levels, are well reproduced by RMF[10]. They are as same level of accuracy as density dependent Hartree-Fock (DDHF) results in the non-relativistic approach. Figure 1 gives an example of the charge density distribution for ^{208}Pb, which is adopted from ref.[10], calculated in RMF and compared with two non-relativistic calculations. Recently, this method has been also extended to odd and deformed nuclei throughout the periodic table. It was found that most of the ground state properties can be successfully described by RMF. Applying RMF to the nuclear reaction, we have investigated the relativistic microscopic optical potential (RMOP). Taking account of the medium effects, we calculated the self-energy of a nucleon in the nuclear medium. It is known that the self-energy of a nucleon is identical with the optical potential of the nucleon. Since the scattering problems are studied in a large energy range. The energy dependence of the scalar and vector potentials are certainly important, which are absent in RMF. The Fock terms contribute a weak energy dependence of the potentials, which are included in our calculations. We let the Hartree and Foch self-energies of

a nucleon be the real part of RMOP and the imaginary parts are calculated in the lowest order diagram. Therefore, the calculated self-energy is complex and momentum and density dependent.

$$\Sigma(k, k_F) = \Sigma_s(k, k_F) - \gamma^o \Sigma_o(k, k_F) + i\gamma \cdot \mathrm{k}\Sigma_v(k, k_F). \tag{7}$$

By the standard local density approximation (LDA) the complex self-energy of a nucleon is substituted into the Dirac equation,

$$[\alpha \cdot \mathrm{p}(1 + \Sigma_v(r)) + \gamma^o(M + \Sigma_s(r)) - \Sigma_o(r)]\psi(r) = E\psi(r). \tag{8}$$

It can be reduced to scalar-vector form,

$$[\alpha \cdot \mathrm{p} + \gamma^o(M + U_s) + U_o]\psi = E\psi, \tag{9}$$

$$U_s = \frac{\Sigma_s - \Sigma_v M}{1 + \Sigma_v}, \quad U_o = \frac{-\Sigma_o + E\Sigma_v}{1 + \Sigma_v}.$$

To solve the Dirac equation, the Schrodinger type equation is obtained by eliminating the small components in the Dirac equations.

$$[\frac{p^2}{2E} + U_{cent}(r) + V_c(r) + U_{so}\sigma \cdot \mathrm{L}]\varphi(r) = \frac{E^2 - M^2}{2E}\varphi(r), \tag{10}$$

$$U_{cent}(r) = U_o + \frac{1}{2E}[U_s(2M + U_s) - (U_o + V_c)^2],$$

$$U_{so}(r) = -\frac{1}{2ErD(r)}\frac{dD(r)}{dr},$$

$$D(r) = M + U_s(r) + E - U_o(r) - V_c(r).$$

There are central and spin-orbit potentials, which are called Schrodinger equivalent potentials. It is quite encouraging that without any readjustable parameters this model could reproduce main features of the phenomenological optical potential. The real parts of the central potentials are changed from attractive at low energies to repulsive at high energies. The imaginary parts of the central potentials have surface absorption at low energies and volume absorption at high energies. Especially, the strong spin-orbit potentials are obtained naturally. It is known that the scattering observables mainly depend on the volume integral of the optical potentials. The comparison of the volume integrals of RMOP with the empirical values are given in Fig.2.

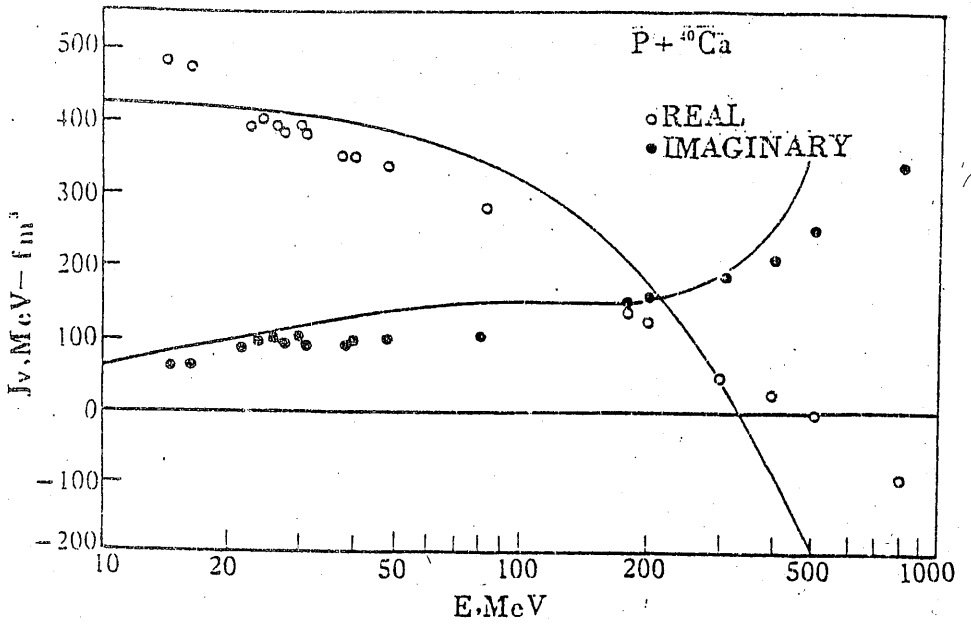

Figure 2: Volume integrals of the central part of the Schrodinger equivalent potentials for ^{40}Ca.

It is found that RMOP obtained in this model is in a reasonable agreement with the empirical values at the energy below 300MeV. We have calculated the scattering observables for various targets at this energy region. A general agreement with the experimental data is found. But, RMOP does not agree with the empirical values at high energies. This is due to the fact that the momentum dependence of self-energy may not be treated properly in this model. In order to show the momentum dependence of the self-energy in Fig.3 the calculated self-energies are compared with that of DPOP, which is given by Hama et al.[13]. From eq. (10) it is found that U_{cent} is roughly equal to $U_s + U_o$ at the low energy and $\frac{1}{2}U_s + U_o$ at the high energy around 1 GeV. Since the real part of U_s is attractive, there is a large cancellation between scalar and vector potentials. As a result, an attractive potential is obtained at low energies. The vector potential dominates at high energies. That is the reason why the central potential changes from attractive to repulsive at high energies. Though the absolute values of U_s and U_o at low energies for DPOP are larger than RMOP, the difference between U_s and U_o are similar. Thus, they have similar Schrodinger equivalent potentials at low energies. The momentum dependence of RMOP due to the Fork term is very weak. Therefore, the vector potential remains strong at high energies. The repulsive central potential of RMOP becomes overlarge at high energies. This may indicate that the density and momentum dependence of the effective interaction in this model is not correctly described. More fundemantal and sophisticated method to deal with many-body problems is RBHF. Starting

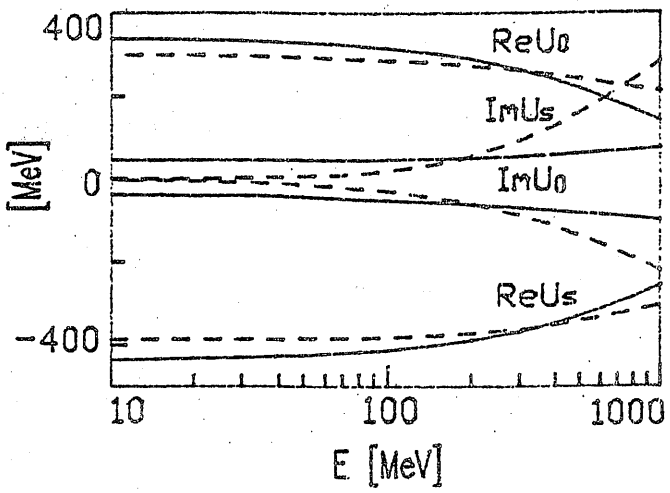

Figure 3: Energy dependence of the scalar and vector potentials at r=0 for ^{40}Ca. The solid curves are phenomenological potentials[13] and dashed curves are calculated in the $\sigma - \omega$ model.

from a bare NN interaction of one boson exchange potential (OBEP) one solves the Bethe-Goldstone equation, which is a three-dimensional reduction of the Bethe-Salpeter equation in the nuclear medium,

$$G = V + VQ\tilde{g}G, \tag{11}$$

where G is the two nucleon correlated effective interaction matrix. V is the bare NN interaction. Q is the Pauli operator, which forbids scattering to intermediate occupied states. $\tilde{g}$ is the single particle proper propagator, which maintains elastic two body unitary in nuclear matter. If V is taken as OBEP with a relatively weak tensor force, the nuclear matter saturation properties are reproduced nearly quantitatively by RBHF[7]. The calculated relativistic G matrix is of strong density dependence and weak momentum dependence. The incompressibility K of nuclear matter for RBHF turns out to be 290 MeV in a good agreement with the generally accepted empirical value. The effective mass M^*/M of a nucleon in nuclear matter depends on the scalar potential, which is about 0.6~0.7. The encouraging results of RBHF in nuclear matter lead us to think that this theory should describe nuclear structure and nuclear reaction reasonably well.

Unfortunately, it is an awkward task to solve RBHF equation for finite nuclei. Though there are a few attempts to work alone this line[14], it is very complicated and under investigation. However, it is feasible for nuclear scattering problems. The self-energy of a nucleon in nuclear matter can be obtained in

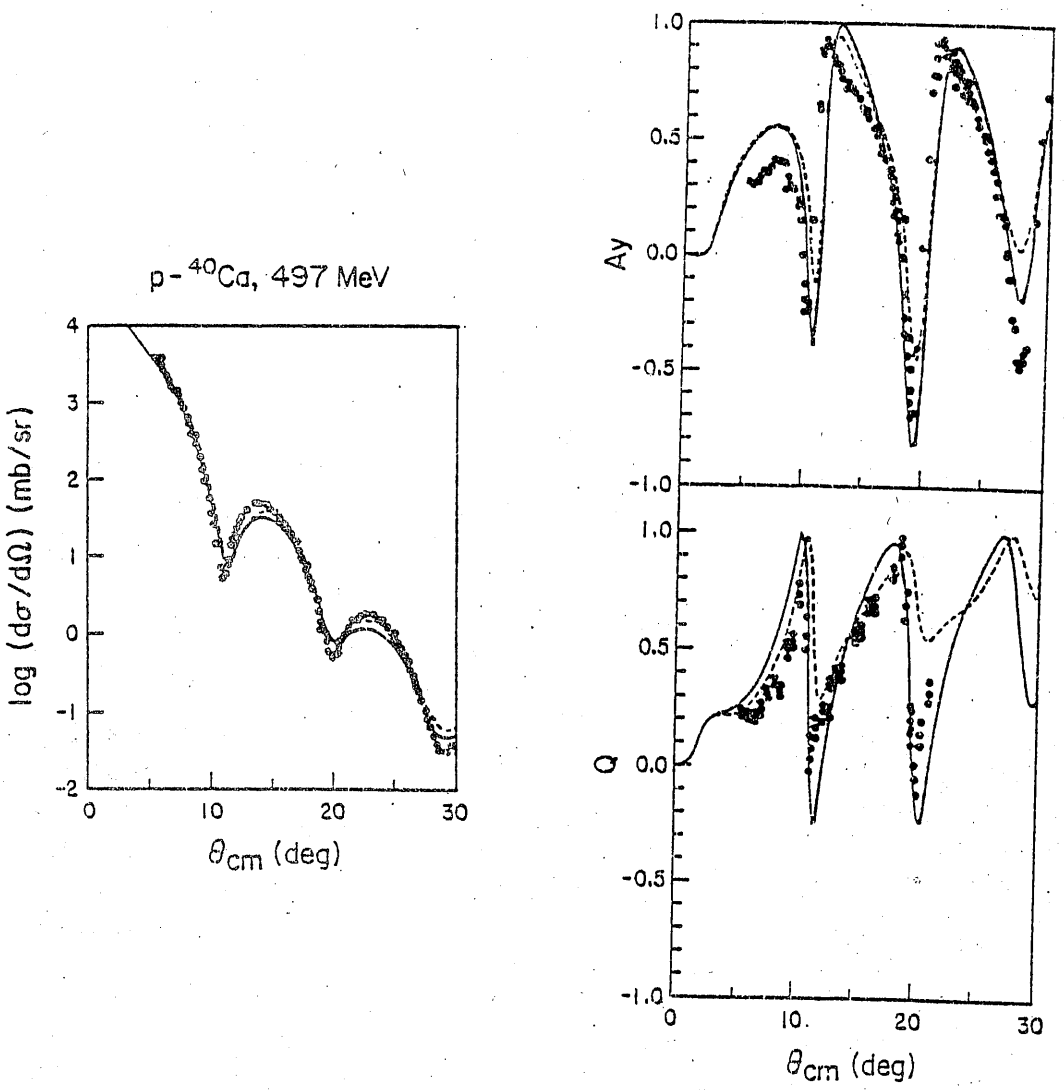

Figure 4: The differential cross section, analyzing power (A_y) and spin rotation function (Q) for the p-^{40}Ca sacttering at 497 MeV. The solid and dashed curves show the results with complex and real effective mass, respectively, calculated in RBHF approach.

RBHF. Using the standard LDA the RMOP for the proton-nucleus scattering is obtained. We calculated proton-nucleus scattering of ^{40}Ca for energy region of 160-800 MeV[15]. The differential cross sections and spin observables are compared with the experimental data. The results show a very good agreement with the experimental data(Fig.4). These may suggest that the effective interactions calculated in RBHF have a good behavior of both density and momentum dependences. Therefore, RBHF is certainly superior to RMF except for its complexity. In regard to some applications the following question may arise. Could we incorpoate the RBHF results in RMF ? That is the idea of the effective interaction, which is commonly used in the non-relativistic approach.

3 Relativitic effective interaction

Only in very recent years there are some attempts to work alone this line. Gmuca[16] proposed a method by using a density dependent scalar meson mass to reproduce the nuclear matter saturation curve. Brockmann and Toki[17] proposed a method based on the analyses of the self-energy. They introduced density coupling constants of σ and ω mesons to reproduce the scalar and vector potentials. Obviously, the information of the momentum dependence of the relativistic G matrix is lost in these approaches, where RMF is used. Fortunately, the momentum dependence of the effective interaction is weak, which may be neglected in the calculation for finite nuclei. Gmuca assumed a density dependent scalar meson mass

$$m_\sigma = m_\sigma^\circ(1 - \alpha\rho + \beta\rho^{5/3}), \tag{12}$$

and adjusted the parameters g_σ, g_ω, α and β to reproduce the nuclear matter saturation curve, which is calculated in RBHF. It is considered to be equivalent to the relativistic G matrix. He has solved Dirac equation with the density dependent scalar meson mass self-consistently for ^{16}O[16]. It is found that the calculated ground state properties of ^{16}O are in a very good agreement with the experimental data. In this approach the scalar and vector components of the self-energy are not individually reproduced.

Brockmann and Toki proposed a method by fitting the scalar and vector potentials with density dependent coupling constants of σ and ω mesons. They called it as relativistic density dependent Hartree approach (RDDH). The scalar and vector potentials calculated in RMF with constant couple constants and in RBHF cross nearly at the nuclear satuation density. Therefore, the coupling constants of g_σ, g_ω in RDDH are similar to those in RMF at the nuclear saturation density. The coupling constants become large at low density and decrease at high density. It is found that the coupling constants at $k_F = 0.8fm^{-1}$, which is just at the nuclear surface for finite nuclei, are about 40% bigger than those at the nuclear matter saturation density. It means that the coupling constants at the nuclear surface are much bigger than those in the interior, which is a rather important surface effect. The

surface effect will improve the rms radius for finite nuclei and certainly influence on the response of nucleus in the quasielastic electron scattering. It is known that the theoretical predictions for the longitudinal response of nucleus overestimate the experimental data about 30% ~50% . This effect will certainly improve the theoretical prediction. It is known that the Fork term could contain the information of momentum dependence in the relativistic G matrix. It is certainly an interesting problem to solve the RHF equation for finite nuclei. Bouyssy and his collaborators[18] did a pioneer work on it. The RHF approach for finite nuclei may reveal some new physics, since it could contain psedoscalar meson π and other important information. But it is rather complicated and the investigations are still under way. To deal with the scattering problems, the momentum dependence of the relativistic G matrix might not be neglected. We have investigated the scattering problems by the effective meson exchange (EME) in RHF approach[19], which was first proposed by Elsenhans et al.[20]. The relativistic G matrix is split into two parts, the bare NN interaction and the correlation term,

$$G = V + \Delta G. \tag{13}$$

The bare NN interaction is chosen as OBEP. The correlation term ΔG is parameterized in terms of an effective meson exchange model in the RHF approach. The coupling constants and masses of the effective mesons explicitly depend on the density, which are listed in Table 1. The largest contribution shows up in the exchange of an effective isoscalar vector meson. The negative coupling strength means that the two-body correlations reduce the repulsive contribution of ω meson in OBEP.

To show the momentum dependence of the self-energy calculated in this model, we give the self-energy as a function of the nucleon energy at a given density in Fig.5 in comparison with those calculated by the $\sigma - \omega$ model in RHF approach. The Hartree contributions are similar in two models. The Fock terms produced by σ and ω mesons are small and very weak energy dependent. They enhance the strength of both scalar and vector potentials in the $\sigma - \omega$ model. Conversely, the Fock terms in EME model have large cancellation among the isoscalar, isovector and the effective meson contribution. The effective isoscalar vector meson contribution with a negative coupling strength sizably reduce the vector self-energy. As a result, both scalar and vector self-energy in EME model are reduced considerably. The vector potential at the energy of 1GeV in EME model is about 100 MeV weaker

meson	σ	ω	π	ρ	δ	η
$g^2/4\pi$	5.7480	8.8562	12.7767	0.7536	1.1396	2.2486
m(MeV)	551.86	783.97	122.75	609.48	611.90	785.97
$k_F(fm^{-1})$		σ'	ω'	δ'	ρ'	
1.0	$g^2/4\pi$	0.2333	-14.0488	-3.2537	-1.8501	
	m(MeV)	403.32	1500.0	928.67	974.73	
1.2	$g^2/4\pi$	0.2056	-7.1425	-2.6242	-2.0438	
	m(MeV)	440.90	1108.3	928.43	1102.5	
1.4	$g^2/4\pi$	-0.0195	-5.8792	-2.6549	-2.4787	
	m(MeV)	250.00	939.15	970.81	1193.1	
1.6	$g^2/4\pi$	-0.0791	-5.9348	-3.3569	-4.4052	
	m(MeV)	275.06	919.23	1097.0	1500.0	

Table 1: The coupling constants and masses of mesons for the bare potential V and effective mesons for the correlation ΔG. The tensor-vector ratio for ρ meson is f_ρ/g_ρ=3.128.

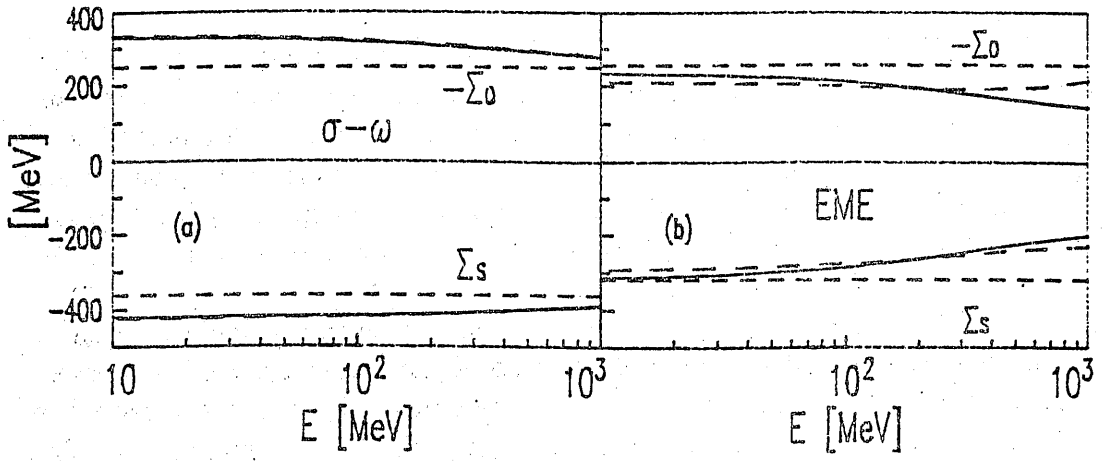

Figure 5: Scalar and vector potentials of the nucleon self-energy Σ (dash-dotted curves) at k_F=1.4 fm^{-1} a) in the $\sigma-\omega$ and b) in the EME model. The dashed lines are the Hartree contributions. The solid curves are scalar and vector potentials U_s, U_o in the Dirac equation (9).

The RBHF approach, starting from a static NN interaction is a more fundamental and sophisticated way to deal with the many-body problems. Taking account of the nuclear short range correlation both the effecctive interactions show a good behavior of both density and momentum dependence. Of course, it is much complicated and time consuming in the numerical calculation.
In regard to possible applications, it is desirable to remedy the deficiencies of RMF and RHF approaches with an effective interaction without losing the features of the relativistic G matrix and at the same time retain the simplicity. This is the idea of the relativistic effective interactions. It has first to be examined in the nuclear system at a normal condition. Then, it is ready to be extrapolated to the nuclear system away from the normal condition.
The direct application could be the study of properties of the nuclei far from the stability line, the nuclear response of quasielastic electron scattering and the phenomena of dense matter at high temperature produced by the nucleus-nucleus collision and astrophysics. Very promising features discussed above have been already seen for these applications.
It is still a challenge to the theoretical physicists to develop a reliable and efficient method, which describes the future experiments at normal and extreme conditions.

References

[1] M.R.Anastasio, L.S.Celenza, W.S.Pong and C.M.Shakin, *Phys. Report* 100(1983), 327.

[2] B.D.Serot and J.D.Walecka, *Adv. in Nucl. Phys.* 16, ed. J.W.Negele and E.Vogt (Plenum, New York, 1986).

[3] B.ter Haar and R.Malfliet, *Phys. Report* 149(1987), 207.

[4] F.Coester, S.Cohen, B.D.Day and C.M.Vincent, *Phys.Rev.* C1(1970), 769.

[5] B.D.Keister and R.B.Wiringa, *Phys.Lett.* 173B(1986), 5.

Effect of tensor coupling of ρ meson in relativistic Hartree theory for Ca isotopes *

Ma Zhongyu[1,2] and Chen Baoqiu[1]
[1)] China Institute of Atomic Energy, Beijing 102413
[2)] Institute of Theoretical Physics, Beijing 100080

The recent experimental program using radioactive nuclear beams has opened a new era in nuclear physics [1]. The study of properties of nuclei far from the stability line is an attractive topic for both experimenters and theorists, because extremely neutron rich nuclei have shown different characteristics from those of nuclei near the stability line. A new aspect of exciting findings in very neutron rich nuclei is neutron halo such as ^{11}Li and ^{11}Be in light nuclei.

The relativistic method[2] is strongly pushed by the success in describing both the properties of finite nuclei in the relativistic Hartree theory and the intermediate proton-nucleus scattering in the relativistic Brueckner Hartree-Fock approximation. Meanwhile, a great effort has been made in a nicroscopic understanding of various nuclear properties starting with interacting nucleon and meson fields within the relativistic framework. The relativistic mean field (RMF) theory with the inclusion of non-linear σ terms and the isovector- vector rho meson field terms provides extremely excellent results for the binding energies and other properties of not only the spherical nuclei. but also of some known deformed nuclei throughout the periodic table[3]. It would be interesting to extend the RMF calculations to nuclei far from the stability line and near the neutron drip line[4,5].

In this work, the isotopes of a given Z till the neutron drip line are studied in RMF using σ, ω, ρ as the interaction between nucleons. It is well known that the ρ meson (an isovector), which couples to the nucleon isospin, is

*This work was supported by The National Natural Science Foundation of China

	M (MeV)	m_σ(MeV)	m_ω(MeV)	m_ρ(MeV)	g_σ	g_ω	g_ρ
HS	939.0	520.0	783.0	770.7	10.47	13.80	4.04
TS	939.0	597.6	783.0	770.0	11.206	12.72	2.78

Table 1: The parameter sets of HS and TS, which are taken from ref.[4,5]

important for the binding energy of neutron rich (or proton rich) nuclei and the location of the neutron drip (proton drip) line. In usual RMF calculations of the stable nuclei, the contribution of the tensor coupling of ρ meson with nucleons is neglected, which is very small [4-6]. Here we emphasize that the contribution of the tensor coupling of the rho meson to binding energy for very neutron rich nuclei may not be neglected and it has not negligible contribution in the neutron drip (proton drip) line when the rate of proton and neutron number becomes very large.

Following the work of Walecka for the description of the relativistic Hartree theory [2], the effective lagrangian density can be written into two parts:

$$\mathcal{L} = \mathcal{L}^0 + \mathcal{L}^I \tag{1}$$

where $\mathcal{L}^0$ is the free lagrangian density including nucleon and meson (σ, ω, ρ) fields and has the following forms:

$$\mathcal{L}^0 = \overline{\psi}(i\,\gamma_\mu\partial_\mu - M)\psi + \frac{1}{2}(\partial_\mu\sigma\partial^\mu\sigma - m_\sigma^2\sigma) - \frac{1}{4}F_{\mu\nu}F^{\mu\nu} + \frac{1}{2}m_\omega^2\omega_\mu\omega^\mu - \frac{1}{4}\vec{G}_{\mu\nu}\cdot\vec{G}^{\mu\nu} - \frac{1}{2}m_\rho^2\vec{\rho}_\mu\cdot\vec{\rho}^\mu \tag{2}$$

where

$$F_{\mu\nu} = \partial_\nu\omega_\mu - \partial_\mu\omega_\nu$$

$$\vec{G}_{\mu\nu} = \partial_\nu\vec{\rho}_\mu - \partial_\mu\vec{\rho}_\nu$$

ψ is an SU(2) baryon field with mass M and σ, ω, $\vec{\rho}_\mu$ are the sigma, omega and rho meson field with mass m_σ, m_ω and m_ρ respectively. The interacting lagrangian density is

$$\mathcal{L}^I = -g_\sigma\overline{\psi}\sigma\psi - g_\omega\overline{\psi}\gamma_\mu\omega^\mu\psi - g_\rho\overline{\psi}\gamma_\mu\vec{\rho}^\mu\cdot\vec{\tau}\psi + \frac{f_\rho}{2M}\overline{\psi}\sigma_{\mu\nu}\partial^\nu\vec{\rho}^\mu\cdot\vec{\tau}\psi \tag{3}$$

The g_σ, g_ω and g_ρ are the NNσ, NNω and NNρ coupling constant, respectively, given in Table 1, which are taken from ref.[4,5]. In the Hartree approximation, the contribution of the pion field is zero, so it is not taken into

account. The Euler-Lagrange equation provides a Dirac equation for the nucleon and Klein-Gordon equation for the meson fields. The detail expression of the equations can be found in ref [4,5,7].

The parameter sets, HS and TS in ref.[4,5], differ in the sigma meson mass m_σ. It was determined in reproducing the meson charge radius for HS and the binding energy for TS, respectively. We can see that the values of g_ρ in HS and TS sets are slightly different. The ratio of tensor to vector coupling f_ρ/g_ρ is chosen to be 3.7 and taken the same for HS and TS. Due to the spherical model we have used, we limit our study to even-even nuclei and choose proton magic nuclei Ca.

The ρNN coupling provides an isospin dependent interaction among nucleons. The interaction produces by the ρNN vector coupling depends on the difference of neutron and proton matter densities,

$$\rho^B_{n\ or\ p} = \frac{1}{4\pi r^2} \sum_a^{N\ (\ or\ Z)} [G_a^2(r) + F_a^2(r)], \tag{4}$$

where $G_a(r)$ and $F_a(r)$ are the upper and lower components of the single particle radial wave functions. The nuclei far from the stability line have a large difference of neutron and proton matter densities. Therefore, their properties are greatly influenced by the isospin dependent interactions.[4]

Patra et al. [8] shown that the tensor coupling of the ρ do not contribute for even-even nuclei in the RMF approximation used and given an exact proof in appendix of ref.[8]. We believe that the contribution of the tensor coupling of ρ meson is not negligible for nuclei far from stability line. The reason is that the tensor coupling of ρNN depends on the tensor densities,

$$\rho^T_{n\ or\ p} = \frac{1}{4\pi r^2} \sum_a^{N\ (\ or\ Z)} 2G_a(r)F_a(r). \tag{5}$$

Though it is usually small due to the interference, the mixing terms of the vector and tensor coupling of ρ meson are not small, which mainly influence the spin-orbit interactions. In order to explore it and to show the influence, the tensor coupling of the ρ meson is included in the RMF calculations in this work. As an example, we show our numerical results for the various nuclear radii and the binding energy of Ca isotopes using TS and HS parameters in Fig 1 and 2, where solid and dashed lines denote the results calculated

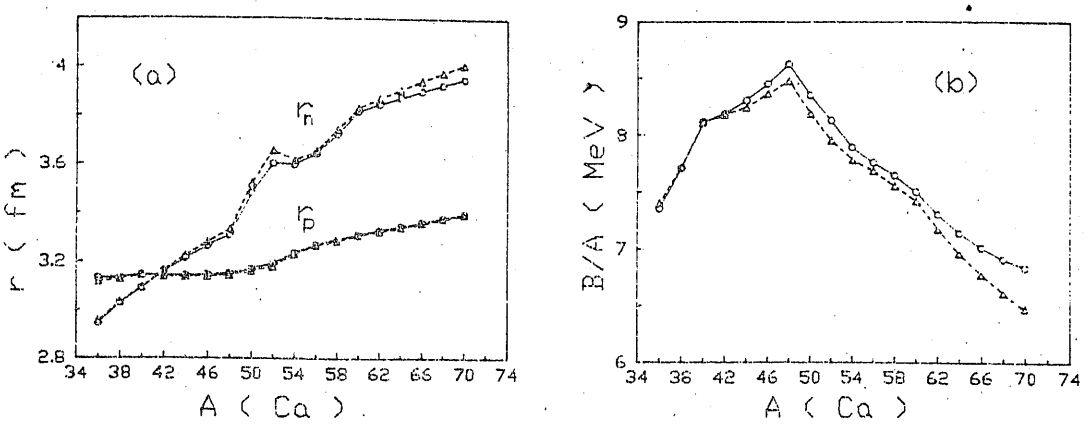

Figure 1: The nuclear properties as function of the neutron number for Ca calculated with the parameter set of TS in table 1. a) the proton and neutron root mean square radii; b) the binding energies per particle B/A. The solid (dotted) lines are for the case without (with) the tensor coupling of the ρ meson.

without and with the tensor coupling of ρ meson, respectively. Our results demonstrate that the tensor coupling of ρ meson is not negligible for neutron drip nuclei. The contribution of the tensor coupling to the binding energy becomes less bound and the neutron rms radius is expanded, when the rate of neutron and proton number becomes very large, and to the rms radii of the proton is small. We also calculate the proton and neutron density distributions for various calcium isotopes as a function of the radial coordinate r with sets HS and TS. When this work was finished, we saw a newly published paper[9], which pointed out the incorrect conclusion of no contribution from the ρ tensor coupling in ref.[8].

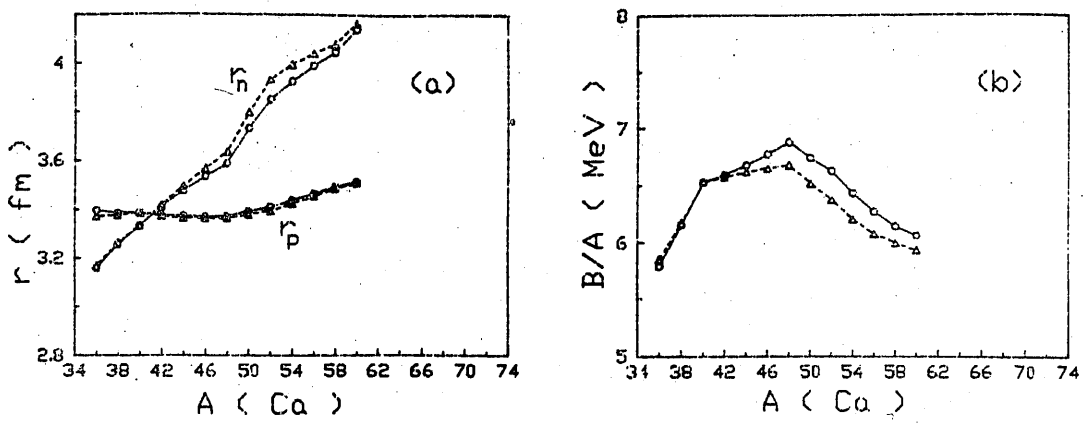

Figure 2: Same as figure 1, except for the parameter set of HS in table 1.

References

1. I. Tanihata, Nucl. Phys. A522(1991)275c
2. B. D. Serot and J.D. Walecka, Adv. Nucl. Phys. 16(1986) 1; B.D. Serot and J.D. Walecka IU/NTC 91-12.
3. Y.K. Gambir, P. Ring and A. Thimet, Ann. Phys. 198(1990) 132.
4. H. Toki, Y. Sugahara, D. Hirata, B.V. Carlson and I. Tanihata, Nucl. Phys. A524,(1991)633
5. D. Hirata, H. Toki, T. Watabe, I. Tanihata and B.V. Carlson, Phys. ReV. C44(1991)1467.
6. J.K. Zhang and D.S. Onley, Nucl. Phys. A526(1991)245
7. Chen Bao Qiu and Ma Zhong Yu , in preparation
8. S.K.Patra and C.R.Praharaj, Phys.Rev. C44(1991)2552
9. J.K.Zhang, Phys.Rev. 46(1992)1558

A functional approach to renormalization in the Walecka model

Wang Zisheng[2] Ma Zhongyu[1-3] Cai Dunjiu[2]

[1]China Center of Advanced Science and Technology(World Laboratory)
[2]China Institute of Atomic Energy
[3]Institute of Theoretical Physics,Beijing 100080,P.R.China

Abstract

A renormalized Scheme based on the functional approach is developed for exchange diagrams and meson propagators in the framework of the Walecka model. The direct and exchange diagrams in the baryon propagator are calculated self-consistently. The effects of the vacuum fluctuations generated by virtual nucleon-antinucleon pairs are included. The result is a set of finite nonlinear integral equation for the baryon self-energy and meson propagator that has to be solved self-consistently.

A model of strongly interacting nucleons and mesons was proposed by Walecka[1] and has been successful in the mean-field theory approximation (MFT) or the one-loop level ("relativistic Hartree approximation" or RHA)[1-10], where the meson fields are replaced by their ground-state expectation values at a finite density of nuclear matter. In the MFT the contribution from the Dirac sea, which includes divergent pieces, is omitted, while a renormalization procedure is performed in the RHA. The original motivation for these studies was that the MFT should become increasingly valid as the density increases and that the MFT and RHA could be good nonperturbative starting points for the calculations at a normal nuclear density[2].

It is well-known that the renormalizable meson-baryon quantum field theory provides a consistent theoretical framework for studying the dynamics of the quantum vacuum in the nuclear medium. Therefore, much work has been done to see if nuclear physics can be adequately described by a renormalizable field theory which employs effective baryonic and mesonic degrees of freedom[1-3,11-22]. To remove the divergences from the Dirac sea, Chin first suggested a diagrammatic treatment method in the RHA[3,11]. Then a functional approach to subtract the divergent terms was presented by Bielajew and Serot[2,13]. During the last a few years, a number of authors have commented on the existence of poles at space-like momenta in the

renormalizable meson–nucleon fields[13–15,17–22].

One decade ago attempts were started to solve the nuclear many–body problem in the relativistic Hartree–Fock approximation(RHF) for the popular σ,ω model[2]. These attempts up to now include self–consistent calculations[4], which keep both the direct and exchange terms, but eliminate the vacuum fluctuations, as well as the discussion of renormalization[13]. The renormalized relativistic Hartree–Fock approximation, which includes contributions from both positive–energy states in the Fermi sea and negative–energy states populating the Dirac sea, proceeds with a suitable definition of counterterms defined in terms of vacuum amplitudes.

In this letter, following the Bielajew and serot's method[2,13] we develop a renormalization technique involves expanding the propagators and self–energies in power series of the free Fermi propagator. By the power counting it is straightforward to extract the divergent terms in the expansion series. These divergent amplitudes may be isolated and removed in terms of spectral functions. A unified and formulated description of the renormalized relativistic Hartree Fock approximation is obtained.

Our considerations are based on the Walecka model [1] (σ, ω model) with Largrangian,

$$\pounds = \bar{\psi}(i\gamma_\mu \partial^\mu - M)\psi + \frac{1}{2}(\partial^\mu \varphi \partial_\mu \varphi - m_\sigma^2 \varphi^2) + \frac{1}{2} m_\omega^2 V^\mu V_\mu - \frac{1}{4} F^{\mu\nu} F_{\mu\nu}$$
$$- g_\sigma \bar{\psi}\varphi\psi - g_\omega \bar{\psi}\gamma^\mu V_\mu \psi + \delta\pounds_{CTC}, \qquad (1)$$

where ψ represents the nucleon field, while $\varphi(V_\mu)$ is the scalar (vector) meson field with mass m_σ (m_ω) and coupling constant g_σ (g_ω). $F_{\mu\nu} = \partial_\mu V_\nu - \partial_\nu V_\mu$ is the vector meson field–strength tensor. The additional term $\delta\pounds_{CTC}$ denotes counterterms that are for the purpose of renormalization.

The noninteracting baryon propagator contains two pieces,

$$G^0(k) = G_F^0(k) + G_D^0(k) = (\gamma_\mu k^\mu + M)\frac{1}{k_\nu^2 - M^2 + i\varepsilon}$$
$$+ \frac{\pi i}{E_k}(\gamma_\mu k^\mu + M)\delta(k_0 - E_k)\theta(k_F - |\mathbf{k}|), \qquad (2)$$

where $E_k = (\mathbf{k}^2 + M^2)^{\frac{1}{2}}$, $k_\nu^2 = k_0^2 - \mathbf{k}^2$ and M is the nucleon mass. G_F^0 incorporates the propagation of virtual nucleons and antinucleons. The density–de-

pendent piece G_D^0 that describes the propagation of nucleon holes in the Femi sea corrects the nucleon part of G_F^0 for the Pauli exclusion principle.

Note that the Feynman propagator satisfies following relations

$$\frac{\partial}{\partial M} G_F^0(k) = [G_F^0(k)]^2, \tag{3}$$

$$\frac{\partial}{\partial k^\mu} G_F^0(k) = -G_F^0(k)\gamma_\mu G_F^0(k). \tag{4}$$

The effect of interactions on the baryon propagation may be included to all orders by Dyson's equation,

$$G(k) = G^0(k) + G^0(k)\Sigma G(k), \tag{5}$$

where Σ is the baryon self-energy. Because of the translational and rotational invariance in the rest frame of infinite nuclear matter, the self-energy may be generally written as

$$\Sigma = \Sigma^s(k) - \gamma_\mu \Sigma^\mu(k) = \Sigma^s(k) - \gamma_0 \Sigma^0(k) + \gamma \cdot \mathbf{k}\Sigma^v(k). \tag{6}$$

The Dyson's equation (5) can be solved formally, yielding

$$G(k) = (\gamma_\mu k^{*\mu} + M^*)\left[\frac{1}{k_\nu^{*2} - M^{*2} + i\varepsilon} + \frac{\pi i}{E_k^*}\delta(k_0^* - E_k^*)\theta(k_F^* - |\mathbf{k}^*|)\right] = G_F(k^*) + G_D(k^*), \tag{7}$$

where $M^* = M + \Sigma^s$, $E_k^* = (\mathbf{k}^{*2} + M^{*2})^{\frac{1}{2}}$, $k^{*\mu} = k^\mu + \Sigma^\mu$, $k_F^* = k_F(1 + \Sigma^v)$. The propagators $G_F(k^*)$ and $G_D(k^*)$ take forms analogous to those in Eq.(2). It can be easily verified that the Feynman piece of the propagator $G_F(k^*)$ still obeys the same Dyson's equation as G(k),

$$G_F(k^*) = G_F^0(k) + G_F^0(k)\Sigma G_F(k^*). \tag{8}$$

Iterating Eq.(8), then using (3),(4) and (6), one finds

$$G_F(k^*)=\sum_{m=0}^{\infty}\sum_{l=0}^{m}\frac{1}{(m-l)!l!}(\Sigma^s\frac{\partial}{\partial M})^{m-l}(\Sigma^\mu\frac{\partial}{\partial k^\mu})^l G_F^0(k). \tag{9}$$

In the RHA, only tadpole diagrams are retained in the baryon propagator,

$$\Sigma^\mu_{\text{Hartree}}=-i\frac{g_\omega^2}{m_\omega^2}\int\frac{d^nk}{(2\pi)^n}tr\gamma^\mu G(k)=\delta^{\mu 0}\frac{g_\omega^2}{m_\omega^2}\rho_B, \tag{10}$$

$$\Sigma^s_{\text{Hartree}}=i\frac{g_\sigma^2}{m_\sigma^2}\int\frac{d^nk}{(2\pi)^n}trG(k)=i\frac{g_\sigma^2}{m_\sigma^2}\int\frac{d^nk}{(2\pi)^n}trG_F(k^*)+i\frac{g_\sigma^2}{m_\sigma^2}\int\frac{d^nk}{(2\pi)^n}trG_D(k^*), \tag{11}$$

where $\rho_B=2k_F^3/3\pi^2$ is the baryon density, n is the dimension of integrals and equal to 4 for the physical case.

The vacuum tadpole in $\Sigma^\mu_{\text{Hartree}}$ from the vector meson exchange vanishes as a result of the symmetric integration. The second term of the scalar self-energy $\Sigma^s_{\text{Hartree}}$ in Eq.(11), which is finite due to the step function $\theta(k_F^*-|\mathbf{k}^*|)$ in G_D that describes the propagation of real nucleons in the Fermi sea. While the first term generated by the propagation of virtual nucleons and antinucleons from the Dirac sea is divergent and a counterterm is required to subtract the divergence. Inserting (9) into (11), one has

$$\Sigma^s_{\text{Hartree}}=i\frac{g_\sigma^2}{m_\sigma^2}\sum_{m=0}^{\infty}\sum_{l=0}^{m}\frac{1}{(m-l)!l!}\int\frac{d^nk}{(2\pi)^n}tr[(\Sigma^s\frac{\partial}{\partial M})^{m-l}(\Sigma^\mu\frac{\partial}{\partial k^\mu})^l G_F^0(k)]$$
$$+\Sigma^s_{CTC}+\text{finite terms}. \tag{12}$$

For the physical dimension n=4, it is clear from simple power counting that only the terms with $0<m<3$ and $l=0$ in Eq.(12) are divergent(see appendix B in ref.2). These divergences may be removed by introducing a counterterm defined as,

$$\delta\mathcal{L}^{(1)}_{CTC}=\alpha_1\varphi+\frac{1}{2!}\alpha_2\varphi^2+\frac{1}{3!}\alpha_3\varphi^3+\frac{1}{4!}\alpha_4\varphi^4. \tag{13}$$

From the Feynman rules for the counterterm vertices, it is easy to see that the counterterm contributes to the scalar self–energy and yields,

$$\Sigma^{s}_{CTC} = \sum_{m=0}^{3} \frac{1}{m!} \left(\frac{g_{\sigma}^{2}}{m_{\sigma}^{2}}\right)(\Sigma^{s})^{m} \alpha_{m+1}. \tag{14}$$

To subtract the divergent terms, one finds

$$\alpha_{m} = -i\int \frac{d^{4}k}{(2\pi)^{4}} tr\left[\frac{\partial^{m-1}}{\partial M^{m-1}} G_{F}(k)\right], \quad 1 \leqslant m \leqslant 4. \tag{15}$$

Therefore, the scalar self–energy in the RHA may be rewritten as

$$\Sigma^{s}_{\text{Hartree}} = i\frac{g_{\sigma}^{2}}{m_{\sigma}^{2}} \int \frac{d^{4}k}{(2\pi)^{4}} tr[G(k)] + \sum_{m=0}^{3} \frac{1}{m!} \frac{g_{\sigma}^{2}}{m_{\sigma}^{2}} \alpha_{m+1} (\Sigma^{s})^{m}. \tag{16}$$

It is as same as Serot and Chin's result[2,3].

In the RHF, the exchange diagrams in the vacuum would lead to momentum–dependent corrections to the baryon propagator. The density dependent baryon propagator G_D gives a finite contribution to the self–energy in the loop integral, while the contribution from the Feynman propagator involves divergent integrals over the occupied negative–energy states. We may carry out the renormalization procedure for the scalar and vector meson term by term. The self–energy from the exchange contribution may be written as,

$$\Sigma_{\text{Fock}}(k) = \Sigma_{F}^{\sigma}(k^{*}) + \Sigma_{F}^{\omega}(k^{*}) + \Sigma_{\text{CTC}}^{\text{Fock}} + \text{finite terms}, \tag{17}$$

where $\Sigma_{F}^{\sigma}(k^{*})$ and $\Sigma_{F}^{\omega}(k^{*})$ are the contribution of σ and ω meson exchanges from the Dirac sea, respectively. They have the forms,

$$\Sigma_{F}^{\sigma}(k^{*}) = ig_{\sigma}^{2}\int \frac{d^{n}q}{(2\pi)^{n}} G_{F}(k^{*} + q^{*})\Delta^{0}(q), \tag{18}$$

$$\Sigma_{F}^{\omega}(k^{*}) = -ig_{\omega}^{2}\int \frac{d^{n}q}{(2\pi)^{n}} \gamma_{\mu} G_{F}(k^{*} + q^{*})\gamma_{\nu} D^{0}(q). \tag{19}$$

The noninteracting meson propagators have their standard relativistic forms,

$$\Delta^0(k) = (k_\mu^2 - m_\sigma^2 + i\varepsilon)^{-1}, \tag{20}$$

$$D_{\mu\nu}(k) = (-g_{\mu\nu} + k_\mu k_\nu / m_\omega^2) D^0(k); \quad D^0(k) = (k_\lambda^2 - m_\omega^2 + i\varepsilon)^{-1}. \tag{21}$$

We have dropped the longitudinal $k_\mu k_\nu$ term in the vector propagator, since it does not contribute to the energy density. Inserting Eq.(9) into (18) and (19), we find

$$\Sigma_F^\sigma(k^*) = ig_\sigma^2 \sum_{m=0}^{\infty} \sum_{l=0}^{m} \frac{1}{(m-l)!l!} \int \frac{d^n q}{(2\pi)^n} [(\Sigma^s \frac{\partial}{\partial M})^{m-l} (\Sigma^\mu \frac{\partial}{\partial k^\mu})^l G_F^0(k+q)] \Delta^0(q), \tag{22}$$

$$\Sigma_F^\omega(k^*) = -ig_\omega^2 \sum_{m=0}^{\infty} \sum_{l=0}^{m} \frac{1}{(m-l)!l!} \int \frac{d^n q}{(2\pi)^n} \gamma_\mu [(\Sigma^s \frac{\partial}{\partial M})^{m-l} (\Sigma^\lambda \frac{\partial}{\partial k^\lambda})^l G_F(k+q)] \times \gamma_\nu D^0(q). \tag{23}$$

From the Feynman parameter integral method and the method of dimensional regularization[23], it can easily be demonstrated that only the terms with $0 \leq m \leq 1$ and $0 \leq l \leq 1$ in Eqs.(22) and (23) are divergent for the physical dimension $n=4$. These divergences can be removed by the following counterterms for the baryon mass and wave function and also the baryon–scalar vertex,

$$\delta \mathcal{L}_{CTC}^{(2)} = M_C \bar{\psi}\psi + \zeta_N \bar{\psi}(\gamma_\mu k^\mu - M)\psi + \zeta_s \bar{\psi}\psi\varphi. \tag{24}$$

The Feynman rules for these counterterms yield

$$\Sigma_{CTC}^{Fock} = M_C + \zeta_N(\gamma_\mu k^\mu - M) + \zeta_s \Sigma^s. \tag{25}$$

Thus, with the definitions we have,

$$M_C = -ig_\sigma^2 \int \frac{d^4 q}{(2\pi)^4} G_F^0(k+q)\Delta^0(q) + ig_\omega^2 \int \frac{d^4 q}{(2\pi)^4} \gamma_\mu G_F^0(k+q)\gamma_\nu D^0(q), \tag{26}$$

$$\zeta_s = -ig_\sigma^2 \int \frac{d^4q}{(2\pi)^4} [\frac{\partial}{\partial M} G_F^0(k+q)]\Delta^0(q)$$

$$+ ig_\omega^2 \int \frac{d^4q}{(2\pi)^4} \gamma_\mu [\frac{\partial}{\partial M} G_F^0(k+q)]\gamma_\nu D^0(q), \tag{27}$$

$$\zeta_N = -ig_\sigma^2 \frac{\Sigma^\lambda}{\gamma_\kappa k^\kappa - M} \int \frac{d^4q}{(2\pi)^4} [\frac{\partial}{\partial k^\lambda} G_F^0(k+q)]\Delta^0(q)$$

$$+ ig_\omega^2 \frac{\Sigma^\lambda}{\gamma_\kappa k^\kappa - M} \int \frac{d^4q}{(2\pi)^4} \gamma_\mu [\frac{\partial}{\partial k^\lambda} G_F^0(k+q)]\gamma_\nu D^0(q). \tag{28}$$

As a result, the self–energy of the Fock term may be rewritten as

$$\Sigma_{\text{Fock}} = ig_\sigma^2 \int \frac{d^4q}{(2\pi)^4} G(k+q)\Delta^0(q) - ig_\omega^2 \int \frac{d^4q}{(2\pi)^4} \gamma_\mu G(k+q)\gamma_\nu D^0(q)$$

$$+ M_C + \zeta_N(\gamma_\mu k^\mu - M) + \zeta_s \Sigma^s. \tag{29}$$

We now apply the technique in the precedings to the meson propagator. The one–loop scalar poplarization insertion is given by

$$\Pi_s(q) = -ig_\sigma^2 \int \frac{d^n k}{(2\pi)^n} tr[G(k)G(k+q)] = \Pi_s^F(q) + \Pi_s^D(q). \tag{30}$$

The nucleon–antinucleon pair $N\bar{N}$ contribution to Π_s, labeled as Π_s^F, involves the integral of $G_F(k^*)G_F(k^*+q^*)$, which is divergent. The particle–hole contribution(Π_s^D) corrects the $N\bar{N}$ contribution for Pauli blocking. It contains at least one G_D in the loop integral and is finite.

$$\Pi_s^F(q) = -ig_\sigma^2 \int \frac{d^n k}{(2\pi)^n} tr[G_F(k^*)G_F(k^*+q^*)], \tag{31}$$

$$\Pi_s^D(q) = -ig_\sigma^2 \int \frac{d^n k}{(2\pi)^n} tr[G_F(k^*)G_D(k^*+q^*) + G_D(k^*)G_F(k^*+q^*)$$

$$+ G_D(k^*)G_D(k^*+q^*)]. \tag{32}$$

Applying Eqs.(9) to (31), one has

$$\Pi_s^F(q) = -ig_\sigma^2 \sum_{m=0}^{\infty} \sum_{j=0}^{m} \sum_{i=0}^{\infty} \sum_{l=0}^{i} \frac{1}{(m-j)!j!} \frac{1}{(i-l)!l!}$$

$$\times \int \frac{d^n k}{(2\pi)^n} tr[(\Sigma^s \frac{\partial}{\partial M})^{m-j} (\Sigma^\mu \frac{\partial}{\partial k^\mu})^j G_F^0(k) (\Sigma^s \frac{\partial}{\partial M})^{i-l} (\Sigma^\mu \frac{\partial}{\partial k^\mu})^l G_F^0(k+q)]. \tag{33}$$

Similary, we use the Feynman parameter integral and the method of dimensional regularization[23]. For the physical dimension n = 4, it is clear that the divergent terms in Eq.(33) are only

$$\text{divergent terms} = -ig_\sigma^2 \int \frac{d^4 k}{(2\pi)^4} tr\{[1 + \Sigma^s \frac{\partial}{\partial M} + \frac{1}{2}(\Sigma^s \frac{\partial}{\partial M})^2$$

$$+ \Sigma^\mu \frac{\partial}{\partial k^\mu} + \frac{1}{2}(\Sigma^\mu \frac{\partial}{\partial k^\mu})^2][G_F^0(k) G_F^0(k+q)]\}. \tag{34}$$

According to Eq.(34), the required counterterms include φ^2, φ^3, φ^4 terms ,which shifts M→ M*. In addition, there are other two counterterms that are required to subtract the divergence in the momentum–dependent terms.

$$\delta \mathcal{L}_{CTC}^{(3)} = \frac{1}{2!} \alpha'_2 \varphi^2 + \frac{1}{3!} \alpha'_3 \varphi^3 + \frac{1}{4!} \alpha'_4 \varphi^4 + \zeta_1 \varphi \gamma_\mu \partial^\mu \varphi + \zeta_2 \varphi \partial_\mu \partial^\mu \varphi. \tag{35}$$

Their contributions can be written explicitly as

$$(\Pi_s(q))_{CTC} = \alpha'_2 + \alpha'_3 \Sigma^s + \frac{1}{2} \alpha'_4 (\Sigma^s)^2 + \zeta_1 \gamma_\mu q^\mu + \frac{1}{2} \zeta_2 q_\mu^2. \tag{36}$$

where

$$\alpha'_2 = ig_\sigma^2 \int \frac{d^4 k}{(2\pi)^4} tr[G_F^0(k) G_F^0(k+q)], \tag{37}$$

$$\alpha'_3 = ig_\sigma^2 \int \frac{d^4 k}{(2\pi)^4} tr\{\frac{\partial}{\partial M}[G_F^0(k) G_F^0(k+q)]\}, \tag{38}$$

$$\alpha'_4 = ig_\sigma^2 \int \frac{d^4 k}{(2\pi)^4} tr\{\frac{\partial^2}{\partial M^2}[G_F^0(k) G_F^0(k+q)]\}, \tag{39}$$

$$\zeta_1 = ig_\sigma^2 \frac{1}{\gamma_\lambda q^\lambda} \int \frac{d^4 k}{(2\pi)^4} tr\{\Sigma^\mu \frac{\partial}{\partial k^\mu}[G_F^0(k) G_F^0(k+q)]\}, \tag{40}$$

$$\zeta_2 = ig_\sigma^2 \frac{1}{q_\lambda^2} \int \frac{d^4k}{(2\pi)^4} tr\{(\Sigma^\mu \frac{\partial}{\partial k^\mu})^2 [G_F^0(k) G_F^0(k+q)]\}. \quad (41)$$

It is clear by power counting that the counterterms of Eq.(36) remove the divergence in (33) and render the scalar meson polarization Π_s finite. The finite result has the form,

$$\Pi_s(q) = -ig_\sigma^2 \int \frac{d^4k}{(2\pi)^4} tr[G(k)G(k+q)] + \sum_{l=0}^{2} \frac{1}{l!} \alpha'_{l+2} (\Sigma^s)^l + \zeta_1 \gamma_\lambda q^\lambda + \frac{1}{2} \zeta_2 q_\mu^2 \quad (42)$$

Next we consider the vector meson propagator. The polarization insertion $\Pi_{\mu\nu}$ is decomposed into an $N\bar{N}$ ($\Pi_{\mu\nu}^F$) and a particle–hole contribution ($\Pi_{\mu\nu}^D$). The $N\bar{N}$ piece is made finite ($\Pi_{\mu\nu}^{RF}$) by subtracting an appropriate counter–term $(\Pi_{\mu\nu}^F)_{CTC}$,

$$\Pi_{\mu\nu}^{RF}(q) = ig_\omega^2 \int \frac{d^4k}{(2\pi)^4} tr[\gamma_\mu G_F(k^*) \gamma_\nu G_F(k^* + q^*)] + (\Pi_{\mu\nu}^F(q))_{CTC}. \quad (43)$$

By analogy, inserting Eq.(9) into (43) and then subtracting divergent terms, we can find that its contribution to vector meson propagator is written explicitly by

$$\Pi_{\mu\nu}(q) = ig_\omega^2 \int \frac{d^4k}{(2\pi)^4} tr[\gamma_\mu G(k) \gamma_\nu G(k+q)] + (\Pi_{\mu\nu}^F(q))_{CTC}. \quad (44)$$

where

$$\begin{aligned}(\Pi_{\mu\nu}^F(q))_{CTC} = & -ig_\omega^2 \int \frac{d^4k}{(2\pi)^4} tr[\gamma_\mu G_F^0(k) \gamma_\nu G_F^0(k+q)] \\ & - ig_\omega^2 \int \frac{d^4k}{(2\pi)^4} tr\{\Sigma^\lambda \frac{\partial}{\partial k^\lambda} [\gamma_\mu G_F^0(k) \gamma_\nu G_F^0(k+q)]\} \\ & - ig_\omega^2 \int \frac{d^4k}{(2\pi)^4} tr\{(\Sigma^\lambda \frac{\partial}{\partial k^\lambda})^2 [\gamma_\mu G_F^0(k) \gamma_\nu G_F^0(k+q)]\}. \end{aligned} \quad (45)$$

This renormalization procedure will naturally guarantee the current conservation relation and Lorentz covariance.

The method presented above is essentially to extract the divergence by expanding propagator $G_F(k^*)$ around $M^* = M$ and $k^* = k$ in nuclear matter. Following the power counting it is easy to find that only first a few terms in this expansion are divergent. To render the expressions finite, a few suitable defined counterterms in terms of vacuum amplitudes are added to remove the divergence.

For the purpose of this letter, we restrict ourselves to describe the effects of vacuum fluctuations in the σ,ω model. It may be straightforward to include other mesons for renormalization in the relativistic many-body theory.

Reference

1.J.D.Walecka,Ann.of Phys.83(1974)491.
2.B.D.Serot and J.D.Walecka,Adv.Nucl.Phys.16,1(1986).
3.S.A.Chin,Ann.of Phys.108(1977)301.
4.C.J.Horowitz and B.D.Serot,Nucl.Phys.A399(1983)529.
5.A.Bouyssy et al.,Rhys.Rev.C36(1987)380.
6.Bernard ter Haar and Rudi Malflict,Phys.Reps.149(1987)207.
7.M.R.Anastasio et al.,Phys.Reps.100(1983)327.
8.C.J.Horowitz,Nucl.Phys.A412(1984)228.
9.Ma Zhongyu et al.,Nucl.Phys.A490(1988)619.
10.M.S.Hussin et al.,Phys.Reps. 201(1991)279.
11.S.A.Chin,Phys.Lett.B62(1976)263.
12.B.D.Serot and J.D.Walecka,Phys.Lett.B87(1979)172.
13.A.F.Bielajew and B.D.Serot,Ann. of Phys.156(1984)215.
14.R.J.Furnstahl,R.J.Perry and B.D.Serot,Phys.Rev.C40(1989)321.
15.R.Friedrich,K.Wehrberger and F.Beck,Phys.Rev.C46(1992)188.
16.C.J.Horowitz,Phys.Lett.B140(1984)181.
17.R.J.Perry,Phys.Lett.B182(1986)269.
18.V.Soni,Phys.Lett.B183(1987)91.
19.T.D.Cohen,M.K.Banerjerjee and C.Y.Ren,Phys.Rev.C36(1987)1653.
20.R.J.Furnstahl and C.J.Horowitz,Nucl.Phys.A485(1988)632.
21.K.Wehrberger and F.Beck,Nucl.Phys.A491(1989)587.
22.Xiangdong Ji,Phys.Lett.B219(1989)143.
23.G.'t Hooft and M.Veltman,Nucl.Phys.B44(1972)189.

Description of the Pion Inelastic Scattering to the Excited State with Negative parity

Yuxin Liu[a,b], Yushun Zhang[a,c], Hongzhou Sun[b,d], and Enguang Zhao[a,b]
[a]CCAST(World Laboratory), P. O. Box 8730, Beijing 100080, China
[b]Institute of Theoretical Physics, Academia Sinica,
P. O. Box 2735, Beijing 100080, China*
[c]Institute of High Energy Physics, Academia Sinica,
P. O. Box 918(4-1), Beijing 100039, China
[d]Department of Physics, Tsinghua University, Beijing 100084, China

December 18, 1992

Abstract

An approach to describe the medium energy pion inelastic scattering from nucleus with an excitation to a negative parity state is proposed by combining the Eikonal approximation with the {spdf} Interacting Boson Model. The calculated differential cross sections of the $\pi^{\pm}-^{118}Sn$ and $\pi^{\pm}-^{152}Sm$ scattering exciting the target from 0_1^+ to 3_1^- state and the deformation parameters of the 3_1^- state agree with experimental data quite well.

Distrorted wave impulse approximation(DWIA) has made considerable successes in describing hadron-nucleus scattering at high energy. However, for some scattering from collective nuclei, DWIA is not accurate at high momentum transfer[1]. Ginocchi et al[2] have devoloped a simple scheme combining the Interacting Boson Model(IBM)[3] and the Glauber or Eikonal approximation[4,5] and applied it to study the electron[6], photon[7], proton[2] and pion[8] elastric scatterings and the inelastric scatterings from ground state to positive parity excited states. The results are encouraging. Untill now, however, there are still no discussion on the pion inelastric scatterings from ground state to negative parity excited state[9-11] in this scheme. Therefore, our purpose in this letter is to apply the scheme to describe this kind of transition. in order to do this, instead of the usual IBM, we have to combine the {spdf} IBM[12-13] with Eikonal approximation.

In the Eikonal Approximation theory[5],for the scattering from a target with an initial state $\{L_i,M_i\}$ to a final state $\{L_f,M_f\}$ the scattering amplitude F in the isospin

*Mailing address

space $\overrightarrow{\tau}$ ($\overrightarrow{\tau} = \mathrm{T} + \overrightarrow{\phi}$ is the operator of total isospin, and T, $\overrightarrow{\phi}$ represent the isospin operators of the nucleus and pion) can be expressed as

$$F^{(\tau)}_{L_f M_f L_i M_i}(q) = ik(-i)^{M_f}\int_0^{\infty} J_{M_f}(q,b)\{\delta_{fi} - e^{-\overline{\psi}^{(\tau)}_0(b)}\langle L_f M_f|e^{-\hat{\psi}^{(\tau)}_l(\mathrm{b})}|L_i M_i\rangle\}bdb \quad (1)$$

where $\mathbf{k}$ is the incident momentum, $\mathbf{q}$ is the momentum transfer, $\mathbf{b}$ is the impact parameter, J_{M_f} is the Bessel function of rank $|M_f|$, $\overline{\psi}^{(\tau)}_0(b)$ is elastic profile function which can be written as

$$\overline{\psi}^{(\tau)}_0(b) = \frac{i}{2k}\int_{-\infty}^{+\infty}(k^2 + \frac{1}{2}\nabla^2)\tilde{\rho}^{(\tau)}_0(r)dz \quad (2)$$

with

$$\begin{aligned}\tilde{\rho}^{(\tau)}_0 &= \lambda^{(1)}_0\rho_0(r) + \gamma^{(1)}(\tau)\lambda^{(1)}_1\rho'_0(r)\\ \rho_0(r) &= (N+Z)\rho^{(i)}_0(r)\\ \rho'_0(r) &= (N-Z)\rho^{(i)}_0(r)\end{aligned} \quad (3)$$

where $\gamma^{(1)}(\tau)$ are C-G coefficients(the values were listed in ref.[14]), $\lambda^{(1)}_0$ and $\lambda^{(1)}_1$ are the isoscalor, isovector parameters of pion-nucleus optical potential respectively[14]. $\rho^{(i)}_0(r)$ is the ground state density for proton or neutron. $\hat{\psi}^{(\tau)}_l(\mathbf{b})$ is the excitation function. It can be expressed as

$$\hat{\psi}^{(\tau)}_l(\mathbf{b}) = \varepsilon^{\tau}_l(\mathbf{b})\cdot\hat{O}^{(l)} \quad (4)$$

in which $\varepsilon^{\tau}_l(\mathbf{b})$ is the transition profile function. $\hat{O}^{(l)}$ is the transition operator of 2^l-pole transition.

For the scattering exciting the target from the ground state to a negative parity state, the excitation is usually recongnized as the electric octupole excitation, i.e.,$\hat{\psi}^{(\tau)}_l(\mathbf{b}) = \hat{\psi}^{(\tau)}_3(\mathbf{b})$.

Assuming that the collective states of the target nucleus can be described in the framework of {spdf}IBM, the most general Hamiltonian involving one-body and two-body interactions of the bosons can be expressed as

$$H = \sum_{l=0}^{3}\varepsilon_l\hat{n}_l + \sum_{L=0}^{6}\kappa_L\hat{Q}^{(L)}\cdot\hat{Q}^{(L)} + \sum_{L=0}^{5}\kappa'_L\hat{O}^{(L)}\cdot\hat{O}^{(L)} \quad (5)$$

where $\hat{n}_l = \sum_\mu b^{\dagger}_{l\mu}b_{l\mu}$ is the nubmer of the boson with spin l. $\hat{Q}^{(L)}_q$, $\hat{O}^{(L)}_q$ are the 2^l-pole magnetic, electric (L=odd) or electric, magnetic(L=even) transition operators respectively, and they can be given as

$$\hat{Q}^{(L)}_q = [1 + (\chi^{(2)}_{dd} - 1)\delta_{L2}](d^{\dagger}\tilde{d})^{(L)}_q + \sum_{\substack{l_1,l_2\\ l_1\le l_2\\ l_1+l_2=even}}\chi^{(L)}_{l_1l_2}[b^{\dagger}_{l_1}\tilde{b}_{l_2} + b^{\dagger}_{l_2}\tilde{b}_{l_1}(1-\delta_{l_1l_2})]^{(L)}_q \quad (6)$$

$$\hat{O}^{(L)}_q = (s^{\dagger}\tilde{p} + p^{\dagger}\tilde{s})^{(1)}_q\delta_{L1} + (s^{\dagger}\tilde{f} + f^{\dagger}\tilde{s})^{(3)}_q\delta_{L3} + \sum_{\substack{l_1,l_2\\ l_1<l_2\\ l_1+l_2=odd}}\chi^{(L)}_{l_1l_2}[b^{\dagger}_{l_1}\tilde{b}_{l_2} + b^{\dagger}_{l_2}\tilde{b}_{l_1}]^{(L)}_q \quad (7)$$

The states of a nucleus can be labelled by the irreducible representations of the group chain

$$U_{spdf}(16) \supset (U_{sd}(6) \supset U_d(5) \supset O_d(5) \supset O_d(3)) \otimes (U_{pf}(10) \supset (U_p(3) \otimes U_f(7)) \supset (O_p(3) \otimes (O_f(7) \supset O_f(3)) \supset O_{pf}(3)) \supset O_{pdf}(3) \tag{8}$$

It means that the basis of the states can be expressed as

$$|LM\rangle^{\pi} = |N[n_{sd}]n_d\nu_d\alpha_d L_d[n_{pf}](n_p L_p n_f \nu_f \alpha_f L_f) L_{pf} L^{\pi} M\rangle \tag{9}$$

The energy spectra and the wave functions of the nucleus can be determined by diagonalizing the Hamiltonian (5) in the space spanned by eq.(9).

Combining the Eikonal approximation theory with the {spdf}IBM, $\hat{\psi}_l^{(\tau)}(\mathbf{b})$ can be written as

$$\hat{\psi}_3^{(\tau)}(\mathbf{b}) = \varepsilon_3^{(\tau)}(\mathbf{b}) \cdot [(s^{\dagger}\tilde{f} + f^{\dagger}\tilde{s})^{(3)} + \chi_{pd}^{(3)}(p^{\dagger}\tilde{d} + d^{\dagger}\tilde{p})^{(3)} + \chi_{df}^{(3)}(d^{\dagger}\tilde{f} + f^{\dagger}\tilde{d})^{(3)}] \tag{10}$$

The octupole excitation profile function is given as

$$\varepsilon_{3\mu}^{(\tau)}(\mathbf{b}) = \frac{i}{2k}\int_{-\infty}^{+\infty}\left[k^2 + \frac{1}{2}\left(\frac{\partial^2}{\partial r^2} + \frac{2}{r}\frac{\partial}{\partial r} - \frac{12}{r^2}\right)\right]\tilde{\alpha}_3^{(\tau)}(r) C_{\mu}^3(\theta,\varphi) dz \tag{11}$$

where

$$\begin{aligned} \tilde{\alpha}_3^{(\tau)}(r) &= \lambda_0^{(1)}\alpha_3(r) + \gamma^{(1)}(\tau)\lambda_1^{(1)}\alpha_3'(r) \\ \alpha_3(r) &= (N+Z)\alpha_3^{(i)}(r) \\ \alpha_3'(r) &= (N-Z)\alpha_3^{(i)}(r) \end{aligned} \tag{12}$$

$$C_{\mu}^3(\theta,\varphi) = \sqrt{\frac{4\pi}{7}} Y_{3\mu}(\theta,\varphi) \tag{13}$$

$\alpha_3^{(i)}(r)$ can be taken as the Tassie form[15] $\alpha_3^{(i)}(r) = \omega_3^{(i)} r \frac{d}{dr}\rho_0^{(i)}(r)$. in which $\omega_3^{(i)}$ is the structure function of octupole excitation. It is something like the octupole deformation parameter. In accordence with the normalization condition, $\omega_3^{(i)}$ can be determined by the experimental data B(E3) with relation

$$\begin{aligned} &B(E3, 0_1^+ \to L^-) = \left[\int_0^{\infty} \alpha_3^{(i)}(r) r^5 dr\right]^2 \\ &\left[\langle L^- \parallel (s^{\dagger}\tilde{f} + f^{\dagger}\tilde{s})^{(3)} + \chi_{pd}^{(3)}(p^{\dagger}\tilde{d} + d^{\dagger}\tilde{p})(3) + \chi_{df}^{(3)}(d^{\dagger}\tilde{f} + f^{\dagger}\tilde{d})^{(3)} \parallel 0_1^+\rangle\right]^2 \end{aligned} \tag{14}$$

According to the characteristic of octupole deformation, $\varepsilon_{3\mu}^{(\tau)}(\mathbf{b})$ have four nonvanished components. They can be decided with eq.(11). Under the peripheral approximation z=0, $\varepsilon_{3\mu}^{(\tau)}(\mathbf{b})$ has only one independent nonvanished component

$$\varepsilon_{31}^{(\tau)}(\mathbf{b}) = \frac{i}{2k}\int_{-\infty}^{+\infty}\left[k^2 + \frac{1}{2}\left(\frac{\partial^2}{\partial r^2} + \frac{2}{r}\frac{\partial}{\partial r} - \frac{12}{r^2}\right)\right]\frac{\sqrt{3}}{4}\tilde{\alpha}_3^{(\tau)}(r) dz \tag{15}$$

and

$$\varepsilon_{33}^{(\tau)}(\mathbf{b}) = -\sqrt{\frac{5}{3}}\varepsilon_{31}^{(\tau)}(\mathbf{b}) \tag{16}$$

Because many-$\{f,p\}$ boson state has not been observed experimentally[16], the positive parity state of nuclei can be regarded as the state with zero-$\{f,p\}$ bosons, and the negative parity state as one-$\{f,p\}$ boson. Then the scattering matrix element can be simply given as

$$\langle N[N-1]n_d\nu_d\alpha_d L_d[1](n_pL_pn_fL_f)L_{pf}L^-M|e^{-i\hat{\psi}_i^{(\tau)}(\mathbf{b})}|Nn_d=L_d=n_{pf}=L_{pf}=L=0\rangle$$
$$=\sqrt{N!}C_{(N-1)n_d\nu_d}\alpha^{N-1-n_d}(\gamma^{(2)}\cdot\gamma^{(2)})^{\frac{n_d-\nu_d}{2}}$$
$$\sum_{m_dM_{pf}}\langle L_dM_dL_{pf}M_{pf}|LM\rangle C_{L_{pf}M_{pf}}B_{\nu_d\alpha_dL_dM_d}(\gamma_0^{(2)},\gamma_2^{(2)}) \tag{17}$$

where

$$C_{(N-1)n_d\nu_d}=\left[\frac{(2\nu_d+3)!!}{(N-1-n_d)!(\frac{n_d-\nu_d}{2})!(n_d+\nu_d+3)!!}\right]^{1/2} \tag{18}$$

$$C_{L_{pf}M_{pf}}=\begin{cases}\beta^{(1)}_{M_{pf}} & (L_{pf}=1)\\ \delta^{(3)}_{M_{pf}} & (L_{pf}=3)\end{cases} \tag{19}$$

$$B_{\nu_d\alpha_dL_dM_d}(\gamma_0^{(2)},\gamma_2^{(2)})=\frac{1}{\nu_d!}([\nu_d]\nu_d\alpha_dL_dM_d|(\gamma^{(2)}\cdot d^\dagger)^{\nu_d}|0\rangle \tag{20}$$

$$\begin{aligned}\alpha&=ch\lambda_0\\ \beta^{(1)}_\mu&=\frac{\xi^{(1)}_\mu}{\lambda_0^2}(\frac{sh\lambda_0}{\lambda_0}-1)\\ \gamma^{(2)}_\mu&=\frac{\xi^{(2)}_\mu}{\lambda_0^2}(1-ch\lambda_0)\\ \delta^{(3)}_\mu&=(-1)^{1+\mu}\frac{\varepsilon^{(\tau)}_{3\mu}(\mathbf{b})}{\lambda_0}sh\lambda_0+\frac{\xi^{(3)}_\mu}{\lambda_0^2}(\frac{sh\lambda_0}{\lambda_0}-1)\end{aligned} \tag{21}$$

$$\lambda_0=\left[-\varepsilon^{(\tau)}_{30}(\mathbf{b})^2+2\varepsilon^{(\tau)}_{31}(\mathbf{b})^2-2\varepsilon^{(\tau)}_{32}(\mathbf{b})^2+2\varepsilon^{(\tau)}_{33}(\mathbf{b})^2\right]^{1/2} \tag{22}$$

$$\begin{aligned}\xi^{(1)}_\mu&=\chi^{(3)}_{pd}\sum_{m_2m_3}(-1)^{m_3}\varepsilon^{(\tau)}_{3m_3}\xi^{(2)}_{m_2}\langle 1\mu 2m_2|3m_3\rangle\\ \xi^{(2)}_\mu&=\chi^{(3)}_{df}\sum_{m_3m_3'}(-1)^{3+m_3'}\varepsilon^{(\tau)}_{3m_3}\varepsilon^{(\tau)}_{3m_3'}\langle 2\mu 3m_3|3m_3'\rangle\\ \xi^{(3)}_\mu&=\chi^{(3)}_{df}\sum_{m_2m_3}(-1)^{m_3}\varepsilon^{(\tau)}_{3m_3}\xi^{(2)}_{m_2}\langle 3\mu 2m_2|3m_3\rangle\end{aligned} \tag{23}$$

Because all the discussions up to now are performed in the isospin space, one should make a transformation from isospin space to the physical channels before a cross section can be calculated

$$\begin{aligned}F^{(\pi^+)}_{L_fM_f00}(q)&=\tfrac{1}{T+1}F^{(T)}_{L_fM_f00}(q)+\tfrac{1}{(T+1)(2T+1)}F^{(T+1)}_{L_fM_f00}(q)+\tfrac{2T-1}{2T+1}F^{(T-1)}_{L_fM_f00}(q)\\ F^{(\pi^-)}_{L_fM_f00}(q)&=F^{(T+1)}_{L_fM_f00}(q)\end{aligned} \tag{24}$$

Finally the differential cross section from the ground state to the L_f state is

$$|\frac{d\sigma}{d\Omega}|^{(\zeta)} = \sum_{M_f} |F^{(\zeta)}_{L_f M_f 00}(q)|^2 \tag{25}$$

where ζ refers to π^- or π^+.

With this approach we describe the $\pi^\pm - ^{118}Sn$ and $\pi^\pm - ^{152}Sm$ inelastic scattering which excite the target from 0_1^+ state to 3_1^- state. In the calculations, the isoscalar parameter $\lambda_0^{(1)}$ and isovector parameter $\lambda_1^{(1)}$ are determined from free pion-nucleus scattering phase shifts[17]. The ground state proton and neutron density distributions in the nucleus are taken from electron scattering experiments, i.e., $\rho_0^{(i)}(r) = \rho_0 / \left[1 + exp\left(\frac{r-R^{(i)}}{a^{(i)}}\right)\right]$, where $R^{(i)}$ is the nuclear radius at half density and $a^{(i)}$ is the thickness parameter.

When the energy spectra and electromagnetic transition rates are reproduced pretty well, we get the matrix elements $\langle 3^- \parallel (s^\dagger \tilde{f} + f^\dagger \tilde{s})^{(3)} + \chi_{pd}^{(3)}(p^\dagger \tilde{d} + d^\dagger \tilde{p})^{(3)} + \chi_{df}^{(3)}(d^\dagger \tilde{f} + f^\dagger \tilde{d})^{(3)} \parallel 0_1^+ \rangle$ for ^{118}Sn and ^{152}Sm as shown in table 1. With the parameters in table 2 and eq.(14) we get the octupole deformation parameters of ^{118}Sn and ^{152}Sm as shown in table 3. Figures 1 and 2 are the calculated differential cross sections of $\pi^\pm - ^{118}Sn$ and $\pi^\pm - ^{152}Sm$ scattering with excitation from 0_1^+ to 3_1^- state and the comparisons with experiments and DWIA calculation results.

Table 1. The matrix elements of E3 transition of ^{118}Sn and ^{152}Sm

	^{118}Sn	^{152}Sm
Matrix Element	5.992	8.3667

Table 2. The parameters of ^{118}Sn and ^{152}Sm

	$a^{(i)}$(fm)	$R^{(i)}$(fm)	B(E3)$\uparrow(e^2fm^6)$
^{118}Sn	0.54	5.275	1.75×10^5
^{152}Sm	0.581	5.804	1.36×10^5

Table 3. The calculated results of $\omega_3^{(i)}$ of ^{118}Sn and ^{152}Sm and the comparison with experiments

	Calculated	Experimental
^{118}Sn	0.177	0.168^a
^{152}Sm	0.117	0.12^b

[a] taken from ref.[18], [b] taken from ref.[9]

From table 3 and figures 1 and 2, we know that without adjusting any parameters the calculated results agree with experiments pretty well. It shows that, with the negative parity boson f and p being taken into account, the inelastic scattering exciting the nucleus from the ground state to a negative parity state can be described quite well in the scheme of combining the Eikonal approximation and the IBM as well as the scattering preserving the parity.

This work is partly supported by the National Natural Science Foundation of China. Helpful discussions with Professor Jimin Hu, Professor Qizhi Han and Professor Mei Zhang are acknowledged with thanks. The authors are grateful to CCAST for their hospitality and supports.

REFERENCES

[1] M. L. Barlett, J. A. McGill, L. Ray, M. M. Barlett, G. W. Hoffmann, N. M. Hintz, G. S. Kybe, M. A. Franey andG. Blanpied, Phys. Rev. **C22** (1980) 408.

[2] J. N. Ginocchio, T. Otsuka, R. D. Amado and D. A. Sparrow, Phys. Rev. **C33** (1986) 247; J. N. Ginocchio, G. Wenes,R. D. Amado, D. C. Cook, N. H. Hintz and M. M. Gazzaly, Phys. Rev. **C36** (1987) 2436; L. Zuffi, G. Maino and A. Ventura , Phys. Rev. **C34**, (1984) 1223.

[3]A. Arima and F. Iachello,Ann. Phys. (N. Y.) **99** (1976) 253; ibid,111 (1978) 201; ibid, 123 (1979) 468.

[4] R. J. Glauber, in: Lecture in Theoretical Physics, eds, W. E. Britten and L. G. Bunham (Interscience, New York, 1959),Vol. 1, p.315.

[5]S. J. Wallace, Ann. Phys. (N. Y.) **78** (1973) 190.

[6] A. E. L. Dieperink, F. Iachello,A. Rinat and C. Creswell, Phys. Lett. **76B** (1978) 135; G. Wenes, T. Otsuka and J. N. Ginocchio, Phys. Rev. **C37** (1988) 1878.

[7] G. Maino, A. Ventura, L. Zuffi and F. Iachello, Phys. Lett. **152B** (1985) 17.

[8] Y. S. Zhang and Y. X. Liu, Commun. Theor. Phys. in press.

[.9] C. L. Morris and S. J. Seestrom Morris, Phys. Rev. **C28** (1983) 2165.

[10] J. L. Ullmann, et.al., Phys. Rev. **C35** (1987) 1099.

[11] N. M. Hintz, et.al., Phys. Rev. **C45** (1992) 601.

[12] J. Engel and F. Iachello, Phys. Rev. Lett. **54** (1985) 1126; ibid, Nucl. Phys. **A472** (1987) 61.

[13] H. Z. Sun, M. Zhang and Q. Z. Han, Chinese J. Nucl. Phys. **13** (1991) 1211.

[14] M. B. Johnson, Phys. Rev. **C22** (1980) 192; M. B. Johnson and E. R. Siciliano, Phys. Rev. **C27** (1983) 1647.

[15]L. T. Tassie, Austral. J. Phys. **9** (1965) 407; P. Ring and P. Schuck, The Nuclear Many-Body Problems (Springer-Verlag, 1980).

[16]R. Julin, J. Kantele, et.al., in: Symmetries and Nuclear Structure, eds, R. A. Meyer and V. Paar (Harwood Academic, Switzerland, 1987).

[17] G. A. Miller and J. E. Spencer, Ann. Phys. (N. Y.) 100 (1976) 562.

[18]R. H. Spear, At. Data Nucl. Data Tables, **42** (1989) 55.

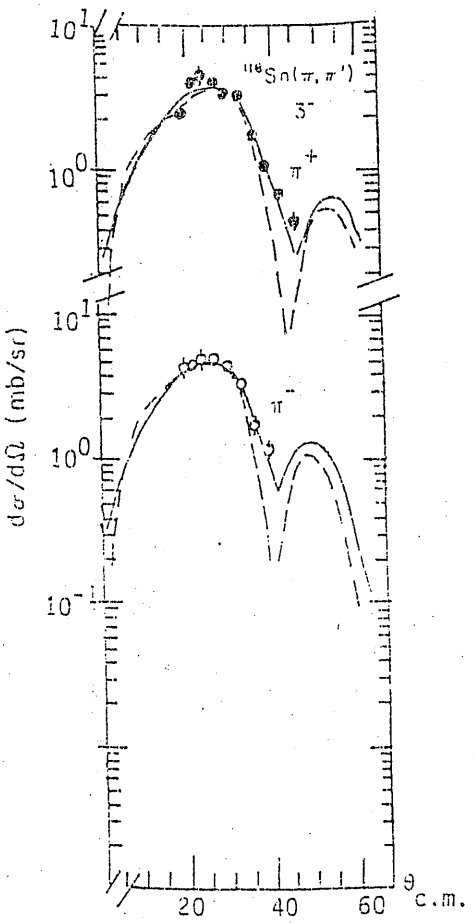

Figure 1: Comparison of the present calculated result(solid curves) of the differential cross section for the inelastric scattering of 163MeV $\pi^{\pm} - {}^{118}Sn$ with an excitation from 0_1^+ state to 3_1^- state with the experimental data(Ref.[10]). The dashed curves are taken from DWIA.

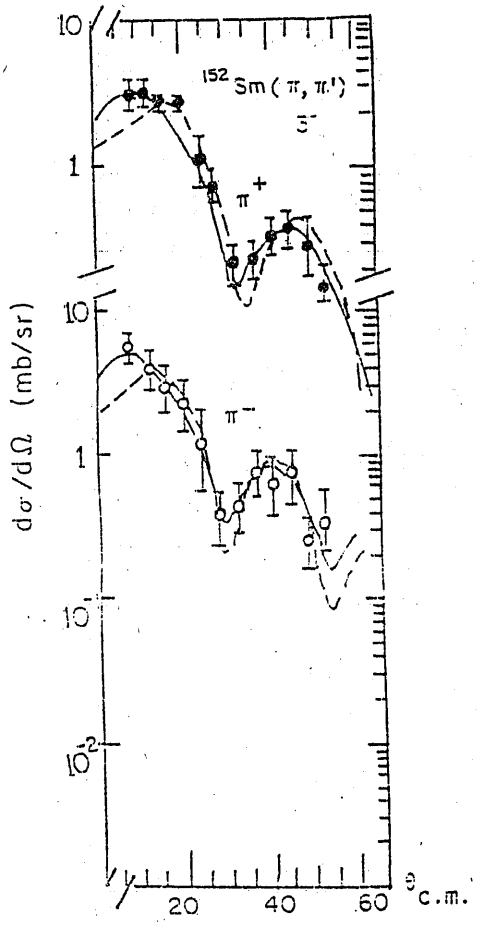

Figure 2: Comparison of the present calculated result(solid curves) of the differential cross section for the inelastric scattering of 180MeV $\pi^{\pm} - ^{152}Sm$ with an excitation from 0_1^+ state to 3_1^- state with the experimental data(Ref.[9]). The dashed curves are taken from DWIA.

PHENOMENOLOGICAL ANALYSIS AND MICROSCOPIC STRUCTURE OF "IDENTICAL" SUPERDEFORMED BANDS

ZENG JINYAN (曾謹言)[1,2,3] AND LEI YI'AN (雷奕安)[3]

[1] *(China Center of Advanced Science and Technology (World Laboratory), Center of Theoretical Physics, P. O. Box 8730, Beijing 100080, China)*

[2] *(Institute of Theoretical Physics, Chinese Academy of Science, Beijing 100080, China)*

[3] *(Department of Physics, Peking University, Beijing 100871, PRC)*

ABSTRACT

A reliable phenomenological analysis of superdeformed (SD) bands shows that the so-called "identical" SD bands in general may have different bandhead moments of inertia ($\delta J_0/J_0 \geq 10^{-2}$). Because the dynamic moment of inertia $J^{(2)}$ varies with ω much faster than the kinematic moment of inertia $J^{(1)}$, and the ω variation of moments of inertia may be quite different for various SD bands, under certain conditions a near equality of $J^{(2)}$ (hence E_γ) of two "identical" SD bands may occur in certain frequency range ($|\delta E_\gamma/E_\gamma| = |\delta J^{(2)}/J^{(2)}| \sim 10^{-3}$), and the angular momentum alignments may appear to be approximately quantized. But the situation turns out to be different in other frequency regions. The present phenomenological analysis seems to be consistent with the configuration assignments made by the available microscopic theory in the framework of strong-coupling model. No pseudospin symmetry is involved in present analysis.

Key words: identical SD bands, kinematic and dynamic moments of inertia, angular momentum alignment, signature splitting, pseudo-spin symmetry.

Recent years have seen tremendous progress in experimental [1] and theoretical [2] studies of nuclear superdeformed (SD) rotational bands. One of the most amazing properties of SD bands is the discovery of "identical" SD bands in some adjacent nuclei [3–5], i. e., the observed cascade $E2$ γ transition energies of SD bands in some adjacent nuclei are almost identical within certain frequency range [3, 4]

$$\delta E_\gamma / E_\gamma \sim 10^{-3}, \tag{1}$$

which implies that their dynamic moments of inertia are almost equal. This fact seems very difficult to understand in classical models. For example, according to the rigid-body or irrotational fluid model, the difference in moment of inertia δJ of adjacent nuclei (assuming the same deformation) is

$$\delta J / J = \delta A / A \sim 10^{-2}, \tag{2}$$

where A is the nuclear mass number. Stephens et al. [4, 5] argued that the very similar SD bands can be characterized as having virtually identical moments of inertia, but different augular momentum alignments, and the difference in angular momentum alignment seems to be quantized (multiples of $\hbar/2$). Stephens et al. considered this phenomenum may be attributed to the pseudo-spin symmetry [6], which has raised serious debate and comments [7, 8]. Until now, the essense of identical SD bands still remains a puzzle.

But, *does the near equality of transition energies observed actually imply a near equality of moments of inertia?* In other words, *does the "identical" SD bands really have identical moments of inertia (bandhead moment of inertia, kinematic and dynamic moments of inertia and their variation with ω, etc.)?* To account for the near equality of transition energies, this paper presents a serious phenomenological analysis, which seems to be consistent with the available microscopic calculations [9, 10, 11] and in which no pseudospin symmetry is involoved.

One of the most serious difficulties in experimental studies on nuclear SD bands is that so far the angular momenta of SD band can not be measured, heuce we can not extract the kinematic moment of inertia $J^{(1)}$ and angular momentum alignment directly from the observed E_γ. Using the usual expression for rotational spectra

$$E(I) = \frac{\hbar^2}{2J} I(I+1), \tag{3}$$

$E2$ γ transition energies can be expressed as (strictly speaking, the momentum of inertia J is I-dependent)

$$E_\gamma(I) \equiv E(I) - E(I-2) = \frac{\hbar^2}{2J}(2I-1). \tag{4}$$

If the angular momenta have been assigned, the kinematic moment of inertia can be extracted from the observed E_γ as follows,

$$J^{(1)}(I-1) = (2I-1)\hbar^2/E_\gamma(I). \tag{5}$$

The difference in E_γ's of two neighboring γ-rays is

$$\Delta E_\gamma(I) \equiv E_\gamma(I+2) - E_\gamma(I) = 4\hbar^2/J, \tag{6}$$

and the dynamic moment of inertia is usually extracted by,

$$J^{(2)}(I) = 4\hbar^2/\Delta E_\gamma(I), \tag{7}$$

where there is no need to know the angular momenta.

Becker et al. [12] developed a method to determine the angular momenta of SD band; i. e., the dynamic moments of inertia $J^{(2)}$ are least squares fit to the Harris three-parameter ω^2-expansion, and then integrated with ω to get the angular momenta. There has been some comments on this method [7, 8]. The main defect of this method in application is its rather large uncertainty about the angular momentum assignment due to the large error in measured ΔE_γ. In refs. [13—15] was presented a more effective and convenient method to determine the angular momenta of SD band. The angular momenta of most SD bands observed in the $A \sim 190$ and 150 regions have been determined by making use of this method. Thus, we can make a thorough analysis of the moments of inertia and angular momentum alignments of SD bands, particularly the "identical" SD bands in the $A \sim 190$ region to clarify the essence of "identical" SD bands.

It is seen from eq. (7) that the near equality of E_γ's of two "identical" SD bands, no doubt, implies the near equality of their dynamical momets of inertia $J^{(2)}$. However, it should be emphasized that the near equality of the E_γ's of "identical" SD bands are established experimentally only in certain angular frequency range [4, 5] (e. g. in $A \sim 190$ region, it is established only within $\hbar\omega \sim 0.2$—0.4 MeV), which, therefore, does not imply the near equality of $J^{(2)}$ outside this range, particularly does not imply the equality of

bandhead moments of inertia J_0. Moreover, it does not imply the near equality of kinematic moments of inertia $J^{(1)}$.

As illustrative examples, let us analyze the SD bands observed in ^{194}Hg and ^{192}Hg, which have been addressed quite widely [4, 5, 12]. To obtain more reliable information on the moments of inertia, in stead of the ab expression adopted in refs. [14] and [15], we will use an improved expression for rotational spectra (abc formula) [18]

$$E(I) = a\left[\sqrt{1 + bI(I+1)} - 1\right] + cI(I+1). \tag{8}$$

The ab formula can be derived from the Bohr Hamiltonian with suitable potential energy under the assumption of small nuclear axial asymmetry [16, 17]. The last term on the right side of eq. (8) is introduced by considering the effect of higher order term (β^4) in the potential energy of Bohr Hamiltonian [18] (to first order perturbation). According to eq. (8), the corresponding kinematic and dynamic moments of inertia are given by

$$\hbar^2/J^{(1)} = ab[1 + bI(I+1)]^{-1/2} + 2c, \tag{9}$$

$$\hbar^2/J^{(2)} = ab[1 + bI(I+1)]^{-3/2} + 2c, \tag{10}$$

and the bandhead moment of inertia is

$$J_0 = \hbar^2/(ab + 2c). \tag{11}$$

The observed E_γ's of the four SD bands, ^{192}Hg and ^{194}Hg(1, 2, 3), are least squares fit by eq. (8), and the results are given in Table 1. It is seen that all the observed transition energies of sixty-nine γ-rays are reproduced incredibly well ($|E_\gamma^{\rm cal} - E_\gamma^{\rm exp}| \leq 0.5$keV). Therefore, the moments of inertia calculated by eqs. (9—10) (using the adjusting parameters a, b and c) are very reliable and more accurate than those extracted by the difference quotient expressions (5) and (7). In Fig. 1 is shown the comparison of the ω variation of the moments of inertia for the SD bands ^{194}Hg(1), (2), (3) and ^{192}Hg. Usually, the yrast SD bands of ^{192}Hg is considered to be identical with the excited SD bands ^{194}Hg(2, 3), but not with the yrast SD band of ^{194}Hg (^{194}Hg(1)).

Let us analyze the bandhead moment of inertia J_0, which is intimately connected with the intrinsic structure (configuration) of SD band at $\omega = 0$ [9—11], particularly depends on the components of high-N intruder configurations [21]. The extracted J_0's (using eq. (11)) of the SD bands in ^{192}Hg and ^{194}Hg are as follows:

Table 1 Comparison of the calculated and observed E_γ's for the SD bands ^{192}Hg and ^{194}Hg(1, 2, 3).

I	^{192}Hg, $\alpha = 0$ $E_\gamma(I)$		^{194}Hg(1), $\alpha = 0$ $E_\gamma(I)$		^{194}Hg(2), $\alpha = 0$ $E_\gamma(I)$		^{194}Hg(3), $\alpha = 1$ $E_\gamma(I+1)$	
	expt [12]	calc	expt [19]	calc	expt [20]	calc	expt [20]	calc
48		881.7		868.1		863.8		879.5
46		852.7	841.0	840.7		835.8		851.3
44		823.3	812.9	812.7	(807)	807.0		822.4
42	793.4	793.4	783.9	784.1	777.7	777.6	(793)	793.0
40	762.8	763.0	754.6	754.9	747.6	747.5	762.7	762.8
38	732.1	732.1	725.4	725.0	716.7	716.6	732.2	732.0
36	700.6	700.6	693.8	594.3	684.5	684.9	700.4	700.4
34	668.6	668.5	662.4	662.9	652.2	652.4	668.0	668.1
32	635.8	635.7	630.5	630.6	619.3	619.2	635.1	635.0
30	602.3	602.1	597.3	597.4	585.2	585.1	600.9	601.2
28	567.9	567.7	563.6	563.3	550.3	550.1	566.4	566.6
26	532.4	532.4	528.3	528.2	514.3	514.4	531.6	531.2
24	496.3	496.3	492.3	492.2	477.7	477.8	494.6	495.0
22	459.1	459.1	455.2	455.1	440.7	440.5	458.3	458.1
20	420.8	420.9	417.1	416.9	402.1	402.3	420.4	420.3
18	381.6	381.7	377.8	377.8	363.7	363.4	382.1	381.3
16	341.1	341.4	337.7	337.6	323.8	323.8	342.8	342.6
14	299.9	300.0	296.2	296.4	283.3	283.5	302.5	302.8
12	257.7	257.7	254.3	254.3	242.7	242.7	262.3	262.3
10	214.6	214.4		211.4	201.3	201.3		221.3
8		170.3		167.8		159.4		179.8
6		125.5		123.6		117.2		137.9
4		80.1		78.8		74.7		95.7
2		34.4		33.8		32.1		53.2
a(keV)		6597.3		10855		22052		19241
$b \times 10^4$		8.168		5.796		3.102		3.297
c(keV)		3.043		2.498		1.923		2.153

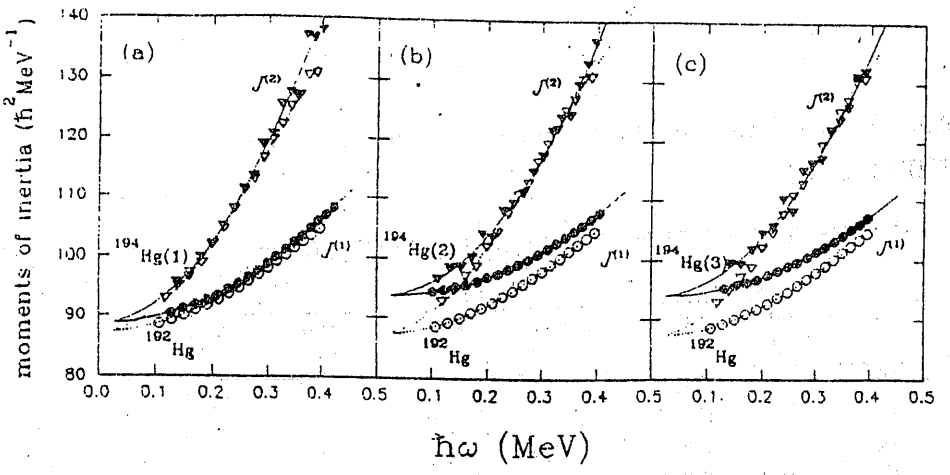

Fig. 1 The ω variation of the moments of inertia of SD bands ^{194}Hg(1, 2, 3) and ^{192}Hg. The calculated moments of inertia using eqs. (9) and (10) are denoted by solid (for ^{194}Hg) and dotted (for ^{192}Hg) curves. The moments of inertia extracted directly from the observed E_γ's using eqs. (5) and (6) are marked by • (^{194}Hg, $\mathcal{J}^{(1)}$), ▼ (^{194}Hg, $\mathcal{J}^{(2)}$), ∘ (^{192}Hg, $\mathcal{J}^{(1)}$), and ▽ (^{192}Hg, $\mathcal{J}^{(2)}$), respectively.

SD bands	^{192}Hg	^{194}Hg(1)	^{194}Hg(2)	^{194}Hg(3)
$J_0(\hbar^2\text{MeV}^{-1})$	87.15	88.59	93.57	93.89

It is clearly seen that the J_0's of the signature partner SD bands, ^{194}Hg(2, $\alpha = 0$) and ^{194}Hg(3, $\alpha = 1$), are very similar ($\delta J_0/J_0 \sim 10^{-3}$), which is not surprising because both SD bands have the same configuration structure at $\omega = 0$. However, it is quite astounding that the difference in J_0's of the usually called "identical" SD bands, ^{192}Hg and ^{194}Hg(2, 3), is rather large ($\delta J_0/J_0 \sim 7\%$), quite similar to the difference in J_0's of ground bands in normally-deformed even-even nuclei ($(\delta J_0/J_0 > 10^{-2})$). On the contrary, the difference in J_0 of the yrast SD bands ^{192}Hg and ^{194}Hg(1), though usually not considered as identical, is much smaller ($\delta J_0/J_0 \sim 1.6\%$), i.e.

$$J_0(^{194}\text{Hg}(1)) - J_0(^{192}\text{Hg}) \ll J_0(^{194}\text{Hg}(2,\ 3)) - J_0(^{192}\text{Hg}).$$

Similarly, it is found that within the observed ω-range, (see Fig. 1)

$$\mathcal{J}^{(1)}(^{194}\text{Hg}(1)) - \mathcal{J}^{(1)}(^{192}\text{Hg}) \ll \mathcal{J}^{(1)}(^{194}\text{Hg}(2,\ 3)) - \mathcal{J}^{(1)}(^{192}\text{Hg}),$$

which is qualitatively consistent with the microscopic calculations for these SD bands. In fact, according to refs. [2, 9—11], both the neutron and proton configurations of the SD

bands ^{192}Hg and ^{194}Hg(1) (at $\omega = 0$) are considered as quasi-particle vacuum, and their high-N components are $\pi 6^4 \nu 7^4$ (π and ν denote proton and neutron respectively, $\pi 6^4$ means that there are four protons occupying the N=6 major shell, $\nu 7^4$ means that there are four neutons occupying the N=7 major shell). Therefore, it is understandable that both SD bands have very similar J_0 values. On the contrary, the configurations of the excited SD bands ^{194}Hg(2, 3) are assigned to be "^{192}Hg core"$\otimes$[ν624 9/2]$\otimes$[ν512 5/2]; i. e., there are two unpaired neutrons occupying the orbits [624 9/2] and [512 5/2]. The blocking effects of unpaired neutrons lead to a larger bandhead moment of inertia for ^{194}Hg(2, 3) than that of ^{192}Hg.

But how can we account for the observed fact that the γ transition energies of "identical" SD bands are almost equal? The essential points are: (a) The near equality is established only in a limited range of frequencies (or angular momenta). (b) In the same SD band the dynamic moment of inertia $J^{(2)}$ changes with increasing ω much more rapidly than the kinematic moment of inertia $J^{(1)}$. (c) The ω variation of the moments of inertia of two "identical" SD bands may be different. Therefore, though the bandhead moments of inertia of two "identical" SD bands are different ($\delta J_0/J_0 > 10^{-2}$), under certain conditions (see below), their $J^{(2)}$'s may be very similar within certain frequency range, hence $\delta E_\gamma/E_\gamma \sim 10^{-3}$. As a rough estimate, using eq. (4), we have

$$\frac{\delta E_\gamma}{E_\gamma} = \frac{\delta I}{I} - \frac{\delta J}{J}. \tag{12}$$

For "identical" SD bands in adjacent nuclei [22], $\delta I/I \sim 1/2I \sim 10^{-2}$. Therefore, if δI and δJ are of the same sign and the difference in kinematic moments of inertia (within certain frequency range) keeps $|\delta J/J| \sim 10^{-2}$), two terms on the right-hand side of eq. (12) may cancel with each other, resulting in

$$\left|\frac{\delta E_\gamma}{E_\gamma}\right| = \left|\frac{\delta J^{(2)}}{J^{(2)}}\right| \sim 10^{-3}. \tag{13}$$

Two beautiful examples are displayed in Fig. 1(b) and (c). From Fig. 1 it is seen that $J_0(^{192}\mathrm{Hg}) < J_0(^{194}\mathrm{Hg}(2,\ 3))$ and within the observed frequency range, $J^{(1)}(^{192}\mathrm{Hg}) < J^{(1)}(^{194}\mathrm{Hg}(2,\ 3))$. However, because $J^{(2)}$ increases with ω much more rapidly than $J^{(1)}$, and in the range $\hbar\omega < 0.4$ MeV the moments of inertia of the SD band ^{192}Hg increase with ω faster than ^{194}Hg(2, 3), it is found that $J^{(2)}(^{192}\mathrm{Hg}) \approx J^{(2)}(^{194}\mathrm{Hg}(2,3))$ holds well within the frequency range $\hbar\omega \sim$(0.2—0.4) MeV as observed ($\delta J^{(2)}/J^{(2)} \sim 10^{-3}$). However, it is

seen that in the range $\hbar\omega < 0.2$ MeV and $\hbar\omega > 0.4$ MeV the calculated $J^{(2)}(^{192}\mathrm{Hg}) < J^{(2)}(^{194}\mathrm{Hg}(2,3))$, just as have been observed in the range $\hbar\omega \sim$ (0.1—0.2) MeV. What afford one much food for thought is, though usually the SD bands ^{192}Hg and ^{194}Hg(1) are not considered as identical, the behavior of their moments of inertia ($J^{(1)}$ and $J^{(2)}$) is quite similar, which implies their quite similar intrinsic structure.

Microscopic calculations [2, 9—11] show that, in the $A \sim 190$ region, there exist a stable SD valley in the potential energy surface even for $I = 0$, which implies that the SD band may extend to $I = 0$ state. In view of the excellent agreement between the calculated E_γ's by the *abc* expression and the observation (see Table. 1), the predicted E_γ values for the γ-rays (not yet observed) in the ranges $I < 10$ and $I > 43$ are meaningful. From Table 1, it is seen that

$$\begin{aligned} & \left|\frac{1}{2}\left[E_\gamma(I+1,\ ^{194}\mathrm{Hg}(3)) + E_\gamma(I-1,\ ^{194}\mathrm{Hg}(3))\right| - E_\gamma(I,\ ^{192}\mathrm{Hg})\right| \\ \approx\ & \left|E_\gamma(I,\ ^{194}\mathrm{Hg}(2)) - E_\gamma(I,\ ^{192}\mathrm{Hg})\right| \gg \left|E_\gamma(I,\ ^{194}\mathrm{Hg}(1)) - E_\gamma(I,\ ^{192}\mathrm{Hg})\right| \end{aligned}$$

However, if we compare $E_\gamma(I+1,\ ^{194}\mathrm{Hg}(3))$ with $E_\gamma(I,\ ^{192}\mathrm{Hg})$, it is found that in the spin range $I \sim$18—42 the following relation holds rather well (deviations not exceeding 1 keV, except for I=24, 28, and 30)

$$E_\gamma(I+1,\ ^{194}\mathrm{Hg}(3,\ \alpha=1)) = E_\gamma(I,\ ^{192}\mathrm{Hg}(\alpha=0)) \tag{14}$$

which is just the reason why people called them as identical SD bands. But, this is only an apparent phenomenon occuring in a limited range of angular momenta. In fact, just as have been observed in the spin range $I \sim$ 10—20, the calculted $E_\gamma(I,\ ^{192}\mathrm{Hg})$'s for $I < 10$ become smaller than the corresponding $E_\gamma(I+1,\ ^{194}\mathrm{Hg}(3))$'s, but become larger than $E_\gamma(I+1,\ ^{194}\mathrm{Hg}(3))$ for $I > 40$.

In Fig. 3 are displayed the angular momentum alignments $I_x = \omega J^{(1)}$ of the three SD bands in ^{194}Hg relative to the SD band ^{192}Hg,

$$i(\omega) = I_x(\omega,\ ^{194}\mathrm{Hg}) - I_x(\omega,\ ^{192}\mathrm{Hg}). \tag{15}$$

Indeed it is seen that $i(\omega) = I_x(\omega,\ ^{194}\mathrm{Hg}(2,3)) - I_x(\omega,\ ^{192}\mathrm{Hg}) \approx 1$ holds in the range $\hbar\omega \approx$ 0.2—0.4 MeV. However, significant deviation of i from 1 occurs in the ranges $\hbar\omega \approx$ 0.1—0.2 MeV (observed), $\hbar\omega < 0.1$ MeV and $\hbar\omega > 0.4$ MeV (not yet observed). In sharp contrast to this, no quantized spin-alignment difference is found for the SD band ^{194}Hg(1) relative to

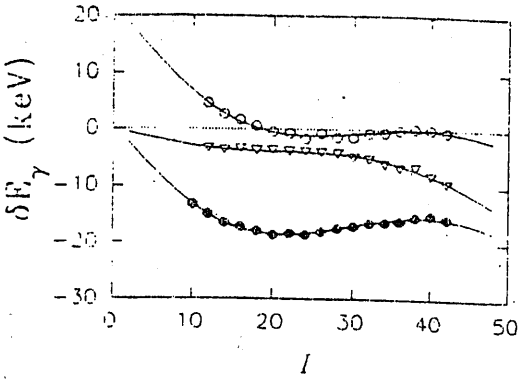

Fig. 2 $\delta E_\gamma = E_\gamma(^{194}\mathrm{Hg}) - E_\gamma(^{192}\mathrm{Hg},\ I)$. The observed δE_γ's for the SD bands ^{194}Hg(1, 2, 3) are denoted by ▽, •, and ◦, respectively. The solid lines are the calculated results using eq. 8.

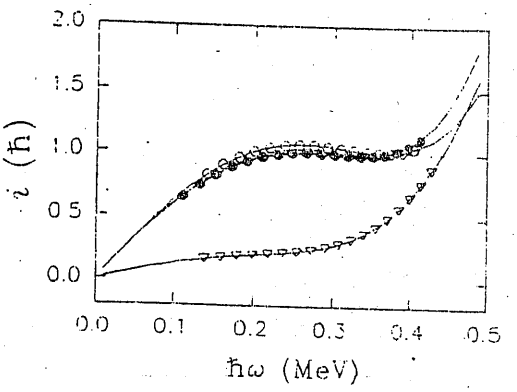

Fig. 3 The same as Fig. 2, but for the angular momentum alignment, $i = I_x(^{194}\mathrm{Hg},\ \omega) - I_x(^{192}\mathrm{Hg},\ \omega)$.

the SD band ^{192}Hg, which reflects that the high-N components of both SD bands gradually change with increasing ω.

So far in the Hg isotopes thirteen SD bands have been observed, six of which (^{194}Hg(1), ^{193}Hg(1), ^{192}Hg, ^{191}Hg(1), ^{190}Hg, ^{189}Hg) are yrast SD bands, and the remainding seven (^{193}Hg(4), and signature partners ^{194}Hg(2, 3), ^{193}Hg(2, 3), and ^{191}Hg(2, 3)) are excited SD bands. Usually, the three signature partners are considered as identical with the SD band ^{192}Hg, and their spin alignments relative to ^{192}Hg are approximately quantized ($i \approx 1$) within the range $\hbar\omega \sim 0.2$—0.4 MeV. Table 2 shows the systematic comparison of the observed and calculated (using eq. (8)) E_γ's of the three signature partners. It can be seen that the agreement is excellent ($|E_\gamma^{\mathrm{cal}} - E_\gamma^{\mathrm{exp}}| \leq 0.5$ keV). It is found that for both the observed and calculated E_γ's, the following relations hold quite well,

$$\begin{aligned}
&\frac{1}{2}\left[E_\gamma(^{191}\mathrm{Hg}(2),\ I+1/2) + E_\gamma(^{191}\mathrm{Hg}(3),\ I-1/2)\right] \\
&= \frac{1}{2}\left[E_\gamma(^{193}\mathrm{Hg}(2),\ I+1/2) + E_\gamma(^{193}\mathrm{Hg}(3),\ I-1/2)\right] = E_\gamma(^{194}\mathrm{Hg}(2),\ I) \\
&\frac{1}{2}\left[E_\gamma(^{191}\mathrm{Hg}(2),\ I-1/2) + E_\gamma(^{191}\mathrm{Hg}(3),\ I+1/2)\right] \\
&= \frac{1}{2}\left[E_\gamma(^{193}\mathrm{Hg}(2),\ I-1/2) + E_\gamma(^{193}\mathrm{Hg}(3),\ I+1/2)\right] = E_\gamma(^{194}\mathrm{Hg}(3),\ I) \qquad (16)
\end{aligned}$$

Table 2 Comparison of the calculated and observed E_γ's for the signature partner SD bands, ^{191}Hg(2, 3), ^{193}Hg(2, 3) and ^{194}Hg(2, 3).

	$E_\gamma(I+1/2)$, $\alpha=1/2$				$E_\gamma(I)$, $\alpha=0$		$E_\gamma(I-1/2)$, $\alpha=-1/2$				$E_\gamma(I+1)$, $\alpha=1$	
	^{191}Hg(2)		^{193}Hg(2)		^{194}Hg(2)		^{191}Hg(3)		^{193}Hg(3)		^{194}Hg(3)	
I	expt [22]	calc	expt [23]	calc	expt [23]	calc	expt [22]	calc	expt [23]	calc	expt [23]	calc
48						863.6						879.5
46				846.3		835.6						851.3
44				817.1	807.0	807.0		798.5				822.4
42		793.5		787.4	777.7	777.6		768.9			793.0	793.0
40		762.9	756.6	757.0	747.6	747.5		738.5		744.3	762.7	762.8
38		731.4	726.3	726.0	716.7	716.6	707.5	707.4		711.6	732.2	732.0
36	699.2	699.1	694.5	694.3	684.5	684.9	675.2	675.4		678.5	700.4	700.4
34	666.0	666.0	661.6	661.8	652.2	652.4	642.6	642.6	645.0	644.9	668.0	668.1
32	631.9	632.0	628.6	628.7	619.3	619.2	609.2	609.0	611.0	610.7	635.1	635.0
30	596.9	597.2	595.0	594.7	585.2	585.1	574.3	574.6	575.4	576.0	600.9	601.2
28	561.8	561.5	559.9	560.0	550.3	550.1	539.5	539.4	540.7	540.8	566.4	566.6
26	525.1	525.1	524.9	524.5	514.3	514.4	503.3	503.3	504.7	504.8	531.6	531.2
24	488.1	488.0	488.1	488.1	477.7	477.8	466.5	466.5	468.7	468.2	494.6	495.0
22	449.9	450.1	451.0	451.0	440.7	440.5	429.1	428.9	431.5	430.9	458.3	458.1
20	411.5	411.6	412.9	413.0	402.1	402.3	390.2	390.5	392.7	392.9	420.4	420.3
18	372.5	372.4	374.2	374.3	363.7	363.4	351.6	351.5	353.5	354.1	382.1	381.8
16	332.9	332.6	334.2	334.9	323.8	323.8	311.8	311.8	314.7	314.6	342.8	342.6
14	292.0	292.3	294.9	294.7	283.3	283.5		271.5	274.6	274.4	302.5	302.8
12		251.4	254.5	254.0	242.7	242.7		230.7	233.7	233.5	262.3	262.3
10		210.2		212.6	201.3	201.3		189.4		192.0		221.3
8		168.6		170.7		159.4		147.7		150.0		179.8
6		126.7		128.4		117.2		105.8		107.5		137.9
4		84.6		85.8		74.7		63.5		64.6		95.7
2		42.3		42.9		32.1						53.2
a(keV)		61411		15181		22052		3726.2		5115.9		19241
$b \times 10^4$		1.594		3.908		3.102		10.00		7.604		3.297
c(keV)		4004		2.405		1.923		3.552		3.447		2.153

The comparison of the moments of inertia of SD bands, ^{194}Hg(2, 3), ^{193}Hg(2, 3) and ^{191}Hg(2, 3) is displayed in Fig. 4. In Figs. 5 and 6 is shown the ω variation of the moments of inertia of SD bands ^{193}Hg(1, 2, 3) and ^{191}Hg(1, 2, 3), in which also is shown the SD band ^{192}Hg as a reference. The corresponding augular momentum alignments of ^{193}Hg(1, 2, 3) and ^{191}Hg(1, 2, 3) relative to ^{192}Hg are displayed in Figs. 7 and 8. It is seen that:
(a) The bandhead moments of inertia of signature partner SD bands are very similar:

SD band	^{191}Hg(2, 3)	^{193}Hg(2, 3)	^{194}Hg(2, 3)
J_0 ($\hbar^2$MeV^{-1})	94.45, 94.34	93.09, 92.72	93.57, 93.89
$(\delta J_0/J_0)\times 10^3$	1.1	3.8	3.4

(b) Almost no signature splitting in moments of inertia is observed for the signature partners ^{193}Hg(2, 3) and ^{194}Hg(2, 3), but there exist a relatively large signature splitting for ^{191}Hg(2, 3), which may be qualitatively understood from their configuration structures (see below).
(c) Though the bandhead moments of inertia J_0 of ^{193}Hg(2, 3) and ^{191}Hg(2, 3) differ significantly from that of ^{192}Hg ($\delta J_0/J_0 \sim 6$—7%), the dynamic moments of inertia $J^{(2)}$ of ^{193}Hg(2, 3) and ^{191}Hg(2, 3) are nearly equal to that of ^{192}Hg in the frequency range $\hbar\omega \sim 0.2$—0.4 MeV, and the spin alignments (relative to ^{192}Hg) are approximately quantized ($i \approx 1$). However, when $\hbar\omega < 0.2$ MeV, systematic differences in their $J^{(2)}$'s occur and and systematic deviations of spin alignment i from 1 occur.

The phenomenological analysis of the SD bands in ^{193}Hg and ^{191}Hg given above is helpful for studying their configuration structure. According to the calculations made in Refs. [2, 9, 10, 11], there exists a gap in the neutron single-particle level scheme at N=112, around which are distributed the following single-particle energy levels (most of them having larger Ω values):

$\cdots$, [642 3/2$^+$], [761 3/2$^-$], $\|N=112\|$, [624 9/2$^+$], [512 5/2$^-$], [752 5/2$^-$], [514 7/2$^-$], $\cdots$

According to the analysis by Meyer et. al. [11], the configurations of the four SD bands in ^{193}Hg nucleus (at $\omega = 0$) may be considered as a valence neutron coupled with the "^{192}Hg core" (or "^{194}Hg core"). The valence neutron occupies the following orbitals:

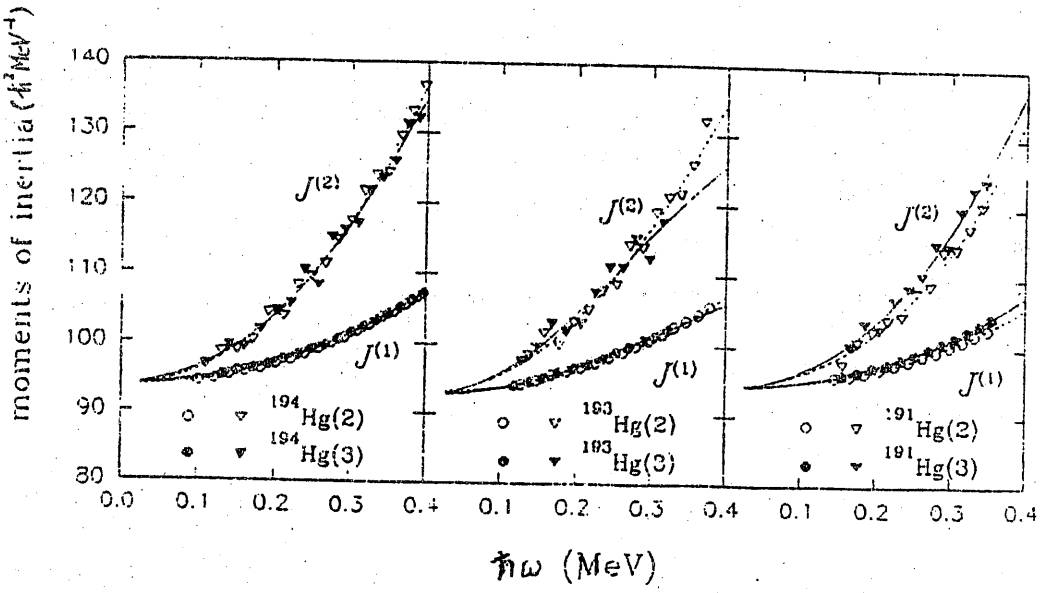

Fig. 4 Comparison of the ω variation of the moments of inertia for the signature partner SD bands, ^{194}Hg(2, 3), ^{193}Hg(2, 3) and ^{191}Hg(2, 3) (cf. Fig. 1).

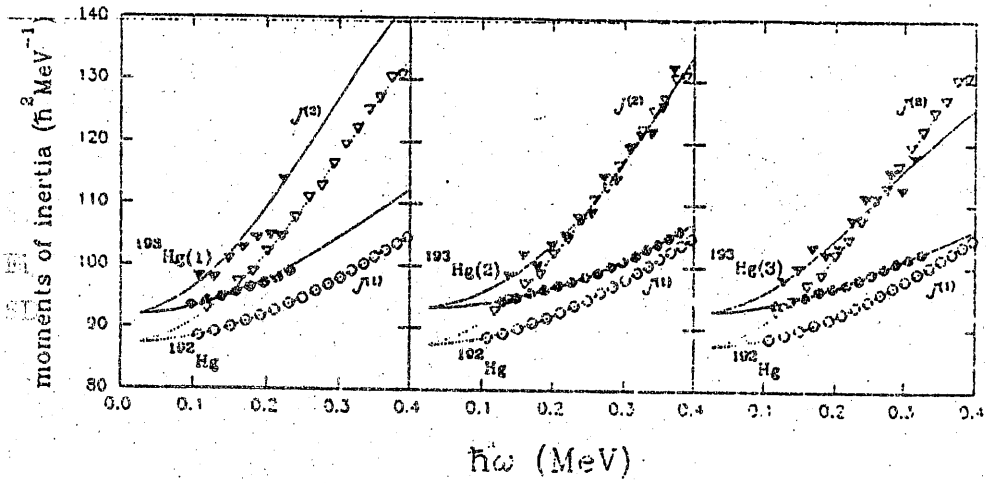

Fig. 5 The ω variation of the moments of inertia of the SD bands ^{193}Hg(1, 2, 3). As a reference, the SD band ^{192}Hg is also presented (cf. Fig. 1).

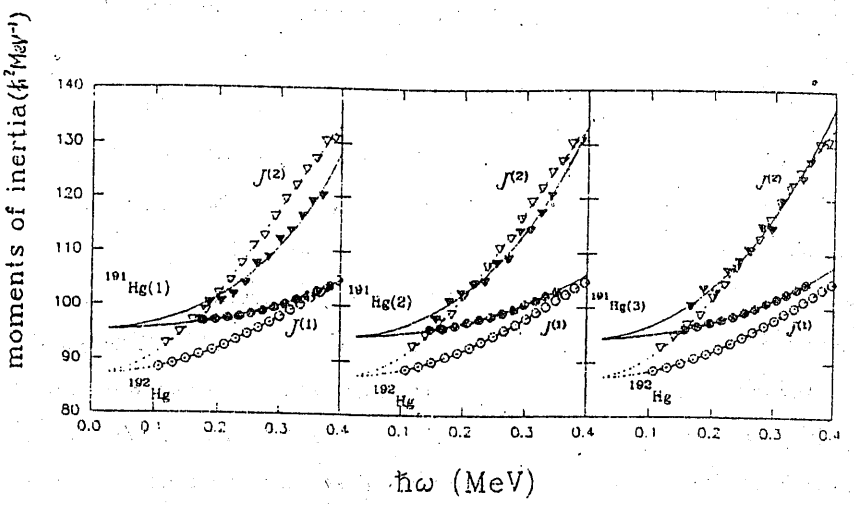

Fig. 6 The same as Fig. 5, but for the SD bands ^{191}Hg(1, 2, 3).

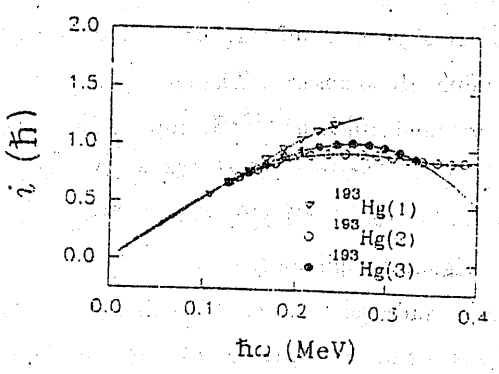

Fig. 7 The angular momentum alignments of the SD bands ^{193}Hg(1, 2, 3) relative to the SD band ^{192}Hg (cf. Fig. 3), $i = I_x(^{193}\mathrm{Hg},\ \omega) - I_x(^{192}\mathrm{Hg},\ \omega)$.

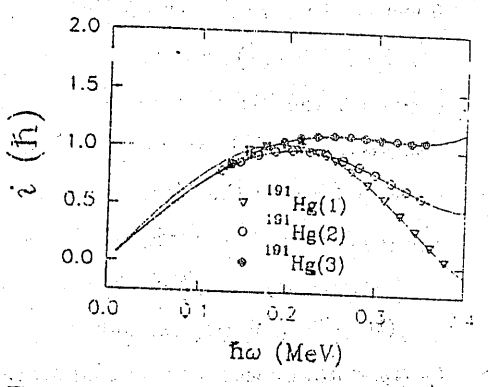

Fig. 8 The same as Fig. 3 and 7, but for the SD bands ^{191}Hg(1, 2, 3).

$[512\ 5/2^-]$, $\alpha = -1/2$, for ^{193}Hg(1), (I_0=15/2, $J_0 = 92.3\hbar^2\mathrm{MeV}^{-1}$)

$[624\ 9/2^+]$, $\alpha = 1/2$, for ^{193}Hg(2), (I_0=21/2, $J_0 = 93.09\hbar^2\mathrm{MeV}^{-1}$)

$[624\ 9/2^+]$, $\alpha = -1/2$, for ^{193}Hg(3), (I_0=19/2, $J_0 = 92.73\hbar^2\mathrm{MeV}^{-1}$)

$[752\ 5/2^-]$, $\alpha = -1/2$, for ^{193}Hg(4), (I_0=27/2, $J_0 = 103.3\hbar^2\mathrm{MeV}^{-1}$)

Because almost no signature splitting is observed in the SD bands ^{193}Hg(2, 3) and there exist large differences in J_0's between ^{193}Hg(2, 3) and ^{192}Hg, it seems reasonable to assign the configuration of ^{193}Hg(2, 3) as a neutron in high-Ω orbital [624 9/2] coupled with the "^{192}Hg core". Other most possible candidates for the orbital of N=113 neutron are [512 5/2$^-$] and [752 5/2$^-$]. The bandmixing between the SD bands ^{193}Hg(1) and ^{193}Hg(4) have been established experimentally [23], which is allowed only when two bands have the same parity and signature. Considering the large difference in J_0's between ^{193}Hg(1) and ^{193}Hg(4) (J_0 = 92.3, 103.7$\hbar^2$MeV^{-1}, respectively), it seems reasonable to assume that the valence neutrons of ^{193}Hg(1) and ^{193}Hg(4) occupy the orbitals [512 5/2$^-$] and [752 5/2$^-$], respectively.

According to Riley, et al. [9] and Satula et al. [10], the configuration of the yrast SD band ^{191}Hg(1) ($\alpha = -1/2$) is "^{192}Hg core"$\otimes[\nu 761\ 3/2]^{-1}$, with high-$N$ component $\pi 6^4\nu 7^3$. Because the high-N orbital [761 3/2] has a large signature splitting, the signature partner SD band ^{191}Hg(1) ($\alpha = 1/2$) is expected to be difficult to observe. The most possible configuration of the excited SD band ^{191}Hg(2, 3) is assigned [10] to be "^{192}Hg core"$\otimes[\nu 642\ 3/2]^{-1}$, as compared with the configuration of ^{193}Hg(2, 3) ("^{192}Hg core"$\otimes[\nu 624\ 9/2]$), which can account for why the features of the moments of inertia of ^{191}Hg(2, 3) and ^{193}Hg(2, 3) are similar (except that ^{191}Hg(2, 3) have a larger signature splitting).

In summary, the phenomenological analysis (bandhead moment of inertia J_0, ω variation of $\mathcal{J}^{(1)}$, $\mathcal{J}^{(2)}$, and angular momentum alignment, signature splitting, etc.) of the SD bands in Hg isotopes seems to be consistent with the following configuration assignments:

^{192}Hg, ^{194}Hg, high-N components are $\pi 6^4\nu 7^4$, $\alpha = 0$

^{193}Hg(2, 3)="^{192}Hg core"$\otimes[\nu 624\ 9/2]$, $\alpha = 1/2, -1/2$

^{191}Hg(2, 3)="^{192}Hg core"$\otimes[\nu 642\ 3/2]^{-1}$, $\alpha = 1/2, -1/2$

^{194}Hg(2, 3)="^{192}Hg core"$\otimes[\nu 624\ 9/2]\otimes[\nu 512\ 5/2]$, $\alpha = 0, 1$

^{193}Hg(1)="^{192}Hg core"$\otimes[\nu 512\ 5/2]$, $\alpha = -1/2$

^{193}Hg(4)="^{192}Hg core"$\otimes[\nu 752\ 5/2]$, $\alpha = -1/2$

^{191}Hg(1)="^{192}Hg core"$\otimes[\nu 761\ 3/2]^{-1}$, $\alpha = -1/2$

References

[1] Twin P. J., Nucl. Phys. **A520** (1990) 17c; **A522** (1991) 13c.

[2] Åberg S., Nucl. Phys. **A520** (1990) 35c, and references therein.

[3] Byrski T. *et al.*, Phys. Rev. Lett. **64** (1990) 1650.

[4] Stephens F. S. *et al.*, Phys. Rev. Lett. **64** (1990) 2623; **65** (1990) 301.

[5] Stephens F. S., Nucl. Phys. **A520** (1990) 91c.

[6] Bohr A., Hamamoto I., and Mottelson B. R., Physica Scripta, **26** (1987) 267.

[7] Wu C. L., Feng D. H., and Guidry M. K., Phys. Rev. Lett. **66** (1991) 1377.

[8] Wyss R. and Pilote S., Phys. Rev. **C44** (1991) R601.

[9] Riley M. A. *et al.*, Nucl. Phys. **A512** (1990) 198.

[10] Satula W., Ćwiok S., Nazarewicz W., Wyss R., and Johnson A., Nucl. Phys. A529 (1991) 289.

[11] Meyer M., Redon N., Quentin P. and Libert J., Phys. Rev. **C45** (1992) 233.

[12] Becker J. A. *et al.*, Phys. Rev. **C41** (1990) R9; **A520** (1990) 187c.

[13] Xing Z., Chen X. Q., High Energy Phys. and Nucl. Phys. **15** (1991), 1020.

[14] Zeng J. Y., Meng J., Wu C. S., Zhao E. G., Xing Z., and Chen X. Q., Phys. Rev. **C44** (1991) R1745.

[15] Wu C. S., Zeng J. Y., Xing Z., and Chen X. Q., Meng J., Phys. Rev. C45 (1992) 261.

[16] Wu C. S. and Zeng J. Y., High Energy Phys. and Nucl. Phys. **8** (1984) 219, 445; **9** (1985) 77, 214.

[17] Wu C. S. and Zeng J. Y., Commun. Theor. Phys. **8** (1987), 51.

[18] Huang H. X., Wu C. S., and Zeng J. Y., Phys. Rev. **C39** (1989) 1617.

[19] Beausang C. W. *et al.*, Z. Phys. **A335** (1990) 325.

[20] Cullen D. M. *et al.*, Nucl. Phys. **A520** (1990) 105c.

[21] Bengtsson T., Ragnarsson I. and Åberg S., Phys. Lett. **B208** (1988) 39.

[22] Mottelson B. R., Nucl. Phys. **A522** (1991) 1c.

[23] Janssens R. V. F. *et al.*, Nucl. Phys. **A520** (1990) 75c.

[24] Fernandez P. B. *et al.*, Nucl. Phys. **A517** (1990) 386.

Spin-Spin Interaction in Cranked Shell Model

C. S. Wu*

CCAST (World Laboratory), Center of Theoretical Physics,
P. O. Box 8730, Beijing 100080, China,
Department of Physics, Peking University, Beijing 100871, China
and
Institute of Theoretical Physics, Chinese Academy of Science,
Beijing 100080, China

Abstract

A $\sigma \cdot \sigma$ interaction added to the cranked shell model Hamiltonian is investigated in the particle-number-conserving approach. The degeneracy between doublets $|\Omega_1 \pm \Omega_2|$ is removed as expected. The gap parameter $\tilde{\Delta}$ is also dependent of the existence of the $\sigma \cdot \sigma$ interaction. However, the bandcrossing frequency and the yrast-yrare interaction strength, spin alignment, and the occupation probabilities over the single particle levels appear to be nearly unchanged when the $\sigma \cdot \sigma$ interaction is included.

*Mailing address: Department of Physics, Peking University, Beijing 100871, China

The importance of the spin-spin (hereafter call $\sigma \cdot \sigma$) interaction has been recognized for a long time in the nuclear structure theory. For example, the splitting of the doublet states $|\Omega_1 \pm \Omega_2|$ existing in the even (even-even or odd-odd) nuclei, the so-called Gallapher-Moskowski coupling scheme, is originated from the $\sigma \cdot \sigma$ interaction between the unpaired nucleons [1]. For reproducing the systematics of the collective parameters, such as nuclear moments of inertia and gyromagnetic ratio, the $\sigma \cdot \sigma$ interaction plays a indispensable role [2]. In some papers [3] the $\sigma \cdot \sigma$ interaction was also introduced to account for the odd-even staggering in the nuclear spectroscopy. However, to our knowledge, this interaction has not been yet included in a variety of cranked shell model (CSM) calculations. Therefore, it should be useful to investigate that to what extent the conclusions drawn from the previous CSM calculations (without $\sigma \cdot \sigma$ interaction) maintain if this interaction is included. This becomes more neccessary in consideration of the fact that the recent experimental advances in the nuclear superdeformed bands have evoked a heated discussion about the influence of the pairing correlation and other residual interactions (e.g. octupole correlation) [4,5]. In this report we would like to discuss the $\sigma \cdot \sigma$ interaction in the framework of the particle-number-conserving (PNC) treatment of the single-j CSM.

A Hamiltonian

The Hamiltonian is taken as

$$H = H_{\rm CSM} + H_\sigma \tag{1}$$

where $H_{\rm CSM}$ is the usual CSM Hamiltonian

$$H_{\rm CSM} = H_{\rm sp} + H_{\rm P} + H_{\rm C} \tag{2}$$

with the single particle Hamiltonian

$$H_{\rm sp} = \sum_{\nu>0} \varepsilon_\nu \left(a_\nu^\dagger a_\nu + a_{\bar\nu}^\dagger a_{\bar\nu} \right), \tag{3}$$

the pairing correlation

$$H_{\rm P} = -G \sum_{\mu,\nu>0} a_\mu^\dagger a_{\bar\mu}^\dagger a_{\bar\nu} a_\nu, \tag{4}$$

and the Coriolis interaction

$$H_{\rm C} = -\omega \sum_{\mu,\nu} \langle \mu | j_x | \nu \rangle a_\mu^\dagger a_\nu. \tag{5}$$

H_σ is the $\sigma \cdot \sigma$ interaction, for simplicity, taken the form of

$$\begin{aligned} H_\sigma &= V_0 \sum_{i<j} \mathbf{S}(i) \cdot \mathbf{S}(j) \\ &= \frac{V_0}{4} \hbar^2 \sum_{i<j} \sigma(i) \cdot \sigma(j) \end{aligned} \tag{6}$$

In this report, we confine ourselves to the single-j model [6], namely, with the single particle energies

$$\varepsilon_\Omega = \kappa \frac{3\Omega^2 - j(j+1)}{j(j+1)}, \qquad |\Omega| = \frac{1}{2}, \frac{3}{2}, \cdots, j, \quad j = \frac{13}{2} \tag{7}$$

which is believed to be a good approximation of the intruder orbits playing a decisive part in the high-spin state physics. The $\sigma \cdot \sigma$ interaction coupling constant V_0 is rather arbitrarily chosen as $V_0/\kappa = 0$, 0.1, 0.2, and 0.3. The pairing correlation strength G is fixed as $G/\kappa = 0.15$ in the calculation of $V_0 = 0$. When $V_0 \neq 0$, a renormalized value of G is adopted to reproduce the first excited 0^+ state (at $\omega = 0$) with the same energy as that in the case of $V_0 = 0$.

The Hamiltonian (1) is diagonalized with the PNC approach which has been proved to be useful and effective in the CSM calculations [7,8]. In the calculation an MPC (many-particle configuration) truncation was used to diminish the MPC space. The truncation energy is assumed to be $E_c/\kappa = 3.5$.

B Routhian

The Hamiltonian (1) has been diagonalized for the systems of even particle numbers, $N = 2, 4, \cdots$, and 12 in the $i13/2$ shell. Only the results of the six particle system are given below for saving space. But the situation is similar for the others.

The eigenenergies for lowest bandheads with signature $\alpha = 0$ in the $N = 6$ system are shown in Fig. 1. It is seen that when $V_0 = 0$ the first excited band $K = 1$ is degenerate to the band $K = 6$ because in these states the unpaired particles occupy the same single particle levels 633$\uparrow$ and 642$\uparrow$. Similarly for the bands $K = 2$ and $K = 5$ (633$\uparrow \mp$ 651$\uparrow$) and the bands $K = 3$ and $K = 4$ (633$\uparrow \pm$ 660$\uparrow$). When the $\sigma \cdot \sigma$ interaction is switched on, the two-fold degeneracy removes. The doublet splitting is $\sim (0.10 - 0.15)\kappa \sim (250 - 400)$keV for $V_0/\kappa = 0.2 - 0.3$, comparable to that observed in the rare-earth region ($\sim 100 - 600$keV).

As pointed out above, the pairing strength G is renormalized under the request that the first excited 0^+ state is located at the same energy as that in the case of $V_0 = 0$. Therefore, with increasing V_0, the G-value decreases step by step. This is understandable because the $\sigma \cdot \sigma$ interaction has also a coherent effect. The values of G and V_0 used in the calculation are as follows.

V_0/κ	0	0.1	0.2	0.3
G/κ	0.1500	0.1404	0.1245	0.0880

The comparison of the eigenenergies obtained in the cases of $V_0/\kappa = 0$ and 0.2 is given in Fig. 2. At least for the lowest four bands, the energies and their variations with frequency are almost the same in these two cases, except for the doublet splitting. This can be shown more clearly in the yrast reference (Fig. 3). For example, the bandcrossing frequency $\hbar\omega_c = 0.123\kappa$ and yrast-yrare interaction $V_c = 0.241\kappa$ for $V_0 = 0$ are very close to $\hbar\omega_c = 0.121\kappa$ and $V_c = 0.227\kappa$ for $V_0 = 0.2\kappa$.

C Spin alignments

The spin alignments

$$i = \langle J_x \rangle = -\frac{\partial E'}{\partial \omega} \tag{8}$$

for the yrast and yrare bands are shown in Fig. 4. One may find that the i's calculated with $V_0/\kappa = 0$ and 0.2 are nearly identical with each other. This is a reflection of the resemblance between the eigenenergies. In both cases, $i_{\rm yrare}$ is larger than $i_{\rm yrast}$ in low frequency region, but $i_{\rm yrare} < i_{\rm yrast}$ at high frequencies. $i_{\rm yrare} = i_{\rm yrare}$ at ω_c.

D Gap parameter

In the PNC approach the gap parameter $\tilde{\Delta}$ is defined as [9]

$$\tilde{\Delta} = G\sqrt{\langle P^\dagger P \rangle}, \quad P^\dagger = \sum_{\mu>0} a^\dagger_\mu a^\dagger_{\bar{\mu}} \tag{9}$$

which coincides with

$$\Delta = G\langle P \rangle \tag{10}$$

adopted in the HFB approximation [9]. Because $\tilde{\Delta}$ depends explicitly on the choice of G, it is expected that the calculated $\tilde{\Delta}$ in $V_0/\kappa = 0.2$ is clearly different from that in $V_0 = 0$. However, the values of $\tilde{\Delta}/G$ obtained in both cases are very similar (see Fig. 5). The $\tilde{\Delta}_{\rm yrast}/G$ is larger than $\tilde{\Delta}_{\rm yrare}/G$. The former decreases smoothly with ω, while the latter remains nearly unchanged in a wide range of frequencies. In both cases, $\tilde{\Delta}_{\rm yrast}/G$ decreases by $10-15\%$ when $\hbar\omega/\kappa$ increases from 0 to 0.15 ($\sim$ 400keV). No pairing collapse is found in these cases.

E Moments of Inertia

The kinematic and dynamic moments of inertia

$$\mathcal{J}^{(1)} = \frac{i}{\omega} \qquad \mathcal{J}^{(2)} = \frac{{\rm d}i}{{\rm d}\omega} \tag{11}$$

can be calculated and the results for the three lowest bands are shown in Fig. 6. When $V_0 = 0$ the kinematic and dynamic moments of inertia for the yrast band remain almost unchanged below the bandcrossing. Afterward, both of them decrease with increasing ω, but $\mathcal{J}^{(2)}$ decreases more rapidly. The $\sigma \cdot \sigma$ interaction seems not to have a remarkable influence, at least in the single-j shell, on the moment of inertia for the yrast band, contrary to the results of ref. [2] which find a reduction by about 15%. When $V_0/\kappa = 0.2$, the kinematic and dynamic moments of inertia reveal similar features, but vary with a rather large amplitude. For the yrare and the second excited bands, $\mathcal{J}^{(1)}$ and $\mathcal{J}^{(2)}$ fluctuate with very large amplitudes, both in the cases of $V_0/\kappa = 0$ and 0.2. This is because the excited bands distribute more densely, so that the cross talk among them is more frequently. In this aspect one may find a distinct result that the dynamic moment of inertia grows up and has a sharp peak at low frequencies when $V_0 = 0$, vis-a-vis that in $V_0/\kappa = 0.2$ which goes down slowly until a shallow valley appears.

It is interesting to note that for the yrast band the ratio

$$R = \sqrt{\frac{\left[\mathcal{J}^{(1)}\right]^3}{\mathcal{J}^{(2)}}} \tag{12}$$

maintains nearly a constant below the bandcrossing. This is expected from the ab expression for the rotational spectrum [10] and R is equal to the bandhead moment of inertia. However, same behavior cannot be found for the excited bands. Of course, this does not contradict with the result obtained from the ab expression because the excited band does not have a stable intrinsic structure [7,8].

F Occupation Probabilities over Single Particle Levels

The occupation probabilities over the single particle levels are shown in Fig. 7 for the yrast and yrare bands. It is clear that the occupation probabilities in $V_0/\kappa = 0.2$ are almost the same as those in $V_0 = 0$. At $\omega = 0$ the yrast band is a coherent state composed of fully-paired configurations, while the yrare band is a pair-broken state with unpaired particles occpying levels 642$\uparrow$ and 633$\uparrow$. As ω increases, they gradually lose their original characters due to the band mixture. In the bandcrossing region ($\hbar\omega_c \sim 0.12\kappa$), the yrast band becomes a complicated composition of fully-paired configurations and pair-broken configurations with appreciable probabilities occupying levels 642$\uparrow$ and 633$\uparrow$ (the total occupation number by the unpaired particles is about 1.1, implying that there is a possibility of about 50% in pair-broken states), while the yrare band has two unpaired particles distributing over levels 660$\uparrow$, 651$\uparrow$, 642$\uparrow$, 633$\uparrow$, and 624$\uparrow$ (with total occupation number of about 2.1).

G Concluded Remarks

The $\sigma \cdot \sigma$ interaction has been investigated in the framework of CSM with the PNC treatment. As for a single-j shell, the appearance of the $\sigma \cdot \sigma$ interaction seems not to alter remarkably the main results (e.g. bandcrossing frequency and yrast-yrare interaction strength, spin alignment, and occupation probabilities over the single particle levels) obtained without spin-spin correlation, except for the removal of the degeneracy between doublets $|\Omega_1 \pm \Omega_2|$, existing widely in the even-even deformed nuclei. In addition, the gap parameter $\tilde{\Delta}$ is also dependent on the existence of the $\sigma \cdot \sigma$ interaction, roughly proportional to the pairing correlation strength G, provided a renormalized G values is sdopted. The moments of inertia for the yrast band are nearly independent of V_0 (at least in the region of $V_0/\kappa = 0-0.3$), but those for the excited bands seem to be V_0-dependent, perhaps more or less randomly.

It should be emphasized that the discussion on the $\sigma \cdot \sigma$ interaction made in this report is limited to the case of a single-j shell. An overall investigation in a more realistic single particle level scheme is needed. Moreover, a simplified form for the $\sigma \cdot \sigma$ interaction is used where the radial dependence and the possible exchange term are ignored. Calculation with the Nilsson potential demonstrates qualitatively a reproduction of the doublet splitting in the rare earth region, but not numerically.

References

[1] H. Frisk, Z. Phys. **A 330** (1988) 241.

[2] J. Meyer, J. Speth, and J. H. Vogeler, Nucl. Phys. A **193** (1972) 60.

[3] A. K. Jain, J. Kvasil, R. K. Sheline, and R. W. Hoff, Phys. Lett. B **209** (1988) 19.

[4] S. Åberg, Nucl. Phys. **A 520** (1990) 35c.

[5] D. M. Cullen et al., Nucl. Phys. **A 520** (1990) 105c.

[6] I. Hamamoto, Nucl. Phys. **A 271** (1976) 15.

[7] C. S. Wu and J. Y. Zeng, Phys. Rev. **C 40** (1989) 998.

[8] C. S. Wu and J. Y. Zeng, Phys. Rev. **C 41** (1990) 1822.

[9] P. Ring and P. Schuck, *The Nuclear Many-Body Problems* (Springer-Verlag, New York, 1980).

[10] C. S. Wu, L. Cheng, C. Z. Lin and J. Y. Zeng, Phys. Rev. **C 45** (1992) 2507.

Figure Captions

Fig. 1 The bandheads of the lowest bands with signature $\alpha = 0$ for $N = 6$ system in $i13/2$ shell.

Fig. 2 The eigenenergies of the lowest bands with signature $\alpha = 0$ for $N = 6$ system in $i13/2$ shell.

Fig. 3 The eigenenergies (yrast reference) of the lowest bands with signature $\alpha = 0$ for $N = 6$ system in $i13/2$ shell.

Fig. 4 The spin alignments for the yrast and yrare bands for $N = 6$ system in $i13/2$ shell.

Fig. 5 The gap parameters $\tilde{\Delta}$ for the yrast and yrare bands for $N = 6$ system in $i13/2$ shell.

Fig. 6 The moments of inertia for the lowest bands for $N = 6$ system in $i13/2$ shell. The kinematic and dynamic moments of inertia are denoted by thin and thick lines, respectively. The open circles stand for the R's defined in eq. (12).

Fig. 7 The occupation probabilities over the single-particle levels for the yrast and yrare bands for $N = 6$ system. The open bar represents the probability occupying by a particle pair, while the shadow bar denotes that by an unpaired particle. The letters A, B, $\cdots$, and F stand for the single particle levels $|\Omega| = 1/2, 3/2, \cdots$, and $11/2$.

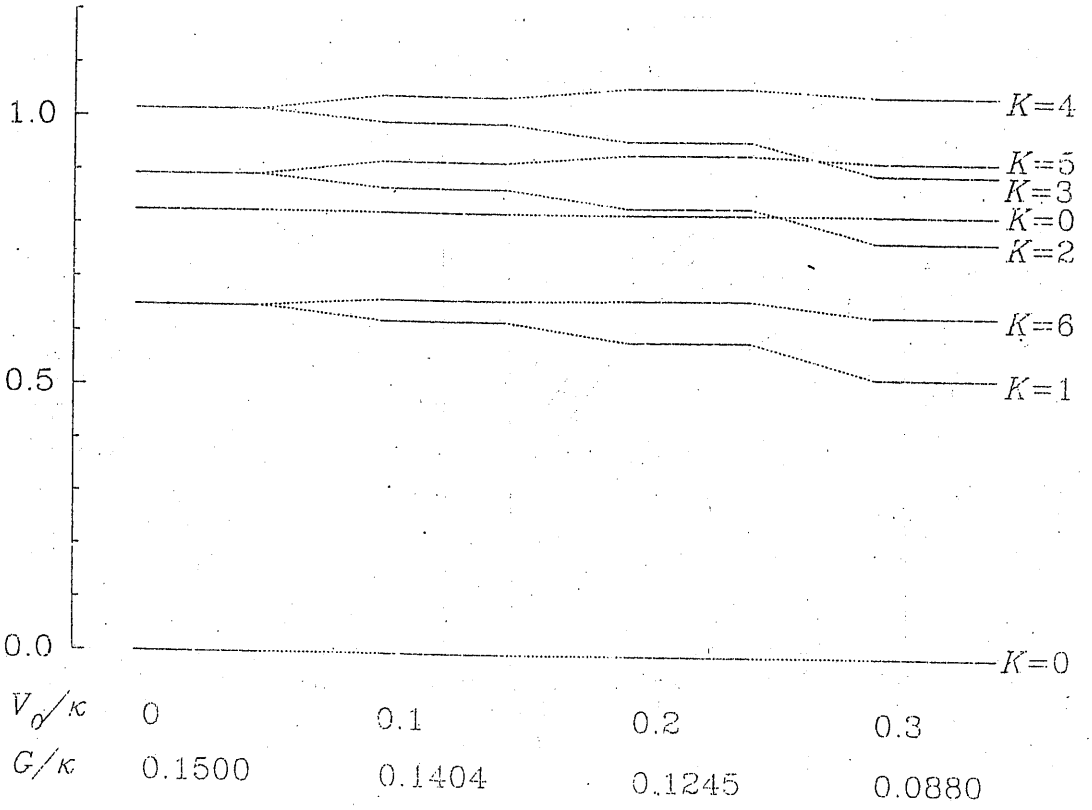

V_0/κ	0	0.1	0.2	0.3
G/κ	0.1500	0.1404	0.1245	0.0880

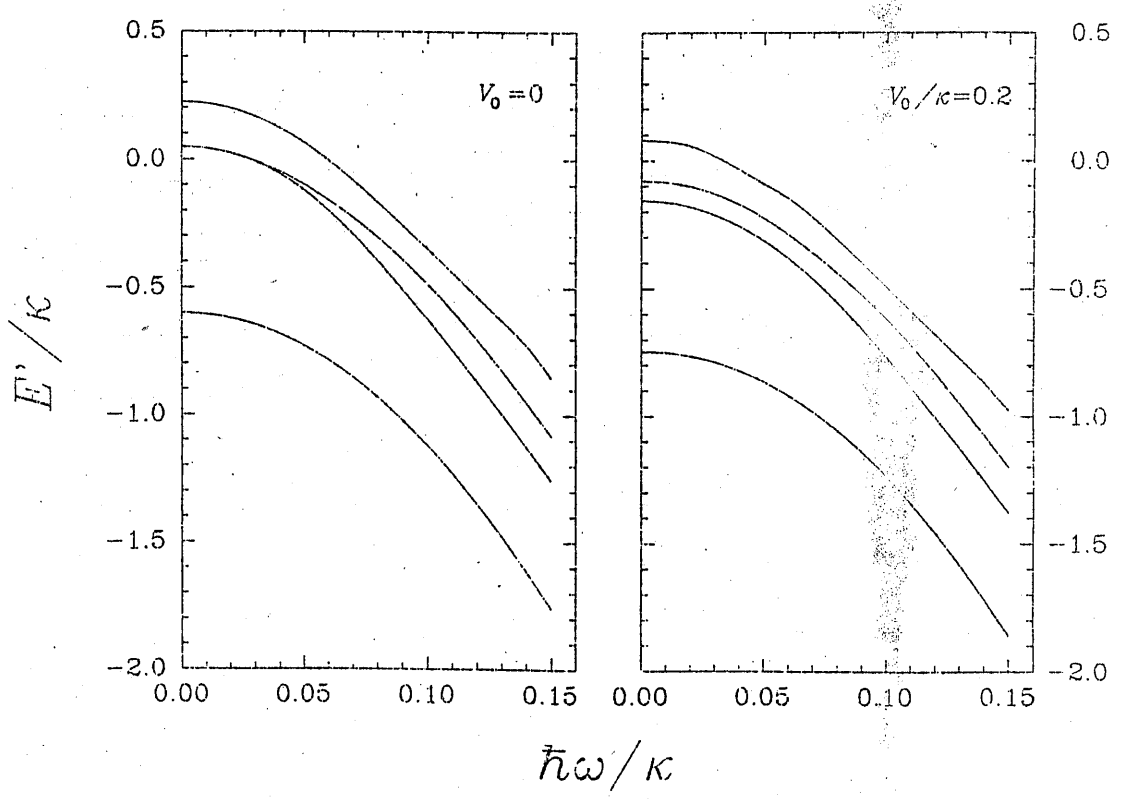
0.5
0.0
−0.5
−1.0
−1.5
−2.0
$V_0 = 0$
$V_0/\kappa = 0.2$
0.00
0.05
0.10
0.15
E'/κ
$\hbar\omega/\kappa$

Fig. 2

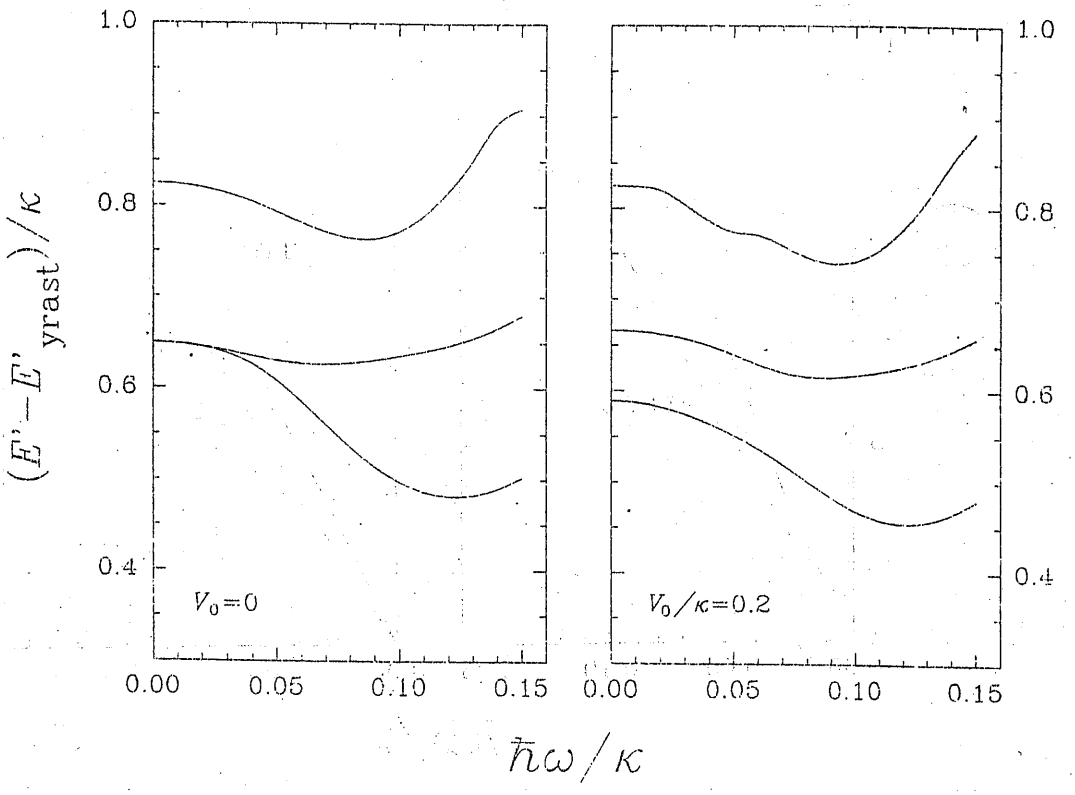
1.0
0.8
0.6
0.4
$(E'-E'_{\mathrm{yrast}})/\kappa$
$V_0=0$
$V_0/\kappa=0.2$
0.00
0.05
0.10
0.15
$\hbar\omega/\kappa$

Fig. 3

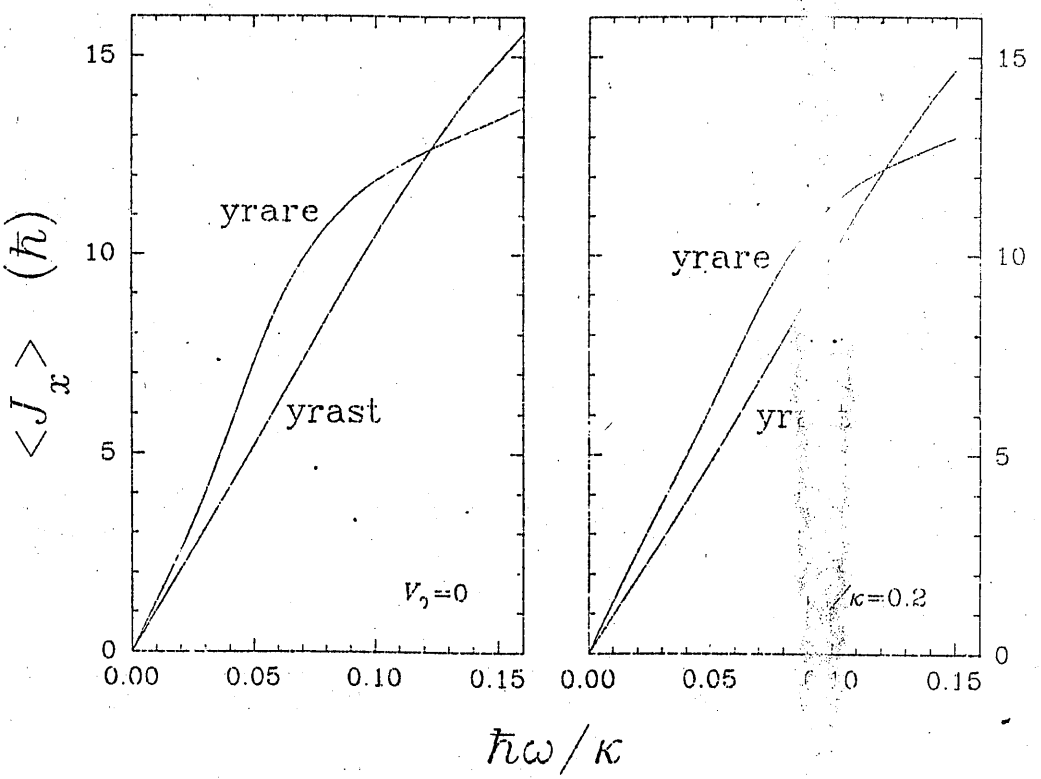
15
10
5
0
$\langle J_x \rangle$ $(\hbar)$
yrare
yrast
V_0=0
0.00
0.05
0.10
0.15
yrare
κ=0.2
$\hbar\omega/\kappa$

Fig. 4

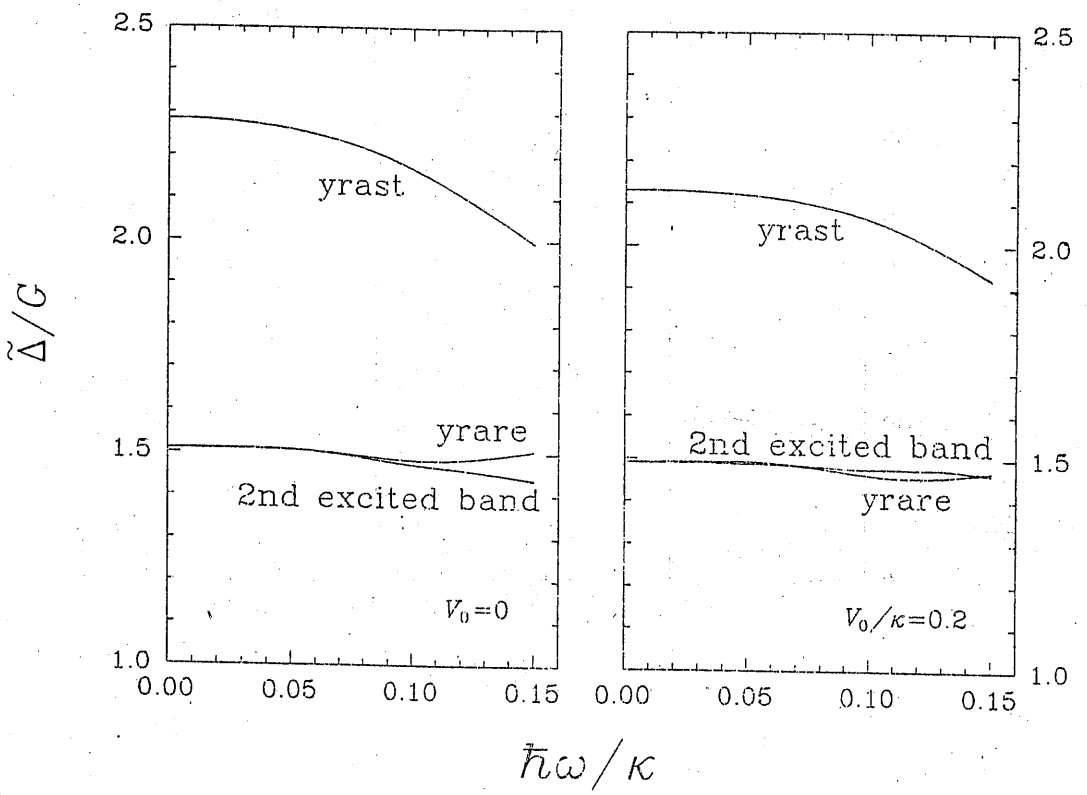
2.5
2.0
1.5
1.0
$\tilde{\Delta}/G$
yrast
yrare
2nd excited band
$V_0=0$
0.00
0.05
0.10
0.15
yrast
2nd excited band
yrare
$V_0/\kappa=0.2$
$\hbar\omega/\kappa$

Fig. 5

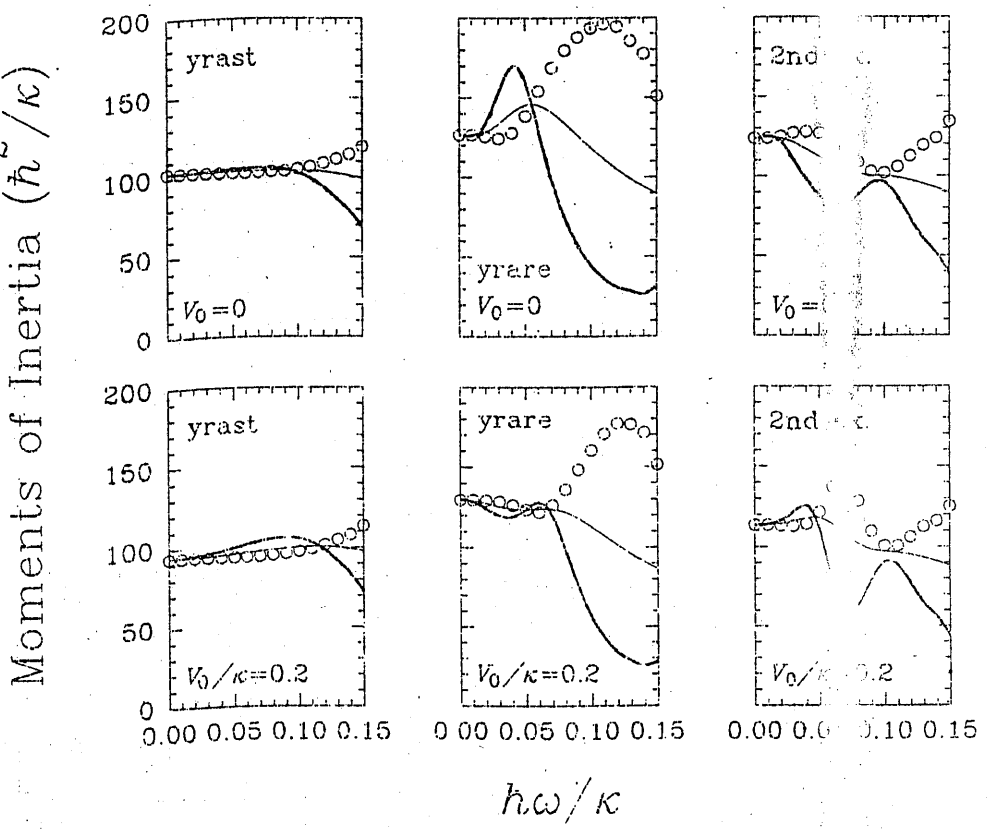
Moments of Inertia ($\hbar^2/\kappa$)
200
150
100
50
0
yrast
$V_0=0$
yrare
$V_0=0$
2nd
$V_0=$
yrast
$V_0/\kappa=0.2$
yrare
$V_0/\kappa=0.2$
2nd
$V_0/$
.2
0.00 0.05 0.10 0.15
0 00 0.05 0.10 0.15
0.00 0.0
.10 0.15
$\hbar\omega/\kappa$

Fig. 6

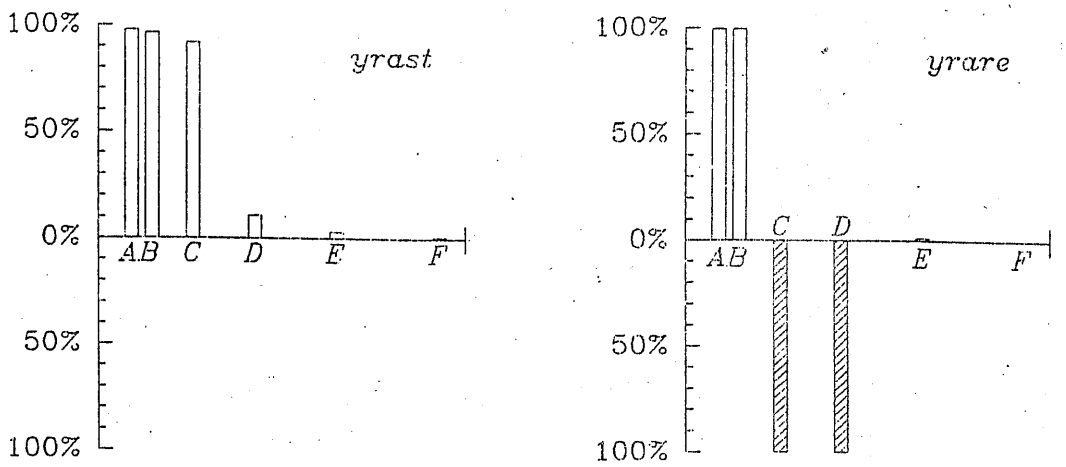

$V_0/\kappa=0$

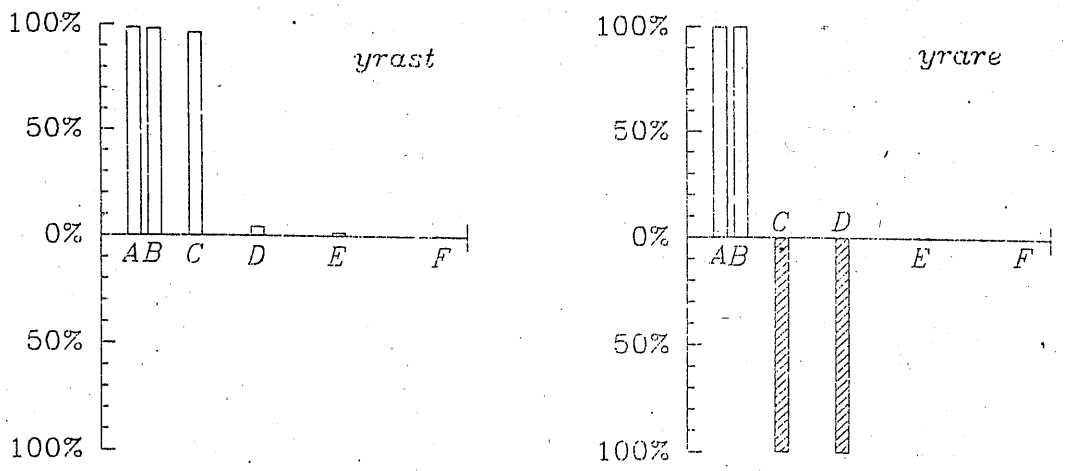

$V_0/\kappa=0.2$

Fig. 7(a) $\hbar\omega/\kappa = 0$

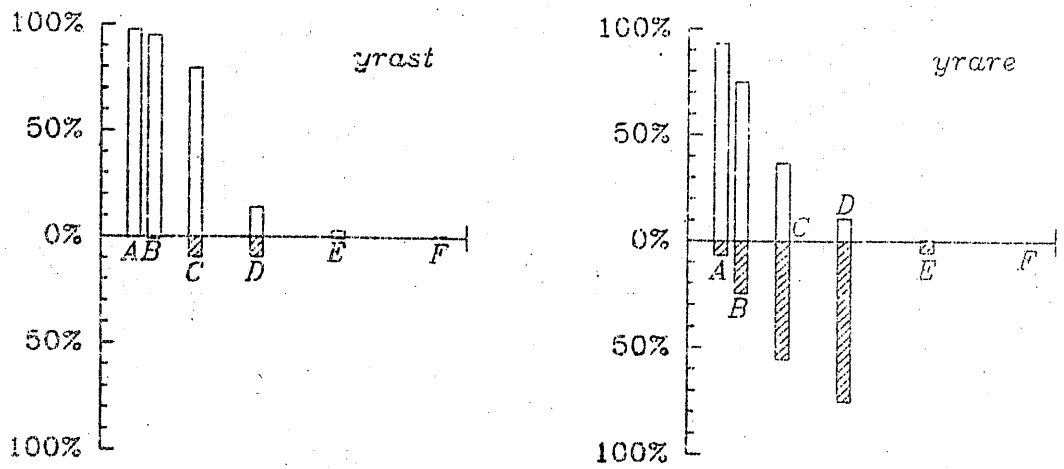

$V_0/\kappa=0$

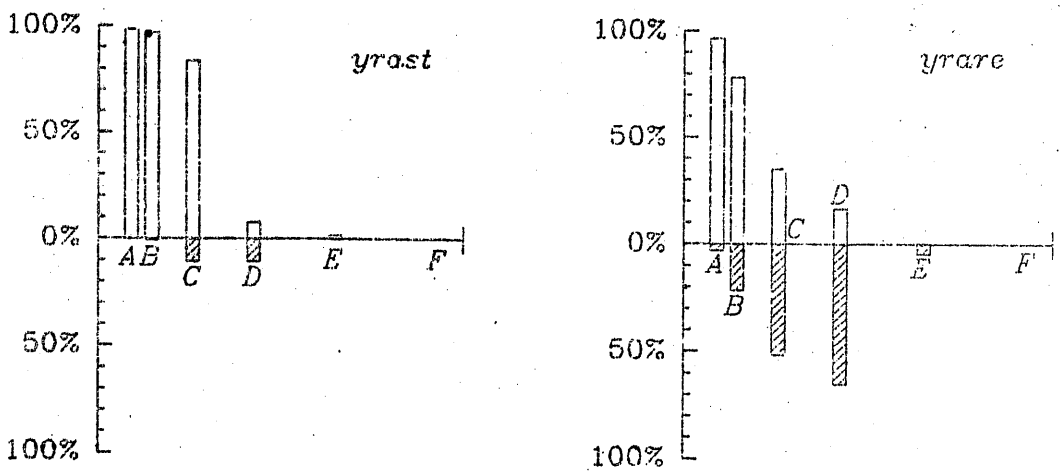

$V_0/\kappa=0.2$

Fig. 7(b) $\hbar\omega/\kappa = 0.04$

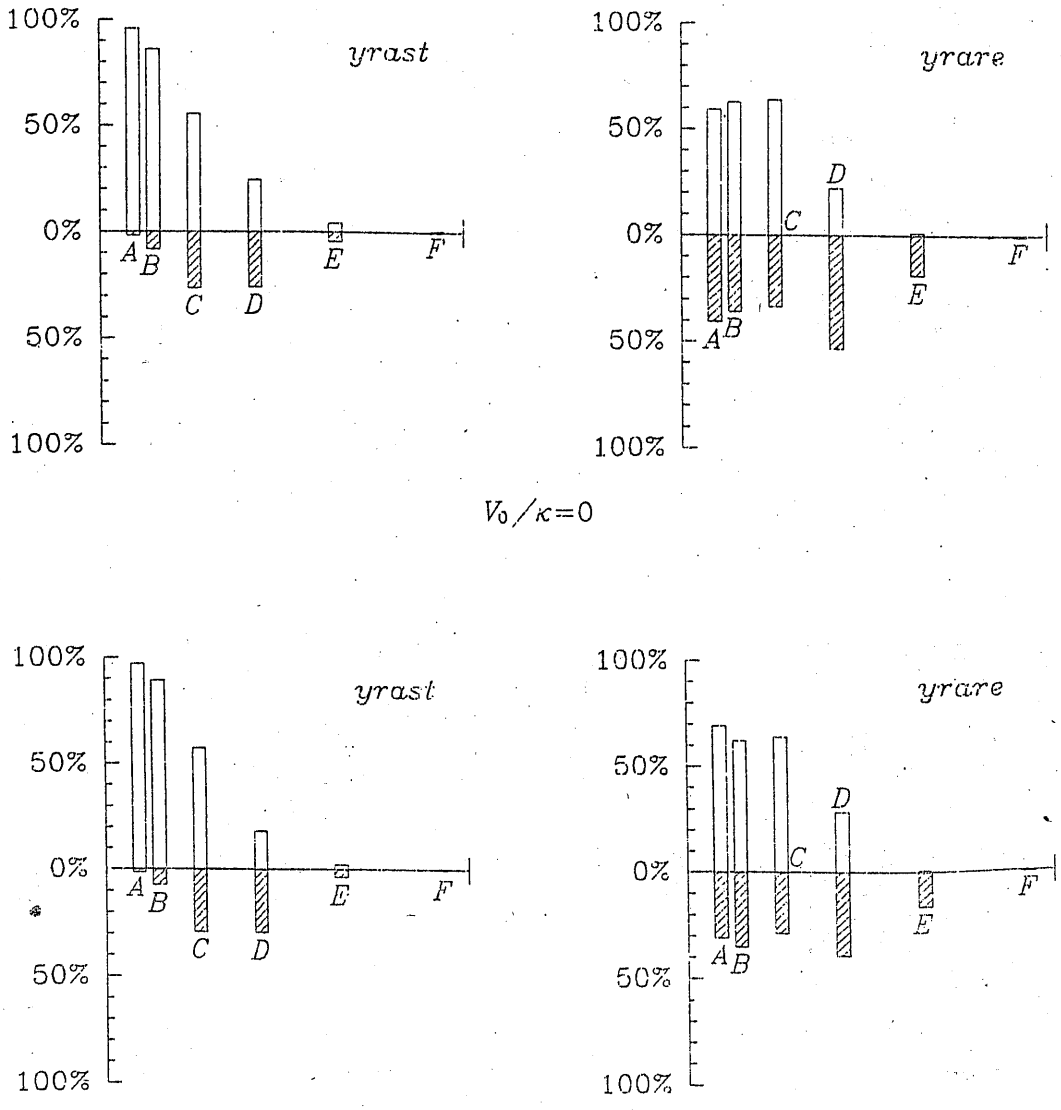

Fig. 7(c) $\hbar\omega/\kappa = 0.08$

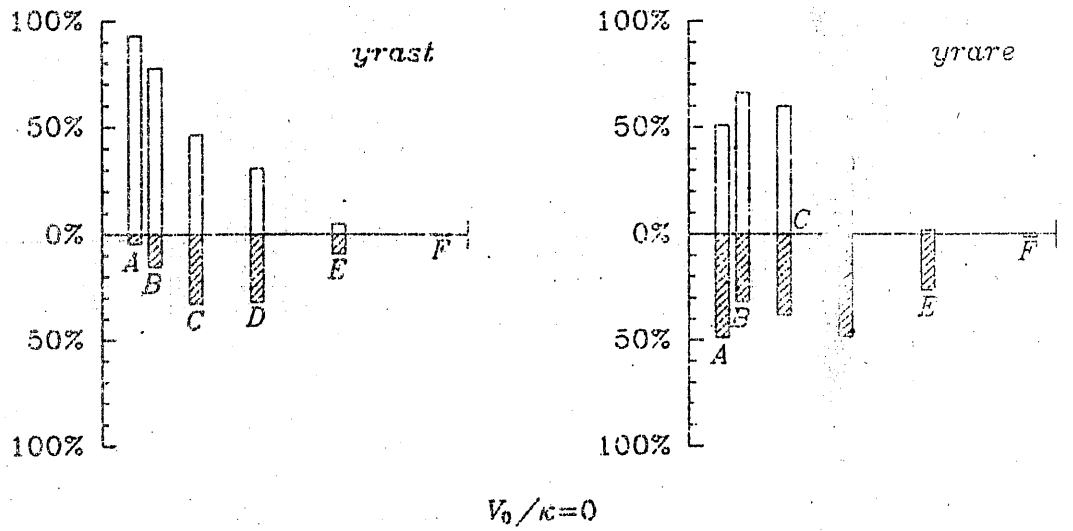

$V_0/\kappa=0$

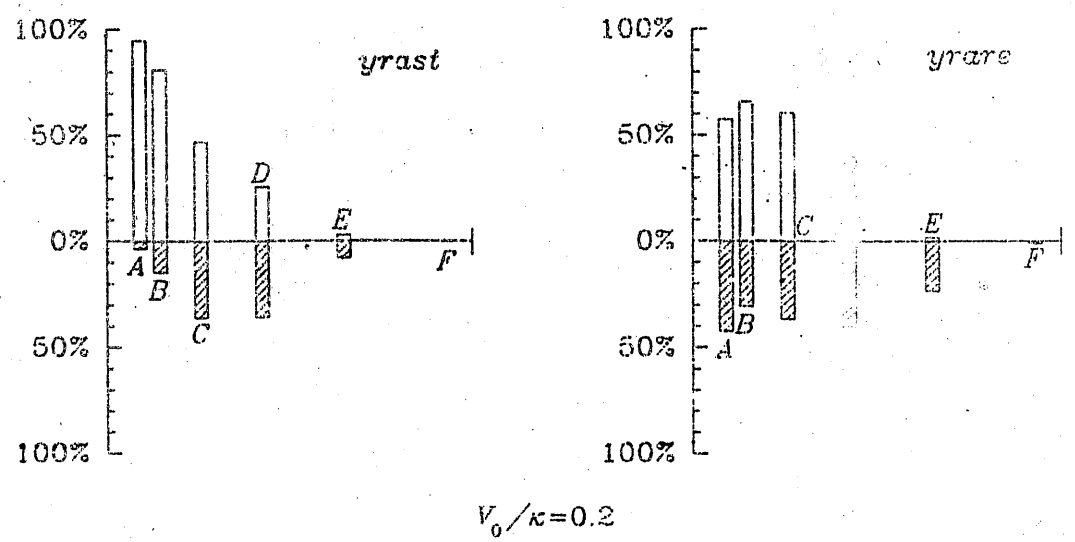

$V_0/\kappa=0.2$

Fig. 7(d) $\hbar\omega/\kappa = 0.10$

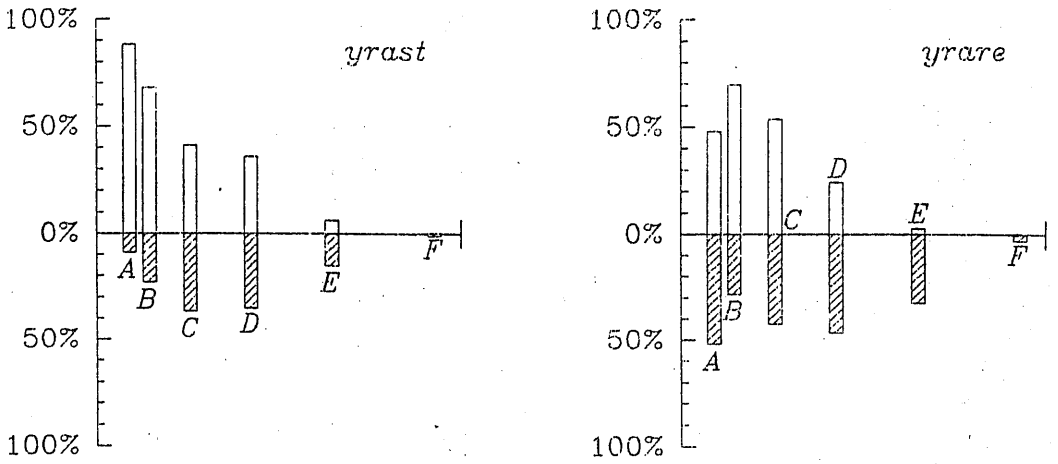

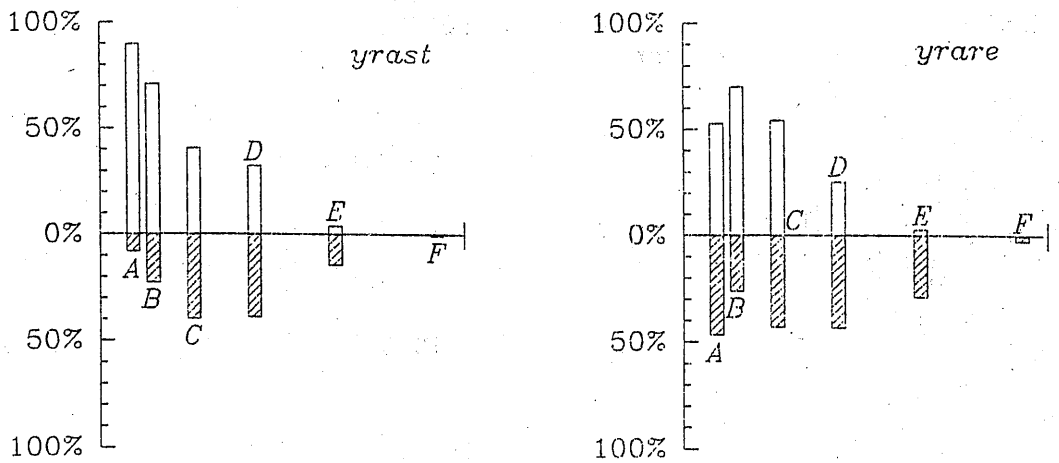

Fig. 7(e) $\hbar\omega/\kappa = 0.12$

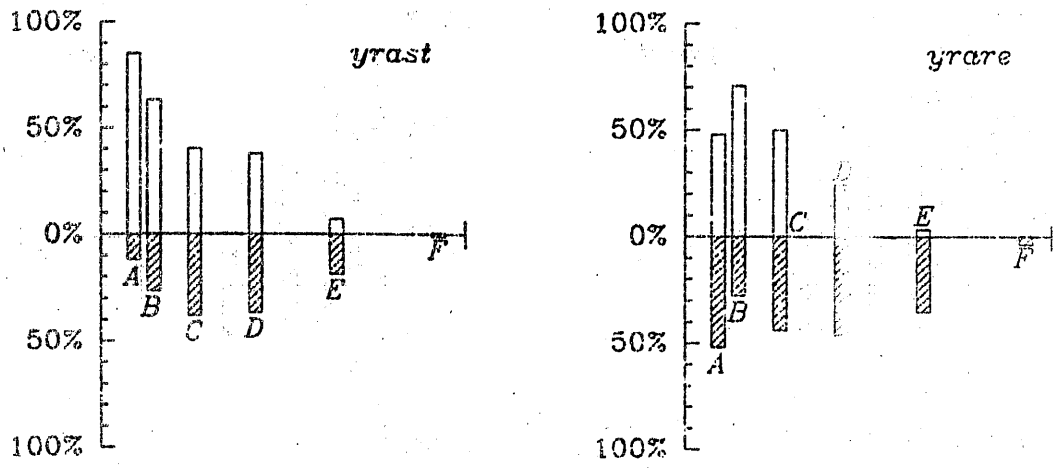

$V_0/\kappa=0$

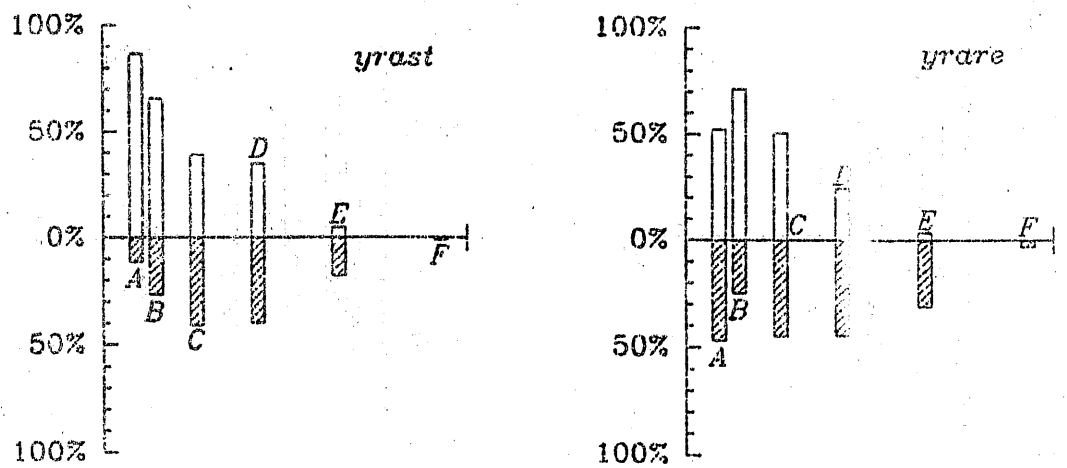

$V_0/\kappa=0.2$

Fig. 7(f) $\hbar\omega/\kappa = 0.13$

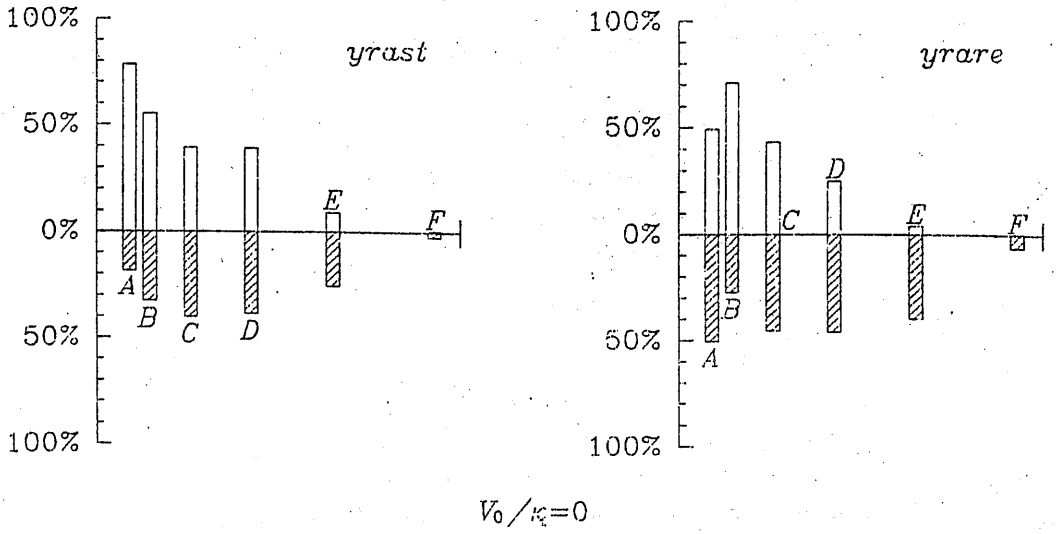

$V_0/\kappa=0$

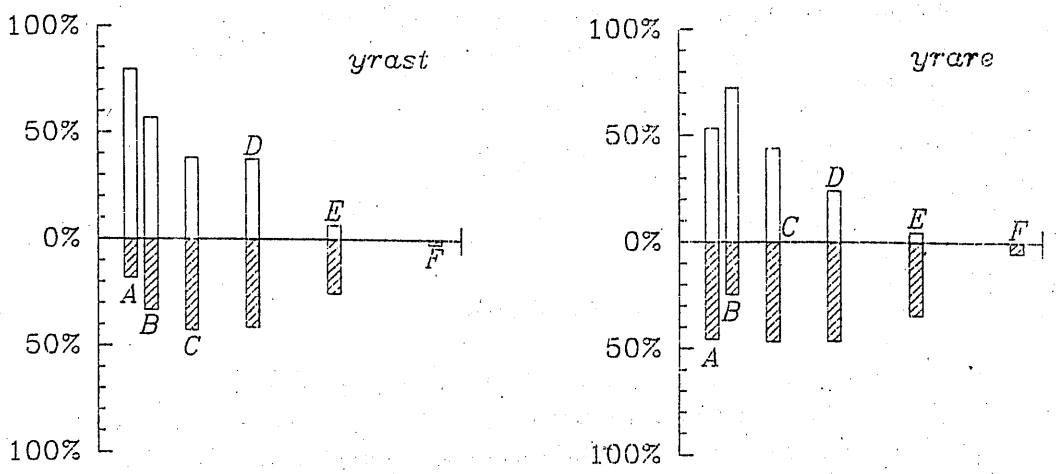

$V_0/\kappa=0.2$

Fig. 7(g) $\hbar\omega/\kappa = 0.15$

The Triaxial Motion In Mo Isotope N clei

Wendong Luo[1,2] and Y.S. Chen[2,3]
[1]CCAST(World Laboratory), P.O.Box 8730, Beiji 100080
[2]Institute of Atomic Energy, Beijing 102413, C ina*
[3]Institute of Theoretical Physics, Academia Sinica, B ing 100080

Abstract

The nuclear shapes of transitional Mo isotope nuclei are calcul by means of the model based on the cranking approximation and Strutinsky method. The recent experimental results of the high spectroscopy and the lifetime measurement of ^{87}Mo are studie detail and explained by the evolution of the γ deformation with quasiparticle configurations. The shape calculations with the M fied Harmonic Oscillator potential, but not the folded Yukawa or so called universal Woods-Saxon potentials, give the correct cri neutron number $N \geq 47$ for the spherical shape of the Mo iso nuclei.

1. Introduction

In nuclei with Z$\sim$ 40 and N$\sim$ 46 the level spectra exhibit a tr sition from the collective rotation to the particle-like motion structures. T mass region thus has been receiving an increasing heed recent years. Mi scopically, the complexity of the nuclear structure in this region is origina from

*mailing address

the abundance of the energy gaps in the Nilsson diagram of the single particle energy, the $N, Z = 38$ gap at a large deformation, the subshell closure $N, Z = 40$ and the major shell closure $N = 50$. Therefore the shell effect manifests itself in a dramatic way: the addition or removal of one or two nucleons is relatively more important in the determination of nuclear shapes, and the region becomes very rich of the shape coexistence. Further more, the energy gaps are located relative to the $g_{9/2}$ high-j shell at just below (40), above (50) and inside (38) the shell. Consequently, there must be a dramatic shape driving effect of rotating $g_{9/2}$ proton and neutron orbits on the soft core of coexisting shapes. It was observed experimentally that the low lying spectra are characterized with the rotational motion of the deformed rotor for the $N \leq 44$, but the particle-like motion for the $N \geq 47$. The $N = 45$ isotone nuclei with $Z \sim 40$ are thus very interesting subjects to study the transitional structure both theoretically and experimentally. Recently, the high spin spectroscopy and the lifetime measurement of ^{87}Mo were completed[1]). The yrast rotational band of positive parity was measured up to the $I^{\pi} = 49/2^{+}$ state, far beyond the backbend, and the tentatively assigned negative parity bands are also rotational. Further more, the deformed shape of this nucleus can be proved by the lifetime measurement which yields large B(E2) values, around 900 $e^2 \cdot fm^4$ for the transitions above the $17/2^{+}$ state, corresponding to a transition quadrupole moment of $Q_t \approx 1.6e \cdot b$. The measured transition quadrupole moments of the yrast states show a drastic rising by about a factor of 2 after the backbend, indicating a change of the structure from the ground band to the aligned band. It is a challenging task for the theory to reproduce all of these experimental results. The purpose of the present model calculation is to investigate the shape evolution caused by the γ deformation drive of the rotating high-j quasiparticle(q.p.) orbits to gain an insight into the interplay between rotation and deformation in transitional nuclei. It is also a goal to achieve a good understanding of the high spin spectroscopy of ^{87}Mo and obtain a correct shape evolution with the neutron number among the Mo isotope nuclei. A brief description of the model is given in section 2, the results of calculation and discussion in section 3, the summary in section 4.

2. A brief description of the model

Obviously, the configuration dependence of nuclear shapes must be taken into account in the study of the structure of this mass region. The Hamiltonian of quasiparticles moving in a quadrupolely deformed potential rotating around the x-axis with a frequency ω may be written as,

$$H^{\omega} = H_{sp}(\varepsilon_2, \varepsilon_4, \gamma) - \lambda N + \Delta(P^{+} + P) - \omega J_x, \qquad (1)$$

where the H_{sp} denotes the deformed hamiltonian of single particle motion, the second term of the right side is the chemical potential, the third term is the pairing interaction and the last term stands for the Coriolis and centrifugal forces. The Modified Harmonic Oscillator (MHO) potential with the parameters κ and μ for the mass region taken from ref.[2]) is employed in the present calculation. The pairing gap parameter is determined empirically by $\Delta = 0.9\Delta_{oe}$, and the Δ_{oe} is got from the experimental odd-even mass difference [3]). The total routhian surface(TRS), namely the total energy in rotating frame as a function of the ε_2 and γ deformations, of (Z, N) nucleus for a fixed q.p. configuration cf may be calculated by

$$E^{cf}(\varepsilon_2, \gamma; \omega) = E_{ld}(\varepsilon_2, \gamma) + E_{corr}(\varepsilon_2, \gamma; \omega = 0) + E^{g}_{rot}(\varepsilon_2, \gamma; \omega) + \Sigma_{i \in cf} e^{\omega}_{i}(\varepsilon_2, \gamma), \qquad (2)$$

where the E_{ld} is the Liquid Drop Model energy [4]), the E_{corr} is the quantal effect correction to the energy, which includes both shell [5]) and the pairing [6]) corrections. The collective rotational energy E_{rot} may be calculated microscopically as the energy difference between the expectation values of the H^{ω} with and without rotation, by using the wave functions for the q.p. vacuum configuration [7]). The last term of the equation (2) is the sum of the q.p. energies belonging to the configuration cf, which generates the deformation drive. The hexadecapole deformation is fixed $\varepsilon_4 = 0$ in the present calculation as a good approximation. All of the terms in equation (2) depend on the (Z, N) numbers which are not written explicitly. The equilibrium deformations of nucleus may be calculated by minimizing the total routhian energy of equation (2) with respect to the ε_2 and γ deformations for each configuration.

3. Results of calculation and discussion

3.1. SIGNATURE SPLITTING AND TRIAXIALITY

It is well studied and generally accepted that the triaxial motion of nuclear shape in an odd mass nucleus may be identified with the signature energy splitting of the rotational bands in question, a change of the signature splitting implies most probably the change of the γ deformation [7-9]. The routhian energies of the lowest two q.p. orbits of the $g_{9/2}$ shell are calculated as functions of the γ deformation and plotted in Fig.1 (a) for $N = 45$ neutron system and Fig.1 (b) for $Z = 42$ and Fig.1 (c) for $Z = 40$ proton systems. The A_i and B_i above the curves denote the two lowest $g_{9/2}$ q.p. rotating orbits with the signature $\alpha = 1/2$ and $-1/2$ respectively, where the $i = (n, p)$ for (neutron, proton). It is seen from Fig.1 (a) that the signature splitting, namely the energy difference between the orbits with the signature $\alpha = 1/2$ (solid) and $\alpha = -1/2$ (dots), is nearly zero at $\gamma \geq 0°$ and becomes large at the negative γ values, and a strong γ drive toward the negative values is visible. This is a typical feature of the γ drive and the signature splitting in an odd mass nucleus when the Fermi level of the odd number of particles lies at the middle of a high-j shell, the $\nu g_{9/2}$ shell in the present case and the $\pi h_{11/2}$ shell in the light rare earth nuclei. The disappearness of the signature splitting after the first backbend observed in the $\pi h_{11/2}$ bands of the light rare earth region [10,11] can be well explained by the mechanism that the γ deformation change from the negative values to near zero, which is caused by the γ deformation drive of the aligned $i_{13/2}$ neutron pair [7,9]. However, the large signature splitting observed in the $\nu g_{9/2}$ bands of ^{87}Mo does not disappear but extends to high spins and maintains almost constant after the backbend [1]. It is not surprising that no disappearness of the signature splitting occurs in ^{87}Mo, since the γ deformation driving tendency of the $g_{9/2}$ proton orbits completely differs from that of the $i_{13/2}$ neutron orbits, the later presents a very strong positive γ driving force since the neutron Fermi level lies at the beginning of the shell. For ^{87}Mo with the $Z = 42$ the proton Fermi level lies at a bit lower than the middle of the $g_{9/2}$ shell so that a strong γ deformation drive of the lowest two q.p. orbits marches toward negative values and there is only a gentle drive from 0° to 60°, as shown in Fig.1 (b). It is expected that the γ deformation of the $g_{9/2}$ 1 q.p. bands has a negative value around $-40°$ due to the γ negative driving tendency as shown in Fig.1 (a) and should not change its negative value when going to the 3 q.p. bands after the backbend due to the negative γ driving property of the aligned $g_{9/2}$ proton pair as shown in Fig.1 (b). Indeed, the calculated equilibrium γ deformation is $-40°$ for the $[A_n]$ 1 q.p. configuration and $-35°$

for the $[A_n A_p B_p]$ 3 q.p. configuration. The almost unchanged γ deformation is responsible for the large and almost constant signature splitting observed in the $\nu g_{9/2}$ bands of ^{87}Mo. The γ driving tendency of the $g_{9/2}$ proton orbits becomes a positive γ drive toward 60° when going from $Z = 42$ to $Z = 40$, as shown in Fig.1 (c). The opposite change of the driving tendency is triggered by the two particle removal of the filling degree of freedom in the $g_{9/2}$ shell. It is expected that the signature splitting of the $\nu g_{9/2}$ bands of ^{85}Zr would disappear after the backbend, caused by the change of the γ deformation from the negative to the positive values due to the alignment of the $g_{9/2}$ proton pair. In the phenomenon of the signature splitting disappearness, the role of the alignment of the $g_{9/2}$ q.p. protons in ^{85}Zr is similar to that for the alignment of the $i_{13/2}$ q.p. neutrons in the light rare earth nuclei [10]. It is certainly interesting to look at experimentally whether such a phenomenon could occur in the $g_{9/2}$ neutron bands of ^{85}Zr. Unfortunately , the bands under the question were measured not well beyond the backbend, although the signature splitting observed in the 1 q.p. neutron bands is large and quenched at the backbend, but no more data for the 3 q.p. bands [12]. However, the signature splitting data of the 3 q.p. bands are important for justifying whether the turning point of the γ driving tendency toward the positive γ values is at $Z = 40$ protons and then providing an accurate test for the theory. According to the mechanism, the other light isotone nuclei of $N = 45$ neutrons, such as ^{83}Sr and ^{81}Kr, are expected to have the signature splitting disappearness, namely a large signature splitting in the ground state bands, but an almost vanishing splitting in the proton pair aligned bands since the $g_{9/2}$ proton q.p. orbits near the Fermi surface become the source of a strong positive γ drive in $Z \leq 40$ isotone nuclei. Indeed, the disappearness of the signature splitting was observed in ^{81}Kr [13]) and explained by the above mechanism [14]). The relevant bands in ^{83}Sr were not measured beyond the backbend[15]), the lack of the experimental data is just like that in ^{85}Zr.

The routhian energies of the lowest four negative parity orbits for the $N = 45$ neutron system are calculated and plotted as functions of the γ deformation in Fig.2. The E_n and G_n orbits have the signature $\alpha = 1/2$ and the F_n and H_n with the signature $\alpha = -1/2$. The present TRS calculation of ^{87}Mo yields a prolate shape rotating around its symmetry axis, namely $\gamma = -120°$, for the $[E_n]$ configuration and a prolate shape, $\gamma \approx 0°$, for the $[G_n]$ and $[F_n]$ configurations. The $I^\pi = 1/2^-$ isomeric state found at around 250 KeV excitation energy in the light $N = 45$ nuclei [12,13,15]) may be based on

the $[E_n]$ configuration and has the nature of the $\nu p_{1/2}$. The low lying negative parity state of configuration $[E_n]$ was not found in ^{87}Mo probably due to the too weak population of this isomeric state in the employed heavy ion reaction [1]) beacuse of its single particle property. The tentatively assigned negative parity bands with a small signature splitting found in ^{87}Mo may be explained as the $[G_n]$ and $[F_n]$ bands which have the γ deformation of $\sim 0°$ and thus a small signature splitting, as shown in Fig.2. It should be mentioned that either the G_n or E_n orbit has the nature of the $\nu p_{1/2}$ and $\nu f_{5/2}$ shells because the strong admixture between these two shells are found at around $\gamma = 0°$.

3.2. TRANSITION QUADRUPOLE MOMENT

The result of the negative γ deformation for ^{87}Mo is contrary to that given in ref.[1]), where the equilibrium γ deformation for the aligned yrast band is positive, $\gamma = 26°$, determined together with the deformation $\beta_2 = 0.28$ as a constrained solution of the equations of the (β_2, γ) variables, namely

$$Q_t = \frac{3}{\sqrt{5\pi}} Z R_0^2 \beta_2 \frac{cos(\gamma + 30°)}{cos30°}, \tag{3}$$

$$J^{(1)} = \frac{2}{5} M R_0^2 (1 + \sqrt{\frac{5}{4\pi}} \beta_2 sin(\gamma + 30°)), \tag{4}$$

where $R_0 = 1.2A^{1/3}$ fm and M is the mass of nucleus, the transition quadrupole moment Q_t and the static moment of inertia $J^{(1)}$ are set to their experimental values for the aligned bands. The ε_2 is approximately equal to $0.94\beta_2$ and the more accurate relation formula with higher order terms can be found in the literature, for an example ref.[16]). The problem is that the positive γ deformation value results in an almost vanishing signature splitting for the $g_{9/2}$ neutron bands in ^{87}Mo after the backbend as discussed above and seen in Fig.1 (a), and thus it is in disagreement with the experiment. And it seems that the rigid body expression (4) of $J^{(1)}$ is incorrect to apply to the rather low spin region where the pairing interaction still play a very important role and the spin alignment of individual quasiparticles contribute significantly to the moment of inertia. The deformations of $(\varepsilon_2, \gamma) = (0.16, -35°)$ obtained in the present calculation, see Fig.3 (b), are more reasonable since they reproduce not only the experimental signature

splitting but also the Q_t data. The calculated Q_t by equation (3) with these deformation parameters is $Q_t = 1.7e \cdot b$ which is in a nice agreement with the experiment.

Fig.3 (a) is the TRS diagram calculated for the ground state band $[A_n]$, $\nu(g_{9/2})^1$ configuration of ^{87}Mo and the equilibrium deformations are determined by the minimum of the total energy as $\varepsilon_2 = 0.19$ and $\gamma = -40°$. The equilibrium deformations for the aligned band $[A_n A_p B_p]$, $\nu(g_{9/2})^1\pi(g_{9/2})^2$ configuration are $(\varepsilon_2 = 0.16, \gamma = -35°)$. The reduction of the ε_2 deformation when going from the ground 1 q.p. band to the aligned 3 q.p. band is caused by the ε_2 deformation drive of the aligned $g_{9/2}$ protons toward small values, as shown in Fig.4, in which plotted are the calculated routhian energies of the lowest two $g_{9/2}$ proton orbits as functions of the ε_2 deformation at a fixed $\gamma = -40°$. One can see from Fig.3 (a) that the potential energy surface exhibits a softness when going from the minimum toward the origin of coordinates along the ε_2-axis at $\gamma \approx -40°$, so that even a gentle ε_2 drive as presented in Fig.4 could have a considerable effect on the reduction of the ε_2 deformation of the soft core. An other striking feature presented in the TRS diagram of Fig.3 (a) is that the γ deformation is extremely soft from $-40°$ to $-90°$ at the equilibrium ε_2 deformation. Such an extremely shallow minimum coexisted with other shallow minima is the characteristics of the calculated TRS diagram for the transitional nuclei. Such a shallow minimum indicates that the rotational motion of a soft rotor may be accompanied with the vibrational motion, most likely the γ vibration. The standard cranking shell model calculation with the calculated ground state deformation parameters and the pairing gap $\Delta_p = 0.13\ \hbar\omega_0$ can not reproduce the band crossing frequency observed in ^{87}Mo, rather too small for the theory. By considering the influence of the vibrational motion, if an effective γ deformation is chosen as $\gamma = -60°$, the average of the γ deformations of the two shallow minima shown in Fig.3 (a), the calculated crossing frequency and the spin alignment is $\hbar\omega_c = 0.43$ MeV and $i_x = 6.7\hbar$ respectively, which are in agreement with the experimental values $\hbar\omega_c = 0.45$ MeV and $i_x = 6.5\hbar$. It should be kept in mind that this treatment is only a qualitative estimation by considering one fact out of others which may effect on the crossing frequency in such a soft nucleus. A striking feature observed in the yrast band of ^{87}Mo is the drastic rising of the transition quadrupole moment Q_t after the backbend, from $\sim 0.7e \cdot b$ in the ground band to $\sim 1.6e \cdot b$ in the aligned band, here the quantum number $K = 5/2$ was taken in the calculation of the Q_t from mea-

sured B(E2) values. The calculated deformation parameters for the aligned band states reproduce well the Q_t data after the backbend, however, those for the ground band states lead to a factor of 2 larger Q_t value for the ground band states and thus can not explain the rising feature of the Q_t. As a guess, the rather small Q_t value of the ground state may be originated from the weakening effect of the possible vibrational motion on the E2 collectivity for a very soft rotor. It was found that the calculations of the Strutinsky type by means of both the folded Yukawa potential [17]) and the Woods-Saxon potential with the universal parameters [18]) give a basically spherical shape for both the ground band and the aligned band states and thus can not reproduce the Q_t data of ^{87}Mo. The possible shape change that would be indicated by the sharp rising of the Q_t after the backbend, is in contradiction with the ε_2 and γ driving tendencies of the $g_{9/2}$ proton orbits, see Fig.2 and Fig.1 (b). Despite of the successful calculations and satisfactory explanations in other aspects, the discrepancy between the theory and the experiment about the sharp rising of the Q_t after the backbend observed in ^{87}Mo remains to answer satisfactorily. It should be noticed that the 879KeV transition just above the $17/2^+$ state which connects the ground and the aligned bands has the biggest B(E2) value, and thus the biggest Q_t. It is hard to understand at the base of the mean field theory why the transition which connects the states with very different deformations can have such a big B(E2) value.

3.3. SHAPES OF MOLYBDENUM ISOTOPE NUCLEI

The total routhian surfaces calculated for the ground state bands for ^{86}Mo, ^{88}Mo, ^{89}Mo and ^{90}Mo are shown in Fig.5. The deformed shape minima are found for the Mo isotope nuclei with the $N \leq 46$, see Fig.3 (a), Fig.5 (a) and (b), and the spherical shape minima found for the $N \geq 47$ Mo isotope nuclei, see Fig.5 (c) and (d). A deformed triaxial shape ($\varepsilon_2 = 0.25, \gamma = -32°$) is found for the ground state configuration [0] of ^{86}Mo, $N = 44$, and a slightly deformed triaxial shape of ($\varepsilon_2 = 0.16, \gamma = -20°$) for the [0] configuration of ^{88}Mo, $N = 46$, which is similar to that for ^{87}Mo shown in Fig.3 (a); A near spherical shape ($\varepsilon_2 = 0.04, \gamma = -120°$) is established for the ground band configuration $[A_n]$ in ^{89}Mo, $N = 47$, shown in Fig.5 (c), and a typical pattern of a spherical shape presents in the TRS diagram of ^{90}Mo, shown in Fig.5 (d). All these calculated results are in excellent agreement with the experiments. The yrast sequence of ^{88}Mo was measured up to the 14^+ state and the strong

backbend is observed at spin $I = 6$ [19]), the observed rotational structure of the spectrum provides a crucial evidence for the deformed shape. With one more neutron added to the system, the rotational structure disappears in ^{89}Mo according to the calculation. Indeed, the high spin level scheme of ^{89}Mo was just established experimentally at Beijing Tandem Lab and found no collective rotational structure in the spectrum [20]). The spherical shapes for the $N \geq 48$ systems are proved in the recently done experiments of the high spin spectroscopies of ^{90}Mo and ^{92}Mo, where the level spectrum obey the spherical single particle coupling scheme [21]). The high spin spectroscopy of ^{86}Mo has not been measured yet, but the well deformed shape for the $N = 44$ system has been well identified with the high spin spectra of the neighbour isotone nuclei, for an example ^{84}Zr [22]). It is noticed that the shape calculations of the same type for the ground-state bands by means of both the folded Yukawa potential [17]) and Woods-Saxon potential with the universal parameters [18]) give a too small critical neutron number $N \geq 43$ for the spherical shapes for the Mo isotope nuclei, and thus are in disagreement with the experiments, indicating a requirement of new sets of potential parameters for the region.

4. The Summary

By considering the configuration dependence of nuclear shapes, the cranking approximation and the Strutinsky method that incorporates the (MHO) potential are applied to the description of the high spin states of the transitional nuclei, as a good example, ^{87}Mo is studied in detail. The large signature splitting of the positive parity bands and the almost vanishing signature splitting of the negative parity bands observed in ^{87}Mo are reproduced by the present calculation and explained by the triaxial motion driven by the high-j rotating $g_{9/2}$ q.p. orbits. The transition quadrupole moment Q_t calculated with the calculated deformation parameters for the $\nu(g_{9/2})^1\pi(g_{9/2})^2$ configuration is in a good agreement with the experiment Q_t value of the aligned band in ^{87}Mo. However, the calculated deformations for the $\nu(g_{9/2})^1$ configuration overestimates the Q_t value of the ground state band, indicating that perhaps the vibrational motion should be taken into account for such a very soft rotor. The nuclear shapes of the Mo isotope nuclei become spherical

when the neutron number increases closing to the magic number $N = 50$, the present calculation yields the correct critical neutron number $N \geq 47$ for the spherical shape. The calculations by means of the folded Yukawa and the so called universal Woods-Saxon potentials are fail to reproduce the experimental transition quadrupole moments for both the ground and the aligned yrast bands in ^{87}Mo, and give a too small critical neutron number $N \geq 43$ for the spherical shape of Mo isotope nuclei, and thus the new sets of potential parameters may be required for this transitional region.

The work is supported by the National Natural Science Foundation of China.

References

1) Ch.Winter, D.J.Blumenthal, P.Chowdhury, B.Crowell, P.J.Ennis, S.J.Freeman, C.J.Lister, C.J.Gross, J.Heese, A.Jungclaus, K.P.Lieb, D.Rudolph, M.A.Bentley, W.Gelletly, J.Simpson, J.L.Durell and B.J. Varley, Nucl. Phys. **A535**(1991)137
2) I.Ragnarsson, R.K.Sheline, Phys. Scripta **29**(1984)385
3) A.H.Wapstra, G.Audi, Nucl. Phys. **A432**(1985)1
4) W.D.Myers, W.Swiatecki, Ari. Fys. **361**(1967)343
5) V.M.Strutinsky, Nucl. Phys. **A122**(1968)1; **A95**(1967)420
6) R.Wyss, J.Nyberg, A.Johnson, R.Bengtsson, W.Nazarewicz, Phys. Lett. **B215**(1988)211
7) Y.S.Chen, S.Frauendorf, L.L.Riedinger, Phys. Lett. **B171**(1986)7
8) Y.S.Chen, S.Frauendorf, G.A.Leander, Phys. Rev. **C28**(1983)2437
9) S.Frauendorf, F.R.May, Phys. Lett. **B125**(1983)245
10) G.B.Hagemann, J.D.Garrett, B.Herskind, J.Kownacki, B.M.Nyakó, P.L.Nolan, J.F.Sharpey-Schafer and P.O.Tjøm, Nucl. Phys. **A424**(1984)365
11) A. J. Larabee, L.H.Courtney, S.Frauendorf, L.L.Riedinger, J.C.Waddington, M.P.Fewell, N.R.Johnson, I.Y.Lee and F.K.McGowan, Phys. Rev. **C29**(1984)1934
12) S.Suematsu, Y.Haruta, B.J.Min, K.Heiguchi, Y.Ishikawa, S.Mitarai, T.Kuroyanagi and Y.Onizuka, Nucl. Phys. **A485**(1988)304

13) L.Funke, J.Döring, P.Kemnitz, E.Will, G.Winter, A.Johnson, L.Hildingsson and Th. Lindblad, Nucl. Phys. A455(1986)206
14) Y. S. Chen, Nucl. Phys. A421(1984)403c
15) S.E. Arnell, S. Sjoberg, O. Skeppstedt, E. Wallander, A. Nilsson and G. Finnas, Nucl. Phys. A334(1980)71
D.Bucurescu, G.Constantinescu, M.Ivaşcu, N.V.Zamfir and M.Avrigeanu, J. Phys. G7(1981)399
16) R.Bengtsson, J.Dudek, W.Nazarewicz and P.Olanders, Phys. Scripta 39(1989)196
17) P. Möller, J.R. Nix, Atom. Data and Nucl. data Tab. 26(1981)165; Nucl. Phys. A361(1981)117
18) J.Dudek, Z.Szymański and T.Werner, Phys. Rev. C23(1981)920
19) S.Wen et al., in Progress Report for Beijing National Tandom Accelerator Laboratory(1990-1991), ed. CIAE (China Ocean Press, Beijing, 1992) p.83
20) S.Wen et al., in Progress Report for Beijing National Tandom Accelerator Laboratory(1990-1991), ed. CIAE (China Ocean Press, Beijing, 1992) p.84
S.Wen et al., in Proc. Int. Nucl. Phys. Conf.(Abstract), Wiesbaden 1992, Germany, ed. U.Grundinger, p.1.2.10
21) Pragya Singh, R.G. Pillay, J.A. Sheikh and H.G. Devare, Phys. Rev. C45(1992)2161
22) H.G.Price, C.J.Lister, B.J.Varley, W.Gelletly and J.W.Olness, Phys. Rev. Lett. 51(1983)1842

Captions of Figures

Fig.1 The routhian energies of the two lowest positive parity rotating $g_{9/2}$ q.p. orbits at $\hbar\omega = 0.025\hbar\omega_0$, plotted as functions of the γ deformation, calculated at the $\varepsilon_2 = 0.18$ and the $\Delta_n = 0.15\hbar\omega_0$ for the $N = 45$ neutron system (panel (a)), the $\Delta_p = 0.10\hbar\omega_0$ for the $Z = 42$ system (panel (b)), the $\Delta_p = 0.10\hbar\omega_0$ for the $Z = 40$ system (panel (c)). The orbits with the

signature $\alpha = 1/2$ and $-1/2$ are denoted by the A_i (solid line) and B_i (dots line) respectively, here $i = (n, p)$ for (neutron, proton) system.

Fig.2 The routhian energies of the four lowest negative parity rotating q.p. neutron orbits at $\hbar\omega = 0.025\hbar\omega_0$, plotted as functions of the γ deformation, calculated with the $\varepsilon_2 = 0.18$ and $\Delta_n = 0.15\hbar\omega_0$ for the $N = 45$ system. The solid (E_n, F_n) and dots (G_n, H_n) lines stand for the signature $\alpha = 1/2$ and $-1/2$ respectively.

Fig.3 The calculated total routhian energy surfaces for ^{87}Mo: (a) for the ground band configuration $[A_n]$, $\nu(g_{9/2})^1$, at spin $I = 9/2$ and (b) for the aligned band configuration $[A_nA_pB_p]$, $\nu(g_{9/2})^1\pi(g_{9/2})^2$, at spin $I = 23/2$. The scale of an unlabeled line relative to its neighbor is 0.2 MeV and the crosses denote the minima.

Fig.4 The routhian energies of the two lowest $g_{9/2}$ rotating $g_{9/2}$ q.p. proton orbits at $\hbar\omega = 0.025\hbar\omega_0$, plotted as functions of the ε_2 deformation, calculated at the $\gamma = -40°$ and $\Delta_p = 0.10\hbar\omega_0$ for the $Z = 42$ system, the solid and dots lines denoted by the A_p and B_p stand for the signature $\alpha = 1/2$ and $-1/2$ respectively.

Fig.5 The calculated total routhian energy surfaces for the ground state band configurations at $\hbar\omega = 0.025\hbar\omega_0$ for (a) ^{86}Mo, (b) ^{88}Mo, (c) ^{89}Mo and ^{90}Mo. The scale of an unlabeled line relative to its neighbor is 0.2 MeV and the crosses denote the minima.

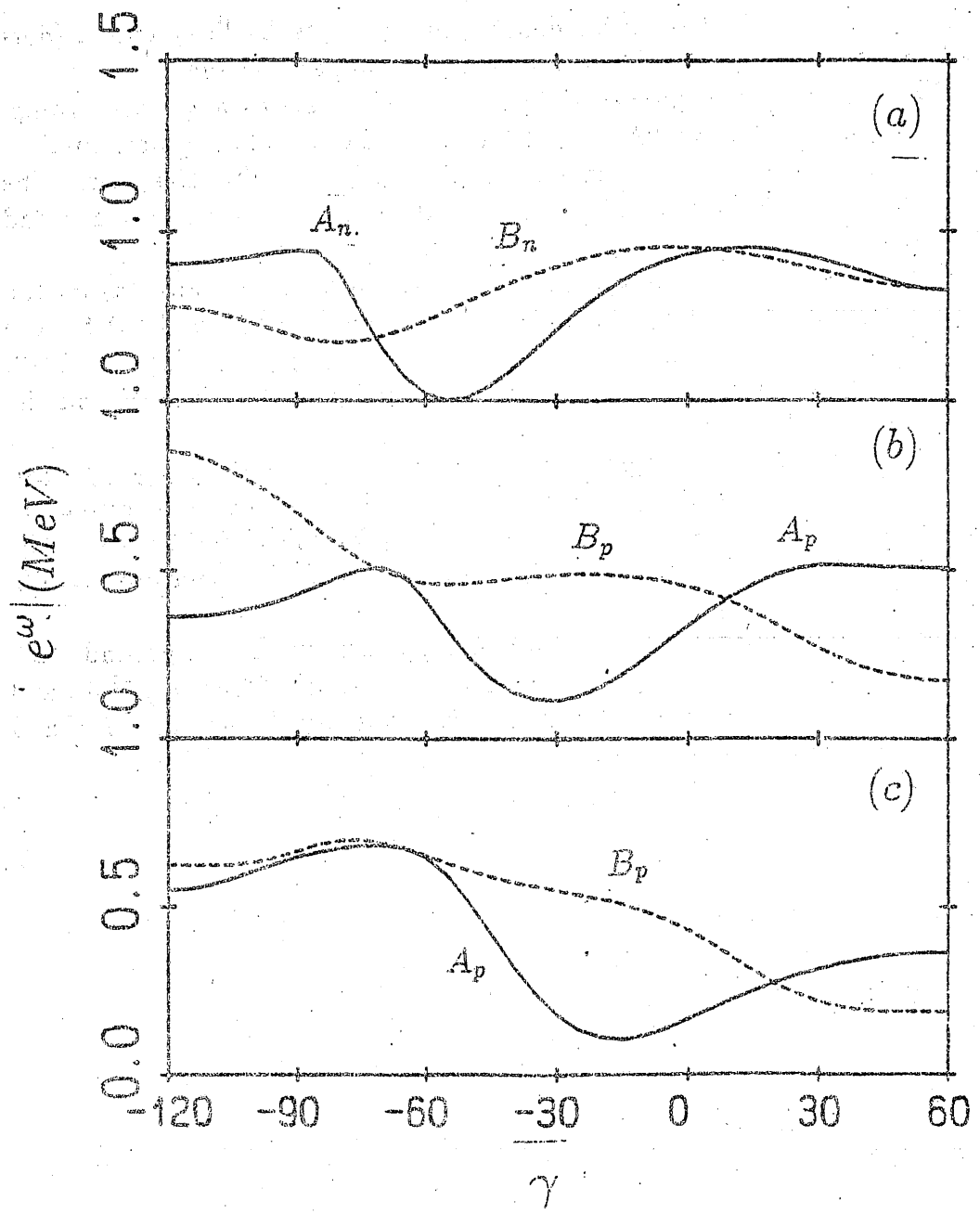
(a)
A_n
B_n
(b)
B_p
A_p
(c)
B_p
A_p
$e^{\omega}|(MeV)$
1.5
1.0
0.5
0.0
-120
-90
-60
-30
0
30
60
γ

Fig 1

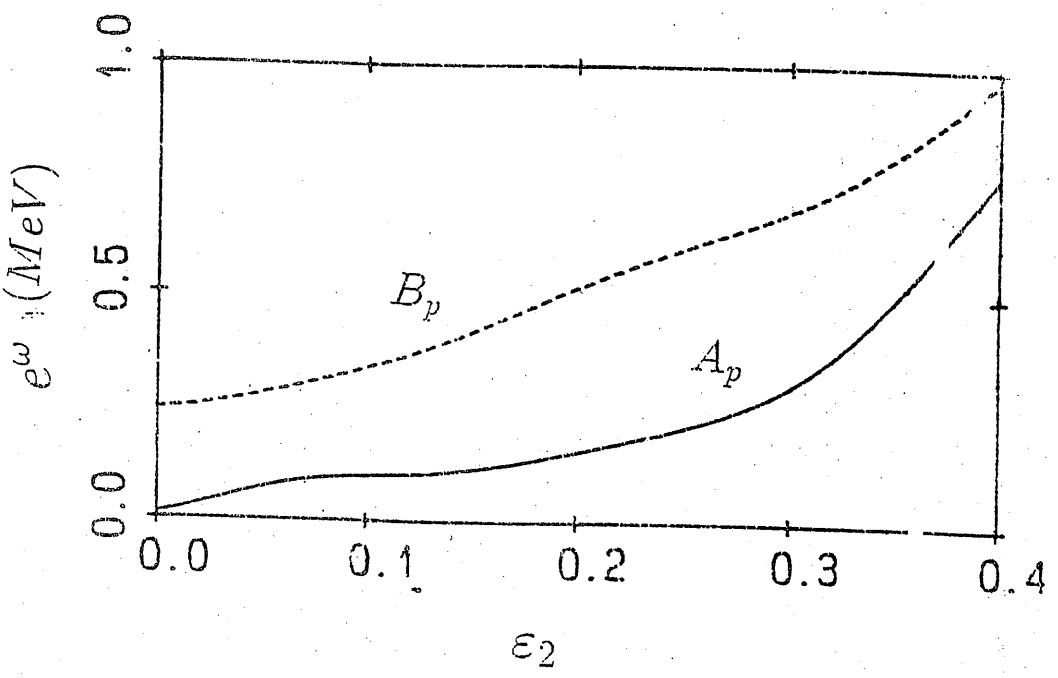

Fig 4

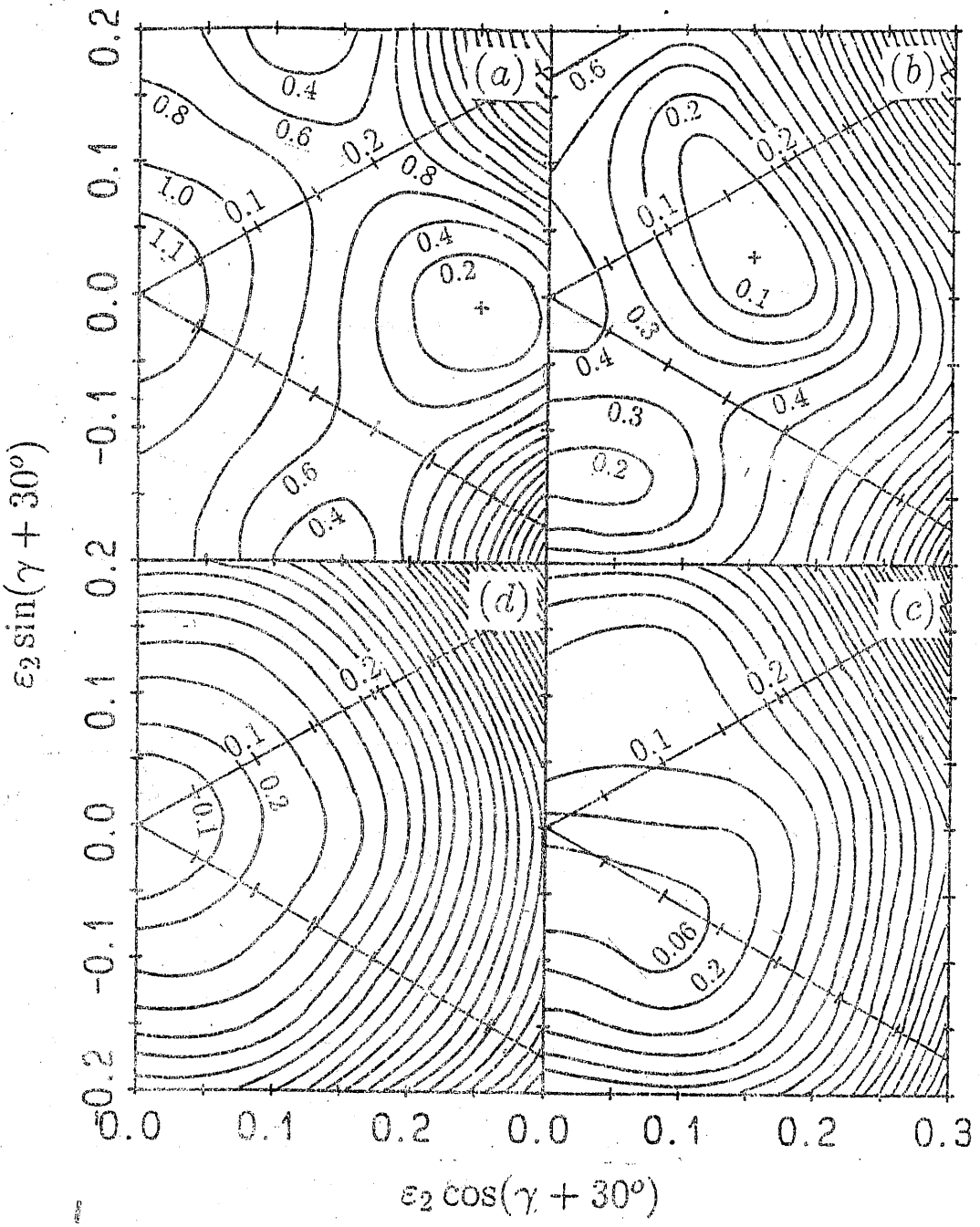
(a)
(b)
(c)
(d)
0.4
0.8
0.6
0.2
1.0
0.1
1.1
0.3
0.06
0.2
0.1
0.0
-0.1
-0.2
0.0
0.1
0.2
0.3
$\varepsilon_2 \sin(\gamma + 30°)$
$\varepsilon_2 \cos(\gamma + 30°)$

Fig. 5

Coefficients of Fractional Parentage of the Boson System with Single l and F-spin 1/2 *

Hong-zhou Sun
Department of Physics, Tsinghua University, Beijing 100084, China
Institute of Theoretical Physics, Academia Sinica, Beijing 100080, China
Qi-zhi Han
Department of Physics, Peking University, Beijing 100871,China
Yu-xin Liu
CCAST(World Laboratory), P. O. Box 8730, Beijing 100080,China
Institute of Theoretical Physics, Academia Sinica, Beijing 100080, China

November 29, 1992

Abstract

A system of identical bosons with single angular momentum l and F-spin 1/2 is under consideration. The classification of it's wave functions and the evaluation of it's coefficients of fractional parentage are discussed by using the generalized Wigner-Eckart theorem of semisimple compact Lie groups.

1 Introduction

It is known that the Interacting Boson Model(IBM) has been successful in describing the nuclear coolective motion[1], and the coefficients of fractional parentage(CFP)[2-5] method is one of the most efficient techneque for constructing the IBM wave functions. Even though many works have been done to study nuclear physics in the framework of IBM, the discussion on the CFP of IBM is relatively meager. As a consequence, the work load of calculation of some computer codes in the framework of IBM is tremendously heavy. Moreover some of them can not be performed for the nucleus including relatively many bosons. These defects have limitted the application region of IBM. It is fortunate that Sun and their colaborators have recently put forward a simple formula to calculate the CFP of IBM1[6]. And a computer code has also been set up[7]. With the code the

*The project supported by Doctoral Programm Foundation of Institution of Higher Education of China and National Natural Science Foundation of China

CFP's of the system including 42 d-bosons can be obtained. It provides us convenience to describe the nuclear superdeformed state and chaotic behavier of many boson system.

In fact, as the nuclear physics being discussed in the framework of IBM, it is usually recongnised that the IBM2[4] is the most efficient version to be used. It is certain that the proton boson and the neutron boson can be treated separately in this case. However the configuration space is enlarged remarkablely. It increases a great amount of the work of calculation, so that the application region is limitted. In the other hand the physical meaning is not transparent enugh. To solve this problem, a formalism to determine the CFP of IBM2, which is just the CFP of boson system with single angular momentum l and F-spin 1/2, is proposed in the light of Lie group theory. In this paper we discuss the classification of the wave function of the system and the factorization of the CFP, and give a recurrent formula to evaluate the CFP with definite seniority and F-spin.

2 Classification of Wave Functions

The wave functions of the system with many bosons, each with angular momentum l and F-spin 1/2, are classified according to the group chain

$$U(2N) \supset (U(N) \supset O(N) \supset O(3)) \otimes SU(2) \quad (N = 2l+1). \tag{2.1}$$

Supposing

$$\begin{aligned} b^{\dagger}_{m\sigma} &= b^{\dagger}_{lm1/2\sigma}, \\ b_{m\sigma} &= b_{lm1/2\sigma}, \end{aligned} \tag{2.2}$$

are the creation and annihilation operators of boson with angular momentum l, F-spin 1/2 and z component m and σ. And let

$$\tilde{d}_{m\sigma} = (-1)^{l+m+1/2+\sigma} b_{l-m1/2-\sigma}$$

be the irreducible tensor corresponding to $b_{m\sigma}$. The generators, Casimir operators, and the labels of IRRPs for each subgroup in the group chain (2.1) are given in Table 1.

Table 1. The generators, Casimir operators and IRRP labels for groups in chain (2.1)

Group	Generators	Casimir Operators	IRRP Labels
$U(2N)$	$B^{kJ}_{qu} = (b^{\dagger}\tilde{b})^{kJ}_{qu}$	$C_{1U(2N)} = \sum_{m,\sigma} b^{\dagger}_{m\sigma} b_{m\sigma} = \hat{N}_b$ $C_{2U(2N)} = \sum_{k,J} B^{kJ} \cdot B^{kJ}$ $= \hat{N}_b(\hat{N}_b + 2N + 1)$	$[n]$
$U(N)$	$P^k_q = \sqrt{2} B^{k0}_{q0}$	$C_{2U(N)} = \sum_k P^k \cdot P^k$ $= \frac{\hat{N}_b(\hat{N}_b + 2N - 4)}{2} + 2\hat{F} \cdot \hat{F}$	$[n_1, n_2]$
$O(N)$	$P^k \quad k = odd$	$C_{2O(N)} = \sum_{k=odd} P^k \cdot P^k$ $= C_{2U(N)} - \hat{N}_b - 2\varphi^1 \cdot \tilde{\varphi}$	(σ_1, σ_2)
$O(3)$	$\hat{L}_q = \sqrt{l(l+1)N/3} P^1_q$	$C_{2O(3)} = \hat{L} \cdot \hat{L}$	L
$SU(2)$	$\hat{F}_u = \sqrt{N/2} B^{01}_{0u}$.	$C_{2SU(2)} = \hat{F} \cdot \hat{F}$	F

in which $\wp_u^\dagger = \sqrt{\frac{N}{2}}(b^\dagger b^\dagger)^{0\,1}_{0\,u}$, $\tilde{\wp}_u = \sqrt{\frac{N}{2}}(\tilde{b}\tilde{b})^{0\,1}_{0\,u}$ is the creation and annihilation operator of boson pair respectively. They are the invariant quantities of group $O(N)$

The wave functions of the boson system can then be written as

$$\begin{array}{l} |[n]_{2N} \quad [n_1\, n_2]_N \quad \langle \sigma_1 \sigma_2 \rangle \;\; \alpha \;\; L \quad \beta \quad F\rangle, \\ \quad U(2N) \;\; U(N) \quad\quad O(N) \quad O(3) \quad SU(2) \end{array} \tag{2.3}$$

where α and β are additional quantum numbers. The reason for including these additional quantum number is that the reductions of $U(N) \supset O(N)$ and $O(N) \supset O(3)$ are not simple reducible.

The eq.(2.3) can be rewritten as

$$|n(sf)\alpha L\beta F\rangle = |[n]_{2N}\,[n_1\, n_2]_N\,\langle \sigma_1\sigma_2\rangle\,\alpha\, L\,\beta\, F\rangle, \tag{2.4}$$

where

$$s = \sigma_1 + \sigma_2, \qquad f = \frac{\sigma_1 - \sigma_2}{2}.$$

From eq.(2.3) we know that it requires 7 parameters to label the wave function completely. These 7 parameters can be chosen as the ones in eq.(2.4), i.e., $n, s, f, \alpha, L, \beta, F$. According to the definition of eq.(2.4), $|n(sf)\alpha L\beta F\rangle$ satisfies the following relations,

$$\begin{bmatrix} C_{2U(2N)} \\ C_{2U(N)} \\ C_{2O(N)} \\ C_{2O(3)} \\ C_{2SU(2)} \end{bmatrix} |n(sf)\alpha L\beta F\rangle = \begin{bmatrix} n(n+2N-1) \\ \dfrac{n(n+2N-4)}{2} + 2F(F+1) \\ \dfrac{n(n+2N-6)}{2} + 2f(f+1) \\ L(L+1) \\ F(F+1) \end{bmatrix} |n(sf)\alpha L\beta F\rangle. \tag{2.5}$$

Because $\wp_u^\dagger, \tilde{\wp}_u$ are the invariant quantities of group $O(N)$, $|n(sf)\alpha L\beta F\rangle$ can be obtained by means of acting the operator $\wp_u^\dagger$ on $|(sf)\alpha L\rangle = |s(sf)\alpha Lf\rangle$ step by step, i.e.,

$$|n(sf)\alpha L\beta F\rangle = C\{(\wp_u^\dagger)^\rho |(sf)\alpha L\rangle\}^{\beta\, F}, \tag{2.6}$$

where $\rho = \dfrac{n-s}{2}$, C is the normalizing constant. $|(sf)\alpha L\rangle$ satisfies the restrictions shown in the following

$$\begin{bmatrix} \hat{N}_b \\ \hat{L}^2 \\ \hat{F}^2 \\ \tilde{\wp}_u \end{bmatrix} |(sf)\alpha L\rangle = \begin{bmatrix} s \\ L(L+1) \\ f(f+1) \\ 0 \end{bmatrix} |(sf)\alpha L\rangle. \tag{2.7}$$

The discussion above shows that s is the seniority and f can be regarded as the reduced F-spin.

3 The branching Rule of the Reduction $U(2N) \supset (U(N) \supset O(N) \supset O(3)) \otimes SU(2)$

(a) The Reduction of $U(2N) \supset U(N) \otimes SU(2)$

The branching rule for this reduction is quite simple. It can be expressed as

$$[n]_{2N} = \sum_{n_1 n_2} [n_1\, n_2]_N \otimes F, \tag{3.1}$$

where

$$n = n_1 + n_2, \qquad F = \frac{n_1 - n_2}{2}.$$

(b) The Reduction of $U(N) \supset O(N)$

Using the representation theory of group $U(N)$ and $O(N)$[9] one can get the following recurrent relations of the branching rule for the reduction $U(N) \supset O(N)$

$$\begin{aligned} [n,\, n]_N &= [n-2,\, n-2]_N + F(n,\, n) - F(n-1,\, n-1); \\ [n,\, n-1]_N &= F(n,\, n-1); \\ [n_1,\, n_2]_N &= [n_1 - 2,\, n_2]_N + F(n_1,\, n_2), \end{aligned} \tag{3.2}$$

where

$$\begin{aligned} F(n_1,\, n_2) &= \sum_{\beta\,\alpha} (n_1 - \beta + \alpha,\, \alpha); \\ \beta &= n_2, n_2 - 2, n_2 - 4, \cdots\cdots\cdots, \geq 0; \\ \alpha &= \beta, \beta - 1, \beta - 2, \cdots\cdots\cdots, 0\,. \end{aligned} \tag{3.3}$$

With the eqs.(3.2) and (3.3), all of the branching rules of this reduction can be obtained.

(c) The Reduction of $O(N) \supset O(3)$

The method to get the branching rules for this reduction analytically has been proposed by Wang et. al.[10]. With the computer codes[10,11] all the branching rules can be obtained.

4 The Coefficient of Fractional Parentage

The coefficient of fractional parentage for the system whose wave founction can be labelled by the group chain (2.1) can be expressed in the second quantization representation as

$$\langle n(sf)\alpha L\beta F\{|n-1(s'f')\alpha' L'\beta' F'\rangle = \sqrt{\frac{1}{n}}\langle n(sf)\alpha L\beta F\|b^{\dagger}\|n-1(s'f')\alpha' L'\beta' F'\rangle, \tag{4.1}$$

where $\langle \cdots \| b^\dagger \| \cdots \rangle$ is the reduced matrix element of the irreducible tensor $b^\dagger_{m\sigma}$. It is easy to show that $b^\dagger_{m\sigma}$ is the irreducible tensor with rank $[1]_{2N}$ under the group chain (2.1), i.e.,

$$\begin{array}{cccccc} b^\dagger_{m\sigma} = b^\dagger([1]_{2N} & [1]_N & \langle 1,0\rangle & lm & 1/2\sigma). \\ U(2N) & U(N) & O(N) & O(3) & SU(2) \end{array} \tag{4.2}$$

Then taking advantage of the generalized Wigner-Eckart theorem the reduced matrix element of $b^\dagger_{m\sigma}$ can be factorized according the group chain (2.1) as

$$\begin{aligned} &\langle n\,(s\ f)\,\alpha\ L\beta\ F\|b^\dagger\|n-1\,(s'\ f')\,\alpha'\ L'\beta'\ F'\rangle \\ &= \sqrt{n}\left[\begin{array}{cc|c} [1]_{2N} & [n-1]_{2N} & [n]_{2N} \\ [1]_N & [n'_1\ n'_2]_N & [n_1\ n_2]_N \end{array}\right]\left[\begin{array}{cc|c} [1]_N & [n'_1\ n'_2]_N & [n_1\ n_2]_N \\ <1> & \beta' <\sigma'_1\ \sigma'_2> & \beta <\sigma_1\ \sigma_2> \end{array}\right] \\ &\quad \left[\begin{array}{cc|c} <1> & <\sigma'_1\ \sigma'_2> & <\sigma_1\ \sigma_2> \\ l & \alpha' L' & \alpha\ L \end{array}\right]. \end{aligned} \tag{4.3}$$

The CFP as shown in eq.(4.1) can then be rewritten as

$$\begin{aligned} &\langle n(sf)\alpha L\beta F\{|n-1(s'f')\alpha' L'\beta' F'\rangle \\ &= \langle n(sf)\beta F\{|n-1(s'f')\beta' F'\rangle\langle (sf)\alpha L\{|(s'f')\alpha' L'\rangle, \end{aligned} \tag{4.4}$$

in which

$$\begin{aligned} &\langle n(sf)\beta F\{|n-1(s'f')\beta' F'\rangle \\ &= \left[\begin{array}{cc|c} [1]_{2N} & [n-1]_{2N} & [n]_{2N} \\ [1]_N & [n'_1\ n'_2]_N & [n_1\ n_2]_N \end{array}\right]\left[\begin{array}{cc|c} [1]_N & [n'_1\ n'_2]_N & [n_1\ n_2]_N \\ <1> & \beta' <\sigma'_1\ \sigma'_2> & \beta <\sigma_1\ \sigma_2> \end{array}\right], \end{aligned} \tag{4.5}$$

can be called as the F-spin part of CFP.

$$\langle (sf)\alpha L\{|(s'f')\alpha' L'\rangle = \left[\begin{array}{cc|c} (1\ 1/2)\ (s'\ f') & & (s\ f) \\ l & \alpha' L' & \alpha\ L \end{array}\right] = \left[\begin{array}{cc|c} <1> & <\sigma'_1\ \sigma'_2> & <\sigma_1\ \sigma_2> \\ l & \alpha' L' & \alpha\ L \end{array}\right], \tag{4.6}$$

can be refered as the orbital part of CFP.

$\langle n(sf)\beta F\{|n-1(s'f')\beta' F'\rangle$ can be calculated using $|n(sf)L_{max}\beta F\rangle$(see eq.(2.6)). For $\langle (s\ f)\alpha\ L\{|(s',f')\alpha'\ L'\rangle$, we find the following simple formula to evaluate it

$$\left[\begin{array}{cc|c} (1\ 1/2)\ (s-1,f') & & (s,f) \\ l & \alpha' L' & (\alpha'_1\ L'_1\ f'_1)\ L \end{array}\right] = C\ \langle (s\ \ f)(\alpha'_1\ L'_1\ f'_1)L\|b^\dagger\|(s-1\ \ f')\alpha' L'\rangle, \tag{4.7}$$

where C is the normalizing constant,

$$\langle (s\ \ f)(\alpha'_1\ L'_1\ f'_1)L\|b^\dagger\|(s-1\ \ f')\alpha' L'\rangle = \frac{P(\alpha'_1\ L'_1\ f'_1\ \alpha'\ L'\ f')}{\sqrt{P(\alpha'_1\ L'_1\ f'_1\ \alpha'_1\ L'_1\ f'_1)}}, \tag{4.8}$$

where

$$P(\alpha_1' L_1' f_1' \alpha' L' f') = \delta(\alpha_1', \alpha')\,\delta(L_1', L')\,\delta(f_1', f')$$

$$- \sum_{f''\alpha''L''} (-1)^{f_1'+f'+L_1'+L'} \sqrt{(2f_1'+1)(2f'+1)(2L_1'+1)(2L'+1)}$$

$$\left[\begin{Bmatrix} 1/2 & f'' & f_1' \\ 1/2 & f & f' \end{Bmatrix} \begin{Bmatrix} l & L'' & L_1' \\ l & L & L' \end{Bmatrix} + \right.$$

$$\left. \frac{(-1)^{f_1'+f'} 6\delta(L'', L)}{(2L+1)((N+s-4) - f''(f''+1) + f(f+1))} \begin{Bmatrix} 1/2 & f'' & f_1' \\ f & 1/2 & 1 \end{Bmatrix} \begin{Bmatrix} 1/2 & f'' & f' \\ f & 1/2 & 1 \end{Bmatrix} \right]$$

$$\langle (s-1\ \ f_1')\alpha_1' L_1' \| b^\dagger \| (s-2\ \ f'')\alpha'' L'' \rangle \langle (s-1\ \ f')\alpha' L' \| b^\dagger \| (s-2\ \ f'')\alpha'' L'' \rangle, \tag{4.9}$$

and we have the reciprocal relation

$$\left[\begin{array}{cc|c} (1\,1/2) & (s,f) & (s-1,f') \\ l & (\alpha_1' L_1' f_1')L & \alpha' L' \end{array} \right] = (-1)^{l+L'+L} \sqrt{\frac{d(s-1,f')(2L+1)}{d(s,f)(2L'+1)}} \left[\begin{array}{cc|c} (1\,1/2) & (s-1,f') & (s,f) \\ l & \alpha' L' & (\alpha_1' L_1' f_1')\,L \end{array} \right], \tag{4.10}$$

where $d(s,f)$ is the dimension of the $IRRP$ (s,f) of group $O(N)$.

In this paper,the classification of wave functions and the factorization of the CFP for the system with single angular momentum l and F-spin 1/2 are discussed. A recurrent formula to evaluate the CFP with well-defined F-spin and seniority is given. We hope these discussion will improve the IBM calculations.

References

[1] F. Iachello and A. Arima, *The Interacting Boson Model*(Cambridge; Cambridge University Press, 1987).

[2] R. F. Bacher and S. Goudsmit, Phys. Rev. **46**(1934)948.

[3] G. Racah, Phys. Rew. **63**(1943)367.

[4] P. J. Redmond, Proc. Roy. Soc. London **A222**(1954)84.

[5] A. de-Shalit and I. Talmi, *Nuclear shell Theory* (Academic, New York, 1963).

[6] H. Z. Sun, M. Zhang, Q. Z. Han ang G. L. Long, J. Phys. **A22**(1989), 4769; ibid, **A23**(1990), 1957.

[7] Y. X. Liu, H. Z. Sun and E. G. Zhao, Comput. Phys. Commun. **70**(1992), 154.

[8] A. Arima, T. Otsuka, F. Iachello and I. Talmi, Phys. Lett. **66B**(1977), 205.

[9] Q. Z. Han and H. Z. Sun, *Group Theory*(Peking University, 1987).

[10] J. J. Wang and H. Z. Sun, High Energy Phys. Nucl. Phys., 14 (1990), 842; H. Z. Sun, J. J. Wang and Y. X. Liu, to be published.

[11] Y. X. Liu, Chinese J. Comput. Phys. **9**(1992), 163.

A new FORTRAN Program for the CFPs of a Fermion System [1]

Jia-jun Wang

CCAST (World Laboratory), P. O. BOX 8730,Beijing,100080,China

Department of Physics, Peking University, Beijing 100871,China

Institute of Theoretical Physics, Academia Sinica, Beijing 100080, China

Qi-zhi Han

Department of Physics, Peking University, Beijing 100871,China

Abstract

A simple FORTRAN program called CFPOF,which calculetes fractional parentage coefficients (CFPs) for a fermion system is introduced.The program CFPOF uses the new recurrent formula of the CFPs with well-defined seniority and the multiplicity of an irreducible representation (Irrep) of $O(3)$ in an Irrep of group $SP(N)$ ($N = 2j + 1$). It provides an efficient algorithm for numerical computation.

[1]The project supported by CCAST (World Laboratory) , Doctoral Programm Foundation of Institution of Higher Education of China and National Science Foundation of China

It is well known that the fractional parentage coefficients (CFPs)[1-2] method is one of the most efficient method for the construction of shell model wave functions. It is an iterative method. Many programs such as JJCFP,[3] GENESIS[4,5] et al were published.However,all these codes are not efficient enough for the system including large number of fermions. They calculated the CFPs of n identical fermions by diagonalizing the quadratic Casimir operators of group $U(N)$ and group $SP(N)$ simultaneously, where $N = 2j + 1$, j is the angular momentum of a fermion. Hong-Zhou Sun et al [7] have given a new recurrent formula of CFPs with well-defined seniority for identical fermions in j-j coupling. Using the new recurrent formula and the multiplicity of an Irrep of group $O(3)$ in an Irrep of group $SP(N)$,[7,8] we wrote a FORTRAN program called CFPOF for calculating the CFPs of identical fermions. This program is faster and more efficient for a fermion system with large fermion number.

We run the GENESIS and CFPOF on the VAX-8550 to calculate all the CFPs of identical fermions, the comparison between GENESIS and CFPOF is shown in teble 1.

Table 1 The Running Time On VAX-8550

j / *name of code*	9/2	11/2	13/2	15/2
CFPOF	5-seconds	21-seconds	6-minutes	3.5-hours
GENESIS	6-minutes	33-minutes	*overflow when* $n = 5$	

There n is the fermion number.

It is clear that the calculation speed depends strongly on the number of fermions and the angular momentum of each fermion. The calculation speed of CFPOF is faster than GENESIS, because the new recurrent formula depends on the seniority ν but not on the total fermion number n. It avoids a lot of repetive computations.Moreover,the dimension of $< 1^{\nu} >$ is much smaller than that of $[1^n]$. These merits of the calculating method make the new code appreciably faster.

Helpful discussions with Professor Hong-Zhou Sun are acknowledged with thanks.

References

[1] R.F. Bacher and S. Goudsmit, Phys. Rev. **46**(1934)948.

[2] G. Racah, Phys. Rev. **63**(1943)367.

[3] L.B.Hubbard,Comput.Phys.Commu. **1**(1970)225.

[4] D. Zwart, *GENESIS* code.

[5] X. Ji and M. Vallieres, Phys. Rev. **C35**(1987)1583.

[6] A. de-Shalit and I. Talmi, Nuclear shell Theory,Academic,New York,1963

[7] H.Z. Sun, Q.Z. Han, M. Zhang and G.L. Long, Commun. Theor. Phys. **11**(1989)441,449.

[8] J.J.Wang and H.Z.Sun. High Energy Phys.and Nucl.Phys,(in Chinese) **14**(1990)842.

Branching Rules for $U(N) \supset SP(N) \supset O(3)$ [1]

Jia-jun Wang

CCAST (World Laboratoory),P. O. Box 8730, Beijing 100080, China

Department of Physics, Peking University, Beijing 100871,China

Institute of Theoretical Physics, Academia Sinica, Beijing 100080, China

Hong-zhou Sun

CCAST (World Laboratoory),P. O. Box 8730, Beijing 100080, China

Department of Physics, Tsinghua University, Beijing 100084, China

Institute of Theoretical Physics, Academia Sinica, Beijing 100080, China

Abstract

The branching rules for Group chain $U(N) \supset SP(N) \supset O(3)$ of the irreducible representations $[2^a\, 1^b]$ of U(N) are discussed in some detail. Simple analytical recurrent formulae of these branching rules for above group chain are obtained. They are very efficient to simplify the calculations of Fractional Parentage Coefficients. This method can be used to find the branching rules for the Group chain $U(N) \supset O(N) \supset O(3)$ too.

[1]The project supported by CCAST (World Laboratoory) ,Doctoral Programm Foundation of Institution of Higher Education of China and National Science Foundation of China

1 Introduction

For the single-j fermion system with isospin 1/2,the wave functions are classified according to the following Group chain

$$U(2N) \supset (U(N) \supset SP(N) \supset O(3)) \otimes SU(2) \tag{1}$$

There are many different ways[1-3] of finding branching rules and some tables of the branching rules have been published.[4,5] In principle,the branching rules for above group chain can be calculated by Schur function method,but it is very complicated when the ranks of groups or the dimensions of representations are large.Using computer one can find some branching rules, but because of the rounding errors,some branching rules cannot be obtained. However, this problem is very important in applications. For example, it is very efficient to simplify the calculations of Fractional Parentage Coefficient(CFP).[6,7]

The reduction of $U(2N) \supset U(N)$ is well know,but the reduction of $U(N) \supset SP(N) \supset O(3)$ is complicated. In practice we only need to discuss the reductions of the irreducible representations (Irrp) $[2^a\,1^b]$ of the group $U(N)$. Thus the problem of reduction of $U(N) \supset SP(N)$ is simplified. In this paper the branching rule formula for $U(N) \supset SP(N)$ is given in Sec.II. The branching rule formula for $SP(N) \supset O(3)$ is given in Sec.III.

2 Branching rule for $U(N) \supset SP(N)$

For Group U(N) we have obtained[11]

$$[1^c] \otimes [1^a] = \begin{cases} [2^a\,1^{c-a}] + [2^{a-1}\,1^{c-a+2}] + \cdots + [1^{c+a}], & c \geq a\,, c+a \leq N; \\ [2^a\,1^{c-a}] + [2^{a-1}\,1^{c-a+2}] + \cdots + [2^{c+a-N}\,1^{2N-c-a}], & c \geq a\,, c+a > N. \end{cases} \tag{2}$$

Using (2),we have

$$[2^a\,1^{c-a}] = [1^c] \otimes [1^a] - [1^{c+1}] \otimes [1^{a-1}] \tag{3}$$

The formula of direct product decomposition of two totally antisymmetric Irrp of SP(N)[11] is

$$\begin{aligned} < 1^c > \otimes < 1^a > &= \sum_{l=0}^{a}\sum_{i=l}^{a} < 2^{a-i}\,1^{c-a+2l} >, c \geq a, c+a \leq N/2 \\ &= \sum_{l=0}^{N/2-c}\sum_{i=l}^{a} < 2^{a-i}\,1^{c-a+2l} >, c \geq a, c+a > N/2 \end{aligned} \tag{4}$$

The branching rules for $[1^a]$ of $U(N)$ can be written as[9]

$$[1^a] = < 1^a > + < 1^{a-2} > + \cdots + \begin{cases} < 0 >, & a = even \\ < 1 >, & a = odd \end{cases}$$

Thus we obtain for $c = a + b \leq N/2$

$$[2^a\,1^b] = [2^{a-2}\,1^b] + \sum_{\alpha}\sum_{\beta} < 2^\beta\,1^\alpha >, \tag{5}$$

where

$$\begin{aligned} \alpha &= 0,\ 2, \cdots \leq c, b = even, \\ &= 1,\ 3, \cdots \leq c, b = odd, \\ \beta_{min} &= MAX(0, a-\alpha), \\ \beta_{max} &= MIN(a, c-\alpha) \end{aligned}$$

For $c = a + b > N/2$,we have

$$[2^a\,1^b] = [2^a\,1^{\bar{c}-a}] + \sum_{\gamma} < 1^{\bar{c}+1} > \otimes < 1^{a-1-\gamma} >, \tag{6}$$

where

$$\begin{aligned} \bar{c} &= N - c \\ \gamma &= 0,\ 2,\ 4, \ldots, a-1 \end{aligned}$$

Using (5),(6) the branching rules for the Irrp $[2^a\,1^b]$ of $U(N)$ with any dimensions can be calculated.We have written a program "ROUN" to calculate these branching rules and the results are checked by the dimensions. For example the branching rules for $U(14) \supset SP(14)$ are listed in Table 1. From Table 1, we can see that the branching rules with $N \leq 8$ are the same as those in ref.[4], many branching rules for Irrp of $U(14)$ with large dimensions are given.The formulae (5),(6) can be used to find all banching rules conveniently without limitation for n and dimension of Irrp. For example, for the single-j fermions system with isospin 1/2 and $j = 15/2$, the Irrp with maximal dimension of $U(16)$ is [16 1](in which $n = 2a+b = 16, T = b/2 = 1$), its dimension is 66745536 , the calculated branching rules for this Irrp is

$$\begin{aligned}
[16\ 1] \supset\ & (14\ 0)+(10\ 0)+(6\ 0)+(2\ 0)+(14\ 1) \\
& +2(12\ 1)+(10\ 1)+2(8\ 1)+(6\ 1)+2(4\ 1) \\
& +(2\ 1)+(12\ 2)+2(10\ 2)+(8\ 2)+2(6\ 2) \\
& +(4\ 2)+(10\ 3)+2(8\ 3)+(6\ 3)+(8\ 4) \qquad (7)
\end{aligned}$$

3 Branching rules for $SP(N) \supset O(3)$

Using (4) we have

$$\begin{aligned}
< 2^{\nu_1}\,1^{\nu_2} > \ =\ & < 1^{\nu_1+\nu_2} > \otimes < 1^{\nu_1} > + < 1^{\nu_1+\nu_2} > \otimes < 1^{\nu_1-2} > \\
& - < 1^{\nu_1+\nu_2+1} > \otimes < 1^{\nu_1-1} > - < 1^{\nu_1+\nu_2-1} > \otimes < 1^{\nu_1-1} > \qquad (8)
\end{aligned}$$

The branching rule formula of $< 1^\nu >$ is[10]

$$< 1^a >= \sum_J J^{\gamma(a,J)}$$

So the branching rules for $SP(N) \supset O(N)$ can be written as

$$< 2^{\nu_1} 1^{\nu_2} >= \sum_{J=J_{min}}^{J_{max}} J^{\chi(2^{\nu_1} 1^{\nu_2}, J)} \tag{9}$$

where

$$\begin{aligned} \chi(2^{\nu_1} 1^{\nu_2}, J) &= \omega(1^{\nu_1+\nu_2}, 1^{\nu_1}, J, j) - \omega(1^{\nu_1+\nu_2+1}, 1^{\nu_1-1}, J, j) \\ &+ \omega(1^{\nu_1+\nu_2}, 1^{\nu_1-2}, J, j) - \omega(1^{\nu_1+\nu_2-1}, 1^{\nu_1-1}, J, j) \end{aligned} \tag{10}$$

and

$$J_{min} = \begin{cases} 0, & 2\nu_1 + \nu_2 = even \\ 1/2, & 2\nu_1 + \nu_2 = odd \end{cases}$$

$$J_{max} = (\nu_1 + \nu_2)(N - (\nu_1 + \nu_2))/2 + \nu_1(N - \nu_1)/2$$

$$\omega(1^a, 1^b, J, j) = \sum_{J_2=J_{2min}}^{J_{2max}} \gamma(b, J_2) \sum_{J_1=|J-J_2|}^{J+J_2} \gamma(a, J_1) \tag{11}$$

We have written a program "ROSPN". Using "ROSPN", the branching rules for $SP(N) \supset O(3)$ are calculated when $N = 4, 6, 8, \ldots, 16$. These results are checked by dimensions too.As an example, the branching rules for $SP(14) \supset O(3)$ are given in Table 2. This method can be used to find the branching rules for the Group chain $U(N) \supset O(N) \supset O(3)$ too.

Helpful discussions with Professor Qi-zhi Han are acknowleged with thanks.

References

[1] R.C.King,Phys.A:Math.Gen.8(1975)429.

[2] G.R.E.Black,R.C.King and B.G.Wybourne,Phys.A:Math.Gen. 16(1983)1555.

[3] F.Gingras andJ.Patera.J.Math.Phys.33(1992)1618.

[4] W.G.Mckay,J.Patera,Tables of dimensions,Indices,and Branching rules for Representations of Simple Lie Algebras, Drekker,New York (1981).

[5] M.R.Bremner,R.V.Moody and J.Patera,Tables of Dominant Weight Multiplicities for Representations of Simple Lie Algbras, Drekker,New York (1985).

[6] H.Z. Sun, Q.Z. Han and J.J. Wang, Fractional Parentrage Coefficients with Isospin, Commun. Theor. Phys. to be published

[7] H.Z. Sun, Q.Z. Han, M. Zhang and G.L. Long, Commun. Theor. Phys. 11(1989)442.

[8] D. Zwart, *GENESIS* code.

[9] M. Hamermash.Group Theory. Addison-Wesley,London (1962)

[10] J.J. Wang and H.Z. Sun,High Energy Phys.and Nucl.Phys.(in Chinese) 14(1990)842.

[11] Q.Z. Han and H.Z. Sun,Group Theory,Peking University Press,Beijing(1987).

Table 1 Branching rules of $U(14) \supset SP(14)$

$j = 13/2, b = even$

s	14	12	10	8	6	4	2	0	12	10	8	6	4	2	10	8	6	4	8	6	d
$2t$	0	0	0	0	0	0	0	0	2	2	2	2	2	2	4	4	4	4	6	6	
n $2T$																					
0 0								1													1
2 0							1														105
4 0						1		1						1							3185
6 0					1		1						1								41405
8 0				1		1		1				1		1				1			273273
10 0			1		1		1				1		1				1				1002001
12 0		1		1		1		1		1		1		1		1		1		1	2147145
14 0	1		1		1		1		1		1		1		1		1		1		2760615
2 2								1						1							91
4 2							1						1	1							4095
6 2						1		1				1	1	2				1			63063
8 2					1		1				1	1	2	1			1	1			455455
10 2				1		1		1		1	1	2	1	2		1	1	2		1	1756755
12 2			1		1		1		1	1	2	1	2	1	1	1	2	1	1	1	3864861
14 2		1		1		1		1	1	2	1	2	1	2	1	2	1	2	1	2	5010005
4 4								1						1				1			1001
6 4							1						1	1			1	1			25025
8 4						1		1				1	1	2		1	1	2		1	225225
10 4					1		1				1	1	2	1	1	1	2	2	1	1	975975
12 4				1		1		1		1	1	2	1	2	1	2	2	3	1	2	2277275
14 4			1		1		1			1	2	1	2	1	1	2	3	2	1	2	3006003
6 6								1						1				1		1	3003
8 6							1						1	1			1	1	1	1	45045
10 6						1		1				1	1	2		1	1	2	1	2	245245
12 6					1		1				1	1	2	1		1	2	2	1	2	637637
14 6				1		1		1			1	2	1	2		1	2	3	1	2	869505
8 8								1						1				1		1	3003
10 8							1						1	1			1	1		1	27027
12 8						1		1				1	1	2			1	2		1	85995
14 8					1		1					1	2	1			1	2		1	124215
10 10								1						1				1			1001
12 10							1						1	1				1			5005
14 10						1		1					1	2				1			8085
12 12								1						1							91
14 12							1							1							195
14 14								1													1

$n = 2a + b$,fermion number,$T = b/2$,isospin.
$s = 2\nu_1 + \nu_2$,seniority,$t = \nu_2/2$ reduce isospin.

continued from Table 1

$j = 13/2, b = odd$

n	$2T$ \ s \ $2t$	13 1	11 1	9 1	7 1	5 1	3 1	1 1	11 3	9 3	7 3	5 3	3 3	9 5	7 5	5 5	7 7	d
1	1							1										14
3	1						1	1										914
5	1					1	1	1					1					19110
7	1				1	1	1	1				1	1					182182
9	1			1	1	1	1	1			1	1	1			1		910910
11	1		1	1	1	1	1	1		1	1	1	1		1	1		2576574
13	1	1	1	1	1	1	1	1	1	1	1	1	1	1	1	1	1	4294290
3	3							1					1					364
5	3						1	1				1	1					12012
7	3					1	1	1			1	1	2			1		140140
9	3				1	1	1	1		1	1	2	2		1	1		780780
11	3			1	1	1	1	1	1	1	2	2	2	1	1	2	1	2342340
13	3		1	1	1	1	1	1	1	2	2	2	2	1	2	2	1	4008004
5	5							1					1			1		2002
7	5						1	1				1	1		1	1		38610
9	5					1	1	1			1	1	2	1	1	2	1	270270
11	5				1	1	1	1		1	1	2	2	1	2	2	1	910910
13	5			1	1	1	1	1		1	2	2	2	1	2	3	1	1639638
7	7							1					1			1	1	3432
9	7						1	1				1	1		1	1	1	40040
11	7					1	1	1			1	1	2		1	2	1	168168
13	7				1	1	1	1			1	2	2		1	2	1	331240
9	9							1					1			1		2002
11	9						1	1				1	1			1		13650
13	9					1	1	1				1	2			1		31850
11	11							1					1					364
13	11						1	1					1					1260
13	13							1										14

$n = 2a + b$,fermion number, $T = b/2$,isospin.

$s = 2\nu_1 + \nu_2$,seniority, $t = \nu_2/2$ reduce isospin.

Table 2 Branching rules of $SP(14) \supset O(3)$

$j = 13/2, \nu_2 = even$

J / s $2t$	0	1	2	3	4	5	6	7	8	9	10	⋯ ⋯	d
0 0	1												1
2 0		1		1		1		1		1		⋯	105
2 2			1		1		1		1		1	⋯	90
4 0	4		7	4	10	6	12	8	12	9	12	⋯	3094
4 2		5	5	10	9	13	12	15	13	15	13	⋯	3900
4 4	1		3	1	4	3	4	3	5	3	4	⋯	910
6 0	2	28	28	56	54	75	74	91	83	99	88	⋯	37400
6 2	17	29	61	71	99	105	128	128	144	138	148	⋯	54978
6 4	3	16	22	33	38	48	49	56	56	59	56	⋯	20020
6 6	2	1	3	4	6	4	8	6	7	7	7	⋯	2002
8 0	45	80	166	196	275	295	360	368	418	412	445	⋯	214200
8 2	43	162	244	353	422	513	562	630	655	697	697	⋯	334152
8 4	29	67	123	156	205	230	268	282	308	310	323	⋯	139230
8 6	3	12	18	26	30	37	40	45	45	47	47	⋯	18018
10 0	57	235	337	508	595	741	809	922	956	1040	1043	⋯	606424
10 2	130	335	585	772	994	1147	1327	1434	1562	1617	1689	⋯	928200
10 4	41	145	230	319	392	473	522	582	617	648	660	⋯	340340
12 0	104	235	429	556	732	829	985	1052	1165	1205	1280	⋯	804440
12 2	103	342	541	764	938	1129	1268	1417	1509	1609	1654	⋯	1021020
14 0	28	118	172	256	304	377	414	476	498	544	551	⋯	379236

$j = 13/2, \nu_2 = odd$

J / s $2t$	1/2	3/2	5/2	7/2	9/2	11/2	13/2	15/2	17/2	19/2	21/2	⋯ ⋯	d
1 1							1						14
3 1	1	1	2	3	3	4	4	4	4	4	3	⋯	896
3 3		1	1	1	2	2	1	2	2	1	2	⋯	90
5 1	9	17	25	32	39	43	48	50	52	52	51	⋯	17850
5 3	6	12	17	22	26	29	32	33	34	34	33	⋯	10752
5 5	1	2	4	4	5	5	6	6	6	6	6	⋯	1638
7 1	53	101	150	196	233	269	298	318	334	344	344	⋯	152320
7 3	40	80	117	151	182	208	229	245	256	260	262	⋯	108290
7 5	11	22	32	41	49	56	61	65	67	68	67	⋯	24960
7 7	2	1	2	4	3	4	5	4	5	5	4	⋯	1430
9 1	166	325	482	627	756	874	976	1053	1116	1159	1180	⋯	616800
9 3	128	260	380	491	599	687	761	827	870	897	915	⋯	452608
9 5	34	67	98	127	154	176	195	209	220	225	227	⋯	102102
11 1	269	533	785	1025	1244	1441	1613	1755	1869	1953	2006	⋯	1188096
11 3	177	350	516	672	816	943	1053	1144	1216	1266	1296	⋯	729300
13 1	183	353	527	690	834	971	1091	1188	1272	1336	1374	⋯	884884

$s = 2\nu_1 + \nu_2$,seniority,$t = \nu_2/2$ reduce isospin.

The Effect of Symmetrical Energy and Shell Correction to the Cluster Formation in QMD

Li Junqing[a,b], Liu Jianye[a,b], Zhao Enguang[a,c] and Zhu Quanling[b]

[a] CCAST(World Laboratory), P. O. Box 8730, Beijing 100080, China
[b] Institute of Modern Physics, Academia Sinica, Lanzhou 730000, China
[c] Institute of Theoretical Physics, Academia Sinica, Beijing 100080, China

Since some time the quantum molecular dynamics(QMD) model[1] has been a powerful tool to investigate the formation of clusters during a heavy ion collision in the intermediate energy region. The model is based on the nucleon-nucleon interaction of Skyrme-type which is supplemented by a long range Yukawa interaction in order to reproduce surface effects and an effective charge Coulomb interaction[2,3]. With this kind of interaction, the model simulates heavy ion reactions on an event-by-event basis, therefore, may preserve correlations and fluctuations, and thus can describe the formation of clusters. The reaction process may be figured out like that: when the projectile collides with the target at a intermediate energy, the composite system is first compressed, during the time some nucleons may be emitted, then the system begins to expand, while clusters may be formed due to the attractive short range nucleon-nucleon force[4]. The propagating process, however, is governed by the classical canonical equation since actually in the model nucleons are considered as classical particles throughout the reaction course. Clusters are identified in the way that if all nualeons within the cluster are close to each other less than $3fm$ and far apart from others more than $3fm$.

Recently we have checked the numbers of protons and neutrons for each cluster which were calculated by QMD model and found that some so-called clusters have very unreasonable N,Z numbers. Actually we found 2, 3 even 4 neutrons or protons stay together and formed so-called mass A=2, 3, or 4 clusters. Several protons can also stay together without the accompaniment of neutrons since the Coulomb force is over simplified so that the system is treated as a uniformly charged sphere, where all particles have a charge Z/A.

Skyrme force is usually used to the normal nucleons. Here in the reaction course the density of the nuclear matter may be extremely dense on one hand or dilute on the other hand. And instead of Schrodinger equation, the characteristic property of nucleus or clusters naturally can be given by the classical canonical equation. For compensation, in addition to the additional Yukawa interaction for acquiring reasonable nuclear surface effects, another interaction which concerns the numbers of neutrons and protons, is considered in the current work.

The Hamiltonian used here is:

$$H = V_{loc} + V_{yuk} + V_{coul} + V(N_i, Z_i) \tag{1}$$

where N_i, Z_i are the neutron and proton numbers of ith cluster. And

$$V_{loc} = t_1 \cdot \delta(\vec{r_1} - \vec{r_2}) + t_2 \cdot \delta(\vec{r_1} - \vec{r_2})\delta(\vec{r_1} - \vec{r_3}) \tag{2}$$

$$V_{yuk} = t_3 \frac{exp(-|\vec{r_1} - \vec{r_2}|/m)}{|\vec{r_1} - \vec{r_2}|/m}, \qquad m = 0.8fm \tag{3}$$

$$V(N,Z) = V_{symmetry} + V_{shell} + V_{pair} \tag{4}$$

and

$$V_{symmetry}(N,Z) = \kappa[a_1 A - a_2 A^{2/3}](\frac{N-Z}{A})^2 \tag{5}$$

which is the symmetry energy from liquid drop model with κ =1.79, a_1 =15.677, a_2 =18.56. N, Z, A are the numbers of neutrons, protons and mass of individual clusters. V_{pair} is the pairing energy. V_{shell} is the shell correction, for which we have a phenomenolagical formular[5] as follows:

$$S(N,Z) = C\{\frac{[F(N) + F(Z)]}{(A/2)^{2/3}} - C_s A^{1/3}\} \tag{6}$$

for axial symmetrical deformation

$$S_{crit} = 2C_s d_0^2 (1 - \frac{C_3 Z^2}{2C_s A}) \tag{7}$$

where $C_s = a_2[1 - \kappa(N - Z/A)^2], d_0 = 0.27, C_3 = 0.717$

$$V_{shell}(N,Z) = S_{crit}[1 + lg(S/S_{crit}] \tag{8}$$

if

$$Q_n = C_q \frac{(M(I)^{5/3} - M(I-1)^{5/3})}{M(I) - M(I-1)}, \qquad C_q = 0.6 \tag{9}$$

M(I)=0,2,8,20,28,50,82,126,184.....
when I=1,2,3.....9.....

$$F(N) = Q_n[N - M(I-1)] - C_q[N^{5/3} - M(I-1)^{5/3}] \tag{10}$$

F(Z) has the same formalism as F(N).

By considering the N,Z dependent potential those clusters which own reasonable neutrons and protons , and Z and/or N are close/equal to any magic number, are more stable than those in the opposite cases. As a price one has to judge in which cluster each nucleon is at each time interval during the numerical calculation.

The N, Z dependent V(N,Z) has been used for calculating ^{40}Ca(30MeV/A) +^{40}Ca reaction for the four different impact parameters b=0,2,4,6. Fig.1) shows the multiplicity distribution of fragments of the reaction. The left column for the case with V(N,Z) and the right column for the case without it. Both cases showed a very similar behaviour. At central collision we observed essentially two components, and the same for other collisions. The first one on the left consists of nucleons and very light particles,

which were emitted during the compression stage and evaporated from some bulk nuclear matter on. The second component distributed nearby the projectile-like as well as the target-like nucleus, which should mostly come from evaporation remanders since $30MeV/A$ is not a very high energy. At $b = 2fm$, this component moves to the left because some angular momentum has been incorporated to the system, so that bigger bulk could not be formed. But when b is getting larger, at $b = 4,\ 6fm$, this component moves back to the right. Since now two nuclei are far from each other, the interaction between the projectile and the target is getting weaker, less relative energy could be dissipated, and thus less particles could be emitted. The component is contributed from incomplete deeply inelastic collisions. For the four cases, the second component in the left column distributed more towards the left as comparing with that in the right column, annoucing deeper disassembling. This is because that ^{40}Ca is a nucleus with double magic number, when two ^{40}Ca nuclei meet together, the composite system no longer has any magic number. The correction of $V(N,\ Z)$ would make the system unstable.

In Fig.2. the number of some extremely unreasonable clusters is indicated as a function of mass A, with circles for the case with modification $V(N,\ Z)$, and with squares for the case without $V(N,\ Z)$. Both are marked with crossing symbols. The number inside circles and squares denotes the Z number. The number of some stable clusters with magic number for N and/or Z is also given for two cases and marked with triangles. These are the results for 10 time simulation of $^{40}Ca(30MeV/A) + ^{40}Ca$ with $b = 2fm$, and at the interaction time $T = 200fm/c$. Obviously the case with $V(N,\ Z)$ has less unreasonable clusters and more stable clusters with magic number in contrast to the case without considering $V(N,\ Z)$.

Fig.3. shows how the unreasonable so-called clusters evolve with reaction time for the case with $V(N,\ Z)$ (denoted with circles) and the case without $V(N,\ Z)$ (denoted with squares). All conditions are the same as that in Fig.2.. One may find that in the case with $V(N,\ Z)$ some unreasonable clusters formed by fluctuations, but it is corrected gradually by having taken the $V(N,\ Z)$ into account. While in the other case, all the unreasonable clusters are governed by randomness throughout the reaction course. Once the cluster is formed, since it is apart from others for at least $3fm$, if any individual nucleon velocity is not extremely large, it usually would stay for ever.

Nevertheless, one may find that even with the $V(N,\ Z)$ correction, unfortunately, still some unreasonable clusters survived. $V(N,\ Z)$ is calculated according to the N, Z number of clusters, it only offers an additional excitation energy to make cluster more stable or unstable. A complete remedy is not achievable. More thorough way might be to calculate the gradient of $V(N, Z)$, i.e. $\frac{\partial V}{\partial N}$ and $\frac{\partial V}{\partial Z}$, to prevent unreasonable clusters from being formed. There are some problems to carry it out, since actually $\frac{\partial V}{\partial N}$ and $\frac{\partial V}{\partial Z}$ are intimately connected with $\frac{\partial H}{\partial \vec{r}}$. To solve the problem is rather sophisticated, nevertheless, the task is in progress.

We are grateful to prof. Ge Linxiao for very fruitful discussions.

References

[1] J.Aichelin Phys. Rep. 202(1991)235

[2] J.Aichelin, G.peilert, A.Bohnet, A.Rosenbauer, H.Stocker, and W.Greiner. Phys.Rev.c 37(1988)2451

[3] G.Peilert, H.Stocker, W.Greiner A.Rosenhauer, A.Bohnet and J.Aichelin Phys.Rev.c 39(1989)1402

[4] H.Stocker, J.A.Maruhn and W.Greiner. Phys.Rev.Lett. 44(1980)725

[5] W.D.Myers et. al., LBL-Report, UCRL-11980(1965)

Figure captions:

[1] The multiplicity ditribution of clusters as a function of mass A for ^{40}Ca(30MeV/A)+^{40}Ca reaction at 4 impact parameters b=0,2,4,6. The left column indicates the results with the cosideration of V(N,Z) and the results in the right column are those without it.

[2] The number of extremely unreasonable clusters and the number of clusters with at least one magic number are given as a function of mass A for both cases with (denoted by circles) and without (denoted by squares) V(N,Z) modification. For details read the text.

[3] The time evolution of some unreasonable clusters for the case with V(N,Z) (circles) and the case without V(N,Z) (squares) . Inside the symbol circle and square are the specific cluster X with mass A, Z protons and N neutrons. The figure before the symbol indicates the number of this kind of clusters.

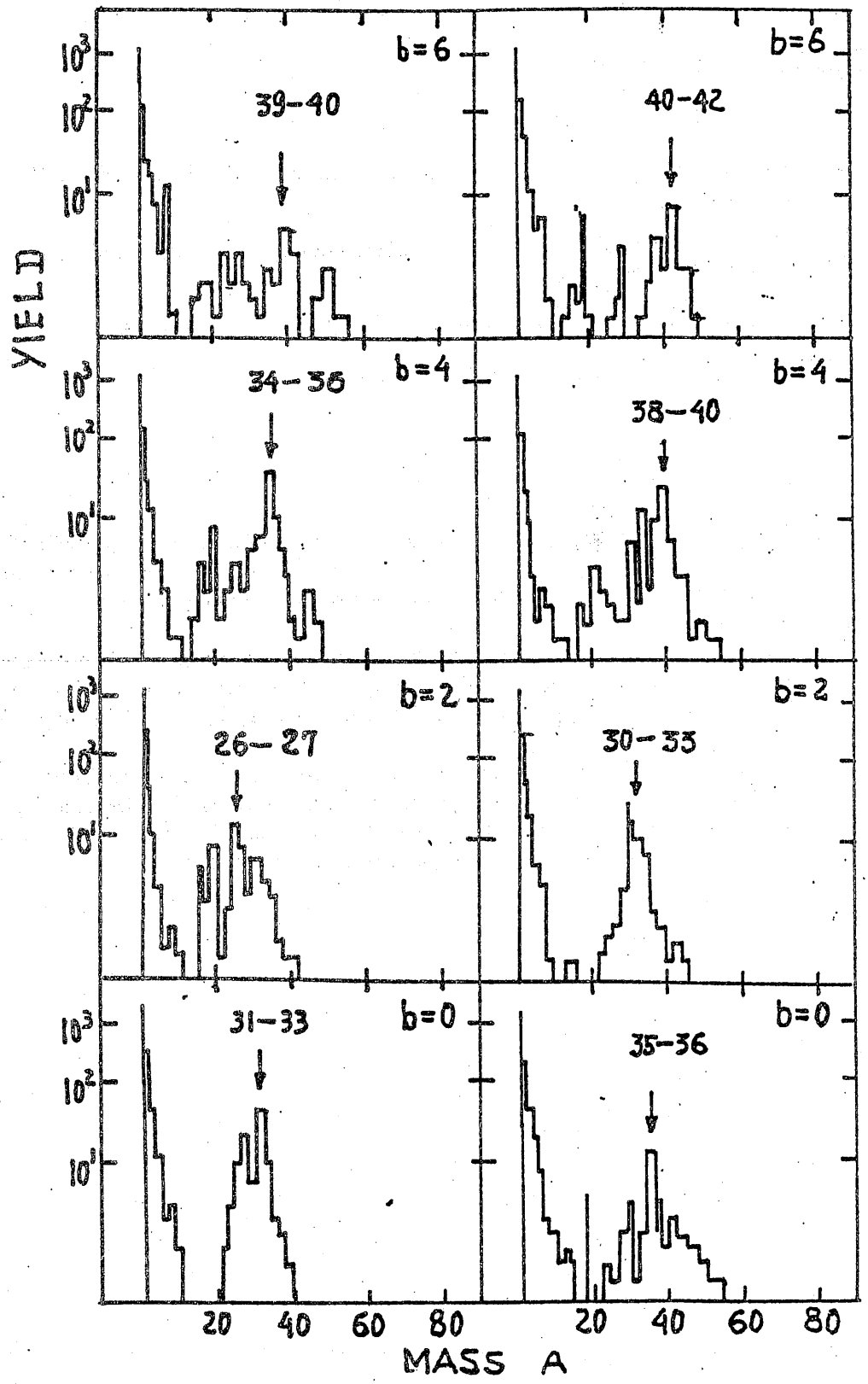
YIELD
b=6
39-40
b=6
40-42
b=4
34-36
b=4
38-40
b=2
26-27
b=2
30-33
b=0
31-33
b=0
35-36
10^3
10^2
10^1
20
40
60
80
MASS A

Fig. 1

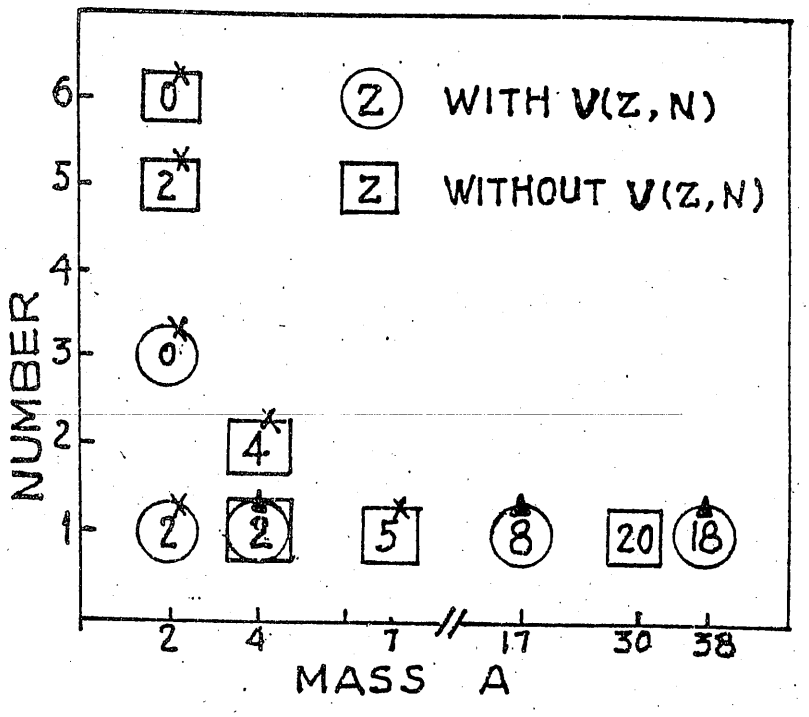
6
5
4
3
2
1
NUMBER
0*
2*
0*
4*
2*
2
5*
8
20
18
(2) WITH V(Z,N)
[2] WITHOUT V(Z,N)
2
4
7
17
30
38
MASS A

Fig. 2

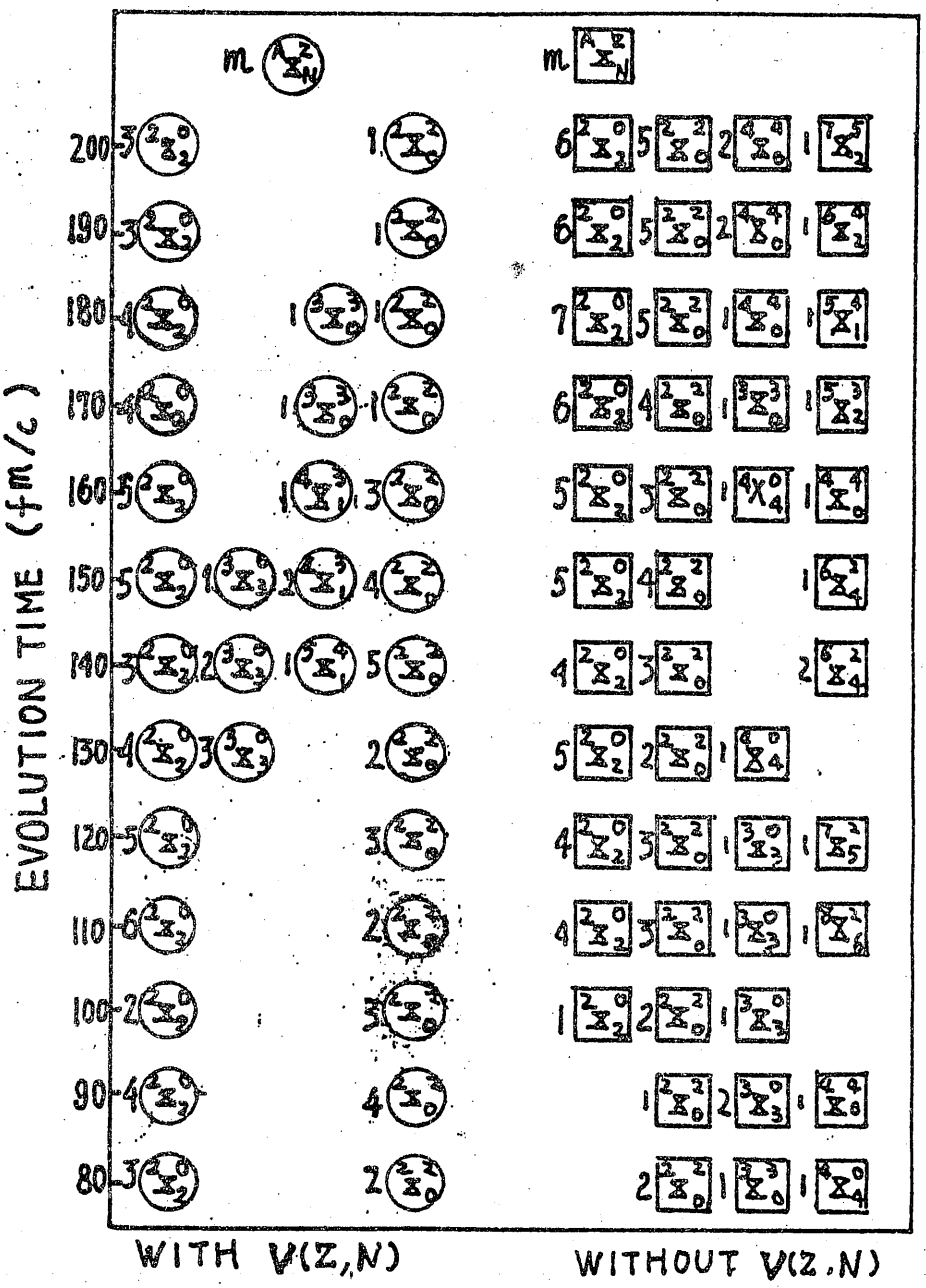
m
m
200
190
180
170
160
150
140
130
120
110
100
90
80
EVOLUTION TIME (fm/c)
WITH V(Z,N)
WITHOUT V(Z,N)

Fig. 3

Alpha particle elastic scattering on ^{16}O in the four α-particle model*

Li Qing-Run

CCAST(World Laboratory), Beijing, China

and

Institute of High Energy Physics, Academia Sinica, Beijing, China

Yang Yong-Xu

Department of Physics, Guangxi Normal University, Guilin, China

Abstract

A folding potential describing the alpha particle scattering on ^{16}O is constructed based on the four α-particle model of the nucleus ^{16}O. This folding potential provides a good description of the experimental data covering a broad energy range.

* Work supported in part by the National Science Foundation of China

1 Introduction

The scattering of light heavy-ion α particle by nuclei has been special interest in the study of heavy-ion reactions [1-4]. The $\alpha + ^{16}O$ elastic scattering is one of the reactions that have relatively systematical and complete experimental data. These data were analysed by using the phenomenological optical potential [5]. Recently, a calculation of $\alpha + ^{16}O$ elastic scattering was performed with the double-folded potential based on the DDM3Y effective interaction and good agreement with the experimental data was obtained [6].

On the other hand, ^{16}O is a typical α structure nucleus, it is assumed to consist of four α-particles and these α-particles remain the features as a free α- particle. This kind of 4α structure model of ^{16}O nucleus has been examined successfully in the electron scattering [7,8], the intermediate energy proton scattering [9,10], and the pion scattering [11].

The purpose of the present work is to consider further the application of the 4α structure model of ^{16}O to the $\alpha + ^{16}O$ elastic scattering.

In the α-particle model, the $\alpha + ^{16}O$ scattering can be considered as the scattering of the incident α by the four α-particles in ^{16}O. Thus using the $\alpha - \alpha$ interaction and the α-particle density in the nucleus, we can obtain the folding potential for the description of the $\alpha + ^{16}O$ scattering. The basic difference between this α-particle folding model and the usual folding model is that, in the former model the α-particle is treated as the "elementary" particle, but in the latter model the nucleon.

El - Azab Farid used a α-folding model in the analysis of the $\alpha + ^{16}O$ scattering at 48.7 MeV [12]. However, because an oversimplified α-particle wavefunction was used in the calculation, so a serious deviation from the data in the angular range of $100^0 - 150^0$ was obtained.

In the present work, a more realistic α-particle wavefunction of ^{16}O nucleus is used in obtaining the $\alpha+^{16}O$ folding potential and the comparison with experimental data is extended to a broad energy range.

In section 2, we briefly present the wavefunction of ^{16}O nucleus in the α-particle model and the folding model. The results and discussion are given in section 3.

2 Folding model and the α-particle wavefunction

In the theory of heavy-ion reactions, the generally used standard folding model is that the real part of the potential is derived by folding a N-N effective interaction with the nucleon densities of the incident and target nuclei. The folded potential (including a renormalization factor), together with a Woods-Saxon imaginary potential and a Coulomb potential, is used to describe the scattering of two composite nuclei.

In the α-particle model, ^{16}O is composed of four alpha particles. We can obtain the $\alpha-^{16}O$ interaction by folding the interaction between the incident α and the α-particle in the nucleus with the α-particle density of ^{16}O. As the alpha particle is treated as "elementary" particle, the real part of the interaction between the incident α and ^{16}O nucleus can be expressed as a single folding potential

$$V(R) = \int d\vec{r}\ V_{\alpha\alpha}(\vec{R}-\vec{r})\ \rho_{\alpha}(\vec{r}) \qquad (1)$$

where $\rho_{\alpha}(\vec{r})$ is the α-particle density distribution in the ^{16}O nucleus and $V_{\alpha\alpha}$ is the interaction between the incident α and the α- particle in ^{16}O nucleus.

In our calculations, $V_{\alpha\alpha}$ was taken as that given by Buck et al. [13], i.e.

$$V_{\alpha\alpha}(r) = -122.6225 \quad exp(-0.22\ r^2) \qquad (2)$$

This potential can reproduce the measured $\alpha+\alpha$ scattering phase shifts very well for c.m. energies up to 40 MeV.

The density $\rho_\alpha(\vec{r})$ in equation (1) can be obtained from the 4α model of ^{16}O. We have proposed an independent α-particle model for the four alpha nucleus ^{16}O [8]. The major points of this model are (i) the α- particles in the nucleus are regarded as "elementary" bosons; (ii) each α-particle in the nucleus moves independently in a mean field with a repulsive core. Basing on this model, the ground state wavefunction of the ^{16}O nucleus can be written as

$$\psi(\vec{r}_1,\vec{r}_2,\vec{r}_3,\vec{r}_4) = \Phi_0^{(\alpha)}(\vec{r}_1)\ \Phi_0^{(\alpha)}(\vec{r}_2)\ \Phi_0^{(\alpha)}(\vec{r}_3)\Phi_0^{(\alpha)}(\vec{r}_4) \tag{3}$$

where $\vec{r}_i (i = 1,2,3,4)$ are the position vectors of the alpha particles in the nucleus, $\Phi_0^{(\alpha)}$ is the lowest orbital wavefunction of an alpha particle in the nuclear field and has been given in [8] as

$$\Phi_0^{(\alpha)}(\vec{r}) = \frac{1}{\sqrt{2}}[O_{10}(r) - O_{20}(r)]Y_{00}(\theta,\varphi) \tag{4}$$

where $Y_{00}(\theta,\varphi)$ is the usual spherical harmonic function, $O_{10}(r)$ and $O_{20}(r)$ are respectively the 1S and 2S harmonic oscillator radial wavefunctions, i.e.

$$\begin{aligned} O_{10}(r) &= 2(a^6\pi)^{-1/4}\ e^{-r^2/2a} \\ O_{20}(r) &= \sqrt{\frac{8}{3}}(a^6\pi)^{-1/4}[\frac{3}{2} - (\frac{r}{a})^2]\ e^{-r^2/2a} \end{aligned} \tag{5}$$

where a is the harmonic oscillator constant, for ^{16}O nucleus $a = 1.2fm$.

This α-particle model of ^{16}O can reproduce the cross sections of electron scattering on ^{16}O very well up to $q^2 \sim 9fm^{-2}$ [8], and also have been applied successfully to the intermediate energy proton scattering [10] and the pion-nucleus scattering [11]. In the present work, we apply this model to heavy-ion scatterings to examine the model once more.

From equations (2)-(5) one can obtain the folding potential defined in equation (1). Then, the total optical potential used to describe the $\alpha + ^{16}O$ scattering can be written as

$$U(R) = N_r V(R) + i\, W(R) + V_c(R) \tag{6}$$

where $V(R)$ is the real folded potential defined in equation (1), N_r is the renormalization factor and $V_c(R)$ the Coulomb potential. The imaginary part of the potential $W(R)$ is taken to have a Woods-Saxon shape, i.e.

$$W(R) = -W_0\{1 + exp(\frac{R - R_w}{a_w})\}^{-1} \tag{7}$$

3 Results and discussion

The general procedure performed in a folding model calculation is that the four parameters N_r, W_0, R_w and a_w are adjusted as free parameters to optimize the fit to the experimental data by using a least-squares program. Because our basic purpose in this work is to examine the predictive ability of the folding model based on the α- particle model, but not to find the optimum fit to the data, so our procedure are (i) taking the parameters R_w, a_w fixed values for all energies in the calculations; only the two parameters N_r and W_0 are adjusted as free parameters to fit the data. (ii) instead of using a least-squares method, the "optimum" fit is obtained by visual evaluation.

According to reference [1], we take $R_w = 1.4\ A^{1/3} fm$, $a_w = 0.7 fm$ and the reduced Coulomb radius $r_c = 1.3 fm$ in our calculations. Using equations (1) - (6), the available experimental data of the $\alpha + ^{16}O$ elastic scattering differential cross section at ten incident energies in the energy region of 20 MeV to 60 MeV are analyzed. As these data cover the whole angular region, thus it makes the test to the model more strict. Although there are also available experimental data for incident energies above 100 MeV (e.g. $T_\alpha = 104$ and $146 MeV$), but as the Buck's $\alpha - \alpha$ interaction is not applicable above 80 MeV, so the folding potential based on equation (2) is no longer suitable for these energies. Thus we did not extend our analysis to the energies above 100 MeV.

The results of our calculations for $\alpha + ^{16}O$ elastic scattering at 25.4, 26.6, 28.1,

29.1, 30.0, 30.9, 32.2, 39.3, 48.7 and 54.1 MeV together with the experimental data are shown in Fig.1 and Fig.2. It can be seen that the α-folding model can reproduce the experimental data quite well. In reference [6], the two angular distributions at incident energies 48.7 and 54.1 MeV were analyzed by using a phenomenological real and imaginary Woods-Saxon potential, but the fits to the experimental data were rather poor. A DDM3Y double-folding model analysis for the same system at four incident energies above 32 MeV was also performed in the same paper, and good agreement with the data was obtained. Comparing our results shown in Fig.1 with those obtained by the DDM3Y double-folding model in reference [6], one can see that both the α-particle folding model and the DDM3Y folding model give almost equally good fits to the experimental data. However, in the DDM3Y model calculations in [6], an imaginary potential with six free parameters (in a form of the sum of Fourier-Bessd functions) and a least-squares program were used to fit the data. In contrast, only one parameter for the imaginary part of the potential is adjustable in our calculation. It is expected that if the same procedure as above are adopted in the α folding model calculations, some improved fits to the data will be obtained. As mentioned above, the purpose of this work is not to get the optimum fit but to examine the predictive ability of the α-particle model, for this goal the results shown in Fig.1 and Fig.2 are sufficiently satisfactory.

The values of N_r and W_0 corresponding to the results of Fig.1 and Fig.2 are plotted in Fig.3. For the DDM3Y model in reference [6] $N_r = 1.40$, 1.39, 1.39 and 1.35 are required to fit the data at incident energies 32.2, 39.3, 48.7 and 54.1 MeV respectively, while for the α-particle model the corresponding values of N_r required are 0.87, 0.84, 0.82 and 0.82. The magnitude of $\mid N_r - 1 \mid$ is a measurement of the successfulness of the folding model, for the DDM3Y model their values are 40%, 39%, 39% and 35%, while for the α-particle model are 13%, 16%, 18% and 18%.

The shape of the unrenormalized (i.e. $N_r = 1$) α folding potential is shown in

Fig.4. The value of the volume integral per nucleon pair for the real part of the potential $J_R/4A$, for the incident energies 48.7 and 54.1 MeV as an example, is 340 MeV fm^3 for the α-particle model, which is in agreement with $J_R/4A \approx 350 MeV\,fm^3$ concluded from the DDM3Y model analysis [6]. This value of 340 MeV fm^3 also agrees with that about 350 MeV fm^3 obtained from a "model independent" analysis for the $\alpha + ^{40}Ca$ system [3]. The above results demonstrate the success of the α folding model in predicting the shape and the strength of the real potential.

Besides the noticeable difference in the renormalization factor mentioned above, it should be emphasized that there is a significant difference between the DDM3Y model and the α-particle model, that is, the elementary interaction used in the DDM3Y model is an effective one, while in the α-particle model is a free $\alpha - \alpha$ interaction (i.e. bare interaction). As shown by Satchler [14] that, if a free N-N interaction is used in constructing the folding potential, the real potential will be overestimated by a factor of two or more, therefore an effective N-N interaction is used to reduce the folding potential. This can be understood as that the interaction for two nucleons embedded in nuclear medium is different from that for two free nucleons. However, in the present work we used a free $\alpha - \alpha$ interaction and obtained a set of the folding potentials more approaching to ones required by the experiments. This fact indicates that the α-particle in the ^{16}O nucleus behaves basically like a free one. This is just the basic physical idea of the nuclear α-particle structure model. This is in agreement with the fact that an α-particle is bound much more weakly than a nucleon in the ^{16}O nucleus. Thus, the present success of using a free elementary interaction may be considered as a strong support to the α structure model of ^{16}O nucleus.

In conclusion, basing on the 4α structure model of ^{16}O nucleus and using a free $\alpha - \alpha$ potential as elementary interaction, a single folding potential is obtained for the description of the interaction between the incident α and the ^{16}O nucleus. This α folding potential provides a satisfactory description of the experimental data in

a broad range of incident energies. This success gives a support for the four alpha structure model of the ^{16}O nucleus.

References

[1] P. P. Singh, R. E. Malmin, M. High and D. W. Devins, Phys. Rev. Lett. 23(1969)1124.

[2] Th. Delbar et al., Phys. Rev. C18(1978)1237.

[3] H. P. Gubler et al., Nucl. Phys. A351(1981)29.

[4] A. M. Kobos et al., Nucl. Phys. A425(1984)205.

[5] F. Michel et al., Phys. Rev. C28(1983)1904.

[6] H. Abele et al., Z. Phys. A326(1987)373.

[7] L. J. McDonald, H. Uberall and S. Numrich, Nucl. Phys. A147(1970)541.

[8] Li Qing-run, Chen Seng-zhong and Zhao En-guang, High Energy Physics. Nucl. Phys. 5(1981)531.

[9] A. N. Antonov, Bulg. J. Phys. 11(1975)287.

[10] Li Qing-run and Zhou Jin-li, to be published.

[11] Li Qing-run, Phys. Rev. C30(1984)1248.

[12] M. El-Azab Farid, J. Phys. G. 16(1990)461.

[13] B. Buck, H. Friedrich and C. Wheathly, Nucl. Phys. A275(1977)246.

[14] G. R. Satcher, Phys. Lett. 59B(1975)121.

[15] A. A. Cowley and G. Heymann, Nucl. Phys. A146(1970)465.

Figure Captions

Fig.1. Differential cross sections for $\alpha + {}^{16}O$ elastic scattering at the incident energies 32.2, 39.3, 48.7 and 54.1 MeV. The curves show the results of the α- particle folding model. The data are from refs.[15], [5], [6].

Fig.2. Differential cross sections for $\alpha + {}^{16}O$ elastic scattering at the incident energies 25.4, 26.6, 28.1, 29.1, 30.0 and 30.9 MeV. The curves show the results of the α-particle folding model. The data are from ref.[15].

Fig.3 Values of the renormalization factor N_r and the central imaginary depth W_0 as a function of the incident energy for the α-particle folding model.

Fig.4 The α model folding potential (unrenormalized) for $\alpha + {}^{16}O$.

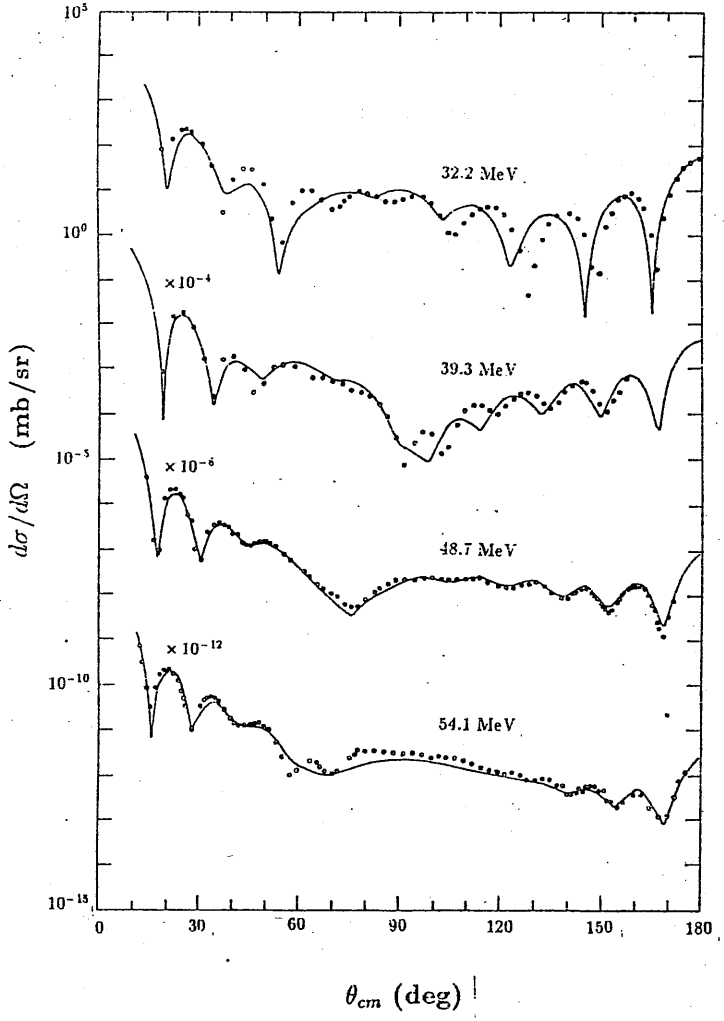
32.2 MeV
×10⁻⁴
39.3 MeV
×10⁻⁸
48.7 MeV
×10⁻¹²
54.1 MeV
dσ/dΩ (mb/sr)
θcm (deg)

Fig.1

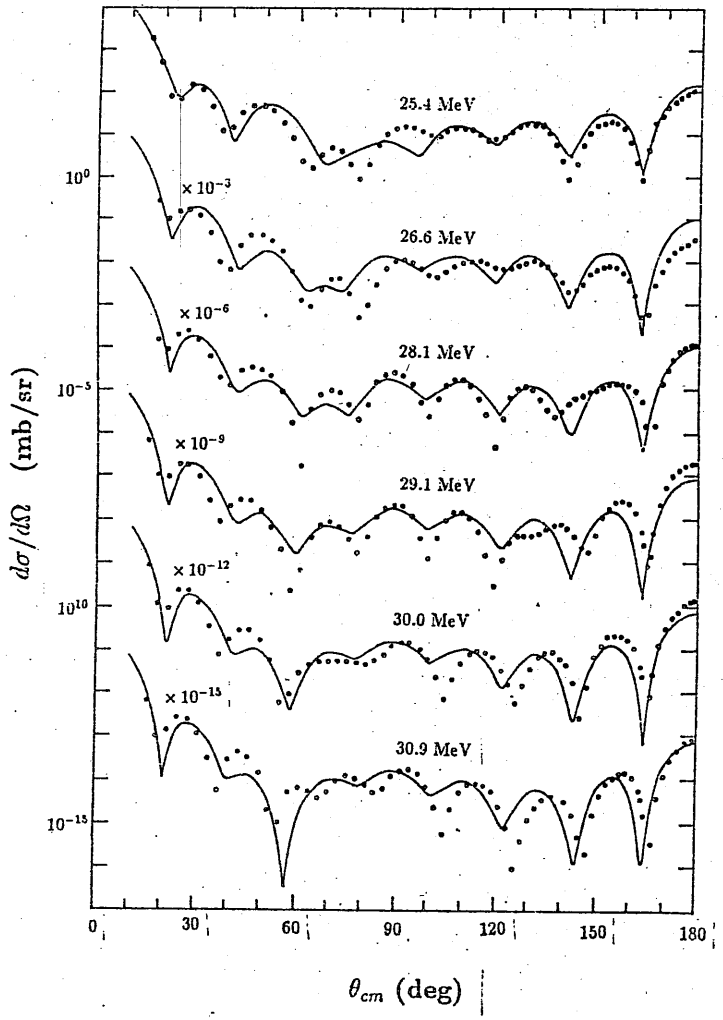
25.4 MeV
×10⁻³
26.6 MeV
×10⁻⁶
28.1 MeV
×10⁻⁹
29.1 MeV
×10⁻¹²
30.0 MeV
×10⁻¹⁵
30.9 MeV
dσ/dΩ (mb/sr)
θcm (deg)

Fig.2

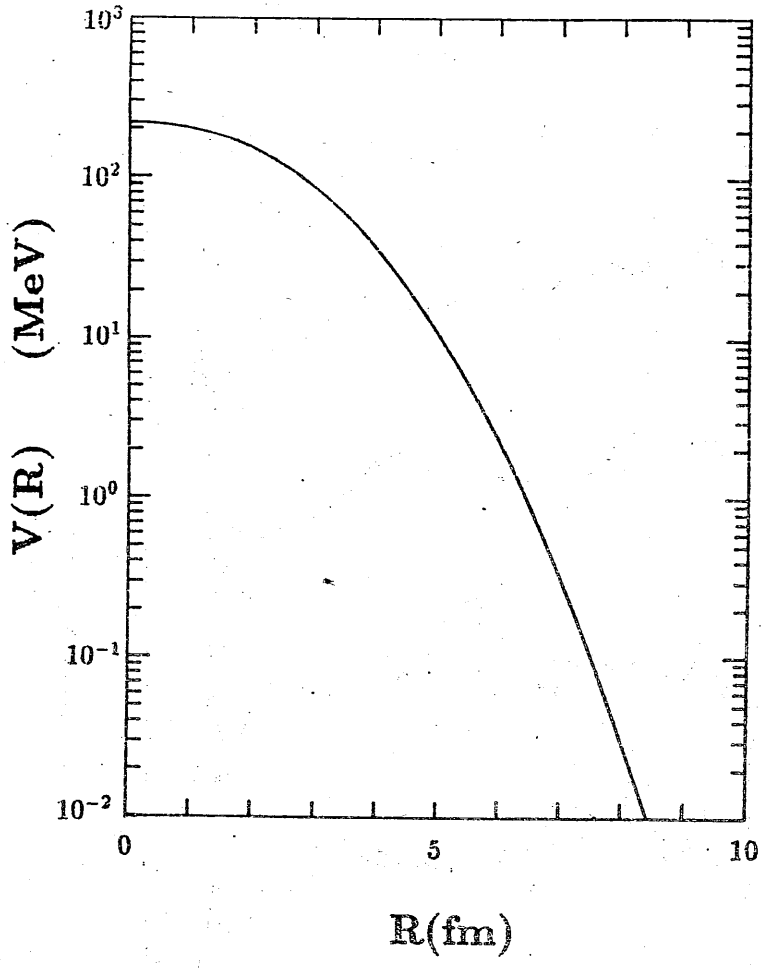
10^3
10^2
10^1
10^0
10^{-1}
10^{-2}
V(R) (MeV)
0
5
10
R(fm)

Fig.4

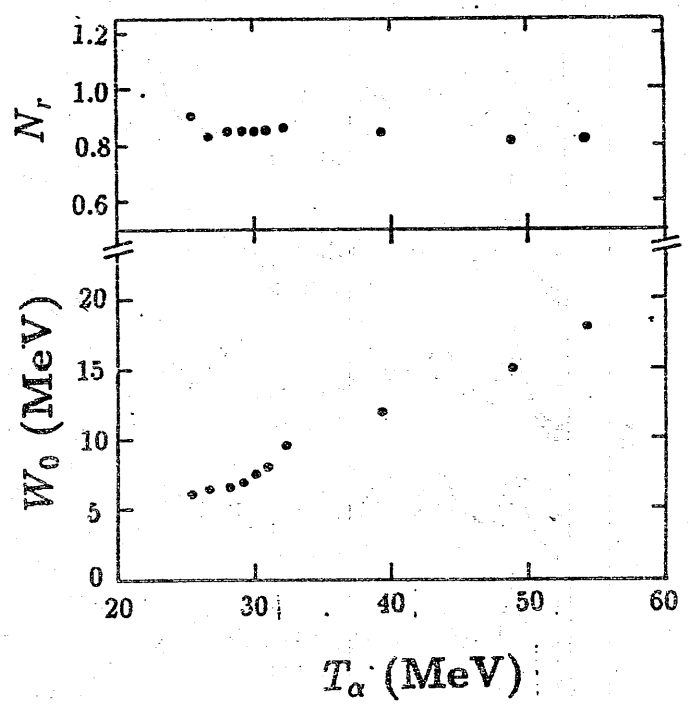
1.2
1.0
0.8
0.6
N_r
20
15
10
5
0
W_0 (MeV)
20
30
40
50
60
T_α (MeV)

Fig.3

PROJECTED ONE PLUS THREE QUASIPARTICLE-SU(5) COUPLING MODEL --Application to the Isotones of ^{147}Pm and ^{149}Eu

Zeng Guo-Mo [a,b], Wu Shi-Shu [b]

a) *The Centre of China Advanced science and Technology (CCAST, World Laboratory), Beijing*
b) *Theoretical Physics Centre of Jilin University, Changchun*

Abstract The calculation method for the transitional odd-A nuclei is studied. The theoretical calculation on the energy level structure of the isotones ^{147}Pm and ^{149}Eu is performed by coupling 1+3 quasiparticle to anharmonic vibration of the core. A particle-number conservation treatment is made by means of the projection method. The effects of the particle-number projection, three-boson excitation and residual interactions on the lower excited states for odd-A nuclei in the transitional region are discussed.

Key words 1+3 quasiparticle, anharmonic vibration, transitional odd-A nuclei, number-projection, truncation method

1. Introduction

In the past decade, several works based on the interacting boson-fermion model (IBFM) [1] and its equivalent the particle-truncated quadrupole-phonon coupling model (PTQM) [2] have been done for the low-lying energy spectra of isotopes $^{147-153}$Eu [3] and $^{147-153}$Pm [4] as well as isotones ^{143}Pr-^{147}Eu [5]. But these works have some shortcomings. First of all, they take the adjacent even-even nuclei as the inert core for every odd-mass nucleus in a sequence of isotopes or isotones and introduce a set of parameters respectively. So, as a whole, there are too much free parameters involved in the calculation and the systematicness is lowered. Secondly, they deal with the core by means of IBM only and the results deviate from the experimental data. In consequence, it is impossible to obtain the accurate description for the higher excited states of odd system. In order to make a systematic and accurate description for odd-A nuclei in the transitional region, we choose a common core for all nuclei in the same series of isotopes or isotones and describe the core with IBM. The extra nucleons are described by one- or three- quasiparticle and the residual interactions between the extra nucleons are taken into account. We hope that the residual interactions will counteract in somewhat

the deviation caused by describing the core with IBM only.

Following from the inclusion of three quasiparticle states, the number of particlies is no longer conserved and the spurious states arise. In order to solve this problem and investigate its influence on the results, the projection method is adopted in this article at a price of a big increase in the computation work. Moreover, that coupling 1+3 quasiparticles to the core results in the rapid expansion of the configuration space and makes the computation very tedious. Therefore, it must be imperative to cut off the configuration space. In the usual method, one should make the truncation in the quasiparticle-core coupling space. But in this way, the computation work is still considerable. Alternatively, we have used an appropriate truncation method. Our calculations show that it is feasible and can simplify remarkably the computations.

With the above model and truncation technique, we have completed the calculations for the low-lying energy spectra of the isotones ^{147}Pm and ^{149}Eu. The experimental results were reproduced quite well.

2. Model and formalism

2.1 Model hamiltonian

The model hamiltonian consists of three parts:

$$H = H_F + H_B + H_{FB} \tag{1}$$

where, H_F describes the quasiparticles outside the core, in which the residual interaction is included. H_B denotes the core hamiltonian. H_{FB} is the particle-core coupling hamiltonian. We give the further explanation for the three hamiltonians respectively as follows:

(1) In the particle representation ,we can write

$$H_F = \sum_\alpha \varepsilon_\alpha a^+_\alpha a_\alpha + \frac{1}{4}\sum \langle\alpha\beta|V|\gamma\delta\rangle a^+_\alpha a^+_\beta a_\delta a_\gamma \tag{2}$$

where, $a^+_\alpha (a_\alpha)$ are the creation (annhilation) operators. $\alpha=(j_\alpha, m_\alpha)$, $\bar{\alpha}=(-)^{j_\alpha - m_\alpha}(j_\alpha, m_\alpha)$ stand for the quasiparticle states. We introduce a z-dependent canonical transformations

$$d^+_\alpha = \gamma_{\bar{\alpha}}(u_\alpha a^+_\alpha - z v_\alpha a_{\bar{\alpha}})$$

$$d^{+}_{\alpha} = \sigma_{\alpha}(u_{a} a^{+}_{\alpha} - z v_{a} a_{-\alpha}) \tag{3}$$

with

$$\sigma_{\alpha} = (u^{2}_{a} + z^{2} v^{2}_{a})^{-1} \tag{4}$$

here v_a and u_a represent the amplitudes of qusiparticle and quasi-hole respectively. Using the inverse transformation of eq.(3), the hamiltonian in (2) can be rewritten as

$$H_F = H_{00} + H_{11} + H_{20} + H_{02} + H_{22} + H_{31} + H_{13} + H_{40} + H_{04}, \tag{5}$$

with

$$H_{02} = H^{+}_{20}; \quad H_{13} = H^{+}_{31}; \quad H_{04} = H^{+}_{40}. \tag{6}$$

The concrete expressions of each terms in eq.(5) can be seen in Ref.[7]. Introducing the generating function of quasiparticle vacuum, one quasiparticle and three quasiparticles states and using the commutation relations of operators $d^{+}_{\alpha}(d_{\alpha})$ we can derive the matrix elements of the hamiltonian (5) and the tensor operators of rank λ between the generating functions and then get the matrix elements of the above operators with the particle-number conserved by the loop integration. In our calculation, the residual interactions contained in H_F are taken as the quadrupole-quadrupole interaction (QQI) and the surface δ interaction (SDI) respectively. Both interactions reflect in some extent the main features of the nuclear force and have simple forms convenient to deal with.

(2) Since the odd-A nuclei that we concern about are close to the spherical region, the core hamiltonian H_B can be taken as the SU(5) limit of IBM, which equals to the anharmonic quadrupole vibration hamiltonian:

$$H_B = H_{SU(5)}$$
$$= \varepsilon \sum_{\mu} d^{+}_{\mu} d_{\mu} + \sum_{L=0,2,4} \frac{1}{2}(2L+1)^{1/2} C_L [(d^{+}d^{+})^{(L)}(dd)^{(L)}]^{(0)} \tag{7}$$

where $d^{+}_{\mu}(d_{\mu})$ are the creation (annhilation) operators of d-bosons. ε is the energy of a d-boson. The corresponding wave functions are $|n\alpha L\rangle$, where n represents the number of d-bosons, L stands for the total angular mementum, α is an additional quantum number needed to classify the states. Since for $n \leq 3$, the states are completely definite for the fixed n and L, in the following we use $|nL\rangle$ only to denote the basis functions of the core.

(3) The particle-core coupling hamiltonian are represented as

$$H_{FB} = -\xi\varepsilon(\pi/2)^{1/2}\sum_{\mu} Q_{2\mu} Y_{2\mu}(\vartheta\phi) \tag{8}$$

where ξ describes the strength of the coupling, $Q_{2\mu}$ is the quadrupole operator for the core. The reduced matrix elements of $Q_{2\mu}$ between the states of the d-bosons are deduced from the experimental $E2$ transition rates and quadrupole moments of the core. In detail, the off-diagonal matrix elements are chosen to be

$$(n'L'\|Q\|nL) = k\,[(2L'+1)\,B(E2:L\longrightarrow L')]^{1/2} \tag{9}$$

the factor k is determined so that $(12\|Q\|00)$ equals to the harmonic value $\sqrt{5}$. The diagonal matrix elements are defined as

$$(nL\|Q\|nL) = k\,\frac{5}{4}\,(7/2\pi)^{1/2}\,Q_{nL} \tag{10}$$

where Q_{nL} is the exprimental quadrupole mement in the state of $|nL\rangle$ and we assume that [8]

$$Q(2_2^+) = -Q(2_1^+),\quad Q(4_1^+) = Q(2_1^+)$$

2.2 Truncation method

In the case of incorporating three-quasiparticle excitations, the dimension of the configurations is too large for the available computer *VAX*8600. For example, for $I=\frac{7}{2}$, even though the number of d-boson are merely taken up to 2, the dimension of configurations become 500. which makes it impossible to adjust the parameters so as to fit the exprimental data. In view of this, the configuration space must be cut off. The method that we adopted are as follows:

(1) freezing the degree of freedom of the core and only considering the excitation of the particles in the open shells. The corresponding wave functions are $|j_a j_b j_{ab} j_c; JM_J\rangle$. solving the energy eigenequations for every J respectively, we can obtain the wavefunction

$$|E^{\alpha J}, JM_J\rangle = \sum C_{\alpha J}(j_a j_b j_{ab} j_c J)\,|j_a j_b j_{ab} j_c; JM_J\rangle \tag{11}$$

and then rearrange the wavefunctions in the size of corresponding eigenvalues $E^{\alpha J}$. Here αJ denotes the order of the wave functions with angular momentum J, which we take as an additional quantum number.

(2) Choosing the truncation energy E_{trun} and coupling all wave functions $|\alpha JJM_J\rangle \equiv |E^{\alpha J}, JM_J\rangle$ with $E^{\alpha J} < E_{trun}$ to the bosons wavefunction to construct the basis functions for the coupled quasiparticle-boson representation

$$|\alpha_J JnL, IM\rangle = \sum_{M_J M_L} (JM_J LM_L | IM) |\alpha_J JM_J\rangle |nLM_L\rangle \qquad (12)$$

where the brackets stand for the *Clebsch-Gordan* coefficients. The total wave functions of the nuclear system can be expanded to the basis functions

$$\Phi^{(i)}_{IM} = \sum_{\alpha_J JnL} C^{(i)} (\alpha_J JnL, I) |\alpha_J JnL, IM\rangle \qquad (13)$$

The matrix elements of the total hamiltonian (1) between the basis functions [eq.(12)] is

$$\begin{aligned}\langle \alpha'_J J'n'L', IM|H|\alpha_J JnL, IM\rangle = & \sum_{\text{all } j} C_{\alpha J}(j'_a j'_b j'_{ab} j'_c J') C_{\alpha J}(j_a j_b j_{ab} j_c J) \\ & \times \{\delta_{n'n}\delta_{L'L}[\langle j'_a j'_b j'_{ab} j'_c J'|H_F|j_a j_b j_{ab} j_c J\rangle \\ & + \langle j'_a j'_b j'_{ab} j'_c J'|j_a j_b j_{ab} j_c J\rangle \langle nL\|H_B\|nL\rangle] \\ & - \xi\varepsilon(\pi/5)^{1/2}(-)^{I+L+J} \begin{Bmatrix} 2 & J' & J \\ I & L & L' \end{Bmatrix} (n'L'\|Q\|nL) \\ & \times \langle j'_a j'_b j'_{ab} j'_c J'\|\sum Y\| j_a j_b j_{ab} j_c J\rangle\}. \end{aligned} \qquad (14)$$

In the first step, the largest dimension of the matrix we need to evaluate is 29. And in the second step it is possible to limit the dimension below 200 by adequatly choosing the truncation energy. Therefore, the configuration space is remarkably reduced and the whole process is convenient to handle by computers.

3. Results and discussion

As an illustration, we have applied the above model and truncation method to calculate the low-lying energy levels for the isotones ^{147}Pm and ^{149}Eu. ^{146}Nd is taken as a common core. ^{147}Pm and ^{149}Eu has one and three protons outside the core respectively. Since there are not complete observed spectra for ^{151}Tb and ^{153}Ho, which have five and seven extra particle respectively, we have not included these two neclei in the calculations. In consideration of that there are only two extra protons in ^{149}Eu more than in ^{147}Pm, we neglect the effects of the Coulomb interaction. The quasiparticle levels are taken as $g_{7/2}$, $d_{5/2}$, $d_{3/2}$ and $s_{1/2}$. We do not solve the gap equations for simplicity. The energies and the occupation

numbers of the quasiparticles are obtained from the experimental values in Ref.[9]. The quasiparticle energies are $E_{7/2}$=0.0, $E_{5/2}$= 125.0, $E_{3/2}$=1300.0 and $E_{1/2}$=1400.0 (keV). The observed excitation energies as well as $E2$ transition rates and quadrupole moments of the core needed to calculate the matrix elements of the H_B and H_{FB} can be found in Ref.[10]. We take the d-boson energy as the first exciting energy of the core , i.e., ε=453.86 keV. The anharmonic parameters are C_0=7.78, C_2=395.48 and C_4=135.45 (keV). The values of reduced quadrupole matrix elements for the core are

$$(12\|Q\|00) = \sqrt{5}, \qquad (24\|Q\|12) = 3.63,$$
$$(20\|Q\|12) = \sqrt{2}, \qquad (12\|Q\|12) = -2.60,$$
$$(22\|Q\|00) = 1.26, \qquad (22\|Q\|22) = 2.60,$$
$$(22\|Q\|12) = \sqrt{10}, \qquad (24\|Q\|24) = -2.60.$$

(1) ^{147}Pm

Since there is only one single proton outside the core ^{146}Nd for ^{147}Pm, it requirs merely one quasiparticle to describe the proton. For comparison, we have completed three different types of calculations as shown in Fig.1 with (a), the experimental results; (b), the results for projected one quasiparticle coupled to the core; (c), as (b), except for unprojecting. We have included boson states up to two bosons in (b) and (c) and three bosons in (d). The later is the same as (b) except for the bosons states. The coupling strength is fixed to ξ=1.5. It can be seen in Fig.1 that the three types of calculations present almost identical results. Up to the energies near 1000 keV, the differences between (b) and (c) are not notable. This is because of that the first excitation energy of the core is relatively larger. Thus, the effects of three boson excitations just appear at even higher states. The observed energy levels can be clearly devided into three groups. The lowest group consists of the ground state and the first excitation state. The levels between 400-700 keV form the second group. And the levels above 900 keV belong to the third group. These have been satisfactorily reprodued by three theoretical spectra. Furthermore, the energy densities of all groups are reproduced quite well.

(2) ^{149}Eu

Fig.2 present calculation results for ^{149}Eu. In which (a) is the observed spectrum; (b) the calculated spectrum obtained by coupling projected 1+3 quasiparticle to the core quadrupole vibration and choosing quadrupole-quadrupole interaction as the residual in-

teraction; (c) as (b) except for taking surface delta interaction as the residual interaction and (d) same with (b) except for unprojecting. The strengths of the residual interaction are $\varkappa$=1.30 keV/fm^4 in (b) and (d) and $\varkappa$=80.0 keV in (c). Comparing the calculated spectra with the observed one, we can see that the theoretical results in (c) deviate far from the observed spectrum. On the other hand both (b) and (c) reproduced the experimental results very well. Especially in (b), not only the energy density fits well, but the order of energy levels of the whole spectrum agrees with the experiments quite well.

According to our calculation and the above analysis, we can make preliminary conclusions that

(1) In the case of single particle outside the core, it wont make much difference whether projecting or not. While, if the number of extra particles more than one, the results obtained by projecting are better than the one by unprojecting.

(2) The three-boson excitations of the core contributes only to the higher lying levels of the odd-A nuclei.

(3) For describing the residual interaction, the quadrupole-quadrupole interaction is better than the surface delta interaction. And the energy level structure of odd-A nuclei is very sensitive to the strength of residual interactions.

In the forthcoming articles, we apply the 1+3 quasiparticle-core coupling model to analyse the energy spectra and electromagnetic qualities for the sequence of isotones ^{149}Pm, ^{151}Eu, ^{153}Tb and ^{155}Ho. The results supports the conclusions mentioned above. We have also obtained some other conclusions by analysing the wave functions. And the validity of the model are indicated further.

REFFERENCES

[1] Iachello, F. and Scholten, O., *Phys. Rev. Lett.*, 1979;43:679
[2] Paar, V. *et al.*, *Nucl. Phys.*, 1982; A378:41
[3] Scholten, O. and Blasi, N., *Nucl. Phys.*, 1982; A380:509
[4] Scholton, O. and Ozzello, T., *Nucl. Phys.*, 1984; A424:221
[5] Baum, E. M. *et al.*, *Phys. Rev.*, 1989; C39:1514
Kusnezov, D. F. *et al.*, *Phys. Rev.*, 1989; C40:924
[6] Aryaeinejad, R. *et al.*, *Phys. Rev.*, 1989; C40:1429
[7] Ottaviani, P. L. and Savoia, M., *Phys. Rev.*, 1969; 187:1306; *Nuovo Cim.*, 1970; 67A: 630; *Phys. Rev.*, 1969; 178: 1594
[8] Castel, B. H. *et al.*, *Nucl. Phys.*, 1971; A162: 273
[9] Wildenthal, B. H. *et al.*, *Phys. Rev.*, 1971; C3: 1199
[10] Peker, L. K., *Nuclear Data Sheets*, 1990; 60: 953

FIG.1. Energy levels of ^{147}Pm.

FIG.2. Energy levels of ^{149}Eu.

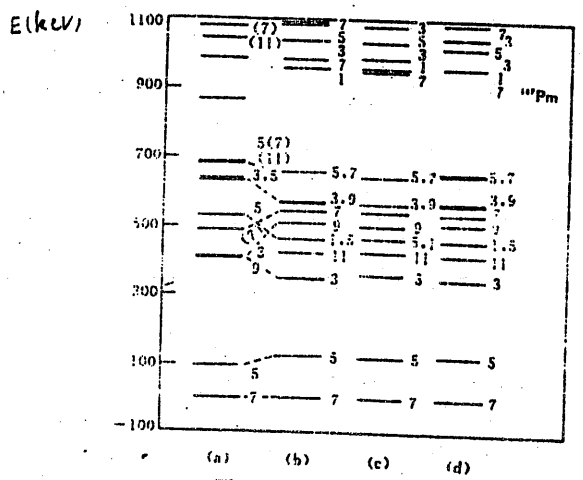

图1 ^{147}Pm的能级图

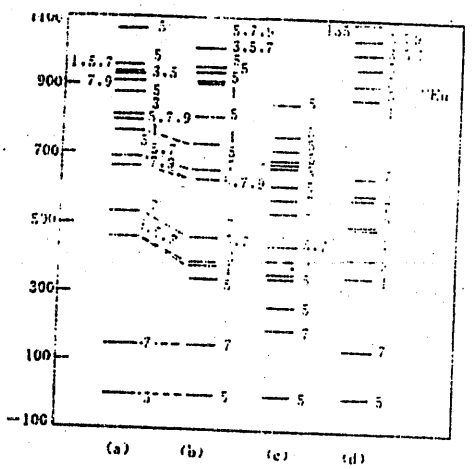

图2 ^{149}Eu的能级图

Dynamical Symmetries of the spdf Interacting Boson Model

Yuxin Liu[a,b], Hongzhou Sun[c,b] and Enguang Zhao[a,b]
[a]CCAST(World Laboratory), P. O. Box 8730, Beijing 100080, China
[b]Institute of Theoretical Physics, Academia Sinica,
P. O. Box 2735, Beijing 100080, China*
[c]Department of Physics, Tsinghua University, Beijing 100084, China

December 23, 1992

Abstract

The dynamical symmetries of the nuclear spdf Interacting Boson Model are discussed systematically. The possible dynamical symmetry group chains are given. The branching rules of reductions in the group chains, the dynamical symmetry Hamiltonians and the energy spectra of the limits $SU_{pdf}(5)$, $O_{spdf}(6)$, $SU_{spdf}(3)$ and $O_{spdf}(4)$ are presented.

1 Introduction

Since the Interacting Boson Model(IBM) was put forward[1], it has been quite successful in describing the collective motoin of nuclei, largely due to the algebraic structure and dynamical symmetry properties of the model[1,2]. In the original version of IBM, positive parity collective excitations are generated by s and d bosons. It points out that there are close connections between collective motion and dynamical symmetries for positive parity states of even-even nuclei, such as vibration corrresponds to U(5) symmetry, rotation to SU(3) symmetry and $\gamma-$unstable to O(6) symmetry. Recently a great number of experimental activities and microscopic analyses have shown that there are probably nuclei with octupole deformation[3]. In order to attempt a collective model description of octupole deformation in nuclei in the framework of IBM, an interacting boson model

*Mailing address

containing s, p, d and f bosons(spdf IBM) has been introduced[4-8] and applied to describe the properties of light actinide nuclei[4,9] and neutron rich rare-earth nuclei[10] with some success.

When the p, f bosons are introduced alongside s and d bosons, the space spanned by single boson states is $1+3+5+7=16$ dimensional. The corresponding algebraic structure is U(16). This structure is quite large and complicated. However Engel and Iachello have discussed the SU(3) and O(4) limits[5]. Nadjakov et.al.[11] and Sun et.al.[8] have discussed some of the SU(5) and O(6) Limits besides the SU(3) limit. Moreover Kusnezov has shown that there are 7 dynamical symmetry limits with 165 group chains. Some of the algebric structure of these groups was given[12]. However there has no systemastic discussion on the description of nucleus with the symmetries.

It is known that nuclear collective motion preserves not only the boson number(duc to the preservation of nucleon number) and angular momentum but also the parity. It means that when the dynamical Hamiltonian is written in the form

$$H=\sum_{l=0}^{3}\varepsilon_l\hat{n}_l+\sum_{l_1,l_2,l_3,l_4,k}V^{(k)}_{l_1,l_2,l_3,l_4}[(b^\dagger_{l_1}\tilde{b}_{l_2})^{(k)}(b^\dagger_{l_3}\tilde{b}_{l_4})^{(k)}]^0 \tag{1.1}$$

there should be $l_1+l_2+l_3+l_4=even(0\le l_1,l_2,l_3,l_4\le 3)$. However, for some group chains given by Kusnezov, the Hamiltonian constructed with the Casimir operators of the subgroups in the symmetry group chain do not meet this restriction, such as the one with interaction $(p^\dagger\tilde{d})^{(k)}\cdot(d^\dagger\tilde{d})^{(k)}$. A thorough analysis shows that there are 142 of the 165 group chains satisfying the restrictions. they can still be classified into 7 dynamical symmetry limits $SU_{pdf}(5)$, $O_{spdf}(6)$, $SU_{pdf}(4)$, $SU_{spdf}(3)$, $O_{pdf}(5)$, $O_{spdf}(4)$ and $O_{pdf}(3)$. Because the symmetry of the $O(5)$ and $O(3)$ limits are quite lower, and $SU(4)$ is isomorphous to $O(6)$, the important ones are the $SU_{pdf}(5)$, $O_{spdf}(6)$, $SU_{spdf}(3)$ and $O_{spdf}(4)$ limits. In this paper we will discuss detailedly the branching rules of reductions in the group chains of these four limits. The dynamical symmetry Hamiltonians, the wave function and the energy spectra of these limits will be constructed. In section 2, 3, 4, 5 we discuss in some details the limits $SU(5), O(6), SU(3)$ and $O(4)$ respectively. Finally in section 6 we give a brief concluding remark.

2 The $SU(5)$ Limit

A systematic analysis shows that there are four kinds of group chains on coupling level $SU_{pdf}(5)$ in spdf IBM. The typical ones are

$$\begin{aligned}&U_{spdf}(16)\supset U_{sd}(6)\otimes U_{pf}(10)\supset U_d(5)\otimes U_{pf}(10)\supset\\ &\qquad SU_d(5)\otimes SU_{pf}(5)\supset SU_{pdf}(5)\supset O_{pdf}(5)\supset O_{pdf}(3)\\ &U_{spdf}(16)\supset O_{spdf}(10)\supset SU_{pdf}(5)\supset O_{pdf}(5)\supset O_{pdf}(3)\end{aligned} \tag{2.1}$$

In $SU_{pdf}(5)$ limit symbolized by the first of eq.(2.1), the dynamical symmetry Hamil-

tonian can be expressed as

$$H = \epsilon C_{1U_{sd}(6)} + \epsilon^{'} C_{1U_{pf}(10)} + AC_{2SU_d(5)} + A^{'} C_{2SU_{pf}(5)} + BC_{2SU_{pdf}(5)} + CC_{2O_{pdf}(5)} + DC_{2O_{pdf}(3)}. \tag{2.2}$$

The wave function can be written as

$$|\psi(L^{\pi})\rangle = |N\ n_{sd}\ [n_d]_5,\ n_{pf}\ [\lambda_1, \lambda_2, \lambda_3, \lambda_4]_5;\ [n_1, n_2, n_3, n_4]_5\ (\nu_1, \nu_2)_5\ \alpha\ L\ \rangle \tag{2.3}$$

$$SU_d(5) \qquad SU_{pf}(5) \qquad SU_{dpf}(5) \quad O_{dpf}(5) \quad O_{dpf}(3)$$

with

$$\pi = \begin{cases} +, & n_{pf} = even; \\ -, & n_{pf} = odd, \end{cases}$$

where α is the additional quantum number to distinguish the same L belonging to the same (ν_1, ν_2). All these values can be determined by the branching rules of the IRRP reductions.

The branching rules for every step of the reductions are the followings.

(1) $U_{spdf}(16) \supset U_{sd}(6) \otimes U_{pf}(10)$

For the total symmetric IRRP $[N]$ of $U_{spdf}(16)$, the branching rule is

$$[N] = \sum \oplus [n_{sd}] \otimes [n_{pf}] \tag{2.4}$$

where n_{sd} and n_{pf} are the posible nonnegative integers satisfying the relation $n_{sd} + n_{pf} = N$.

(2) $U_{sd}(6) \supset SU_d(5)$

This reduction has been detailed in sd IBM. For the symmetric IRRP $[n_{sd}]$, the result is

$$[n_{sd}]_6 = [0]_5 \oplus [1]_5 \oplus [2]_5 \oplus \cdots \oplus [n_{sd}]_5 \tag{2.5}$$

(3) $U_{pf}(10) \supset SU_{pf}(5)$

This reduction has been discussed in refs.[8,12]. For the IRRP $[n_{pf}]$

$$[n_{pf}]_{10} = [n_{pf}, n_{pf}, 0, 0]_5 \oplus [n_{pf} - 1, n_{pf} - 1, 1, 1]_5 \oplus [n_{pf} - 2, n_{pf} - 2, 2, 2]_5 \oplus \cdots$$
$$\oplus \begin{cases} [\frac{n_{pf}}{2}, \frac{n_{pf}}{2}, \frac{n_{pf}}{2}, \frac{n_{pf}}{2}]_5 & (n_{pf} = even); \\ [\frac{n_{pf}+1}{2}, \frac{n_{pf}+1}{2}, \frac{n_{pf}-1}{2}, \frac{n_{pf}-1}{2}]_5, & (n_{pf} = odd). \end{cases} \tag{2.6}$$

(4) $SU_d(5) \otimes SU_{pf}(5) \supset SU_{pdf}(5)$

Using Young tableaux techneque[13–16] or Schur function method[17,18] we can get the branching rules of this reduction. It can be concluded as

$$[\lambda, \lambda, 0, 0]_5 \otimes [n_d]_5 = \sum_{m_1, m_2} \oplus [\lambda + m_1, \lambda, m_2]_5 \tag{2.7}$$

where $m_1 + m_2 = n_d$, $0 \leq m_2 \leq \lambda$.

$$[\lambda_1, \lambda_1, \lambda_2, \lambda_2]_5 \otimes [n_d]_5 = \sum_{m_1, m_2, m_3} \oplus [\lambda_1 + m_1 - m_3, \lambda_1 - m_3, \lambda_2 + m_2 - m_3, \lambda_2 - m_3]_5 \tag{2.8}$$

in which $m_1+m_2+m_3=n_d$, $0\le m_2\le\lambda_1-\lambda_2$, $0\le m_3\le\lambda_2$.

(5) $SU_{pdf}(5)\supset O_{pdf}(5)$

With the Young tableaux techneque or Schur function method being used, the branching rules of this reduction can be obtainned. For the lowest negative parity states, which contain only one p,f boson, the IRRPs of $SU_{pdf}(5)$ can be $[n_d+1]$ and $[n_d,1,1]$, the IRRPs of $O_{pdf}(5)$ can be written as

$$[n_d+1,1]_5=\begin{cases}(n_d+1,1)_5\oplus(n_d-1,1)_5\oplus(n_d-3,1)_5\oplus\cdots\\ \qquad\oplus(3,1)_5\oplus(1,1)_5\\ \oplus(n_d,0)_5\oplus(n_d-2,0)_5\oplus(n_d-4,0)_5\oplus\cdots\\ \qquad\oplus(2,0)_5, & (n_d=even);\\ (n_d+1,1)_5\oplus(n_d-1,1)_5\oplus(n_d-3,1)_5\oplus\cdots\\ \qquad\oplus(4,1)_5\oplus(2,1)_5\\ \oplus(n_d,0)_5\oplus(n_d-2,0)_5\oplus(n_d-4,0)_5\oplus\cdots\\ \qquad\oplus(3,0)_5\oplus(1,0)_5, & (n_d=odd).\end{cases}\tag{2.9}$$

$$[n_d,1,1]_5=(n_d,1)_5\oplus(n_d-1,1)_5\oplus(n_d-2,1)_5\oplus\cdots\oplus(2,1)_5\oplus(1,1)_5$$

(6) $O_{pdf}(5)\supset O_{pdf}(3)$

This reduction has been discussed in details[14-22]. With the computer codes[18,21,22] all of the branching rules can obtained.

The energy of the state L can be expressed as

$$\begin{aligned}E(L^\pi)=&E_0+\epsilon n_{sd}+\epsilon' n_{pf}+A\tfrac{4}{5}n_d(n_d+5)\\&+A'[\lambda_1(\lambda_1+4)+\lambda_2(\lambda_2+2)+\lambda_3^2+\lambda_4(\lambda_4-2)-\tfrac{1}{5}(\lambda_1+\lambda_2+\lambda_3+\lambda_4)^2]\\&+B[n_1(n_1+4)+n_2(n_2+2)+n_3^2+n_4(n_4-2)-\tfrac{1}{5}(n_1+n_2+n_3+n_4)^2]\\&+C[\nu_1(\nu_1+3)+\nu_2(\nu_2+1)]+DL(L+1).\end{aligned}\tag{2.10}$$

The typical energy spectrum can be shown in figure 1.

In $SU_{pdf}(5)$ limit indicated by the second of eq.(2.1), the dynamical symmetry Hamiltonian is

$$H=\epsilon C_{1U_{spdf}(16)}+AC_{2O_{spdf}(10)}+BC_{2SU_{pdf}(5)}+CC_{2O_{pdf}(5)}+DC_{2O_{pdf}(3)}.\tag{2.11}$$

The wave function can be expressed as

$$|\psi(L^\pi)\rangle=|N\,(m_1,m_2,m_3,m_4,m_5)_{10}\,[n_1,n_2,n_3,n_4]_5\,(\nu_1,\nu_2)_5\,\alpha\quad L\ \rangle\tag{2.12}$$

$$O_{spdf}(10)\qquad SU_{dpf}(5)\quad O_{dpf}(5)\quad O_{dpf}(3)$$

With the reductions of the IRRPs being accomplished, the wave functions with this symmetry can be determined. The branching rules that have not discussed above are the followings.

(1) $U_{spdf}(16)\supset O_{spdf}(10)$

The branching rules of this reduction have been discussed in refs. [12] and [18]. The result is

$$[N]_{16} = (\tfrac{N}{2}\tfrac{N}{2}\tfrac{N}{2}\tfrac{N}{2}\tfrac{N}{2})_{10} \oplus (\tfrac{N}{2}, \tfrac{N}{2}-1, \tfrac{N}{2}-1, \tfrac{N}{2}-1, \tfrac{N}{2}-1)_{10} \oplus \cdots$$
$$\oplus \begin{cases} (\frac{N}{2},0,0,0,0)_{10}, & \text{(N=even);} \\ (\frac{N}{2},\frac{1}{2},\frac{1}{2},\frac{1}{2},\frac{1}{2})_{10}, & \text{(N=odd).} \end{cases} \tag{2.13}$$

(2) $O_{spdf}(10) \supset SU_{pdf}(5)$

This reduction is rather complicated, however, it can be realized with the Schur function method[17,18]. For some special IRRPs of $O_{spdf}(10)$, we have branching rules analytically as

$$(\nu,\nu,\nu,\nu,\nu)_{10} = \sum_{i,j} \oplus [\nu-i, \nu-i, j, j]_5 \tag{2.14}$$

where $i = 0, 1, 2, \cdots, \nu$, and $j = 0, 1, 2, \cdots \nu - i$

$$(\nu,0,0,0,0)_{10} = \sum_{k} \oplus [\nu, k, k, k]_5 \tag{2.15}$$

where $k = 0, 1, 2, \cdots, \nu$.

The energy level of state L can be expressed as

$$\begin{aligned} E(L^\pi) = E_0 &+ \epsilon N + A[m_1(m_1+8) + m_2(m_2+6) + m_3(m_3+4) + m_4(m_4+2) + m_5^2] \\ &+ B[n_1(n_1+4) + n_2(n_2+2) + n_3^2 + n_4(n_4-2) - \tfrac{1}{5}(n_1+n_2+n_3+n_4)^2] \\ &+ C[\nu_1(\nu_1+3) + \nu_2(\nu_2+1)] + DL(L+1). \end{aligned} \tag{2.16}$$

where

$$\pi = \begin{cases} +, & n_2 + n_4 = even; \\ -, & n_2 + n_4 = odd. \end{cases}$$

3 The $O(6)$ Limit

There are two $O_{spdf}(6)$ dynamical group chains in spdf IBM. They are

$$\begin{aligned} &U_{spdf}(16) \supset U_{sd}(6) \otimes U_{pf}(10) \supset O_{sd}(6) \otimes O_{pf}(6) \supset O_{spdf}(6) \supset O_{pdf}(5) \supset O_{pdf}(3) \\ &U_{spdf}(16) \supset SU_{spdf}(4) \otimes SU_{spdf}(4) \supset SU_{spdf}(4)(\approx O_{spdf}(6)) \supset O_{pdf}(5) \supset O_{pdf}(3) \end{aligned} \tag{3.1}$$

For the $O_{spdf}(6)$ limit shown by the first of eq.(4.1), the dynamical symmetry Hamiltonian can be expressed as

$$H = \epsilon C_{1U_{sd}(6)} + \epsilon' C_{1U_{pf}(10)} + A C_{2O_{sd}(6)} + A' C_{2O_{pf}(6)} + B C_{2O_{spdf}(6)} + C C_{2O_{pdf}(5)} + D C_{2O_{pdf}(3)}. \tag{3.2}$$

The wave function can be written as

$$|\psi(L^\pi)\rangle = |N\ n_{sd}\ (\sigma_{sd},0,0)_6,\ n_{pf}\ (\sigma_{(pf)1},\sigma_{(pf)2},\sigma_{(pf)3})_6;\ (\sigma_1,\sigma_2,\sigma_3)_6\ (\nu_1,\nu_2)_5\ \alpha\ L\rangle \tag{3.3}$$

$$O_{sd}(6) \qquad O_{pf}(6) \qquad O_{spdf}(6)\ \ O_{dpf}(5)\ \ O_{dpf}(3)$$

in which α is the additional quantum number. They can be decided by the branching rules in this group chain.

The branching rules of the reductions $U_{spdf}(16) \supset U_{sd}(6) \otimes U_{pf}(10)$ and $O_{pdf}(5) \supset O_{pdf}(3)$ in this group chain have also been discussed in section 2. The other branching rules are shown in the following.

(1) $U_{sd}(6) \supset O_{sd}(6)$

This reduction has been detailed in sd IBM[1,2]. The result is

$$[n_{sd}]_6 = \sum \oplus(\sigma_{sd})_6 \qquad \sigma_{sd} = n_{sd}, n_{sd}-2, n_{sd}-4, \cdots 0 \text{ or } 1. \tag{3.4}$$

(2) $U_{pf}(10) \supset O_{pf}(6)$

This reduction has ever been discussed in refs.[8]and [12]. The branching rule is

$$[n_{pf}]_{10} = \sum_{\alpha\beta\gamma} \oplus(\alpha-2\beta, \alpha-2\beta-2\gamma, \alpha-4\beta-2\gamma)_6 \tag{3.5}$$

where $\alpha = n_{pf}, n_{pf}-4, n_{pf}-8, \cdots$, and $\alpha-2\beta \geq \alpha-2\beta-2\gamma \geq |\alpha-4\beta-2\gamma| \geq 0$. For the lowest excited p,f boson states, we have

$$\begin{aligned} [1]_{10} &= (1,\ 1,\ 1)_6, \\ [2]_{10} &= (2,\ 2,\ 2)_6 \oplus (2,\ 0,\ 0)_6, \\ [3]_{10} &= (3,\ 3,\ 3)_6 \oplus (3,\ 1,\ 1)_6 \oplus (1, 1, -1)_6. \end{aligned} \tag{3.6}$$

(3) $O_{sd}(6) \otimes O_{pf}(6) \supset O_{spdf}(6)$

This reduction can be realized with the Young tableaux techneque or Schur function method. For the lower excited p,f boson states, the branching rules are

$$\begin{aligned} n_{pf}=1, \quad & (\sigma_{sd},\ 0,\ 0)_6 \otimes (1,\ 1,\ 1)_6 = (\sigma_{sd}+1,\ 1,\ 1)_6 \oplus (\sigma_{sd},\ 1,\ 0)_6 \oplus (\sigma_{sd}-1,\ 1,\ -1)_6 \\ n_{pf}=2, \quad & (\sigma_{sd},\ 0,\ 0)_6 \otimes (2,\ 2,\ 2)_6 = (\sigma_{sd}+2,\ 2,\ 2)_6 \oplus (\sigma_{sd}+1,\ 2,\ 1)_6 \oplus (\sigma_{sd},\ 2,\ 0)_6 \\ & \oplus (\sigma_{sd}-1,\ 2,\ -1)_6 \oplus (\sigma_{sd}-2,\ 2,\ -2)_6 \\ & (\sigma_{sd},\ 0,\ 0)_6 \otimes (2,\ 0,\ 0)_6 \\ = & \begin{cases} (2,\ 0,\ 0)_6, & (\sigma_{sd}=0); \\ (3,\ 0,\ 0)_6 \oplus (2,\ 1,\ 0)_6 \oplus (1,\ 0,\ 0)_6, & (\sigma_{sd}=1); \\ (\sigma_{sd}-2,\ 0,\ 0)_6 \oplus (\sigma_{sd},\ 0,\ 0)_6 \oplus (\sigma_{sd}+2,\ 0,\ 0)_6 & \\ \quad (\sigma_{sd}-1,\ 1,\ 0)_6 \oplus (\sigma_{sd}+1,\ 1,\ 0)_6 \oplus (\sigma_{sd},\ 2,\ 0)_6, & (\sigma_{sd} \geq 2). \end{cases} \end{aligned} \tag{3.7}$$

and in general

$$(\sigma_{sd},\ 0,\ 0)_6 \otimes (l,\ l,\ l)_6 = \sum_{j=0}^{k} \oplus(\sigma_{sd}+l-j,\ l,\ l-j)_6 \qquad (k = min(2l, \sigma_{sd})). \tag{3.8}$$

(4) $O_{spdf}(6) \supset O_{pdf}(5)$

The branching rules of this reduction can be obtained directly with the Gel'fand-Zetlin rule[23]. It can be expressed as

$$(\sigma_1,\ \sigma_2,\ \sigma_3)_6 = \sum_{\substack{\sigma_2 \leq \nu_1 \leq \sigma_1 \\ \sigma_3 \leq \nu_2 \leq \sigma_2}} \oplus(\nu_1,\ \nu_2)_5 \tag{3.9}$$

The energy of the state L can be expressed as

$$E(L^{\pi}) = E_0 + \epsilon n_{sd} + \epsilon^{'} n_{pf} + A\sigma_{sd}(\sigma_{sd}+4) \\ +A^{'}[\sigma_{(pf)1}(\sigma_{(pf)1}+4) + \sigma_{(pf)2}(\sigma_{(pf)2}+2) + \sigma^2_{(pf)3}] \\ +B[\sigma_1(\sigma_1+4) + \sigma_2(\sigma_2+2) + \sigma_3^2] + C[\nu_1(\nu_1+3) + \nu_2(\nu_2+1)] + DL(L+1). \tag{3.10}$$

where

$$\pi = \begin{cases} +, & n_{pf} = even; \\ -, & n_{pf} = odd. \end{cases}$$

The typical energy spectrum for the system N=3 is shown in figure 2.

The dynamical symmetry Hamiltonian of the limits shown as the second of eq.(3.1) can be written as

$$H = \epsilon C_{1U_{spdf}(16)} + AC_{2SU^{(a)}_{spdf}(4)\otimes SU^{(b)}_{spdf}(4)} + BC_{2O_{spdf}(6)} + CC_{2O_{pdf}(5)} + DC_{2O_{pdf}(3)}. \tag{3.11}$$

The wave function can be written as

$$|\psi(L^{\pi})\rangle = |N\ [n_1,n_2,n_3]_4\ (\sigma_1,\sigma_2,\sigma_3)_6\ (\nu_1,\nu_2)_5\ \alpha \quad L\rangle \tag{3.12}$$

$$SU_{spdf}(4) \quad O_{spdf}(6) \quad O_{dpf}(5) \quad O_{dpf}(3)$$

where α is the additional quantum number. Their values can be obtained by the following branching rules and those momentioned above.

(1) $U_{spdf}(16) \supset SU_{spdf}(4) \otimes SU_{spdf}(4)$

This reduction has been discussed in refs [5] and [12]. For the IRRP [N] of $U_{spdf}(16)$, the branching rule is

$$[N]_{16} = {}^{'}\sum_{n_1,n_2,n_3} \oplus [n_1,n_2,n_3]_4 \otimes [n_1,n_2,n_3]_4 \tag{3.13}$$

in which $n_1 \geq n_2 \geq n_3 \geq 0$, $n_1+n_2+n_3 = N-4k$, $k = 0,1,2,\cdots,[N/4]$.

(2) $SU_{spdf}(4) \otimes SU_{spdf}(4) \supset O_{spdf}(6)$

Considering the isomorphous relation of $SU(4)$ and $O(6)$, this reduction can be realized by the reduction of $SU_{spdf}(4) \otimes SU_{spdf}(4) \supset SU_{spdf}(4)$, of which the branching rule can be determined with the Young tableaux techneque or Schur function method. Then, with the following relations we can get the IRRPs $(\sigma_1,\sigma_2,\sigma_3)$ of $O_{spdf}(6)$ from the IRRP $[n_1,n_2,n_3]$ of $SU_{spdf}(4)$

$$\sigma_1 = \tfrac{1}{2}(n_1+n_2-n_3)$$

$$\sigma_2 = \tfrac{1}{2}(n_1-n_2+n_3) \tag{3.14}$$

$$\sigma_3 = \tfrac{1}{2}(n_1-n_2-n_3)$$

The energy of the state L with this symmetry can be expressed as

$$E(L^{\pi}) = E_0 + \epsilon N + A\tfrac{1}{4}[3(n_1^2+n_2^2+n_3^2) - 2(n_1n_2+n_2n_3+n_3n_1) + 4(3n_1+n_2-n_3)] \\ +B[\sigma_1(\sigma_1+4) + \sigma_2(\sigma_2+2) + \sigma_3^2] + C[\nu_1(\nu_1+3) + \nu_2(\nu_2+1)] + DL(L+1). \tag{3.15}$$

4 The $SU(3)$ Limit

There is only one group chain on the coupling level $SU_{spdf}(3)$, whose Hamiltonian keeps the parity preserved. It can be written as

$$U_{spdf}(16) \supset U_{sd}(6) \otimes U_{pf}(10) \supset SU_{sd}(3) \otimes SU_{pf}(3) \supset SU_{spdf}(3) \supset O_{pdf}(3) \qquad (4.1)$$

The dynamical symmetry represented by this group chain is the so called $SU(3)$ limit. Its dynamical symmetry Hamiltonian can be expressed as

$$H = \epsilon C_{1U_{sd}(6)} + \epsilon^{'} C_{1U_{pf}(10)} + AC_{2SU_{sd}(3)} + A^{'} C_{2SU_{pf}(3)} + BC_{2SU_{spdf}(3)} + DC_{2O_{pdf}(3)}. \quad (4.2)$$

The wave function can be labelled by the IRRPs of the groups in the chain, and it can be written as

$$|\psi(L^{\pi})\rangle = |N\, n_{sd}\,(\lambda_{sd},\ \mu_{sd})_3\, n_{pf}\,(\lambda_{pf},\ \mu_{pf})_3;\ (\lambda,\ \mu)_3 \quad K \quad L\rangle \qquad (4.3)$$

$$SU_{sd}(3) \qquad SU_{pf}(3) \quad SU_{spdf}(3) \quad O_{dpf}(3)$$

where K is the additional quantum number to differate the same L in the (λ, μ). The reduction rules that have not appeared previously are the followings.

$(1) U_{sd}(6) \supset SU_{sd}(3)$

This reduction has been solved completely in sd IBM[1,2]. The branching rule is

$$[n_{sd}]_6 = \sum_{p,q} \oplus (2n_{sd} - 4p - 6q, 2p)_3. \qquad (4.4)$$

i.e.,

$$\begin{aligned}(\lambda_{sd}, \mu_{sd})_3 = {} & (2n_{sd}, 0), (2n_{sd} - 4, 2), (2n_{sd} - 8, 4), \cdots, \\ & (2n_{sd} - 6, 0), (2n_{sd} - 10, 2), (2n_{sd} - 14, 4), \cdots, \\ & \cdots\cdots\end{aligned} \qquad (4.5)$$

$(2) U_{pf}(10) \supset SU_{pf}(3)$

This reduction is rather complicated, but it can be realized with the usual Elliott method[25]. For the lower excited p,f boson states, refs.[5] and [8] have given the branching rules

$$\begin{aligned}&[1]_{10} = (3,0) \\ &[2]_{10} = (6,0), (2,2) \\ &[3]_{10} = (9,0), (5,2), (3,3), (0,3), (3,0) \\ &[4]_{10} = (12,0), (8,2), (6,3), (6,0), (3,3), (4,4), (4,1), (0,6), (2,2), (0,0) \\ &\qquad\qquad \cdots\cdots\cdots\cdots \\ &[n_{pf}]_{10} = (3n_{pf}, 0), (3n_{pf} - 4, 2), (3n_{pf} - 8, 4), \cdots, \\ &\qquad\qquad (3n_{pf} - 6, 0), (3n_{pf} - 10, 2), \cdots, \\ &\qquad\qquad (3n_{pf} - 6, 3), (3n_{pf} - 9, 3), \cdots, \\ &\qquad\qquad \cdots\cdots\cdots\cdots\end{aligned} \qquad (4.6)$$

(3)$SU_{sd}(3) \otimes Su_{pf}(3) \supset SU_{spdf}(3)$

This reduction can be realized by means of the Young tableaux technique or the Schur function method. The branching rule can be analytically expressed as[24]

$$(\lambda_1, \mu_1) \otimes (\lambda_2, \mu_2) = \sum_{p,q} \oplus K(\lambda_1, \mu_1, \lambda_2, \mu_2, p, q)(\lambda_1 + \lambda_2 - p - 2q, \mu_1 + \mu_2 - p + q). \quad (4.7)$$

where $K(\lambda_1, \mu_1, \lambda_2, \mu_2, p, q)$ should satisfy the following relations

$$\begin{aligned} K(\lambda_1, \mu_1, \lambda_2, \mu_2, p, q) &= K(\mu_1, \lambda_1, \mu_2, \lambda_2, p - q, -q) \\ K(\lambda_1, \mu_1, \lambda_2, \mu_2, p, q) &= K(\lambda_2, \mu_2, \lambda_1, \mu_1, p, q) \end{aligned} \quad (4.8)$$

Then taking $\mu_1 = min(\lambda_1, \mu_1, \lambda_2, \mu_2)$, the values of $K(\lambda_1, \mu_1, \lambda_2, \mu_2, p, q)$ can be listed in the following table.

Table 1. The Values of $K(\lambda_1\ \mu_1\ \lambda_2\ \mu_2\ p\ q)$

p	p_0	p_0+1	$\cdots$	p_1	p_1+1	$\cdots$	p_2	p_2+1	$\cdots$	$p_1-p_2-p_0$
K	1	2	$\cdots$	p_1-p_0+1	p_1-p_0+1	$\cdots$	p_1-p_0+1	p_1-p_0	$\cdots$	1

in which

$$\begin{aligned} &p_0 = -min(0, q), \qquad q = -\mu_1, -\mu_1 + 1, \cdots, 0, \cdots, min(\lambda_1, \lambda_2) \\ &p_1 = min(a,\ b), \qquad p_2 = max(a,\ b), \\ &a = min(\mu_2,\ \lambda_1 - q), \quad b = min(\mu_1,\ \lambda_2 - q). \end{aligned}$$

(4)$SU_{spdf}(3) \supset O_{pdf}(3)$

This reduction has also been solved[24]. For the IRRP (λ, μ) of $SU_{spdf}(3)$, the values of L are

$$L = \begin{cases} K, K+1, K+2, \cdots, K + max(\lambda, \mu), & (K \neq 0); \\ max(\lambda, \mu), max(\lambda, \mu) - 2, max(\lambda, \mu) - 4, \cdots, \begin{cases} 0 & (\mu = even) \\ 1 & (\mu = odd) \end{cases} & (K = 0). \end{cases} \quad (4.9)$$

where $K = min(\lambda, \mu), min(\lambda, \mu) - 2, \cdots, 1$ or 0.

The energy of the state L can be experssed as

$$\begin{aligned} E(L^\pi) = {} & E_0 + \epsilon n_{sd} + \epsilon' n_{pf} + A[\lambda_{sd}^2 + \lambda_{sd}\mu_{sd} + \mu_{sd}^2 + 3(\lambda_{sd} + \mu_{sd})] \\ & + A'[\lambda_{pf}^2 + \lambda_{pf}\mu_{pf} + \mu_{pf}^2 + 3(\lambda_{pf} + \mu_{pf})] + B[\lambda^2 + \lambda\mu + \mu^2 + 3(\lambda + \mu)] \\ & + DL(L+1), \end{aligned} \quad (4.10)$$

where

$$\pi = \begin{cases} +, & n_{pf} = even; \\ -, & n_{pf} = odd. \end{cases}$$

The typical energy spectrum is shown in figure 3.

5 The $O(4)$ Limit

There are three group chains on coupling level $O_{spdf}(4)$. They are

$$\begin{array}{l} U_{spdf}(16) \supset SU_{spdf}(4) \otimes SU_{spdf}(4) \supset SP^{(a)}_{spdf}(4) \otimes SP^{(b)}_{spdf}(4) \supset O_{spdf}(4) \supset O_{pdf}(3) \\ U_{spdf}(16) \supset O_{spdf}(16) \supset SP^{(a)}_{spdf}(4) \otimes SP^{(b)}_{spdf}(4) \supset O_{spdf}(4) \supset O_{pdf}(3) \\ U_{spdf}(16) \supset O_{spdf}(10) \supset SP^{(a)}_{spdf}(4) \otimes SP^{(b)}_{spdf}(4) \supset O_{spdf}(4) \supset O_{pdf}(3) \end{array} \quad (5.1)$$

We can symbolize them as $O(4)(I)$ limit, $O(4)(II)$ limit and $O(4)(III)$ limit respectively.

For the $O(4)(I)$ limit, the dynamical symmetry Hamiltonian can be expressed as

$$H = \epsilon C_{1U_{spdf}(16)} + AC_{2SU^{(a)}_{spdf}(4)\otimes SU^{(b)}_{spdf}(4)} + BC_{2SP^{(a)}_{spdf}(4)\otimes SP^{(b)}_{spdf}(4)} + CC_{2O_{spdf}(4)} + DC_{2O_{pdf}(3)}. \quad (5.2)$$

The wave function of the system can be written as

$$|\psi(L^\pi)\rangle = |N\ [n_1,n_2,n_3]_4\ \langle l^{(a)}_1, l^{(a)}_2\rangle_4\ \langle l^{(b)}_1, l^{(b)}_2\rangle_4\ \alpha\ (\omega_1,\omega_2)_4\quad L\ \rangle \quad (5.3)$$

$$SU_{spdf}(4)\quad SP^{(a)}_{spdf}(4)\quad SP^{(b)}_{spdf}(4)\quad O_{spdf}(4)\quad O_{dpf}(3)$$

where α is the additional quantum number to distinguish the same (ω_1,ω_2) belonging to the same $\langle l^{(a)}_1, l^{(a)}_2\rangle \otimes \langle l^{(b)}_1, l^{(b)}_2\rangle$.

The branching rules that have not discussed in previous sections are given in the following.

(1)$SU_{spdf}(4) \otimes SU_{spdf}(4) \supset SP_{spdf}(4) \otimes SU_{spdf}(4)$

This reduction can be easily realized by means of the Young tableaux technique or Schur function method. For the IRRP $[n_1,n_2,n_3]$ of $SU_{spdf}(4)$, the branching rule is

$$[n_1,n_2,n_3]_4 = \sum_i (n_1-i, n_2-n_3-i)_4. \quad (5.4)$$

where $i = 0,1,2,\cdots,min(n_3, n_1-n_2)$

(2)$SP_{spdf}(4) \otimes SP_{spdf}(4) \supset O_{spdf}(4)$

This reduction is, in fact, the reduction $SP_{spdf}(4) \otimes SP_{spdf}(4) \supset SU_{spdf}(2) \otimes SU_{spdf}(2) \approx O_{spdf}(4)$, in which reduction $SP_{spdf}(4) \supset SU_{spdf}(2)$ has been solved[14-19]. Then the IRRP (ω_1,ω_2) of $O_{spdf}(4)$ can be decided with the relations $\omega_1 = j_a + j_b$, $\omega_2 = |j_a - j_b|$, where $(j_a) \otimes (j_b)$ is the IRRP of $SU_{spdf}(2) \otimes SU_{spdf}(2)$.

(3)$O_{spdf}(4) \supset O_{pdf}(3)$

This reduction is quite easy. For the IRRP $\langle \omega_1,\omega_2\rangle$ of $O_{spdf}(4)$, the branching rule is

$$(\omega_1,\ \omega_2)_4 = \sum \oplus L \quad (5.5)$$

where $L = \omega_2, (\omega_2+1), (\omega_2+2), \cdots, \omega_1$.

Then the energy of the state with $O(4)(I)$ symmetry can be expressed as

$$E(L^\pi) = E_0 + \epsilon N + A\tfrac{1}{2}[3(n_1^2+n_2^2+n_3^2) - 2(n_1n_2+n_2n_3+n_3n_1) + 4(3n_1+n_2-n_3)] + 2B[l_1(l_1+4) + l_2(l_2+2)] + C[\omega_1(\omega_1+2) + \omega_2^2] + DL(L+1). \quad (5.6)$$

For the $O(4)(II)$ limit, The dynamical symmetry Hamiltonian is

$$H = \epsilon C_{1U_{spdf}(16)} + AC_{2O_{spdf}(16)} + BC_{2SP^{(a)}_{spdf}(4)\otimes SP^{(b)}_{spdf}(4)} + CC_{2O_{spdf}(4)} + DC_{2O_{pdf}(3)}. \quad (5.7)$$

The wave function can be written as

$$|\psi(L^\pi)\rangle = |N \quad (\nu)_{16} \quad \langle l_1^{(a)}, l_2^{(a)}\rangle_4 \ \langle l_1^{(b)}, l_2^{(b)}\rangle_4 \ \alpha \ (\omega_1,\omega_2)_4 \quad L \ \rangle \quad (5.8)$$

$$O_{spdf}(16) \ SP^{(a)}_{spdf}(4) \ SP^{(b)}_{spdf}(4) \quad O_{spdf}(4) \ O_{dpf}(3)$$

in which α is the additional quantum number.

Except for the reduction $U_{spdf}(16) \supset O_{spdf}(16)$ and $O_{spdf}(16) \supset SP_{spdf}(4) \otimes SP_{spdf}(4)$, the branching rules in this group chain have been discussed. The reduction $U_{spdf}(16) \supset O_{spdf}(16)$ is trivial. For the IRRP $[N]$ of $U_{spdf}(16)$, we have

$$[N]_{16} = \sum \oplus (\nu)_{16}. \quad (5.9)$$

where $\nu = N, N-2, N-4, \cdots, 0 \ or \ 1$.

The reduction $O_{spdf}(16) \supset SP_{spdf}(4) \otimes SP_{spdf}(16)$ can be realized in the light of the reductions $U_{spdf}(16) \supset O_{spdf}(16)$ and $U_{spdf}(16) \supset SU_{spdf}(4) \otimes SU_{spdf}(4) \supset SP_{spdf}(4) \otimes SP_{spdf}(4)$. The result is

$$\{(\nu)\} = \{[\nu]\} - \{[\nu-2]\}. \quad (5.10)$$

where $\{(\nu)\}$ is the IRRPs of $SP_{spdf}(4) \otimes SP_{spdf}(4)$ belonging to the IRRP (ν) of $O_{spdf}(16)$. $\{[\nu]\}$ refers to the IRRPs of $SP(4) \otimes SP(4)$ belonging to the IRRP $[\nu]$ of $U_{spdf}(16)$.

The energy of the state L with dynamical symmetry $O(4)(II)$ can be expressed as

$$E(L^\pi) = E_0 + \epsilon N + A\nu(\nu+14) + 2B[l_1(l_1+4) + l_2(l_2+2)] + C[\omega_1(\omega_1+2) + \omega_2^2] + DL(L+1). \quad (5.11)$$

For the $O(4)(III)$ limit, the dynamical symmetry Hamiltonian can be written as

$$H = \epsilon C_{1U_{spdf}(16)} + AC_{2O_{spdf}(10)} + B[C_{2SP^{(a)}_{spdf}(4)} + C_{2SP^{(b)}_{spdf}(4)}] + CC_{2O_{spdf}(4)} + DC_{2O_{pdf}(3)}. \quad (5.12)$$

The wave function can be written as

$$|\psi(L^\pi)\rangle = |N \ (m_1,m_2,m_3,m_4,m_5)_{10} \ \langle l_1^{(a)}, l_2^{(a)}\rangle_4 \ \langle l_1^{(b)}, l_2^{(b)}\rangle_4 \ \alpha \ (\omega_1,\omega_2)_4 \quad L \ \rangle \quad (5.13)$$

$$O_{spdf}(10) \qquad SP^{(a)}_{spdf}(4) \ SP^{(b)}_{spdf}(4) \quad O_{spdf}(4) \ O_{dpf}(3)$$

where α is the additional quantum number. The reduction of the IRRPs in this chain that should be solved is only $O_{spdf}(10) \supset SP_{spdf}(4) \otimes SP_{spdf}(4)$. The results are

$$(a) \qquad (N,\ 0,\ 0,\ 0,\ 0)_{10} = \sum_{l_1,l_2} \oplus \langle 0, l_1\rangle_4 \otimes \langle 0, l_2\rangle_4. \quad (5.14)$$

where

$$l_1 = k, k-2, k-4, \cdots, 1 \ or \ 0; l_2 = N-k; k = N, N-1, N-2, \cdots, 0.$$

$$(b) \qquad (N,\ N,\ N,\ N,\ N)_{10} = \sum_{l_1,l_2} \oplus \langle l_1, l_2 \rangle_4 \otimes \langle l_1, l_2 \rangle_4. \tag{5.15}$$

where

$$l_1 = N, N-2, N-4, \cdots, 1 \text{ or } 0; l_2 = 0, 1, 2, \cdots, [l_1/2].$$

$$(c) \qquad (N+1,\ 1,\ 1,\ 1,\ 1)_{10} = \sum_{l_1,l_2} \oplus \langle 1, l_1 \rangle_4 \otimes \langle 1, l_2 \rangle_4. \tag{5.16}$$

in which

$$l_1 = N - 2i - l_2 - k; l_2 = 0, 1, 2, \cdots, N - 2i; i = 0, 1, 2, \cdots, [N/2]; k = 0, 1.$$

The energy of the system can be given as

$$\begin{aligned} E(L^\pi) = E_0 &+ \epsilon N + A[m_1(m_1+8) + m_2(m_2+6) + m_3(m_3+4) + m_4(m_4+2) \\ &+ m_5 m_5] + 2B[l_1^{(a)}(l_1^{(a)}+4) + l_2^{(a)}(l_2^{(a)}+2) + l_1^{(b)}(l_1^{(b)}+4) + l_2^{(b)}(l_2^{(b)}+2)] \\ &+ C[\omega_1(\omega_1+2) + \omega_2^2] + DL(L+1). \end{aligned} \tag{5.17}$$

In $O(4)$ limit, the parity of the system is determined by the IRRP of $O_{spdf}(4)$. For the state with IRRP (ω_1, ω_2), if $\omega_2 = 0$, the energy level sequence is $0^+, 1^-, 2^+, 3^-, \cdots$. If $\omega_2 \neq 0$, the states are parity doublets, i.e., the energy sequence is $\omega_2^{\pm}, (\omega_2+1)^{\mp}$, $(\omega_2+2)^{\pm}, \cdots$ (for even ω_2) or $\omega_2^{\mp}, (\omega_2+1)^{\pm}, (\omega_2+2)^{\mp}, \cdots$ (for odd ω_2).

Form eqs.(6.6), (6.11), (6.17) we know that the energy of the state with $O(4)$ symmetry can be simplified as

$$E(L^\pi) = E_0 + C[\omega_1(\omega_1+2) + \omega_2^2] + DL(L+1). \tag{5.18}$$

The typical energy spectrum is shown in figure 4.

6 Concluding Remark

In this paper, the possible dynamical symmetries of the spdf Interacting Boson Model have been discussed. They are classified into 7 kinds of dynamical symmetry limit, of which the $SU_{pdf}(5)$, $O_{spdf}(6)$, $SU_{spdf}(3)$ and $O_{spdf}(4)$ limits are investigated in detail. The branching rules of reductions in the group chains, the dynamical symmetry Hamiltonians and the energy spectra of the limits are given. From figures 1-4 of the typical energy spectra, we can see that the $SU(5)$ limit includes some characteristics of rotation besides that of vibration of the sd IBM. The $O(4)$ limit is analogous to the motion of molecular vibration-rotation. The $SU(3)$ and $O(6)$ limits remain the aspects of rotation and $\gamma-$unstable motion respectively, and give much more energy bands.

These discussions on the limits of the spdf Interacting Boson Model are much helpful for us to understand the symmetries of the octupole and quadrupole deformation.

Moreover the phase transition between different kinds of collective motion can be investigated by considering the changing between the corresponding dynamical symmetry limits. Otherwise, real nuclei do not have one of these so strong symmetries, but the mixture of some of these symmetries. To describe the nuclear collective motion with some quadrupole and octupole deformation, it is necesary to perform numerical calculation. To this end we set up a computer code SPDFBOS[26]. It has been checked by means of the group chain method[27] with respect to the $SU(5)$, $O(6)$, $SU(3)$ and $O(4)$ limits. With this code the nuclei with total boson number $N = n_s + n_d + n_p + n_f = 15$ can be described. The application results will be presented elsewhere.

This work is partly supported by the National Natural Science Foundation of China. Helpful discussions with Professor Qizhi Han and Professor Mei Zhang are acknowledged with thanks.

REFERENCES

[1]A. Arima and F. Iachello,Ann. Phys. (N. Y.) **99**, 253(1976); ibid,111, 201(1978); ibid, 123, 468(1979).
[2] F.Iachello and A Arima, The Interacting Boson Model(Cambridge: Cambridge University Press, 1987).
[3] W. Nazarewicz, Nucl. Phys. **A520**, 333c(1990) and refs. therein.
[4] C. S. Han, D. S. Chuu, S. T. Hsieh and H. C. Chiang, Phys. Lett. **163B**, 295(1985).
[5] J. Engel and F. Iachello, Phys. Rev. Lett. **54**, 1126(1985); ibid, Nucl. Phys. **A472**, 61(1987).
[6] T. Otsuka, Phys. Lett. **182B**, 256(1986).
[7] F. Catara, M. Sambataro, A. Insolia and A. Vitturi, Phys. Lett. **180B**, 1(1986).
[8] H. Z. Sun, M. Zhang and Q. Z. Han, Chinese J. Nucl. Phys. **13**, 121(1991).
[9] T. Otsuka and M. Sugita, Phys. Lett. **209B**, 140(1988).
[10] D. Kusnezov and F. Iachello, Phys. Lett. **209B**, 420(1988).
[11] E. G. Nadjakov and I. N. Mikhailov, J. Phys. **G.13**,1221(1987).
[12] D. Kusnezov, J. Phys. **A22**, 4271(1989); ibid, **A23**, 5673(1990).
[13] D. E. Littlewood, Theory of Group Characters(2nd ed.)(Oxford University Press, 1940).
[14] Q. Z. Han and H. Z. Sun, Group Theory(Peking University Press, 1987).
[15] M. Hamermesh, Group Theory and its Application to Physical Problems (Reading MA: Addison Wesley, 1962).
[16] B. R. Judd, Operator techniques in Atomic Spectropy(New York: McGraw-Hill, 1963).
[17] B. G. Wybourne, Classical Groups for Physicists(New York: Wiley, 1974).
[18] B. G. Wybourne, Provate Communication.

[19] B. G. Wybourne, Symmetry Principles and Atomic Spectroscopy(New York: Wiley, 1970).
[20] R. Gaskell, A. Peccia and R. T. Sharp, J. Math. Phys. **19**, 727(1978).
[21] J. J. Wang and H. Z. Sun, High Energy Phys. Nucl. Phys. **14** (1990), 842; H. Z. Sun, J. J. Wang and Y. X. Liu, to be published.
[22] Y. X. Liu, Chinese J. Comput. Phys. **9**(1992), 163
[23] E. M. Loebl, Group Theory and its Applications(New York: Academic, 1971), Vol. 1;A. O. Barut and R. Raczka, Theory of Group Representations and Applications(Warszawa; Polish Scientific,1980).
[24] H. Z. Sun, Q. Z. Han, X. J. Chen and M. Zhang, Scientia Sinica, A9(1982),818.
[25] J. P. Elliott, Proc. Roy. Soc. **A245**,129(1958);idib;562(1958).
[26] Y. X. Liu, H. Z. Sun and E. G. Zhao, to be published.
[27] G. L. Long, Ph. D. Thesis(Tsinghua University, 1987).

Figure Caption:

Figure 1. The Energy Spectrum of $SU_{pdf}(5)$ Limit($N = 3$, $\epsilon = 0.02MeV$, $\epsilon^{'} = 0.8MeV$, $A = A^{'} = 0$, $B = 0.02MeV$, $C = 0.01MeV$, $D = 0.08MeV$).

Figure 2. The Energy Spectrum of $O_{spdf}(6)$ Limit($N = 3$, $\epsilon = \epsilon^{'} = A = A^{'} = 0$, $B = -0.01MeV$, $C = 0.015MeV$, $D = 0.005MeV$).

Figure 3. The Energy Spectrum of $SU_{spdf}(3)$ Limit($N = 3$, $\epsilon = 0$, $\epsilon^{'} = -0.6934MeV$, $A = A^{'} = 0$, $B = -0.02MeV$, $D = 0.006MeV$).

Figure 4. The Energy Spectrum of $O_{spdf}(4)$ Limit($N = 4$, $C = -0.005MeV$, $D = 0.006MeV$).

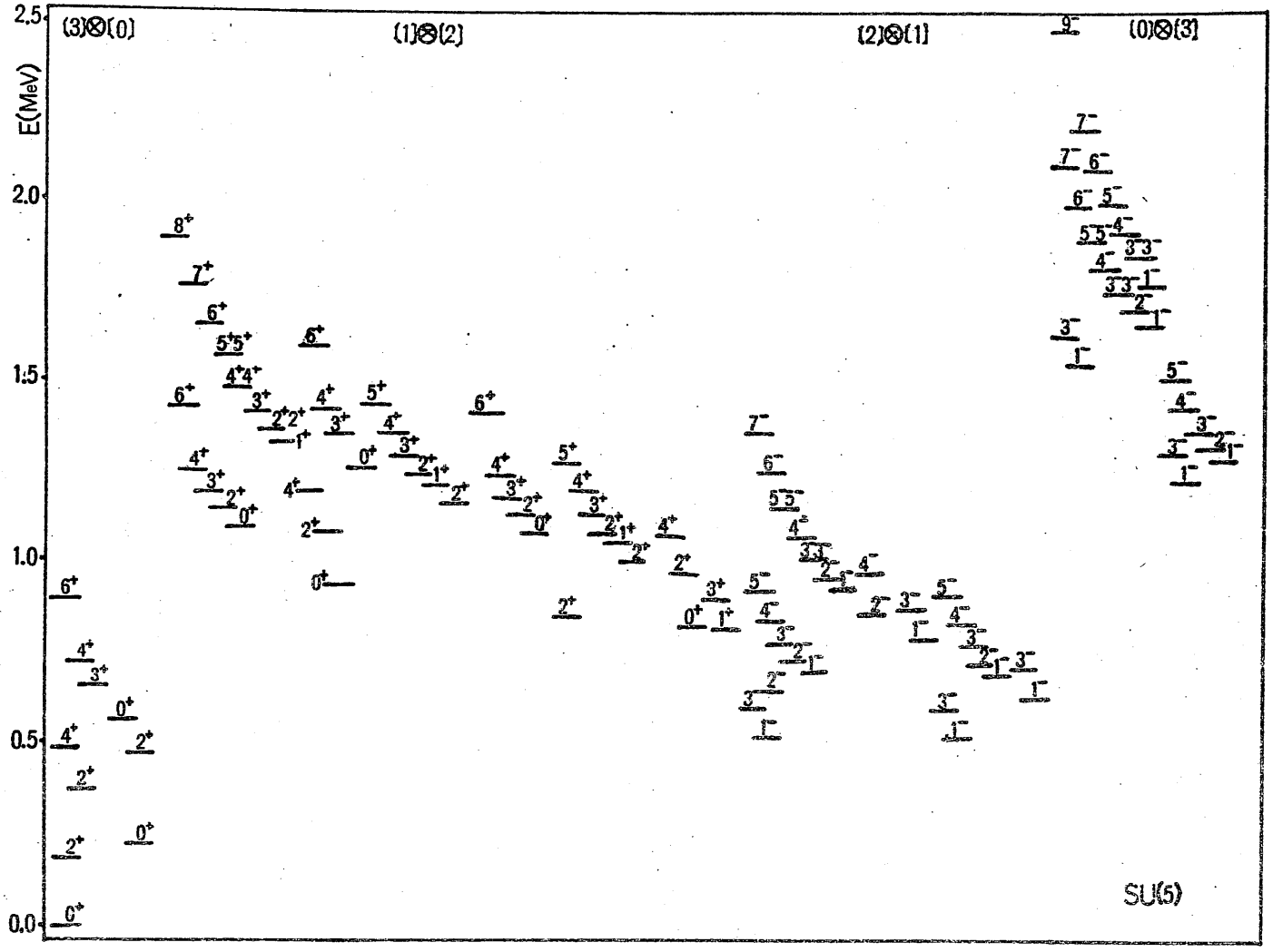
(3)⊗(0)
(1)⊗(2)
(2)⊗(1)
(0)⊗(3)
E(MeV)
2.5
2.0
1.5
1.0
0.5
0.0
SU(5)

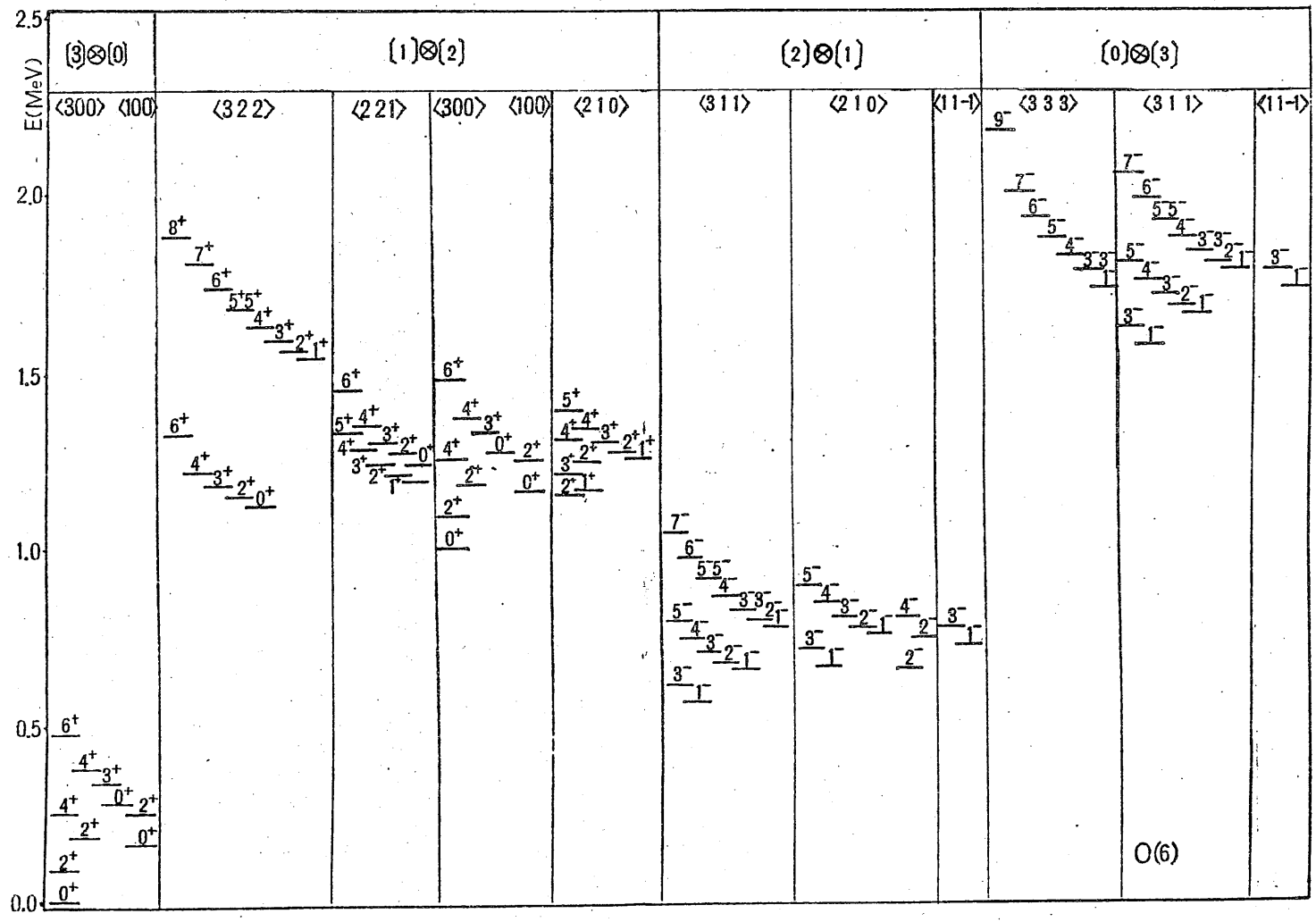
E(MeV)
2.5
2.0
1.5
1.0
0.5
0.0
[3]⊗[0]
[1]⊗[2]
[2]⊗[1]
[0]⊗[3]
⟨300⟩
⟨100⟩
⟨322⟩
⟨221⟩
⟨300⟩
⟨100⟩
⟨210⟩
⟨311⟩
⟨210⟩
⟨11-1⟩
⟨333⟩
⟨311⟩
⟨11-1⟩
O(6)

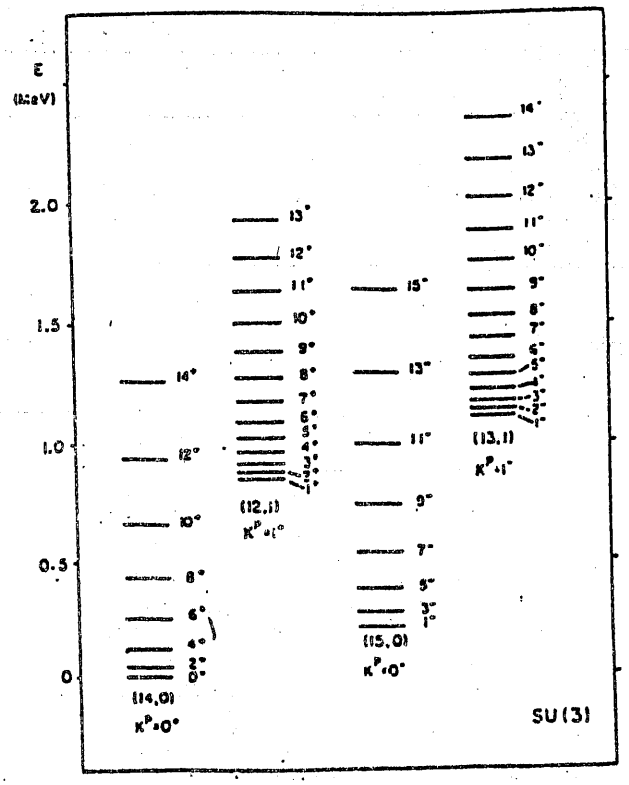
E
(MeV)
2.0
1.5
1.0
0.5
0
(14,0)
(12,1)
(15,0)
(13,1)
SU(3)

Fig. 3.

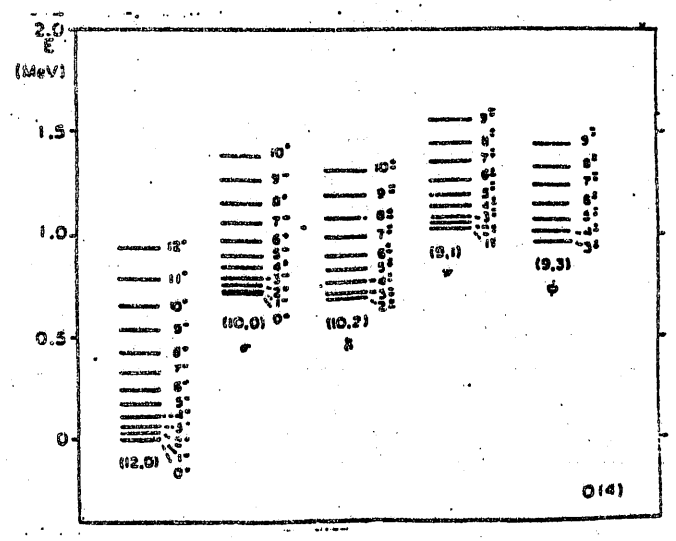
E
(MeV)
2.0
1.5
1.0
0.5
0
(12,0)
(10,0)
(10,2)
(9,1)
(9,3)
O(4)

Fig. 4.

Diadabolic neutron-pair transfer in isotopic chain of Hf-nuclei

J. Meng[a,b], J. Y. Zeng[a,b,c], and E. G. Zhao[a,b]

[a]CCAST(World Laboratory), P. O. Box 8730, Beijing 100080, China,

[b]Institute of Theoretical Physics, Chinese Academy of Science,

P. O. Box 2735, Beijing 100080, China *

[c]Department of Physics, Peking University, Beijing 100871, China

December 25, 1992

ABSTRACT

The neutron pair transfer matrix element (diabolic pair transfer) between neighboring even N particle systems (yrast band to yrast band) for isotopic chain of Hf nuclei are calculated by a particle-number-conserving treatment for the eigenvalue problem of the cranked Nilsson Hamiltonian. The results clearly show that sign change (diabolic points) does exist for a neutron pair transfer of ^{168}Hf $\rightarrow$ ^{166}Hf, in contrast to the previous conclusion that no such sign change occurs drawn from the cranked single-j shell model.

PACS numbers: 21.10._k,21.60.Cz,03.65.Bz,21.60.Ev,27.70.+q

1 INTRODUCTION

In Quantum Mechanics it is well known that the wavefunction of a state is determined to a phase factor $e^{-iEt/\hbar}$. However, it has been proved by Berry in his 1984's article that apart from this dynamical phase, the wavefunction also acquires a non-integrable topological phase when a system is transported adiabatically around a path in parameter space, i. e. , in a cyclic adiabatic process[1]. This phase now usually refered as Berry phase does not vanish in cases the path enclosing a diabolic point (A diabolic point is an exceptional point, in the sense that it violates the no-crossing rule of the Von Neumann and Wigner[2], in parameter space where the interaction between the two energy surfaces with the same symmetry vanishes) and has been generalized to a very abstract definitionin of the manifold of line bundles, as given in the paper of Aharonov and Anandan[3], where the concept of adiabaticity and slow and fast variables is not used. For the past several years, Berry Phase and its generalization have been found to be of interest in a number recent investigations in diverse field of physics, for a review see [4,5].

In Nuclear Physics, especially in the high spin physics, the reaction for the transfer of a pair of identical nucleons coupled to zero angular momentum has been investigated with keen interests recently. As the transfer of a pair of identical nucleons coupled to zero angular momentum to a state in the yrast band (states of the lowest energy for a given angular momentum I) of a neighbouring deformed nucleus can give informations about the pair correlation near the Fermi level, the study of Berry phase in nuclear physics has been an quite active research field during the past several years[6-14]. It was Nikam and Ring who first realized that an oscillating behavior of the pair transfer matrix element as a function of rotational frequency (diabolic pair transfer) is the direct consequence of the Berry phase[6], which is analogous to the DC-Josephson effect in superconductor in the presence of a magnetic field. It was also noted that the oscillating behavior of the pair transfer amplitude is closely connected with the oscillating behavior of the backbending[15]. So far, however, the occurrence of this phenomenon has only been predicted theoret-

ically. Even worse, for one side, without exception, all the calculation are confined to even-neutron even-proton nucleus and no calculations about odd-odd or even-odd nucleus are available. For the other, experimentally, all the physical quantities are only defined on the discrete points on lattice in the particle number and angular momentum (N, I) space. However, most of the above results have been demonstrated within the framework of cranked Hatree-Fock-Bogoliubov (HFB) approach. For example, in the HFB approximation, the actual discrete quantum numbers, the particle number N and the angular momentum I, are respectively replaced by the continuous parameters, the chemical potential λ and the angular frequency ω. The continuous parameters λ and ω are based on semiclassical consideration and are not observables in strict sense[12]. So the crucial problem arises is that the number of nucleons in a nucleus ($\sim 10^2$), particularly, the number of valence nucleons (~ 10) which dominate the features of low-lying excited states, is very limited. Therefore, the serious defects (particle number nonconservation, excessive spurious states, blocking effect, etc.)[16] should be taken into account and the conclusions drawn from the HFB approximation need reexamination. A well-known example[17] is that in all self-consistent solutions to the cranked HFB equation a pairing collapse is always found[18], but calculation with particle-number projection before variation showed that the gap parameter decreases very slowly and no sharp phase transition is found[19]. Similar result was obtained in the exact particle-number-conserving (PNC) treatment for the eigenvalue problem of H'_{CSM}[20]. However, it should be emphasized that *the particle-number projected HFB method (NHFB) is not equivalent to the PNC treatment*, in which the particle-number is stictly conserved from beginning to end. A striking difference can be found in the investigation of the yrast-yrare interaction V. (The particle-number-conserving calculation in ref. [12] seems to be wrong for the reason that for a single-j CSM it showed an ω-independent yrast rounthian (eg. see Fig.1(a) in ref.12) below the first bandcrossing ($\omega < \omega_c$, no Coriolis response) and a sharp bandcrossing between the yrast and yrare bands occurs at $\omega \sim \omega_c$). The exact PNC calculation in the same single-j CSM[14,20]

showed that there only exists yrast bands with strong Coriolis response, because all the particles in a high-j shell have strong Coriolis response and no abrupt exchange of feature between the yrast and yrare bands occurs aroud $\omega \sim \omega_c$.In other words, the yrast-yrare interaction is always strong and no periodic oscillation of V with the degree of shell filling is obtained[20]. In ref. [14], the behaviors of the pair transfer matrix element has been discussed in a cranked single-j shell model using the particle-number-conserving (PNC) method, and no sign change of the pair transfer matrix element occurs for cranked single-j shell in contrast to the previous conclusions. Theoretically and experimentally, much work has to be done in order to gain a better understanding of the Berry phase, backbending and the variation of pair correlation in high spin physics. However, more realistic calculations are absent except the cranking calculation for ^{168}Hf[6,7] and angular momentum projected Tamm Dancoff approximation for Yb- and Hf-nuclei (with unconserved particle number N)[11]. It is not fully clear whether the conclusions drawn from the approximating approach are reliable in the realistic cases. In this paper we will generalize the study of ref. [14] to the isotopic chain of Hf nuclei and address the behavior of the pair transfer matrix element for Hf-nuclei in the cranked shell model with PNC approach.

2 PAIR TRANSFER MATRIX ELEMENT

As usual, the PNC CSM Hamiltonian is expressed as[21]

$$H_{CSM} = H_{sp} + H_{pair} - \omega J_x \tag{1}$$

$$H_{sp} = \sum_{\nu} \varepsilon_\nu a_\nu^+ a_\nu \tag{2}$$

$$H_{pair} = -GP^+P, \quad P^+ = \sum_{\nu>0} a_\nu^+ a_{\bar{\nu}}^+ \tag{3}$$

where H_{sp} is the single particle Hamiltonian and ε_ν the single particle energy, H_{pair} is the pairing interaction with constant pairing strength G ($\Delta = G < P >$ being

the gap parameter), and ωJ_x is the Coriolis interaction with cranking frequency ω about x axis (perpendicular to the symmetry z axis). It should be pointed out that although cranked HFB formalism allows the use of the general result of Berry phase[1] concerning the eigenstates of a Hamiltonian which is function of several continuous parameters (here $H'_{CSM} = H'_{CSM}(\lambda,\omega)$), the PNC cranked formalism does not hinder the appearence of Berry phase[3]. As we are interested in the diabolic pair transfer between the yrast bands of neighbouring Hf nuclei, which is easy to observe experimentally and mainly connected with the neutron bandcrossing, the effect of proton are negelected for the following discussion.

The PNC calculation for ^{166}Hf-^{174}Hf is carried out to illustrate how the pair transfer matrix elements vary with the rotational frequency. It should be emphsized that in the calculation no free parameter is introduced. Since the deformation parameters does not change very much in Hf nuclei we have used fixed parameters $\varepsilon_2 = 0.235$ and $\varepsilon_4 = 0.005$ of ^{168}Hf in the calculation, which are chosen according to the Lund systematics (including the choice of the modified oscillator parameters κ and μ[22]). The reproduced single-particle level is given in Fig. 1, which has been truncated according to $\varepsilon_{below} = 0.40\hbar\omega_0$ and $\varepsilon_{above} = 0.45\hbar\omega_0$ relative to the fermi surface of ^{168}Hf with:

$$\hbar\omega_0(neutron) = 41A^{-1/3}[1 + (N - Z)/3A] \sim 7.78\text{MeV} \qquad (4)$$

According to the truncated single particle level scheme, the numbers of the valence particle for $^{166-174}$Hf are respectively $N = 20 - -28$. The details of the PNC treatment can be found in ref. [16]. The accurate solution to the lowlying eigenstates and eigenenergies of Hf nuclei are obtained by diagonalizing the Hamiltonian H_{CSM} in the truncated many-particle configuration (MPC) space with truncated MPC energy $e_{CE} = 0.40\hbar\omega_0$. For $^{166-174}$Hf the dimensions of the truncated MPC spaces of signature $r = 1$ for neutron systems of ^{166}Hf,^{168}Hf,^{170}Hf,^{172}Hf and ^{174}Hf are 364, 300, 122, 253, and 209, respectively. Consider the quite different character of each large shell, depending on whether they belong to the same large shell, the pairing

interaction strength is reasonably but somewhat arbitrarily chosen as:

$$G = \begin{cases} G_0 & Same\ large\ shell \\ 0.2G_0 \exp[-10^2\omega^2] & Different\ large\ shell \end{cases} \tag{5}$$

with $G_0 = 0.04\hbar\omega_0$. Calculation shows that the conclusions drawn below remain valid for other G values within a reasonable reigon. The lowest nine eigenenergies $E_i/\hbar\omega_0$ [i = 0(yrast),1(yrare),2,...,8] for N = 20,22,...,28 particle system are displayed in Figs. 2 and 3. The first (yrast-yrare) backbending frequencies are about $\omega_c/\hbar\omega_0$ = 0.01,0.03,0.02,0.03 and 0.15 for N = 20,22,24, 26, and 28, respectively. It should be pointed out that the interaction strength between yrast and yrare bands for Hf nuclei

$$V = 1/2\{E_{yrare} - E_{yrast}\}_{\omega=\omega_c} \tag{6}$$

oscillating with different neutron numbers, in contrast with the single-j CSM the interaction strength between yrast and yrare bands there is always strong[14]. For realistic Hf chains cases, in fact, the yrast surface $E_0(N,\omega)$ and yrare surface $E_1(N,\omega)$ in the parameter (N,ω) space may touch. Therefore we will focus on the investigation of the ω variation of the pair transfer matrix element

$$P(\omega) = < N+2,\omega|P^+|N,\omega > \tag{7}$$

where $|N,\omega>$ is the PNC wave function of H_{CSM} for a N particle system at frequency ω. However, the eigen-function of H_{CSM} at each point (N,ω) in the parameter space is determined up to an arbitrary phase. In the PNC calculation the relative phase of wave functions are chosed in such a way that at $\omega = 0$ the matrix element in eq. (7) is positive and the concept of natural Hermitian connection[23] is used; i.e. the overlap between two neighboring PNC wave functions $|N,\omega>$ and $|N,\omega+\epsilon>$ should be unity up to quadratic terms in the infinitesimal parameter ϵ

$$< N,\omega|N,\omega+\epsilon >= 1 + \mathcal{O}(\epsilon^2) \tag{8}$$

The pair transfer matrix element (normalized to unit for $\omega = 0$)

$$< N+2,\omega|P^+|N,\omega > / < N+2,\omega=0|P^+|N,\omega=0 > \tag{9}$$

for yrast band to yrast band as a function of ω is shown in Fig. 4. Although the pair transfer matrix element soon decrases to zero, still it is clearly seen that in the PNC treatment *sign change* of the pair transfer matrix element (yrast band to yrast band) occurs around the rotational frequency $\omega = 0.10\hbar\omega_0$ for a neutron pair transfer reaction in ^{168}Hf $\rightarrow$ ^{166}Hf, in contrast with the previous result obtained by the single-j CSM[14]. Here the rotational frequency at which the sign change of the nuetron pair transfer matrix element occurs seem have nothing with the related bandcrossing frequency, this means that diabolic pair transfer is closely connected with diabolic point not bandcrossing. It could be understood from the N(λ) variation of the the interband interaction of yrast bands and yrare band. In fact, a oscillating N(λ) variation of the interband interaction of yrast bands and yrare band is clearly demonstrated in Fig. 3 and diabolic points between the yrast and yrare bands may appear around $\omega = \omega_c$. Therefore, it is not surprising that an oscillating behavior of pair transfer matrix element is found for a neutron pair transfer reaction in ^{168}Hf $\rightarrow$ ^{166}Hf, as shown in Fig. 4.

3 Summary

Based on PNC cranked Nilsson model we have carried out a systematic investigation of the occurence of Berry phase and diabolic neutron pair transfer for isotopic chain of Hf nuclei. In the calculation we have adopted a reasonable truncated MPC configuration space and a fully quantum mechanical treatment of particle number degree of freedom.

Since the particle number here is quantized, we no longer have continuous parameters and no longer apply the arguement of Berry[1]. Therefore we have introduced another kind of Berry phase on a discretized path similar to ref. [10,11]. As we are only interested in the diabolic neutron pair transfer between yrast bands of neighbouring even isotopic chain of Hf nuclei, which is maily determined by neutron if the proton-neutron residual interaction are negelected, so the calculation are

carried out in neutron MPC space. we have found that the sign of the neutron pair transfer matrix element (yrast band to yrast band) changes around the rotational frequency $\omega = 0.10\hbar\omega_0$ for ^{168}Hf $\rightarrow$ ^{166}Hf, in contrast with the previous result that no such sign change occurs for yrast band to yrast band obtained in the single-j PNC CSM[14]. However this does that means that the calculation of ref. [14] is wrong, instead it is because that in single-j shell no states of normal parity exist.

It should be emphasized that the unique role of atomic nuclei among many body quantum system is based on the strong short range attractive interaction between its constitient particles and its large but yet "finite" number of such constituent particles. Though great success has been achieved since the transplant of the BCS method and the concept of quasiparticle excition from the superconducting theory of metal to nuclear physics at the end of fifties, some important conclusions drawn from the BCS or HFB methods (pairing collapse, oscillating behavior of backbending and pair transfer matrix element in a single-j model) have been turned out to be unsuitable, mainly due to the finiteness of particle number ($\sim 10 - -10^2$) in a nucleus. These results remind us that some statements for nuclear system drawn from the BCS or HFB approximation should be reexamined carefully. The realistic calculation here and a single-j PNC CSM in ref. [14] give a strong support for the above statement.

The authors are grateful to Prof. C. S. Wu for helpful discussion and to CCAST for the hospitality and supports during the workshop period. This work is partly supported by the National Natural Science Foundation of China, and the Grant LWTZ-1298 of Chinese Academy of Science.

*mailing address.

REFERENCES

[1]M. V. Berry, Proc. Roc. Soc. **A392**,45 (1984).

[2]J. Von Neumann and E. P. Wigner, Phys. Z. 30, 467 (1929).

[3]Y. Aharonov and J. Anandan, Phys. Rev. Lett. **58**, 1593 (1987).

[4]I. J. R. Aitchison, Phys. Scr. **T23**, 12 (1988).

[5]J. W. Zwanziger, M. Koenig, and A. Pines, Annu. Rev. Phys. Chem. 41, 601 (1990).

[6]R. S. Nikam, P. Ring and L. F. Canto, Z. Phys. **A324**, 241(1986).

[7]R. S. Nikam, P. Ring, and L. F. Canto, Phys. Lett. **185B**,269 (1987).

[8]L. F. Canto, R. Donangelo, R. S. Nikam, and P. Ring, Phys. Lett. **192B**, 4 (1987).

[9]R. S. Nikam and P. Ring, Phys. Rev. Lett. **58**, 980(1987).

[10]R. S. Nikam, P. Ring, Y. Sun and E. R. Marshalek, Phys. Lett. **235B**,225(1990).

[11]Y. Sun, P. Ring, and R. S. Nikam, Z. Phys. **A339**,51 (1991).

[12]N. Rowley, K. E. Pal, and M. A. Nagarajan, Phys. Lett. **201B**,187(1988).

[13]M. Hasegawa, S. Tazaki and K. Muramatsu, Phys. Lett. **226B**, 1 (1989).

[14]J. Meng, J. Y. Zeng, and E. G. Zhao, Preprint, AS-ITP-92-34.

[15]R. Bengtsson, I. Hamamoto and B. R. Mottelson, Phys. Lett. **73B**, 259 (1978).

[16]J. Y. Zeng and T. S. Cheng, Nucl. Phys. **A405**, 1 (1983).

[17]L. F. Canto, P. Ring, and J. O. Rasmussen, Phys. Lett. **161B**, 21 (1985).

[18]e.g. A. Goodman, Nucl. Phys. **A256**,113 (1976).

[19]U. Mutz and P. Ring, J. Phys. **G10**, L39 (1984).

[20]C. S. Wu and J. Y. Zeng, Phys. Rev. **C40**, 998 (1989); *ibid* **C41**, 1822 (1990).

[21]R. Bengtsson and J. D. Garret, Int. Rev. Nuc. Phys. **2**, 193 (1984).

[22]R. Bengtsson, S. Frauendorf and F. R. May, At. Data Nucl. Data Table **35**, 15 (1986).

[23]B. Simon, Phys. Rev. Lett. **51**, 2167 (1983).

Figure Captions

Figure 1: The truncated neutron Nilsson single particle level scheme in ^{168}Hf (Lund systematics [22]).

Figure 2: The ω variation of the lowest nine eigenenergies (signature $r = 1$) of H_{CSM} for the neutron systems of Hf-chains ^{166}Hf-^{174}Hf in the nilsson model ($e_2 = 0.235$, $e_4 = .005$) obtained by exact diagonalization of H_{CSM} in the truncated MPC space (for the details see the text). The lowest MPC configuration energy is chosen as zero.

Figure 3: The same as Fig. 1, but the yrast band is taken as reference.

Figure 4: The pair transfer matrix elements (normalized to unit for $\omega = 0$) $< N+2, \omega | P^+ | N, \omega > / < N+2, \omega = 0 | P^+ | N, \omega = 0 >$ (solid lines) for $N = 18, 20, 22, 24$, and 26 (yrast band to yrast band) . The dashed lines represent the gap parameters $\tilde{\Delta} \equiv G < P^+ P >$[20] averaged over the initial and final systems: $[\tilde{\Delta}(N) + \tilde{\Delta}(N+2)]/2$. It could be seen that an oscillating behavior occurs for the neutron pair transfer reaction in ^{168}Hf $\rightarrow$ ^{166}Hf.

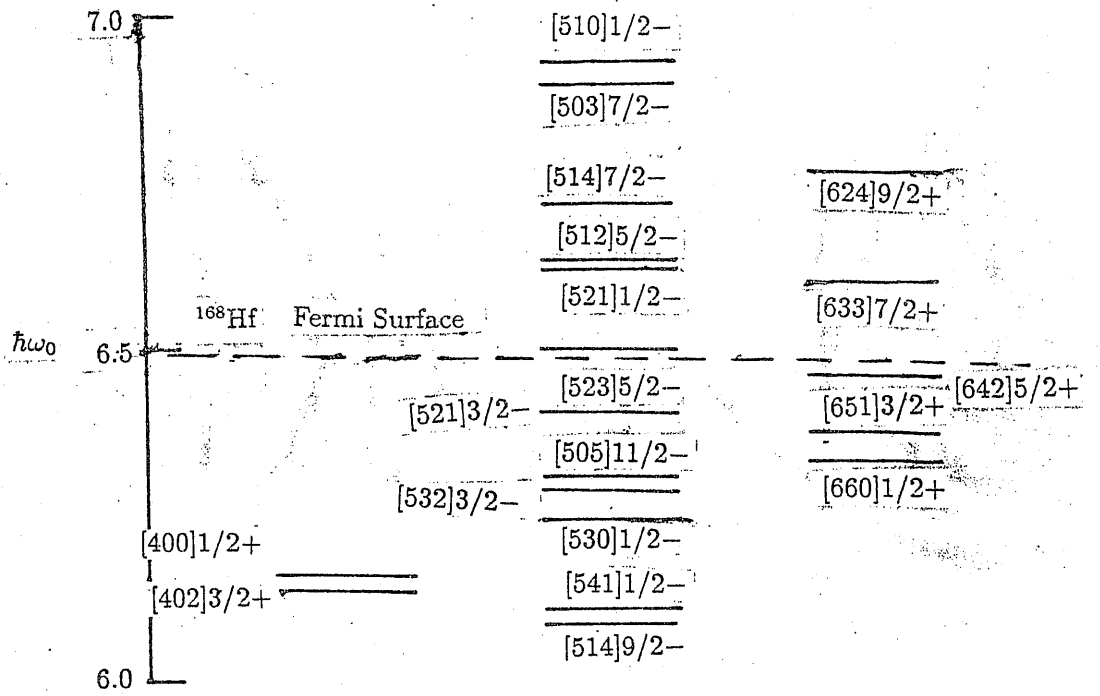
7.0
[510]1/2−
[503]7/2−
[514]7/2−
[624]9/2+
[512]5/2−
[521]1/2−
[633]7/2+
^{168}Hf
Fermi Surface
$\hbar\omega_0$
6.5
[523]5/2−
[642]5/2+
[521]3/2−
[651]3/2+
[505]11/2−
[532]3/2−
[660]1/2+
[400]1/2+
[530]1/2−
[402]3/2+
[541]1/2−
[514]9/2−
6.0

Figure 1:

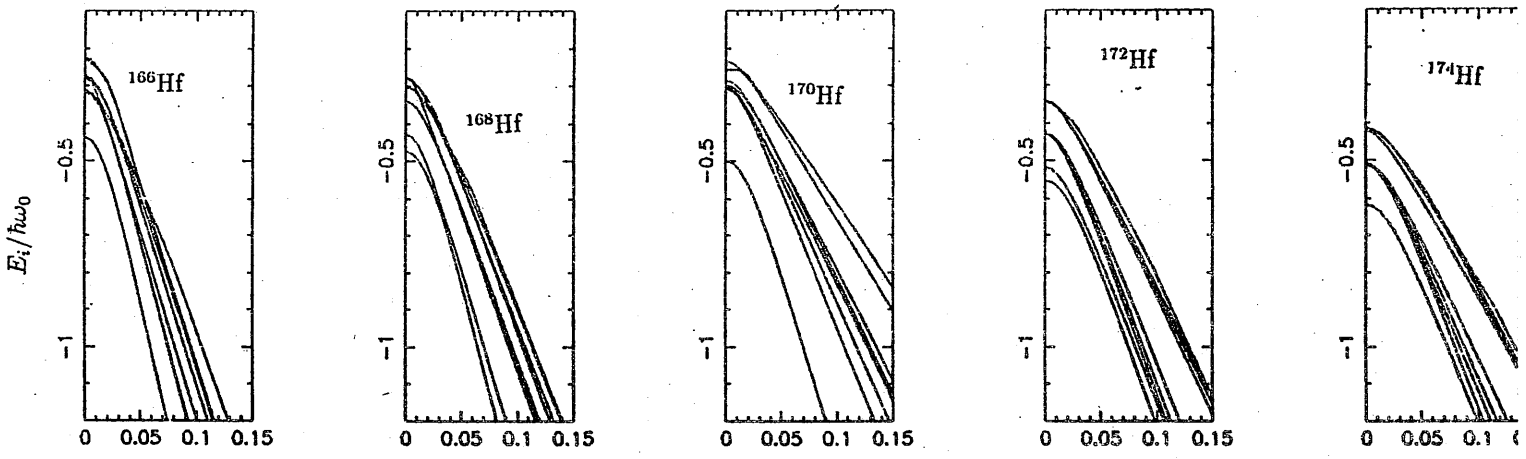

Figure 2:

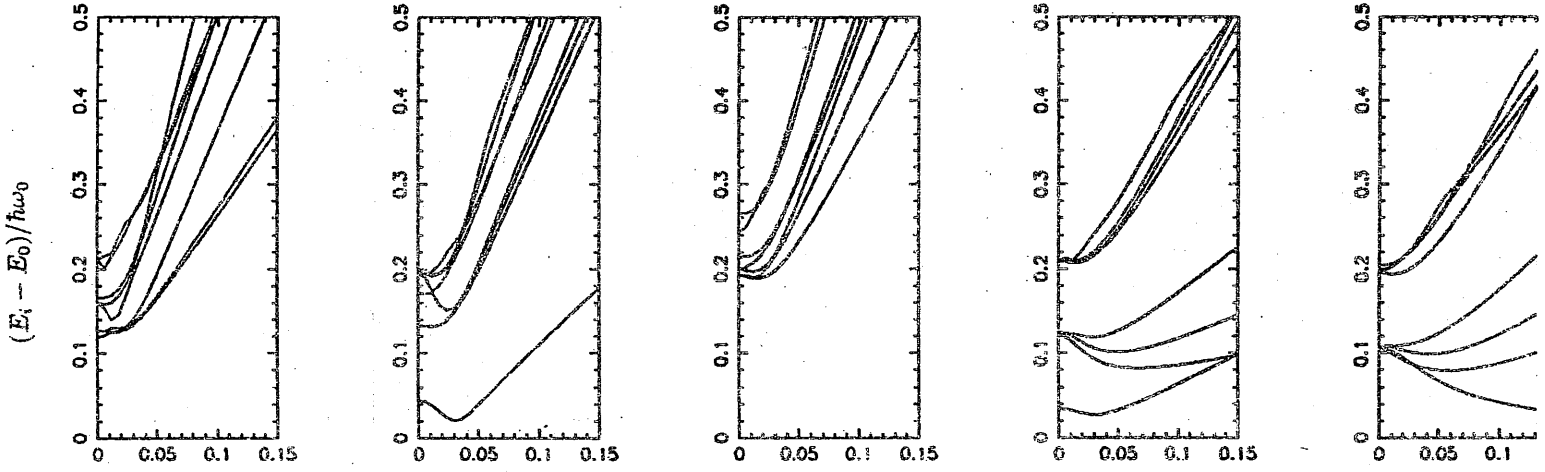

Figure 3:

$P(\omega)/P(\omega = 0)$

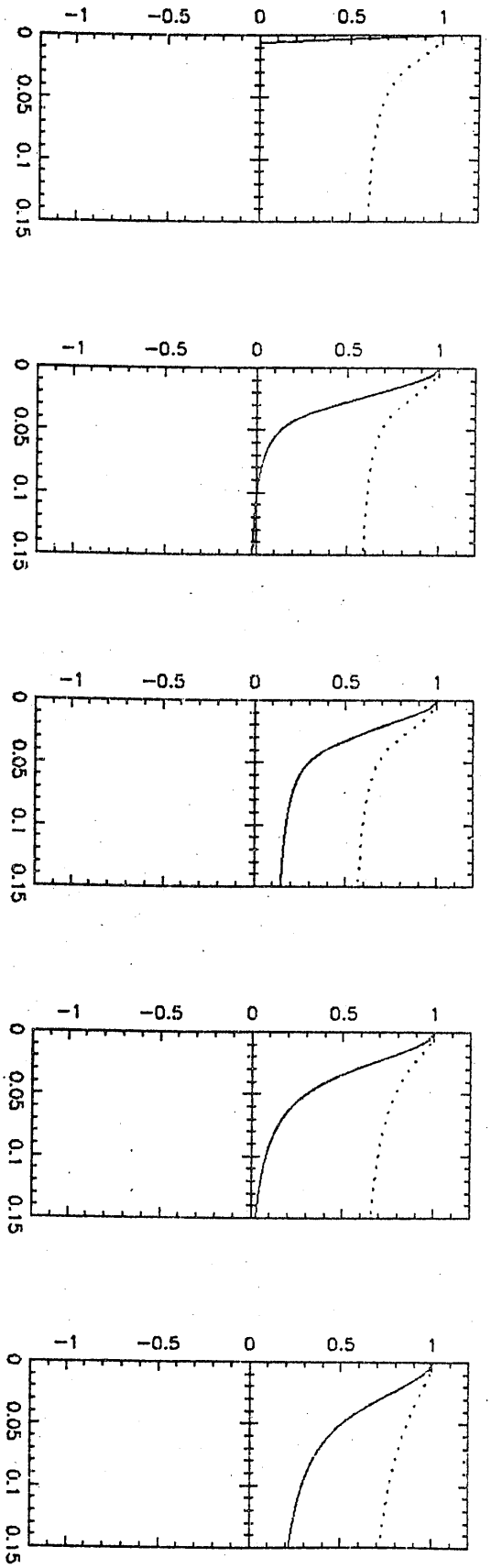

Figure 4: